



MIT  
SEA  
GRANT  
PROGRAM

CIRCULATING COPY  
Sea Grant Depository

# MATHEMATICAL MODELING OF DISPERSION IN STRATIFIED WATERS

by

George C. Christodoulou

Jerome J. Connor

and

Bryan R. Pearce



Massachusetts Institute of Technology

Cambridge, Massachusetts 02139

Report No. MITSG 76-14

November 15, 1976

MATHEMATICAL MODELING OF DISPERSION  
IN STRATIFIED WATERS

by

George C. Christodoulou  
Jerome J. Connor  
and  
Bryan R. Pearce

Report No. MITSG 76-14  
Index No. 76-314-Cbc

## ABSTRACT

### MATHEMATICAL MODELING OF DISPERSION IN STRATIFIED WATERS

by

GEORGE C. CHRISTODOULOU

JEROME J. CONNOR

and

BRYAN R. PEARCE

A numerical model is developed for the quantitative description of the dispersion process in a two-layer system which represents an approximation for a natural water body during the summer season, when a distinct thermocline usually exists. The model can handle any passive constituent, dissolved or suspended, possessing (small) vertical mobility and arbitrary decay characteristics, in a domain of irregular geometry and bottom topography. The formulation is based on the convection-diffusion equation, vertically integrated between the layer boundaries. Layer velocities and thicknesses are assumed to be obtained from a separate hydrodynamic model. The processes of entrainment and mixing through the density interface are presented with a unified view and general quantitative expressions in terms of the stability of the system and the mean flow characteristics are proposed. The modeling of horizontal dispersion mechanisms and the relation of eddy diffusivity to the characteristic grid size and of shear dispersion to the local velocity profile are discussed.

The finite element method is chosen for numerical implementation because of its great flexibility in grid layout and easier handling of spatial or temporal variability. Triangular elements with linear interpolation functions are used for the spatial discretization, while a simple implicit iterative scheme based on the trapezoidal rule is employed for time integration. The method is shown to be unconditionally stable for an arbitrary grid for both one- and two-layer problems, in the case of no iteration and constant parameters. General convergence criteria required by the iteration procedure are developed and expressed in terms of the basic parameters of the problem and are also confirmed by numerical experiments. The accuracy of the computational scheme is investigated on a regular grid. It is found to be satisfactory with respect to numerical amplitude and phase errors; a criterion is presented for avoiding spatial oscillations caused by the approximation of steep concentration gradients.

Analytical solutions are derived for one- and two-dimensional counterflow conditions and are subsequently used for verification purposes. The sensitivity of the phenomenon to the intensity of interfacial mixing and other parameters is studied and is found to vary in different classes of problems. Lastly, the numerical model is applied to two particle dispersion experiments carried out recently in the Massachusetts Bay and comparisons with field measurements are presented.

## AUTHORS

George C. Christodoulou, Ph.D. candidate, Department of Civil Engineering

Jerome J. Connor, professor, Department of Civil Engineering

Bryan R. Pearce, assistant professor, Department of Civil Engineering

## ACKNOWLEDGEMENTS

This two-volume report is the text of a Ph.D. thesis describing the results of research done under the auspices of the M.I.T. Sea Grant Program with support from the Office of Sea Grant in the National Oceanic and Atmospheric Administration, U.S. Department of Commerce, through grant number 04-5-158-1; and from the Massachusetts Institute of Technology; and from the Ralph M. Parsons Laboratory for Water Resources and Hydrodynamics, Department of Civil Engineering, Massachusetts Institute of Technology.

## RELATED REPORTS

Devanney, John W., III, et al. PRIMARY PHYSICAL IMPACTS OF OFF-SHORE PETROLEUM DEVELOPMENTS; REPORT TO COUNCIL ON ENVIRONMENTAL QUALITY. MITSG 74-20; NTIS COM-74-1125/AS. Cambridge: M.I.T. Sea Grant Program, 1974. 432 pp.

Moore, Stephen F., et al. POTENTIAL BIOLOGICAL EFFECTS OF HYPOTHETICAL OIL DISCHARGES IN THE ATLANTIC COAST AND GULF OF ALASKA. MITSG 74-19; NTIS COM-74-11089/AS. Cambridge: M.I.T. Sea Grant Program, 1974. 121 pp.

Moore, Stephen F., Robert L. Dwyer, and Arthur M. Katz. A PRELIMINARY ASSESSMENT OF THE ENVIRONMENTAL VULNERABILITY OF MACHIAS BAY, MAINE, TO OIL SUPERTANKERS. MITSG 73-6; NTIS COM-73-10564. Cambridge: M.I.T. Sea Grant Program, 1973. 162 pp.

Robbins, Phillips W. STUDENT PROJECTS ON THE OXIDATION BY MARINE BACTERIA OF AROMATIC COMPOUNDS FOUND IN OIL. MITSG 71-10; NTIS COM-71-00878. Cambridge: M.I.T. Sea Grant Program, 1971. 55 pp.

NOTE: The preceding publications may be ordered from the National Technical Information Service, U.S. Department of Commerce, Springfield, Virginia, 22151. Use the NTIS number when ordering; prices are variable.

## TABLE OF CONTENTS

	<u>Page</u>
Title Page	1
Abstract	2
Acknowledgments	4
Table of Contents	5
List of Figures	8
List of Tables	12
List of Symbols	13
Chapter 1 Introduction	19
Chapter 2 Model Formulation	26
2.1 Integrated Governing Equations	26
2.2 Applicability, Limitations and Extensions of the Formulation	36
2.3 Boundary Conditions	38
Chapter 3 The Dispersion Process in a Layer	42
3.1 Mechanisms of Dispersion	42
3.2 The Horizontal Eddy Diffusion Coefficient	45
3.3 The Shear Dispersion Coefficients	57
3.4 The Vertical Diffusion Coefficient	68
Chapter 4 Interfacial Transport	73
4.1 Description of the Phenomenon	73
4.2 Review of Related Work	79
4.3 Generalizations and Conclusions	90

	<u>Page</u>
Chapter 5 Analytical Solutions	94
5.1 1-D Instantaneous Injection	96
5.2 1-D Continuous Injection	106
5.3 2-D Continuous Injection	114
Chapter 6 Sensitivity Analysis	121
6.1 One-Dimensional One-Layer Flow	122
6.1.1 Instantaneous Source	122
6.1.2 Continuous Source	126
6.2 Two-Dimensional One-Layer Flow	133
6.2.1 Instantaneous Source	133
6.2.2 Continuous Source	137
6.3 Two-Layer Flow	144
6.3.1 1-D Instantaneous Source	144
6.3.2 1-D Continuous Source	146
6.3.3 2-D Continuous Source	148
Chapter 7 The Finite Element Formulation	154
7.1 The Weak Form	154
7.2 The Finite Element Approximation	158
7.3 Time Integration Strategy	170
Chapter 8 Stability and Accuracy of the Numerical Scheme	174
8.1 Background from Finite Difference Methods	176
8.2 Analysis of a Regular Finite Element Grid	183

	<u>Page</u>
8.2.1 Stability	183
8.2.2 Amplitude Errors	187
8.2.3 Phase Errors	190
8.2.4 Spatial Oscillations	192
8.3 Matrix Analysis for an Arbitrary Grid	198
8.3.1 Time Integration Stability	198
8.3.2 Iteration Convergence	204
8.4 An Approximate Criterion for the Time Step	206
8.5 Experimental Results	216
8.6 Stability of Two-Layer Model	225
Chapter 9 Verification and Applications	234
9.1 1-D Verification Studies	236
9.2 2-D Verification Studies	241
9.3 Application to the NOMES Experiment	244
9.3.1 The Experiment	244
9.3.2 The Flow Field	247
9.3.3 Dispersion Results	260
9.4 Application to the MIT Experiment	279
9.4.1 The Experiment	279
9.4.2 The Flow Field	281
9.4.3 Dispersion Results	282
9.5 Discussion of Results	288
Chapter 10 Conclusions	298
References	301



## LIST OF FIGURES

<u>Figure</u>	<u>Title</u>	<u>Page</u>
2.1	The Two-Layer Idealization	27
3.1	Dependence of the Horizontal Diffusion Coefficient on the Scale of the Phenomenon (58)	48
3.2	Okubo's Diffusion Data (55) and 4/3 Power Lines	48
3.3	Length Scale for Sub-grid Scale Eddy Diffusivity	55
3.4	Velocity Components in Two Coordinate Systems	55
3.5	Comparison of Expressions for the Horizontal Eddy Diffusivity	56
4.1	Schematization of Interfacial Transport	77
4.2	Experimental Results of Lofquist, Replotted in (7)	77
4.3	Experimental Results of Kato and Phillips (35)	83
4.4	Experimental Results of Moore and Long (52)	83
5.1	Flow Field Assumed for Analytical Solutions	95
5.2	Mass Balance at the Location of the Source	95
5.3	Concentration Distributions in 2-D Counter-flow Case	116
6.1	Typical Distribution after an Instantaneous Injection in 1-D Flow	124
6.2	Typical Steady State Distribution for a Continuous Source in 1-D Flow	129
6.3	Sensitivity Curves for 1-D Continuous Source	132
6.4	Typical Distribution after an Instantaneous Injection in a 2-D Domain	134

<u>Figure</u>	<u>Title</u>	<u>Page</u>
6.5	Typical Steady State Distribution for a Continuous Source in a 2-D Domain	138
6.6	Sensitivity Curves for 2-D Continuous Source	141
6.7	Sensitivity Curves for a Continuous Source in a 2-Layer 1-D Counterflow	149
6.8	Sensitivity Curves for a Continuous Source in a 2- Layer 2-D Counterflow	149
7.1	Solution Field and Boundary Conditions	155
7.2	Local Element Coordinate System	159
7.3	Local Boundary Segment Coordinate System	159
8.1	Example of a Regular Grid	185
8.2	Definition of Angles for an Arbitrary Triangle	185
8.3	Comparison of Theoretical Bounds on the Time Step with 1-D Runs	218
8.4	One-Dimensional Finite Element Test Grid	220
8.5	Two-Dimensional Finite Element Test Grid	220
8.6	Comparison of Theoretical Bounds on the Time Step with 2-D Runs	222
8.7	Comparison of Different Loading Strategies in a 2-D Grid	224
9.1	1-D Distribution at t=10 sec. after an Instantaneous Injection	238
9.2	1-D Steady State Distribution	240
9.3	2-D Steady State Distribution along the x-axis	242
9.4	2-D Steady State Profiles Normal to x-axis	243

<u>Figure</u>	<u>Title</u>	<u>Page</u>
9.5	Massachusetts Bay Finite Element Grid and Location of the NOMES Experiment	246
9.6	Interface Motion in FTB Run	253
9.7	Comparison of Predicted Velocities at St. 5	254
9.8	Current Data at St. 5 and FTB Model Results	255
9.9	Flow Field at Flood Tide for FTB Run	257
9.10	Flow Field at Ebb Tide for FTB Run	258
9.11	Seven-Day Particle Paths for FTB Run	259
9.12	Flow Field at Flood Tide for HTB Run	261
9.13	Flow Field at Ebb Tide for HTB Run	262
9.14	Seven-Day Particle Paths for HTB Run	263
9.15	Experimental Data at Day D+2 (54)	265
9.16	Experimental Data at Day D+3 (54)	266
9.17	Surface Measurements at Day D+7 (54)	267
9.18	Model Results for FTB Run at Day D+2	269
9.19	Model Results for FTB Run at Day D+3	270
9.20	Model Results for FTB Run at Day D+7	271
9.21	Model Results for HTB Run at Day D+2 (Release at Low Water)	273
9.22	Model Results for HTB Run at Day D+3 (Release at Low Water)	274
9.23	Model Results for HTB Run at Day D+7 (Release at Low Water)	275
9.24	Model Results for HTB Run at Day D+2 (Release at Ebb Tide)	276

<u>Figure</u>	<u>Title</u>	<u>Page</u>
9.25	Model Results for HTB Run at Day D+3 (Release at Ebb Tide)	277
9.26	Model Results for HTB Run at Day D+7 (Release at Ebb Tide)	278
9.27	Location of the MIT Experiment	280
9.28	Velocity Comparison at St. BE	283
9.29	Experimental Results at Day D+1	284
9.30	Experimental Results at Day D+2	285
9.31	Experimental Results at Day D+3	286
9.32	Computed Concentrations at Day D+1 (Large Tidal Tilt)	289
9.33	Computed Concentrations at Day D+2 (Large Tidal Tilt)	290
9.34	Computed Concentrations at Day D+3 (Large Tidal Tilt)	291
9.35	Computed Concentrations at Day D+1 (Small Tidal Tilt)	292
9.36	Computed Concentrations at Day D+3 (Small Tidal Tilt)	293
9.37	Computed Concentrations at Day D+3 (Small Tidal Tilt)	294

# LIST OF TABLES

<u>Table</u>	<u>Title</u>	<u>Page</u>
3.1	Constants of 4/3 Power Law Fitted to Individual Sets of Data of Figure 3.2	49
3.2	Constants $\lambda$ in Shear Dispersion Coefficient Expressions (Eqs. 3.22)	67
6.1	Parameter Sensitivity for 1-D Instantaneous Injection	124
6.2	Parameter Sensitivity for 1-D Continuous Source	129
6.3	Parameter Sensitivity for 2-D Instantaneous Injection	134
6.4	Parameter Sensitivity for 2-D Continuous Source	138
6.5	Parameter Sensitivity in Two-Layer Systems	152
8.1	Amplitude Error after 100 Time Steps, for $U\Delta t/\Delta s = 0.1$	188
8.2	Phase Error $\theta/ku\Delta t$ , for $E=0$	191
8.3	Phase Error $\theta/ku\Delta t$ , for $u\Delta t/\Delta s = 0.1$	192
8.4	Definition of Symbols Used in Figures 8.3 and 8.6	219
9.1	Parameters Used in Verification Studies	237
9.2	Summary of Circulation Runs for the NOMES Application	251

# LIST OF SYMBOLS

$a_j, b_j$	element constants ( $j = 1, 2, 3$ )
$a, a^*$ $\sim, \sim^*$	amplification matrices
$a_s, a_{ss}$	scalars
$c$	local concentration
$\bar{c}$	average concentration over layer thickness
$c''$	spatial deviation from $\bar{c}$
$c_I$	interfacial friction factor
$d$	scalar
$e$	rate of energy input (dissipation), also turbulent kinetic energy
$f_1, f_2$	functions
$g$	acceleration of gravity
$h$	total water depth
$-h_1$	interface elevation
$-h_2$	bottom elevation
$i$	$\sqrt{-1}$
$j, j_x, j_y$	space discretization indices
$k$	decay rate, also von-Karman constant
$k, k_x, k_y$	wavenumber
$\ell$	length scale for diffusion, also for interfacial transport
$m$	source input per unit time, also scalar
$m_{12}, m_{21}$	one-way interfacial transport rates
$n$	time discretization index

$p$	internal source/sink term, per unit volume
$q_x, q_y, q_z$	turbulent diffusion fluxes
$q_s, q_b$	diffusive flux through surface and bottom, respectively
$q_i$	diffusive flux through interface
$r$	radius of plume
$r_1, r_2, r_3, r_4$	roots of characteristic equations
$s, y$	Laplace transform variables
$t$	time
$u, v, w$	local velocity components
$\bar{u}, \bar{v}$	average velocities over layer thickness
$u'', v''$	spatial deviations from $\bar{u}, \bar{v}$
$u_*$	shear velocity
$w_e$	entrainment velocity
$w_s$	settling velocity
$x, y, z$	Cartesian coordinates
$A$	area
$A_1, A_2, A_3, A_4$	constants
$\tilde{A}$	advection matrix
$\tilde{A}_s, \tilde{A}_{ss}$	symmetric and skew-symmetric part of $\tilde{A}$
$\tilde{B}$	matrix
$C$	layer-integrated concentration
$\hat{C}$	trial solution
$C^*$	prescribed concentration as boundary condition
$C_T$	true solution

$C_N$	numerical solution
$C_o$	initial wave amplitude
$\bar{C}$	specified concentration defining the edge of plume
$D$	layer-integrated decay term
$\tilde{D}$	decay matrix
$E_x, E_y, E$ $E_{xx}, E_{yy}, E_{xy}$	dispersion coefficients
$E, E^*$	interfacial transport matrices
$\tilde{F}^b$	boundary force vector
$F_1, F_2, G$ $\tilde{F}_1, \tilde{F}_2, \tilde{G}$	matrices
$H$	layer depth
$K$ $\tilde{K}$	dispersion matrix
$L$	length scale for diffusion
$L_r, L_a$	relative and absolute length of plume
$M$	amount of instantaneous load, also a large value
$M_1, M_2$	total masses in layers 1, 2
$M$ $\tilde{M}$	geometrical matrix
$N$ $\tilde{N}$	element expansion vector
$P$	term including sources, decay and interfacial transfer
$P_s, P_b$	gain (or loss) through top and bottom boundary of a layer, respectively
$\tilde{P}$	overall forcing vector
$\hat{\tilde{P}}$ $\tilde{P}$	$\tilde{P} - \tilde{F}^b$
$Pe$	Peclet number
$Q_x, Q_y$	total dispersive fluxes



$Q_n, Q_n^*$	dispersive flux normal to boundary and prescribed value
$Q_{21}$	overall interfacial transport
$R$	layer integrated source term, also residual
$R_r, R_a$	relative and absolute radius of plume
$\tilde{R}$	matrix
$Re$	Reynolds number
$Ri_o, Ri_o^*$	overall Richardson numbers
$\tilde{S}$	source vector
$S_c, S_q$	concentration and flux specified boundary segment, respectively
$T$	tidal period
$T_c$	time scale for mixing
$T_I$	initial time for mixing
$\tilde{T}$	coordinate transformation matrix
$U$	velocity magnitude, also velocity scale for interfacial transport
$U_s$	shear velocity
$W$	weighting function, also width of plume
$\tilde{X}$	matrix
$\alpha$	proportionality factor for interfacial diffusion
$\alpha'$	$\alpha/H$
$\beta$	percentage used in defining relative plume boundary
$\beta, \gamma, \delta$	defined in Equation (8.19)
$\epsilon_{xx}, \epsilon_{xy}, \epsilon_{yy}, \epsilon_z, \epsilon$	turbulent diffusion coefficients
$\epsilon$	scalar

$\eta$	surface elevation
$\theta$	phase of $\lambda$ , also angle of coordinate rotation
$\theta_j$	angles of triangular element ( $j = 1,2,3$ )
$\kappa$	molecular diffusivity, also scalar
$\lambda, \lambda^*$	complex amplification factors
$\lambda, \mu$	proportionality constants
$\nu$	kinematic viscosity
$\xi_j$	local element coordinates ( $j = 1,2,3$ )
$\rho$	density, also modulus of $\lambda$
$\sigma^2$	variance
$\phi_j$	angles defined in Figure 8.2
$\vec{\phi}$	vector
$\omega$	variable
$\vec{\psi}, \vec{\Omega}$	matrices
$\Delta\rho$	density difference between the layers
$\Delta U$	velocity difference between the layers
$\Delta s$	grid size
$\Delta t$	time step

#### Subscripts

0	peak value, or value at origin
1	layer 1
2	layer 2
j	space discretization index
n or t	time discretization index

$x, t, z$	components along the coordinate directions
$\sim$	matrix quantity

### Superscripts

$b$	boundary quantity
$d$	shear dispersion quantity
$e$	element quantity
$(i)$	iteration index
$n$	time discretization index
$T$	transpose of matrix
$-$	layer average value
$\sim$	turbulent fluctuation
$\cdot$	time derivative

## CHAPTER 1

### INTRODUCTION

Coastal areas have traditionally been centers of urban and industrial growth. In addition to the convenience of sea transportation, a basic reason for their attractiveness had been the seemingly infinite capacity of the nearby water to receive all kinds of unwanted effluents. In recent years, however, the rapidly increasing quantities of such effluents, and the developing trend for exploration of coastal waters for oil, mineral deposits and other resources, coupled with the growing concern over conservation of environmental quality has led to the necessity for rational planning of the coastal zone utilization, instead of allowing uncontrolled expansion.

A major technical problem associated with such planning strategies is the prediction of how an effluent will spread in a given body of water. The answer to this question is by no means simple. It involves knowledge of the flow field on the one hand and the characteristics and possible interactions of the pollutants on the other. The flow patterns in near shore waters are usually extremely complex and depend on meteorological conditions, bottom topography, boundary geometry, etc. To gain insight into the processes that take place in nature, three approaches may be followed:

- (i) Direct measurements
- (ii) Hydraulic modeling
- (iii) Mathematical modeling

Measurements in coastal waters are normally very expensive and mostly site and time specific, so that by themselves they cannot provide an adequate overall view of the processes of interest. However, they are necessary in conjunction with models of categories (ii) and (iii), since they provide data required for input or for verification purposes. Hydraulic models can yield a very detailed picture of the phenomena, but considerable difficulties are encountered in the proper scaling of all relevant factors, inevitably resulting in some degree of simplification of the representation. They are in general site-specific and also are much more expensive than mathematical models. This last category consists essentially of the representation of the actual processes by mathematical equations, which are subsequently solved by some sort of analytical or numerical technique. The more complex the mathematical representation, the more difficult, but supposedly the more accurate, the solution becomes. Mathematical models are relatively inexpensive and general enough so that they can be applied to different areas with only minor changes.

With the widespread use of high-speed computers, increasingly detailed mathematical formulations can be handled by various numerical methods. Initially, two-dimensional one-layer models, treating the flow field as uniform over the depth, were developed to describe the transient circulation patterns in near-shore waters. This approach is justified because of the characteristic shallowness of coastal waters relative to their horizontal dimensions and yields the simplest approximation to the actual flow field. Finite difference techniques have been used for several years, but lately finite element models, allowing greater flexibility in the representation of complex geometries, have emerged.

From a practical viewpoint, of main interest is not the flow field, but rather the transport and dispersion of some substance due to a given flow field. Therefore, the information obtained from a hydrodynamic model is subsequently used as input to a transport model. The latter normally solves some form of the convection-diffusion equation, expressing the mass balance of the constituent of interest. Again, primarily finite difference schemes have been used in the past and only recently have finite element techniques been employed ( 2, 77, 44).

During the winter season, a water body is generally well-mixed through the depth. However, this is not the case during the summer. Due mainly to increased heat input near the surface, a density stratification begins to develop in the spring and by mid-summer a strong thermocline exists and practically divides the water column into two distinct layers. The dynamics of such a system cannot be adequately represented by a one-layer approximation, as severe velocity differences, and even counter-flows, may exist between the layers. The effect of stratification on the flow pattern has been evaluated by means of two-layer analytical solutions for oceans (87) and coastal waters (6). In lakes, where the wind is the primary forcing mechanism—as opposed to tide—the vertical dimension has been treated in more detail in both analytical (40) and numerical (45) investigations, at the expense of eliminating one of the horizontal dimensions. Severe simplifications of the geometry and of the governing equations had to be introduced, understandably, in order to obtain analytical results. To achieve a better description of both the vertical structure and the horizontal variability of the flow in a natural water

body of arbitrary geometry and bottom topography, multi-layer or quasi-three-dimensional numerical models were formulated (41, 72, 86). Simultaneous with solving the hydrodynamic equations, one has to keep track of density changes, as they may significantly affect the flow field. Therefore, most multilayer circulation models are coupled with dispersion models which describe the transport of heat and salt, on which the water density depends. This implies that concentrations of heat and salt along open boundaries have to be specified and gain or loss through the water surface or through the boundaries has to be taken into account.

The development of large multilayer computer codes has recently been initiated (1, 41, 38, 72). Primary emphasis is being placed on improving the computational techniques for solving the increasingly complex relevant equations more efficiently and in software organization for easier use. Little attention has been given so far to the proper choice of the values of the parameters involved or the sensitivity of the solution to parameter variations. As the number of parameters and the boundary conditions that have to be specified increases with the number of layers, model verification becomes a very difficult and costly task. Extensive field data are generally required for the proper application of multilayer models to a given area, since, in the absence of realistic inputs (especially boundary conditions), the confidence in their results diminishes rapidly. So, despite their great potential, the usefulness for predictive purposes becomes doubtful.

The question of complexity of the mathematical representation of the physical processes vs. the cost and data requirements is an important one

from a practical viewpoint. A less ambitious, two-layer model, while still containing a small number of parameters, and requiring minimal "tuning", provides a significantly different picture of the phenomena than its one-layer counterpart and is quite appropriate under strong natural stratification. The two-layer idealization is a natural one with the distinct thermocline being almost a "material" interface, allowing little transfer through it and lending itself to a clearer representation of the physical processes of entrainment. By contrast, in a multilayer approach, the layers are necessarily separated in an arbitrary way by imaginary (mostly horizontal) interfaces. Of course, this is necessary when a strong thermocline is absent and the change in density is more or less continuous from the surface to the bottom.

The objective of this study is to investigate problems associated with properly describing the dispersion of matter in a two-layer system. Transport of constituents, notably water quality parameters, is being incorporated in the multilayer models mentioned above. However, the fundamental physical behavior of dispersion in a layered system has not so far been fully investigated. It is felt that this can be best understood in the simplest two-layer case, which therefore has to precede a multilayer approach. This work attempts to establish this behavior by studying first the physical processes involved and developing simple analytical solutions which identify the essential features of the problem, before proceeding to the numerical aspects of the solution. Then, the details of the finite element method are discussed and its stability requirements and accuracy characteristics for this class of problems are established.



The numerical model is intended to describe the dispersion of an arbitrary constituent, possessing in general vertical mobility, in a two-layer coastal water body of variable bottom topography and boundary geometry, under transient flow conditions. This being primarily a study of the dispersion phenomenon, the velocity field in both layers, as well as their thicknesses, will be assumed known, presumably obtainable through a separate hydrodynamic model. By uncoupling the hydrodynamic and dispersion models, the same flow pattern can be used to investigate very economically the spreading of several different substances and to experiment with different source locations, loading strategies, parameter values etc. However, this can only be done provided that the constituent of interest does not affect significantly the flow field or the density structure.

After the mathematical formulation of the problem (Chapter 2), the nature of the dispersion coefficients is examined in detail (Chapter 3). The horizontal eddy diffusivity is related to the grid size of the finite difference or finite element discretization, while the contribution of vertical shear is handled through an extension of Taylor's method (76) to two-dimensional flows. A brief discussion of the vertical diffusion coefficient is made at the end of this chapter. In Chapter 4, the physical mechanisms responsible for material transfer between the layers are examined. Through a literature review of theoretical and experimental investigations, mostly related to simple one-dimensional flows, quantitative relations expressing the interfacial transport in terms of the mean flow characteristics are proposed.

Analytical solutions for simple flow conditions are derived in Chapter 5. These show some of the peculiarities of the dispersion process in a two-layer system. The sensitivity of both one- and two-layer dispersion phenomena to changes in the parameters involved is examined in Chapter 6. While this is done only for simple flow conditions for which analytical solutions are available, the results are believed to hold to some extent in more general cases as well.

The relatively new finite element method has been chosen for numerical implementation, after its successful application in one-layer dispersion models. The basic formulation along with a discussion of the solution procedure is presented in Chapter 7. Approximate stability criteria based on a simple theoretical examination of the finite element formulation are developed in Chapter 8. The effect of the finite element discretization on the accuracy of the solution is also investigated. Numerical experiments are carried out to supplement and confirm the theoretical results. Knowledge from analogous finite difference approximations is used to some extent, since their stability requirements and other restrictions have been studied extensively. Despite rapid developments in the application of finite element methods to fluid problems, rigorous theoretical stability analysis has not yet succeeded in yielding practical results.

Verification of the numerical scheme against the analytical solutions presented in Chapter 5 is performed in the last chapter. Finally, applications to Massachusetts Bay serve partly as further verification of the model by comparison to large scale field experiments and partly as examples of its applicability to "real world" problems.

## CHAPTER 2

### MODEL FORMULATION

#### 2.1 Integrated Governing Equations

The mass balance of a constituent introduced in a water body is expressed by the three-dimensional convection-diffusion equation which, for negligible density changes either in the ambient conditions or due to the inclusion of the constituent, has the form

$$\frac{\partial c}{\partial t} = - \frac{\partial}{\partial x} (u_c c + q_x) - \frac{\partial}{\partial y} (v_c c + q_y) - \frac{\partial}{\partial z} (w_c c + q_z) + p \quad (2.1)$$

where

$c$  is the local volumetric concentration

$u_c$ ,  $v_c$ ,  $w_c$  are the constituent velocities in the  $x$ ,  $y$ ,  $z$  directions respectively

$q_x$ ,  $q_y$ ,  $q_z$  are the diffusive fluxes in the  $x$ ,  $y$ ,  $z$  directions

$p$  represents the generation or decay of the constituent per unit volume.

To obtain the equations pertaining to a layered system, integration of Equation (2.1) between the layer boundaries is required. In what follows, these equations are derived for the two-layer case defined in Figure 2.1. The procedure is analogous for a multi-layer formulation.

Using Leibnitz's rule one obtains for the top layer:

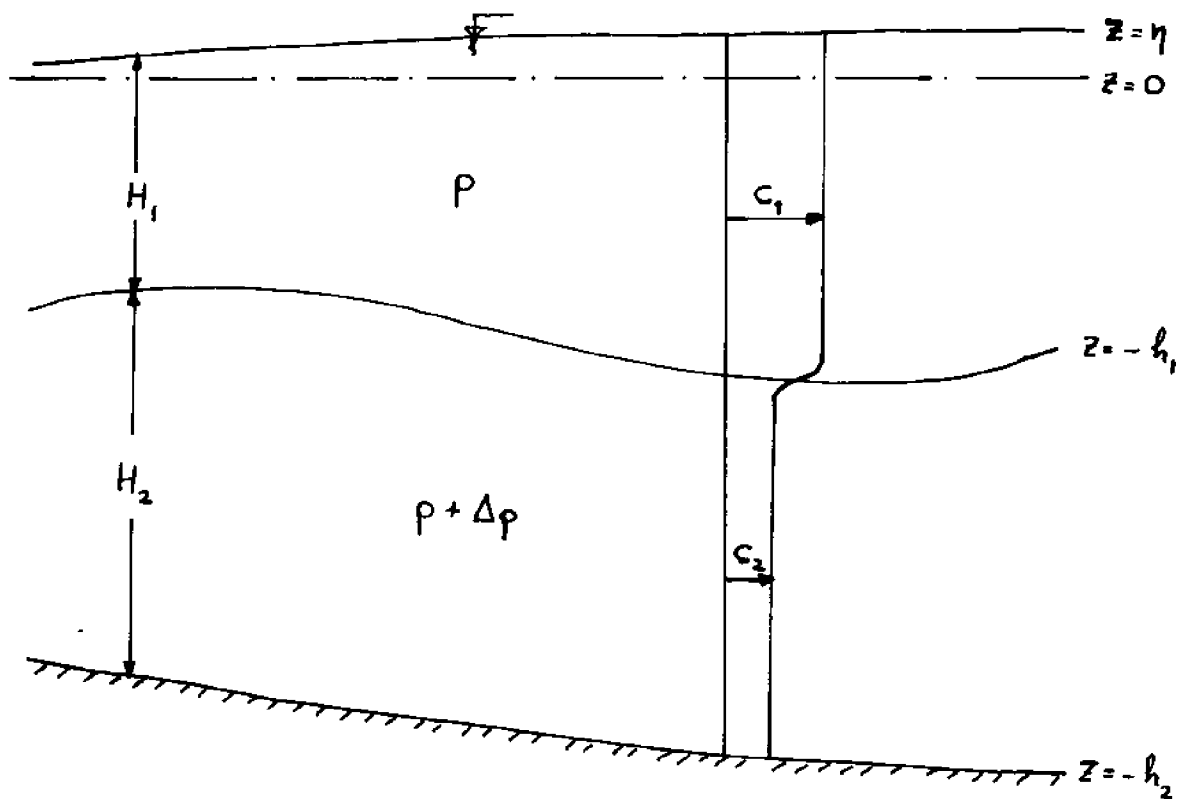


Figure 2.1 The Two-Layer Idealization

$$\begin{aligned}
\frac{\partial}{\partial t} \int_{-h_1}^{\eta} c dz - [c \frac{\partial \eta}{\partial t}]_{\eta} - [c \frac{\partial h_1}{\partial t}]_{-h_1} = & - \frac{\partial}{\partial x} \int_{-h_1}^{\eta} (u_c c + q_x) dz - \frac{\partial}{\partial y} \int_{-h_1}^{\eta} (v_c c + q_y) dz + \\
& + \int_{-h_1}^{\eta} p dz - [w_c c + q_z - (u_c c + q_x) \frac{\partial \eta}{\partial x} - (v_c c + q_y) \frac{\partial \eta}{\partial y}]_{\eta} + \\
& + [w_c c + q_z + (u_c c + q_x) \frac{\partial h_1}{\partial x} + (v_c c + q_y) \frac{\partial h_1}{\partial y}]_{-h_1}
\end{aligned}$$

which, after rearranging, results in:

$$\begin{aligned}
\frac{\partial}{\partial t} \int_{-h_1}^{\eta} c dz = & - \frac{\partial}{\partial x} \int_{-h_1}^{\eta} (u_c c + q_x) dz - \frac{\partial}{\partial y} \int_{-h_1}^{\eta} (v_c c + q_y) dz + \int_{-h_1}^{\eta} p dz + \\
& + [c (\frac{\partial \eta}{\partial t} + u_c \frac{\partial \eta}{\partial x} + v_c \frac{\partial \eta}{\partial y} - w_c) + (q_x \frac{\partial \eta}{\partial x} + q_y \frac{\partial \eta}{\partial y} - q_z)]_{\eta} + \\
& + [c (\frac{\partial h_1}{\partial t} + u_c \frac{\partial h_1}{\partial x} + v_c \frac{\partial h_1}{\partial y} + w_c) + (q_x \frac{\partial h_1}{\partial x} + q_y \frac{\partial h_1}{\partial y} + q_z)]_{-h_1}
\end{aligned} \tag{2.2}$$

This form expresses the time rate of change of the constituent mass within a control volume of length  $dx$ , width  $dy$  and bounded by the lines  $z = -h_1$  and  $z = \eta$ . The first two terms in the right hand side represent the advective and diffusive fluxes through the sides, the third term represents the generation or decay of material within the control volume and the last two terms define the exchange through the top and bottom boundaries, which are, in general, moving.

Normally, the horizontal velocity of the constituent is considered equal to the local water velocity, i.e.,  $u_c \approx u$  and  $v_c \approx v$ . However, unless the material is neutrally buoyant, this will not hold for the vertical component. By introducing the (positive

downwards) settling velocity  $w_s$ , and noting  $w_c = w - w_s$ , the bracketed terms in Equation (2.2) can be written as

$$\begin{aligned} P_{s_1} &= [c(\frac{\partial \eta}{\partial t} + u \frac{\partial \eta}{\partial x} + v \frac{\partial \eta}{\partial y} - w + w_s) - (q_z - q_x \frac{\partial \eta}{\partial x} - q_y \frac{\partial \eta}{\partial y})]_{\eta} = \\ &= [c(\frac{D\eta}{Dt} - w + w_s) - q_s]_{\eta} \\ P_{b_1} &= [c(\frac{\partial h_1}{\partial t} + u \frac{\partial h_1}{\partial x} + v \frac{\partial h_1}{\partial y} + w - w_s) + (q_z + q_x \frac{\partial h_1}{\partial x} + q_y \frac{\partial h_1}{\partial y})]_{-h_1} = \\ &= [c(\frac{Dh_1}{Dt} + w - w_s) - q_i]_{-h_1} \end{aligned}$$

where  $q_s$  and  $q_i$  are the diffusive fluxes normal to the free surface and interface respectively, per unit projected area on the horizontal plane, and are considered positive when outward from the layer. The kinematic condition at the free surface requires

$$[\frac{D\eta}{Dt} - w]_{\eta} = 0$$

and consequently

$$P_{s_1} = c_{\eta} w_s - q_s \quad (2.3)$$

This term represents the gain (or loss) of material from the atmosphere and in most cases vanishes. The interface, defined as the position of steepest density gradient, is not necessarily a material surface. Its location is given by

$$z = -h_1(x, y, t)$$

The position of a particle in the neighborhood of the interface can be

expressed in terms of the boundary and a deviation  $\Delta z$ , i.e.,

$$z = -h_1 + \Delta z$$

Then,

$$w = \frac{Dz}{Dt} = -\frac{Dh_1}{Dt} + \frac{D\Delta z}{Dt}$$

or

$$\left[w + \frac{Dh_1}{Dt}\right]_{-h_1} = w_e \quad (2.4)$$

The relative vertical velocity,  $w_e$ , of the water particles with respect to the layer boundary will be referred to herein as "entrainment" velocity and, by convention, it will be considered positive when directed upwards. Since  $w_e > 0$  implies  $\frac{D\Delta z}{Dt} > 0$  and the latter indicates that the water particle moves upward relative to the boundary, it follows that a positive entrainment velocity is associated with a net water motion from the bottom to the top layer.

We may now write

$$P_{b_1} = c_{-h_1}(w_e - w_s) - q_1 \quad (2.5)$$

Equation (2.5) shows that settling counteracts entrainment. In the case of a neutrally buoyant contaminant ( $w_s = 0$ ) the top layer would gain material through the interface at a rate  $w_e c_{-h_1}$ , provided  $w_e > 0$ . This gain is reduced for settling particles and actually becomes zero when  $w_s = w_e$  and changes to a loss when  $w_s > w_e$ . The latter case simply indicates that the downward settling rate of the particles relative to the water is faster than the upward rate of advance of the water through the interface.

The concept of entrainment is quite familiar in the field of fluid mechanics. It is usually associated with a relatively fast moving or highly turbulent layer (e.g. jet) that draws some mass from the adjacent ambient (and usually quiescent) fluid. In large water bodies, such as lakes or oceans, the term entrainment commonly refers to "erosion" of the quiescent bottom layer by the top layer moving under the influence of the wind or other driving mechanism. In coastal waters both layers are quite turbulent and possess velocities of the same order of magnitude. Therefore, there should be exchange of water mass both ways through the interface, and  $w_e$  will represent only the net result of this exchange. Viewing the concentration as continuous over the whole depth (Figure 2.1), but assuming that the transition zone between the layers is very narrow - consistent with the two layer idealization of the system - it is reasonable to approximate the concentration at the interface by the average of the concentrations of the adjacent layers. Therefore, we set

$$c_{-h_1} \approx \frac{c_1 + c_2}{2} \quad (2.6)$$

in Equation (2.5). This becomes more "exact" as the concentration gradient increases, approaching a discontinuity at the interface. The other component,  $q_i$ , of the interfacial transport is a diffusive flux and is generally expressed in terms of the difference in concentration between the layers, i.e.,

$$q_i = \alpha (c_1 - c_2) \quad (2.7)$$

where  $\alpha$  may depend on flow parameters and the concentration difference.



A detailed discussion of the interfacial transport process follows in Chapter 4.

With respect to the remaining terms of Equation (2.2), the following notation is introduced:

$$C_1 = \int_{-h_1}^{\eta} c dz = H_1 \bar{c}_1 \quad (2.8)$$

$$\begin{aligned} c_1 &= \bar{c}_1 + c_1'' \\ u_1 &= \bar{u}_1 + u_1'' \\ v_1 &= \bar{v}_1 + v_1'' \end{aligned} \quad (2.9)$$

where the overbar denotes the average value over the layer and the double prime the deviation from the average.

$$\int_{-h_1}^{\eta} p dz = R_1 - D_1 \quad (2.10)$$

where  $R_1$  represents the input or creation and  $D_1$  the decay of the constituent within the layer, per unit projected area.

In the simplest case of linear decay,

$$D_1 = kC_1 \quad (2.10a)$$

where  $k$  denotes the decay rate.

Equation (2.2) is now written as

$$\begin{aligned} \frac{\partial C_1}{\partial t} + \frac{\partial}{\partial x}(\bar{u}_1 C_1) + \frac{\partial}{\partial y}(\bar{v}_1 C_1) &= - \frac{\partial}{\partial x} \int_{-h_1}^{\eta} (q_x + u''c'') dz - \frac{\partial}{\partial y} \int_{-h_1}^{\eta} (q_y + v''c'') dz + \\ &+ R_1 - D_1 + P_{s_1} + P_{b_1} \end{aligned}$$

or

$$\frac{\partial \bar{c}_1}{\partial t} + \frac{\partial}{\partial x} (\bar{u}_1 \bar{c}_1) + \frac{\partial}{\partial y} (\bar{v}_1 \bar{c}_1) = -\frac{\partial}{\partial x} Q_{x_1} - \frac{\partial}{\partial y} Q_{y_1} + P_1 \quad (2.11)$$

The horizontal turbulent diffusion fluxes  $q_x$ ,  $q_y$  are usually expressed in terms of the gradients of the layer-average concentration and the turbulent diffusion coefficient, which in its most general form is a second order symmetrical tensor:

$$q_x = -\epsilon_{xx} \frac{\partial \bar{c}}{\partial x} - \epsilon_{xy} \frac{\partial \bar{c}}{\partial y}$$

$$q_y = -\epsilon_{yx} \frac{\partial \bar{c}}{\partial x} - \epsilon_{yy} \frac{\partial \bar{c}}{\partial y}$$

Integrating through the layer thickness, and taking into consideration the fact that  $\frac{\partial \bar{c}}{\partial x}$ ,  $\frac{\partial \bar{c}}{\partial y}$  are constant over  $z$ :

$$-\int_{-h_1}^{\eta} q_x dz = H_1 (\bar{\epsilon}_{xx_1} \frac{\partial \bar{c}_1}{\partial x} + \bar{\epsilon}_{xy_1} \frac{\partial \bar{c}_1}{\partial y}) \quad (2.12)$$

$$-\int_{-h_1}^{\eta} q_y dz = H_1 (\bar{\epsilon}_{yx_1} \frac{\partial \bar{c}_1}{\partial x} + \bar{\epsilon}_{yy_1} \frac{\partial \bar{c}_1}{\partial y})$$

where the overbars denote layer-average values. Under horizontally isotropic conditions,  $\bar{\epsilon}_{xx} = \bar{\epsilon}_{yy} = \epsilon$  and  $\bar{\epsilon}_{xy} = \bar{\epsilon}_{yx} = 0$ .

By analogy, the horizontal transport terms associated with vertical velocity variations are expressed by means of shear dispersion coefficients, as follows:

$$- \int_{-h_1}^{\eta} u''c''dz = H_1 (E_{xx_1}^d \frac{\partial \bar{c}_1}{\partial x} + E_{xy_1}^d \frac{\partial \bar{c}_1}{\partial y}) \quad (2.13a)$$

$$- \int_{-h_1}^{\eta} v''c''dz = H_1 (E_{yx_1}^d \frac{\partial \bar{c}_1}{\partial x} + E_{yy_1}^d \frac{\partial \bar{c}_1}{\partial y}) \quad (2.13b)$$

The horizontal dispersion processes in a layer will be examined in Chapter 3.

In a similar way, by integrating Equation (2.1) between the bottom layer boundaries, we obtain:

$$\begin{aligned} \frac{\partial C_2}{\partial t} + \frac{\partial}{\partial x} (\bar{u}_2 C_2) + \frac{\partial}{\partial y} (\bar{v}_2 C_2) = & - \frac{\partial}{\partial x} \int_{-h_2}^{-h_1} (q_x + u''c'') dz - \frac{\partial}{\partial y} \int_{-h_2}^{-h_1} (q_y + v''c'') dz + \\ & + R_2 - D_2 + P_{s2} + P_{b2} \end{aligned}$$

or

$$\frac{\partial C_2}{\partial t} + \frac{\partial}{\partial x} (\bar{u}_2 C_2) + \frac{\partial}{\partial y} (\bar{v}_2 C_2) = - \frac{\partial}{\partial x} Q_{x_2} - \frac{\partial}{\partial y} Q_{y_2} + P_2 \quad (2.14)$$

where

$$\begin{aligned} P_{s2} = & - [c (\frac{\partial h_1}{\partial t} + u \frac{\partial h_1}{\partial x} + v \frac{\partial h_1}{\partial y} + w - w_s) + (q_z + q_x \frac{\partial h_1}{\partial x} + q_y \frac{\partial h_1}{\partial y})]_{-h_1} \\ = & - [c(w_e - w_s) - q_1]_{-h_1} = - P_{b1} \end{aligned} \quad (2.15)$$

and

$$\begin{aligned}
P_{b2} &= [c \left( \frac{\partial h_2}{\partial t} + u \frac{\partial h_2}{\partial x} + v \frac{\partial h_2}{\partial y} + w - w_s \right) + (q_z + q_x \frac{\partial h_2}{\partial x} + q_y \frac{\partial h_2}{\partial y})]_{-h_2} = \\
&= [c \left( \frac{Dh_2}{Dt} + w - w_s \right) - q_b]_{-h_2}
\end{aligned}$$

The kinematic condition at the bottom requires

$$\left[ \frac{Dh_2}{Dt} + w \right]_{-h_2} = 0$$

and the loss of material to the bottom reduces to

$$P_{b2} = -w_s c_{-h_2} - q_b \quad (2.16)$$

This term may also be written as (34, 11)

$$P_{b2} = -Aw_s c_{-h_2} \quad (2.16a)$$

where

$A = 1.0$  for perfectly absorbing bottom

$A = 0.0$  for perfectly reflecting bottom

In summary, the governing equations for the two layers are:

$$\begin{aligned}
\frac{\partial C_1}{\partial t} + \frac{\partial}{\partial x}(\bar{u}_1 C_1) + \frac{\partial}{\partial y}(\bar{v}_1 C_1) &= \frac{\partial}{\partial x} (E_{xx1} H_1 \frac{\partial \bar{c}_1}{\partial x} + E_{xy1} H_1 \frac{\partial \bar{c}_1}{\partial y}) + \\
&+ \frac{\partial}{\partial y} (E_{yx1} H_1 \frac{\partial \bar{c}_1}{\partial x} + E_{yy1} H_1 \frac{\partial \bar{c}_1}{\partial y}) + \\
&+ (w_e - w_s) \frac{\bar{c}_1 + \bar{c}_2}{2} + \alpha(\bar{c}_2 - \bar{c}_1) - k C_1 + R_1
\end{aligned} \quad (2.17a)$$

$$\begin{aligned}
\frac{\partial c_2}{\partial t} + \frac{\partial}{\partial x} (\bar{u}_2 c_2) + \frac{\partial}{\partial y} (\bar{v}_2 c_2) = & \frac{\partial}{\partial x} (E_{xx_2} H_2 \frac{\partial \bar{c}_2}{\partial x} + E_{xy_2} H_2 \frac{\partial \bar{c}_2}{\partial y}) + \\
& + \frac{\partial}{\partial y} (E_{yx_2} H_2 \frac{\partial \bar{c}_2}{\partial x} + E_{yy_2} H_2 \frac{\partial \bar{c}_2}{\partial y}) - \\
& - (w_e - w_s) \frac{\bar{c}_1 + \bar{c}_2}{2} - \alpha (\bar{c}_2 - \bar{c}_1) - A w_s \bar{c}_2 - k c_2 + R_2
\end{aligned}
\tag{2.17b}$$

where the turbulent diffusivities have been absorbed in the dispersion coefficients and it was assumed that the concentrations are approximately uniform within each layer. These expressions include both integrated and average concentrations; by substituting  $C/H$  for  $\bar{c}$ , the latter can be eliminated. The layer-integrated concentration is chosen here to be the solution variable, being more convenient to work with in the integral form of the governing equations. In addition, it is a more "natural" quantity when the vertical concentration distribution over the layer is not uniform.

## 2.2 Applicability, Limitations and Extensions of the Formulation

The two-layer density stratification is a reasonable approximation of natural conditions during the summer season in the absence of severe weather phenomena. A temperature difference of more than 10°C between the top and the bottom layer is quite common in coastal areas such as the Massachusetts Bay (22). In addition, there is a difference in salinity between the layers, which is more than 1 ppt for the Bay (8). The combined effects of temperature and salinity imply a density difference of about 3<sup>0</sup>/oo between the

layers. In the model the layer densities are assumed to be known as functions of space and in the simplest case, to be constant. Density variation is assumed to be treated by the hydrodynamical model which is also used to provide necessary inputs of layer velocities and thicknesses. It is well known (79) that the thermocline depth can remain essentially fixed for substantial periods of time (of the order of weeks) when a balance exists between surface heating and mechanical energy input. The two-layer idealization of the system is based on the assumption that such statistically steady-state conditions exist for time intervals longer than the time scale associated with the dispersion phenomena of interest.

The densities do not enter in the calculations except for establishing the Richardson number upon which, as will be seen later, the interfacial transport depends. However, the assumption of prescribed densities seems to limit the applicability of the model to dispersion of passive constituents, i.e., not affecting the density structure. The most interesting non-passive pollutant is heat, released from power plants in the sea. A temperature rise of  $3^{\circ}\text{C}$  over the ambient, which is practically an upper limit on allowable heat discharges, causes a density change of  $0.6^{\circ}/\text{oo}$ , which is of the order of 20% of the initial density stratification. For such small density changes, the model can be still considered applicable.

The formulation in terms of the layer-integrated concentrations treats, in general, the total quantity of material within the layer. Certainly, the two-layer discretization is more appropriate when the

concentrations, as well as the flow parameters, are approximately uniform within each layer. This may be unrealistic in the case of heat, for example, or suspended sediments but it seems reasonable for neutrally buoyant constituents. The uniform distribution is the simplest profile that can be chosen. A choice of a different profile is permissible, provided that the assumption of self-similarity is acceptable. The specific profile choice will affect the boundary terms and, in addition, the dispersion and advection terms (11), which have to be expressed in terms of the constituent mean velocities. Such extensions do not present any conceptual difficulties.

Multilayer formulations may be evoked when more refined treatment of flow and concentration variations over the depth is desired. In this case the interfaces are not identified with density discontinuities. As coastal waters seldom exhibit a distinct stratification other than in two-layers, multiple layers are almost purely mathematical, aiming at a more detailed description of the phenomena under consideration. Normally these layers are separated by arbitrary horizontal surfaces that are fixed in time (41, 86, 72). The formulation presented in the previous section can be readily extended to  $n$  layers.

### 2.3 Boundary Conditions

The boundary conditions along horizontal boundaries confining the domain under consideration may be of two types, since the problem involves second order spatial derivatives:

- (a) Concentration specified, in terms of either layer-average or layer-integrated value
- (b) Concentration gradient normal in the boundary specified, or, alternatively, normal dispersive flux ( $Q_n$ ) specified.

The second kind of boundary condition is commonly used along land boundaries, where the normal dispersive flux is set naturally to zero (reflecting boundaries). Ideally, there is no advection through the land boundary, either. The velocity inputs have to be obtained from a hydrodynamic model that allows no water mass transport through the discretized boundary segments. This would imply that, if the pollutant concentration is constant over a segment, there will be no loss or gain of material through it. However, when the concentration is not constant, mass conservation may, in general, be violated and this has to be taken into consideration in the dispersion model.

Of major concern is the treatment of the ocean boundary. As long as the plume remains well within the domain, the concentration may be simply set and maintained at zero along that boundary. However, when the plume, after some time, approaches the boundary, the zero concentration cannot be imposed any more, since it will create an unnatural barrier to the plume that would otherwise extend out of the domain being modelled. The ideal solution to the problem would be to make the grid as big as to be sure that the plume never reaches the boundary. This is not usually possible in practice. Therefore an "engineering" approach has to be taken. This depends on the particular problem being solved and the judgement of the modeler, but



generally different boundary conditions are prescribed for inflows and outflows.

In models of salinity intrusion in estuaries (1-D), during ebb tide the salinity gradient is specified at the boundary as equal to that obtained from the neighboring interior zone; during flood tide the salinity itself is prescribed at the boundary, starting with the value acquired at the end of ebb and increasing up to the ocean salinity following some postulated function, as discussed in (27). In a 2-D domain, there is not, in general, inflow or outflow over the whole ocean boundary at the same time. It is easy, however, to keep track of the velocities at the boundary to determine their direction at any point and any time. Whenever there is outflow, in principle, the concentration gradient should be specified, by analogy to the one-dimensional case. Whenever there is inflow, however, things are more difficult. In general, the concentration should be specified, but this will not only depend on the last outflow concentration at that point, but essentially on the conditions and the mixing out of the boundary, since in pollution problems there is no reference value, as was the ocean salinity in the salinity intrusion problems. The presence of decay further complicates the matter. As Leendertse states (42) the specification of the boundary concentration depends on the modeller's intuition and feeling of the mixing processes out of the boundary.

A simpler procedure for outwards flow is to specify the gradient as zero, allowing the material simply to advect through the boundary.

The gradient near the boundary is small anyway, unless the source is close by, in which case the boundary has probably to be moved further out. The same boundary condition may be kept for a subsequent inflow period provided its duration is substantially smaller than the outflow period. This type of boundary condition, which essentially assumes complete mixing in the neighborhood of the ocean boundary, was tried in earlier applications of the one-layer model to Massachusetts Bay (65). The results are satisfactory provided the plume reaches the boundary in a segment of predominantly outward flow, which is usually the case. It must be noted that in the remaining segment of the ocean boundary, far from the plume, the concentration must be specified, normally at zero, to provide a reference value for the computations in the interior. In a multilayer model, obviously the boundary conditions have to be specified for each layer separately.

## CHAPTER 3

### THE DISPERSION PROCESS IN A LAYER

#### 3.1 Mechanisms of Dispersion

In this chapter the physical mechanisms causing horizontal spreading of a constituent within a given "layer", neglecting the interaction between the layers, will be examined. As evident from the convection-diffusion equations (Section 2.1), there are basically three processes responsible for the dispersion of a substance in the context of a horizontally two-dimensional flow field:

- a) Advection, most importantly temporal or spatial variations of the layer-averaged velocities; mathematically represented by the advection terms in the equations.
- b) Turbulent diffusion, that is, mixing due to small scale turbulent velocity fluctuations; quantified by the turbulent (or eddy) diffusivity, based on the widely used analogy between turbulent mixing and molecular diffusion. This hypothesis has proved very convenient for studying diffusion problems, although it is not necessarily correct, especially for transient problems (14,51).
- c) Dispersion due to vertical shear, that is, velocity nonuniformities over the layer thickness. These variations create an additional effective horizontal spreading in the 2-D concentration field. Their contribution is represented by the shear dispersion coefficient, the concept of which is based again on the assumption of analogy between shear dispersion and turbulent diffusion. The validity of this assumption will be discussed in Section 3.3.

From the above it can be seen that the differentiation between mechanisms and the introduction of diffusion and dispersion coefficients is basically due to the simplified representation of the velocity field. In a three dimensional description the shear effect would be incorporated in the first mechanism. With respect to the relative importance of processes (a) and (b), normally the term advection is associated with the large scale circulation, while diffusion refers to smaller scale turbulent mixing. However, the separation point is not always clear and generally depends on the level of detail in which the advection process can be modeled. In fact, if only an overall "mean" velocity is known over the whole area of interest, even large size eddies that would otherwise be considered as part of the circulation field have to be included somehow in the diffusion terms. It is clear that in that case the magnitude of the diffusion coefficient should increase, while at the same time the uncertainty in its estimate would also increase. These parallel effects are always present when the velocity field is simplified since a larger number of contributions to mixing are lumped into a single "diffusion" coefficient. Therefore, the need for a reasonably detailed description of the flow field is obvious, since the turbulent diffusivity concept is an approximation to the mixing phenomenon to begin with. On the other extreme, if the velocity field is known in great detail, the scale of mixing represented by the turbulent diffusivity is reduced and the contribution of the corresponding term in the equation diminishes.

Let us consider the description of the diffusion of a cloud after

an instantaneous injection in a two dimensional domain. At the beginning, moderate size eddies contribute to the advection of the cloud as a whole, while mixing takes place in very small scales. As the size of the cloud increases over time, larger and larger eddies become involved in the internal mixing of the cloud, while its center moves under an even larger scale circulation. Consequently, the effective diffusion coefficient increases with time (or size). This behavior has been studied in the past (56, 16) and relations between diffusion coefficient and either cloud size or diffusion time have been proposed. However, when the flow field is specified, e.g. by a hydrodynamic model, at a certain spatial discretization, such continuous growth of the diffusion coefficient is not justified any more. Once the cloud size increases beyond the level of discretization of the finite difference or finite element grid, eddies of the scale of the grid size that now contribute to the internal mixing of the cloud are still described by the advection terms in the equation. Therefore the diffusion coefficient should only represent mixing up to the length scale of the spatial discretization of the mathematical model.

The dispersion process in a two-dimensional flow field is undoubtedly extremely complex to handle, because of the incomplete understanding of the several mechanisms involved and the difficulties in their mathematical description. An authority on the subject, A. Okubo, states in concluding a chapter on horizontal and vertical mixing in the sea (56): "Diffusion is Confusion. Nobody but Maxwell's demon really knows what's going on"! Without attempting here an exhaustive

investigation of the phenomenon, some important aspects are examined in the subsequent sections with the particular goal of giving rational quantitative expressions for mechanisms (b) and (c) (described above), useful in mathematical modeling applications.

### 3.2 The Horizontal Eddy Diffusion Coefficient

The introduction of the eddy diffusivity concept is based on the convenient assumption that the small scale mixing due to turbulent velocity fluctuations is analogous, although much more intensive, to molecular diffusion. In the application of this concept to models of diffusion processes in large water bodies, the coefficient is commonly used to incorporate any large scale mixing not accounted for explicitly by the advective terms, as discussed in Section 3.1. For estimating the value of this coefficient for a particular problem, of primary importance are the intensity of the turbulence as measured by either the r.m.s. velocity fluctuations or the supply or dissipation of turbulent energy, and the length scale over which the mixing takes place.

From the theory of locally isotropic turbulence the well-known 4/3-law is derived. This is based on the condition that the eddies responsible for mixing belong to the inertial subrange of turbulence, that is, the range where the energy influx from larger size eddies is balanced by energy transfer and dissipation to smaller size eddies. As presented by Osmidov (62) the 4/3-law is written :

$$\epsilon = c e^{1/3} L^{4/3} \quad (3.1)$$

where

$\epsilon$  = the eddy diffusivity

$e$  = the rate of energy dissipation

$L$  = the length scale

$c$  = a dimensionless constant, or order 0.1 (61).

Alternatively, for diffusion on the sea surface under relatively calm conditions,  $\epsilon$  has been simply expressed as (61):

$$\epsilon = k L^{4/3} \quad (3.2)$$

where  $k$  is of the order of 0.01 in CGS units (varying from 0.005 to 0.016). Nevertheless, the value of  $c$  or  $k$  cannot be discussed independently of the value of the length scale used in the above formulas.

Certainly, the structure of oceanic turbulence is not necessarily isotropic. It is argued, however, that eddy sizes much different than the areas of direct energy influx are essentially isotropic in the horizontal directions (62). Of course, this isotropy is not extended to the vertical direction due to the limitation of the bottom or strong density stratification. Consequently, the vertical diffusion coefficient should be much smaller than the horizontal coefficient since it is associated with a smaller length scale. Moreover, in the areas of significant energy influx the corresponding eddies will not follow the laws of the inertial subrange, that is, the 4/3 law will not hold and a plateau in the value of horizontal diffusivity should be reached.

Qualitative agreement of these considerations with measurements is presented in (58) and shown in Figure 3.1. The length scale was defined as  $\ell = 3\sigma$ , where  $\sigma^2$  is the radial variance of the horizontal distribution of the patch. The eddy diffusivity was determined from

$$\epsilon = \frac{\sigma^2}{4t} \quad (3.3)$$

which is apparently based on a circular idealization of the patch and the assumption of two-dimensional Gaussian distribution.

According to Figure 3.1 :

$$\begin{aligned} \epsilon &\approx 2 \times 10^{-3} \ell^{4/3} & ; & \quad \ell < 10^5 \\ \epsilon &\approx 10^4 & ; & \quad 10^5 < \ell < 5 \cdot 10^5 \\ \epsilon &\approx 10^{-3} \ell^{4/3} & ; & \quad \ell > 5 \cdot 10^5 \end{aligned} \quad (3.4)$$

where  $\epsilon$  in  $\text{cm}^2/\text{sec}$  and  $\ell$  in cm.

It is seen that the constant of the 4/3 law decreases at larger length scales.

A very good collection of diffusion data in the ocean was presented by Okubo (55), who proposed as best fit to all the data the relation

$$\epsilon = 0.01 \ell^{1.15} \quad ; \quad 10^3 < \ell < 10^8 \text{ cm} \quad (3.5)$$

where  $\epsilon$  and  $\ell$  as defined above.

While (3.5) is useful as a first estimate of  $\epsilon$  under any conditions, it is not based on any theoretical arguments. Most



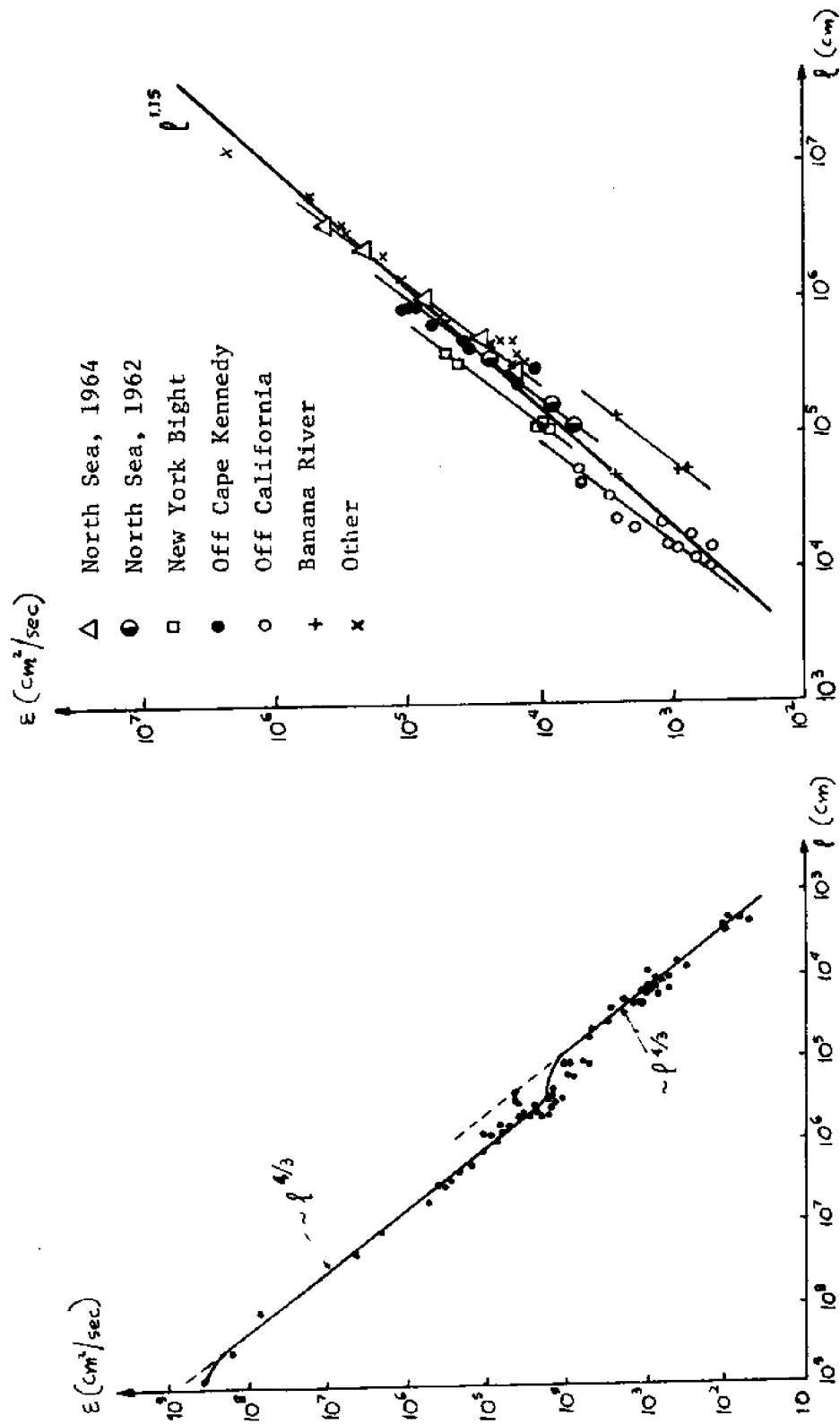


Figure 3.1 Dependence of the Horizontal Diffusion Coefficient on the Scale of the Phenomenon (58)

Figure 3.2 Okubo's Diffusion Data (55) and 4/3 Power Lines

importantly, the individual sets of data (which necessarily extend over smaller ranges of  $\ell$ ) seem to follow quite closely the 4/3-law, but with different constants of proportionality. These 4/3-power lines are drawn (by eye) in Figure 3.2 along with Equation (3.5) given by Okubo. It appears that the slower growth of  $\varepsilon$  with  $\ell$  indicated by (3.5) does not prove that the 4/3 law is not valid, but may be simply due to general shifts in the 4/3 dependence (as seen from Figure 3.1) and also to some differences of energy intensities between the individual areas where the measurements were taken from. The constants of the 4/3-power fits are of the order of  $10^{-3}$  CGS units, as shown in Table 3.1.

Table 3.1

Constants  $k$  of 4/3 - power law fitted  
to individual sets of data of Figure 3.2

Location	$k(\text{CGS units})$
North Sea (1964)	$0.7 \times 10^{-3}$
North Sea (1962 II)	$1.0 \times 10^{-3}$
Cape Kennedy	$1.0 \times 10^{-3}$
N. York Bight	$1.6 \times 10^{-3}$
Off California	$2.2 \times 10^{-3}$
Banana River	$0.4 \times 10^{-3}$

These values are consistent with (3.4) but both appear an order of magnitude too low if compared to the average value of  $k$  in Equation (3.2). This apparent contradiction is, however, caused by different definitions of the length scale used in the formulas. Indeed,  $L$  in (3.2) is defined as the typical distance between diffusing particles and the diffusion coefficient was measured as

$$\epsilon = \frac{1}{2} \frac{\overline{\Delta L^2}}{\Delta t} \quad (3.6)$$

Then,  $L = \sqrt{2} \sigma$  and consequently  $\ell = 3L/\sqrt{2}$ . By also comparing the forms of (3.3) and (3.6) it is seen that there must be an overall factor of  $4(\frac{3}{\sqrt{2}})^{4/3} = 10.9$  between the constants in Equation (3.2) and Table 3.1. The order of magnitude discrepancy is thus explained.

Earlier data reported by Orlob (59) also agree quantitatively with (3.2). Thus, the 4/3 law seems theoretically and experimentally acceptable for expressing the horizontal eddy diffusivity in the sea, provided the length scales of interest are not of the order of the size of the energy containing eddies. In addition, the 4/3 law is not fully acceptable near the shore (92), due to the shoreline and bottom interference and the presence of a strong wave energy band - the waves being neglected in deeper water throughout the present work.

A more general way of expressing the eddy diffusivity is in the form (16, 5):

$$\epsilon = \tilde{U} L \quad (3.7)$$

where  $\tilde{U}$  = the r.m.s. turbulent velocity fluctuation  
and  $L$  = the (horizontal) length scale of turbulence

Arguing that temporal and spatial variability are analogous, it is seen that in isotropic turbulence Equation (3.7) is equivalent to the 4/3 law, since  $\tilde{U} \propto \Delta U \propto (\epsilon L)^{1/3}$ . Therefore, the length scales of (3.7) and (3.1) or (3.2) are equivalent within a dimensionless constant. An expression of the eddy diffusivity in the form (3.7) or (3.1) instead of single length dependence as in (3.2) or (3.5) presents the advantage of incorporating specific knowledge of the turbulence intensity in the area under consideration and can be more useful when the effect of varying mixing intensity caused by changes in meteorological conditions over time has to be taken into account. Of course, the simpler formulas can be used as good approximations in less ambitious modeling efforts. In any case, the appropriate length scale to be used in a finite difference or finite element model needs to be examined.

The concept of the length scale of turbulence is not precisely defined and is commonly quantified indirectly through measurement of other turbulent quantities. Various investigations carried out mainly in boundary layer flows and summarized in (83) show that, far from the wall, the length scale tends to an asymptotic value of 0.08 to 0.10 of the pipe radius or the channel depth; this is an order of magnitude smaller than the size of the largest eddy that

could conceivable be formed in the flow. Similar conclusions have been reached in free turbulent flows (39).

Extending the above to coastal waters, where the flow field is prescribed (known) at certain grid points, it may be argued that the internal horizontal mixing within the grid "cells" can again be represented by using a length scale an order of magnitude smaller than the typical grid size. In fact, some investigations have been carried out with respect to the so-called "sub-grid scale" eddy coefficient applicable to high-speed numerical computations of turbulent flows. This is introduced into the various schemes to account for the turbulent exchange due to eddies smaller than the characteristic grid size and thus not explicitly representable in the computations. The length scale used for the evaluation of such sub-grid scale eddy viscosity coefficient is generally given as

$$L = c\Delta \quad (3.8)$$

where  $\Delta$  is the finite difference grid interval and  $c$  is a numerical constant, with a value ranging from 0.20 for isotropic turbulence to 0.10 in shear flows (17). However, the resolution capabilities associated with large-scale averaging of the hydrodynamic model being used have to be taken into account. For example, it has been found (84) that it is not possible to reproduce horizontal eddies of diameter less than five times the grid size. In this case, a factor of 5 should be incorporated in Equation (3.8).

With respect to the dependence of the eddy coefficient on the

velocity fluctuations, an order of magnitude estimate can be obtained by using such values as 10% of the local velocity. Alternatively, employing the mixing length hypothesis (39):

$$\tilde{U} \propto \frac{\Delta U}{\Delta L} L$$

where  $\frac{\Delta U}{\Delta L}$  = the velocity gradient over the distance L.

In a two-dimensional flow field  $\frac{\Delta U}{\Delta L}$  is expressible in terms of derivatives in both x and y directions and finally Equation (3.7) becomes equivalent to (24):

$$\epsilon = L^2 \sqrt{\phi} \quad (3.9)$$

$$\text{where } \phi = 2 \left( \frac{\partial \bar{u}}{\partial x} \right)^2 + 2 \left( \frac{\partial \bar{v}}{\partial y} \right)^2 + \left( \frac{\partial \bar{u}}{\partial y} + \frac{\partial \bar{v}}{\partial x} \right)^2$$

This form has been used for modeling the eddy diffusivity (17,4) although in the latter reference the length scale was associated with the flow depth and not with the horizontal grid size.

As discussed in (39), a better way of expressing  $\tilde{U}$ , especially in areas with small mean velocity gradients is

$$\tilde{U} \propto \sqrt{e}$$

where e the turbulent kinetic energy. However, additional equations would be needed for the transport and distribution of e, and this is beyond the scope of the present work.

Equation (3.9) permits a straightforward calculation of the turbulent diffusion coefficient in terms of the grid size and the

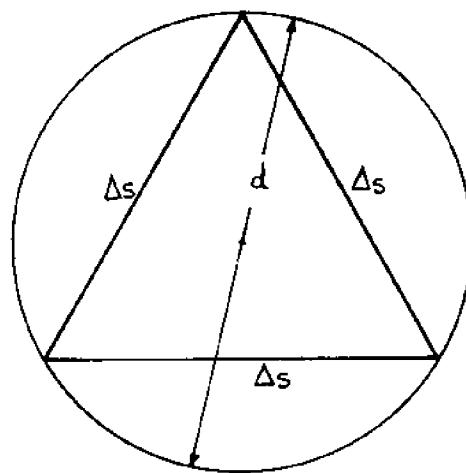
(supposedly known) values of the mean velocities at the grid points. It is particularly convenient with respect to a finite element grid with linear expansions because the velocity gradients are then constant over each element (see Chapter 7). The value of  $L$  can be approximately given, based on the equilateral triangle case (Figure 3.3):

$$L_{\min} \approx \frac{1}{10} d = \frac{1}{10} \frac{2}{\sqrt{3}} \Delta s = 0.12 \Delta s \quad (3.10a)$$

Alternatively, using the fact that  $A = \frac{\sqrt{3}}{4} \Delta s^2$ , one obtains:

$$L_{\min} \approx 0.17 \sqrt{A} \quad (3.10b)$$

Before closing this section, a graphic comparison of the various expressions is worthwhile. In Figure 3.5 formulas (3.2) (with  $k = 0.01$ ), (3.6) (multiplied by 10.9, as discussed earlier) and (3.7) are compared in the range of 0.2 to 5 km, which are common length scales in numerical modeling of coastal waters. In Equation (3.7) the value of  $\bar{U}$  is set equal to 10%  $\bar{U}$ , where  $\bar{U} = 5$  cm/sec, a typical current velocity under calm conditions, which pertain to most of the measurements used to support the other two formulas.



$$d = \frac{2}{\sqrt{3}} \Delta s$$

$$A = \frac{\sqrt{3}}{4} \Delta s^2$$

$$L_{\text{min}} \approx d/10$$

Figure 3.3 Length Scale for Sub-grid Scale Eddy Diffusivity

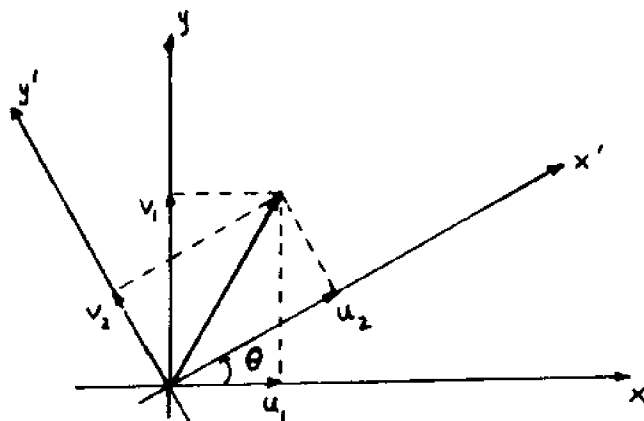


Figure 3.4 Velocity Components in Two Coordinate Systems



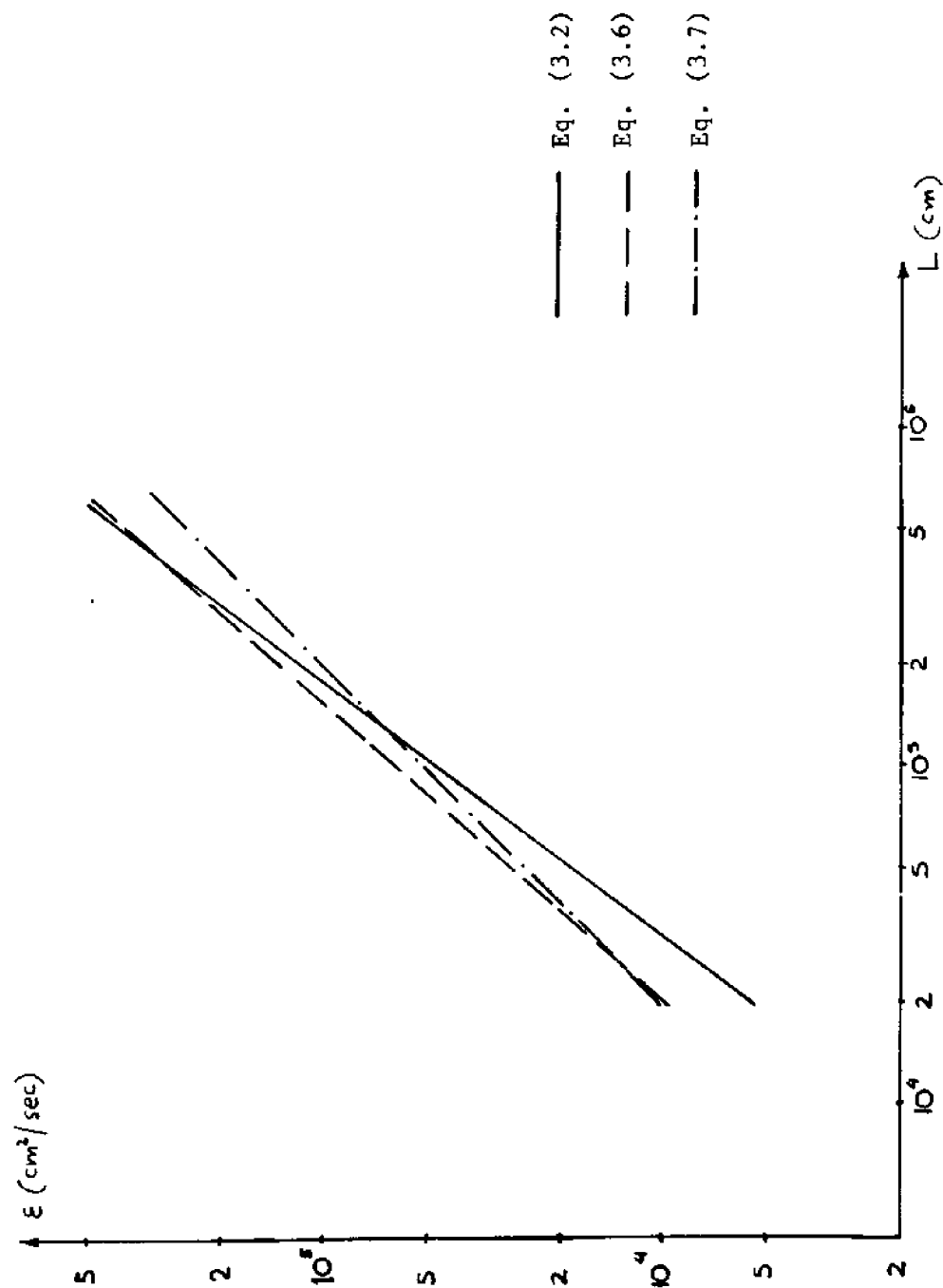


Figure 3.5 Comparison of Expressions for the Horizontal Eddy Diffusivity

### 3.3 The Shear Dispersion Coefficients

These coefficients are used to quantify the effective horizontal transport caused by velocity and concentration nonuniformities over a layer depth. For one-dimensional steady pipe flow the "diffusion analogy"

$$-\frac{1}{A} \int_A u''c'' dA = E_x^d \frac{\partial \bar{c}}{\partial x}$$

where A is the cross sectional area, was introduced by G.I. Taylor (76). Subsequently, the value of the shear dispersion coefficient has been theoretically determined for a uniform steady flow in a straight channel by Elder (18) and extensively investigated, theoretically and experimentally, in less ideal one-dimensional flows (21, 27, 30). An extension to two-dimensional flows has not, so far, been introduced. The validity and the limitations of such an extension will now be examined.

In the three-dimensional convection-diffusion equation, where the vertical velocity component has been neglected,

$$\frac{\partial c}{\partial t} + u \frac{\partial c}{\partial x} + v \frac{\partial c}{\partial y} = \frac{\partial}{\partial x} \left( \epsilon_x \frac{\partial c}{\partial x} \right) + \frac{\partial}{\partial y} \left( \epsilon_y \frac{\partial c}{\partial y} \right) + \frac{\partial}{\partial t} \left( \epsilon_z \frac{\partial c}{\partial z} \right)$$

set (as in Section 2.1)

$$u = \bar{u} + u''$$

$$v = \bar{v} + v''$$

$$c = \bar{c} + c''$$

and neglect the horizontal eddy diffusion terms. Paralleling Taylor's assumptions, consider the concentration fairly well distributed over the layer thickness, i.e.,  $c'' \ll \bar{c}$ , after sufficiently long time. Then, seek a solution satisfying

$$\frac{\partial c}{\partial t} + u \frac{\partial c}{\partial x} + v \frac{\partial c}{\partial y} = 0$$

which implies

$$u'' \frac{\partial c}{\partial x} + v'' \frac{\partial c}{\partial y} = \frac{\partial}{\partial z} (\epsilon_z \frac{\partial c''}{\partial z})$$

or, since  $c'' \ll \bar{c}$ :

$$u'' \frac{\partial \bar{c}}{\partial x} + v'' \frac{\partial \bar{c}}{\partial y} = \frac{\partial}{\partial z} (\epsilon_z \frac{\partial c''}{\partial z}) \quad (3.11)$$

This equation expresses the balance, at any point, between the inhomogeneous convective transfer of the admixture and the vertical diffusion associated with small variations in concentration over the depth (51). These variations can be viewed as adapting themselves to the flow field variability so that, after a sufficiently long time, the balance is achieved.

Integrating (3.11) over  $z$ :

$$\frac{\partial \bar{c}}{\partial x} \int_0^z u'' d\zeta + \frac{\partial \bar{c}}{\partial y} \int_0^z v'' d\zeta = \epsilon_z \frac{\partial c''}{\partial z}$$

Integrating again one obtains for  $c''$ :

$$c'' = \frac{\partial \bar{c}}{\partial x} \int_0^z \frac{d\zeta^*}{\epsilon_z} \int_0^{\zeta^*} u'' d\zeta + \frac{\partial \bar{c}}{\partial y} \int_0^z \frac{d\zeta^*}{\epsilon_z} \int_0^{\zeta^*} v'' d\zeta + \text{const.} \quad (3.12)$$

Substituting this expression for  $c''$  and noting that the constant of integration, when multiplied by  $u''$  or  $v''$  and integrated over  $H$ , will give no contribution, the integral

$$\int_0^H u'' c'' dz \text{ takes the form:}$$

$$\int_0^H u'' c'' dz = \frac{\partial \bar{c}}{\partial x} \int_0^H u'' dz \int_0^z \frac{d\zeta^*}{\epsilon_z} \int_0^{\zeta^*} u'' d\zeta + \frac{\partial \bar{c}}{\partial y} \int_0^H u'' dz \int_0^z \frac{d\zeta^*}{\epsilon_z} \int_0^{\zeta^*} v'' d\zeta$$

Employing partial integration, recalling that

$$\int_0^H u'' dz = \int_0^H v'' dz = 0$$

and multiplying both sides by  $-1$ , we obtain:

$$- \int_0^H u'' c'' dz = \frac{\partial \bar{c}}{\partial x} \int_0^H \frac{1}{\epsilon_z} \left( \int_0^z u'' d\zeta \right)^2 dz + \frac{\partial \bar{c}}{\partial y} \int_0^H \frac{1}{\epsilon_z} \left( \int_0^z u'' d\zeta \right) \left( \int_0^z v'' d\zeta \right) dz$$

(3.13a)

By similar manipulations:

$$-\int_0^H v''c''dz = \frac{\partial \bar{c}}{\partial x} \int_0^H \frac{1}{\epsilon_z} \left( \int_0^z u''d\zeta \right) \left( \int_0^z v''d\zeta \right) dz + \frac{\partial \bar{c}}{\partial y} \int_0^H \frac{1}{\epsilon_z} \left( \int_0^z v''d\zeta \right)^2 dz \quad (3.13b)$$

It is seen that the integrated transport due to the spatial deviations of velocity and concentration from their depth-averaged values have been expressed in terms of the horizontal gradients of the average concentrations. Thus, the representation of this transport by Equations (2.13a,b) is justified. In particular, the shear dispersion coefficients are now identified as:

$$E_{xx}^d = \frac{1}{H} \int_0^H \frac{1}{\epsilon_z} \left( \int_0^z u''d\zeta \right)^2 dz \quad (3.14a)$$

$$E_{yy}^d = \frac{1}{H} \int_0^H \frac{1}{\epsilon_z} \left( \int_0^z v''d\zeta \right)^2 dz \quad (3.14b)$$

$$E_{xy}^d = E_{yx}^d = \frac{1}{H} \int_0^H \frac{1}{\epsilon_z} \left( \int_0^z u''d\zeta \right) \left( \int_0^z v''d\zeta \right) dz \quad (3.14c)$$

These expressions represent an extension of Elder's (18) one-dimensional formula (similar to 3.14a) to a two-dimensional flow field. Because velocity variations in two directions are now explicitly considered, it is believed that Equations (3.14) will be valid under less restrictive conditions than its one-dimensional counterpart. Certainly, the derivation was made under certain simplifying assumptions and

the resulting expressions cannot always be adequate. The velocity field as well as the velocity profiles, represented by  $u''$  and  $v''$  may in reality vary over both space and time. Inherent in the derivation is, however, the condition that this variation is not too severe. As already pointed out, Taylor's approximate treatment of the dispersion process is valid only a sufficiently long time after the material has been introduced into the flow, ensuring a more or less uniform distribution over the depth. Fischer (21) has found that the "initial time",  $T_I$ , is about half the time scale for cross sectional mixing,  $T_c$ . For vertical mixing (5), this is given by

$$T_c = \frac{H^2}{\pi^2 \epsilon_z} \quad (3.15)$$

For values of  $H \sim 20\text{m}$  and  $\epsilon_z \sim 50 \text{ cm}^2/\text{sec}$  it is found that  $T_I$  is of the order of 1 hour. Consequently, Equations (3.14) may be considered approximately valid provided there are no significant velocity changes within this period.

Of particular interest is the effect of a tidal flow component on the dispersion coefficients. Previous investigations on the subject for one-dimensional flow (57,30,12) have revealed that of primary importance is the ratio of the tidal period to the mixing time scale  $T_c$ . It was found (30) that for

$$T/T_c \gtrsim 1 \quad (3.16)$$

the dispersion coefficient is essentially the same as if the flow is steady at any point in the tidal cycle. As a consequence, and since

the dispersion coefficient involves the square of the velocity, its average value over the tidal cycle is half the value it would have for a steady current equal to the maximum tidal current (57). Condition (3.16) seems to be normally satisfied in coastal waters.

The importance of the vertical diffusion coefficient  $\epsilon_z$  for the horizontal dispersion process cannot be underestimated. Equations (3.14) show that a decreased vertical diffusivity leads to a direct increase in the shear dispersion coefficients. However, the dispersion approximation itself could at the same time be questionable, since the vertical mixing time may become unacceptably high.

The arguments so far have been developed for the case of a neutrally buoyant constituent. The treatment can be modified to handle settling particles as done by Elder (18) in the one-dimensional case. The shear dispersion coefficient will in that case depend not only on the flow characteristics but also on the settling velocity. However, unless a settling velocity term is included in Equation (3.11) such an extension will be restricted to very fine particles, the vertical transfer of which is dominated by the vertical eddy diffusivity rather than the settling velocity, i.e.

$$\frac{w_s H}{\epsilon_z} \ll 1 \quad (3.17)$$

Further analytical expressions for the shear dispersion coefficients in the case of falling particles can be found in (74).

It will now be shown that the shear dispersion coefficients given by Equations (3.14 a,b,c) define a second order (symmetrical) tensor:

$$\tilde{E}^d = \begin{bmatrix} E_{xx}^d & E_{xy}^d \\ E_{xy}^d & E_{yy}^d \end{bmatrix} \quad (3.18)$$

It suffices to prove that the expressions of  $\tilde{E}^d$  in two different coordinate systems are related by tensor multiplication. In the system (x,y) let the velocity components be  $(u_1, v_1)$  and in  $(x', y')$  be  $(u_2, v_2)$ , as shown in Figure 3.4.

Then:

$$\begin{bmatrix} u_2 \\ v_2 \end{bmatrix} = \tilde{T} \begin{bmatrix} u_1 \\ v_1 \end{bmatrix} \quad (3.19a)$$

where

$$\tilde{T} = \begin{bmatrix} \cos\theta & \sin\theta \\ -\sin\theta & \cos\theta \end{bmatrix}$$

is the coordinate transformation rotation matrix.

Since the rotation  $\theta$  is constant with  $z$ , the layer-average velocities are

$$\begin{bmatrix} \bar{u}_2 \\ \bar{v}_2 \end{bmatrix} = \tilde{T} \begin{bmatrix} \bar{u}_1 \\ \bar{v}_1 \end{bmatrix} \quad (3.19b)$$



and consequently, by subtracting (3.19a) and (3.19b):

$$\begin{bmatrix} u_2'' \\ v_2'' \end{bmatrix} = \underset{\sim}{T} \begin{bmatrix} u_1'' \\ v_1'' \end{bmatrix} \quad (3.19c)$$

Therefore,

$$\begin{aligned} E_{xx}^{(2)} &= \frac{1}{H} \int_0^H \frac{1}{\epsilon_z} \left( \int_0^z u_2'' d\zeta \right)^2 dz = \frac{1}{H} \int_0^H \frac{1}{\epsilon_z} \left[ \int_0^z (u_1'' \cos\theta + v_1'' \sin\theta) d\zeta \right]^2 dz \\ &= \cos^2\theta E_{xx}^{(1)} + \sin^2\theta E_{yy}^{(1)} + 2\cos\theta \sin\theta E_{xy}^{(1)} \end{aligned} \quad (3.20a)$$

where the superscripts (1) and (2) denote the coordinate systems (x,y) and (x',y') respectively.

Similarly,

$$E_{yy}^{(2)} = \sin^2\theta E_{xx}^{(1)} + \cos^2\theta E_{yy}^{(1)} - 2\cos\theta \sin\theta E_{xy}^{(1)} \quad (3.20b)$$

and

$$E_{xy}^{(2)} = -\cos\theta \sin\theta E_{xx}^{(1)} + \cos\theta \sin\theta E_{yy}^{(1)} + (\cos^2\theta - \sin^2\theta) E_{xy}^{(1)} \quad (3.20c)$$

In compact form, Equations (3.20 a,b,c) can be written as

$$\underset{\sim}{E}^{(2)} = \underset{\sim}{T} \underset{\sim}{E}^{(1)} \underset{\sim}{T}^{-1} \quad (3.21)$$

and this proves that indeed  $\underset{\sim}{E}^d$  is a second order tensor.

The transformation relation (3.21) permits the evaluation of the shear dispersion coefficients for any coordinate system, provided the velocity profiles along any two (arbitrary) perpendicular directions are known. Such knowledge may be available either through measurements or from experience with the general characteristics of coastal currents, particularly in the area of interest (9). In general the velocity vector at any level will not necessarily be parallel to the layer-average velocity vector. In other words the velocity profiles in the x and y directions may have different shapes. Unless very detailed supporting information is available, accepting different profiles in x and y (as was done, for example, in (36)) implies that the results will be dependent on the coordinate system chosen. Thus, when one has only a vague idea about the velocity distribution over the vertical, the establishment of a relation between the dispersion coefficients and the flow characteristics should be based on an assumption of some kind of self-similarity of the velocity profile in the layer; that is, on the assumption that the profile shape remains the same irrespective of direction. This shape need not be constant but it may change over space and time. It can be more uniform when the flow is dominated by the tide and less uniform when the wind exerts a strong influence. In any case, once this assumption is acceptable, it can be readily seen from Equations (5.14 a,b,c) that the shear dispersion coefficients are expressible in the form

$$E_{xx}^d = \lambda \frac{\bar{u}^2 H^2}{\epsilon_z} \quad (3.22a)$$

$$E_{yy}^d = \lambda \frac{\bar{v}^2 H^2}{\epsilon_z} \quad (3.22b)$$

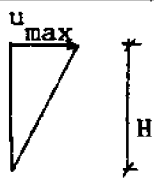
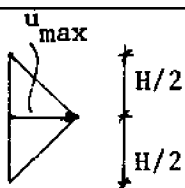
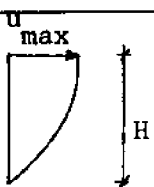
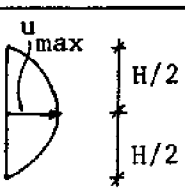
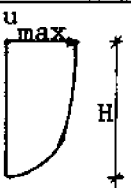
$$E_{xy}^d = \lambda \frac{\bar{u}\bar{v}H^2}{\epsilon_z} \quad (3.22c)$$

with the same constant of proportionality  $\lambda$ . The values of  $\lambda$  for some simple profiles are listed in Table 3.2. It is assumed that  $\epsilon_z$  is constant over the layer thickness and also that there are no flow reversals in the velocity profile, being unlikely because of the definition of the "layer" with the natural boundary of the thermocline. Such reversals, of course, can be easily handled in the general formulas (3.14) but the outcome will have to be expressed through some other velocity scale rather than the mean.

The principal axes of the dispersion coefficient tensor can be found from Equation (3.20c), by requiring that  $E_{xy}^{(2)} = 0$  and solving for the angle  $\theta$ . In the simple case that Equations (3.22) are used it is easily seen that  $E_{xy}^d = 0$  when either  $\bar{u}$  or  $\bar{v}$  vanish, implying that the principal axes coincide with the direction of the mean flow and the normal to it. It is, furthermore, evident that, if  $\bar{v} = 0$ , the lateral dispersion coefficient  $E_{yy}^d$  also vanishes. Thus, the lateral spreading of the constituent is left to the horizontal eddy diffusivity alone. These conclusions agree with the generally observed higher "overall" diffusion coefficients along the flow direction in several experiments in the ocean (56).

Table 3.2

Constants  $\lambda$  in Shear Dispersion Coefficient Expressions (Eqs. 3.22)

Profile		$\lambda$
Linear $\bar{u} = \frac{1}{2} u_{\max}$		$\frac{1}{30}$
Bi-linear $\bar{u} = \frac{1}{2} u_{\max}$		$\frac{1}{120}$
Parabolic $\bar{u} = \frac{2}{3} u_{\max}$		$\frac{2}{105}$
Bi-Parabolic $\bar{u} = \frac{2}{3} u_{\max}$		$\frac{1}{210}$
Logarithmic $\bar{u} = u_{\max} - \frac{u_*}{k}$		$\frac{1}{600}^*$

\*Note: for  $k = 0.4$  and  $u_* = 0.06 \bar{u}$ .

### 3.4 The Vertical Diffusion Coefficient

As for the horizontal exchange, the concepts of vertical eddy viscosity and diffusivity have long been used to describe the turbulent exchange in the vertical direction of momentum and mass, respectively. The two coefficients are considered approximately equal in well-mixed regions. In this section the relation of the vertical exchange coefficient within each layer, which plays an important role in the horizontal dispersion rate (as seen in the previous Section) to the mean flow parameters is examined.

In a given layer there is ideally no density gradient, although in reality there may be a small one. Under such homogeneous conditions, the vertical turbulent diffusivity (viscosity) is usually related to the velocity profile. Prandtl introduced the concept of mixing length, as representative of the exchange distance of vertical eddies and expressed the vertical eddy viscosity as:

$$\epsilon_z \sim \ell^2 \left| \frac{\partial \bar{u}}{\partial z} \right|$$

where  $\frac{\partial \bar{u}}{\partial z}$  is the local velocity gradient. This indicates a larger coefficient in regions of high shear, however it is not applicable when  $\frac{\partial \bar{u}}{\partial z} = 0$ . The determination of the mixing length is a source of difficulty in this kind of approach. It is generally related to the dimensionless distance from the wall, for wall-generated turbulence. The functional form of the mixing length would yield the form of the vertical eddy viscosity and this in turn is related to the velocity

profile also. A review of various eddy viscosity profiles, associated with different velocity distributions, along with experimental measurements is included in (83). For the logarithmic velocity profile, commonly used in open channels, the vertical eddy viscosity distribution is parabolic:

$$\epsilon_z = k u_* H \eta (1 - \eta) \quad (3.23)$$

where  $k = 0.4$ , is the Von-Karman constant

$u_*$  is the shear velocity at the wall

and  $\eta$  is the dimensionless distance from the wall

For the region far from the wall a constant value was proposed, based on experiments by Reichardt:

$$\epsilon_z = 0.067 u_* H \quad (3.24)$$

This is precisely equal to the average value of the parabolic distribution of Equation (3.23), and may be considered a good typical value to be used in the absence of any other information.

If the profile is actually logarithmic,  $u_* \approx 0.06 \bar{U}$  (depending on the friction coefficient), therefore Equation (3.24) can be rewritten in terms of the mean flow velocity

$$\epsilon_z \approx 4.10^{-3} \bar{U} H \quad (3.25)$$

Considering a layer in the sea, as defined in this work, the conclusions derived from open channel hydraulics are relevant to some extent. Near the interface the value of  $\epsilon_z$  does not go to zero but still to a rather small value, under stable stratification (Chapter 4). Near the surface, wind and wave effects cause an increase in vertical exchange intensity and raise the value of  $\epsilon_z$ . It appears that the distribution of  $\epsilon_z$  in such a layer would be more uniform than a parabolic profile. Of course, the actual velocity profile may not be logarithmic, either. The use of a constant value for  $\epsilon_z$  in the layer is consistent with the mathematical idealization of the system. The two-layer (or n-layer) discretization implies that variability of the parameters over a layer thickness is not handled explicitly because either it is really unimportant or is neglected for simplification.

For a layer of 10m thickness and a mean velocity of 0.10 m/sec, Equation (3.25) yields for the vertical eddy diffusivity  $\epsilon_z \approx 4 \cdot 10^{-3} \text{ m}^2/\text{sec} = 40 \text{ cm}^2/\text{sec}$ . This is well within the range of field data in the sea. Kullenberg (37) has carried out extensive measurements of vertical diffusion in shallow waters. For a layer of 14m depth, with almost non-existing stratification  $\left(\frac{1}{\rho} \frac{\partial \rho}{\partial z} = 2.2 \times 10^{-6} \text{ m}^{-1}\right)$ , i.e., total density difference over the depth 0.03 ‰ he found a mean  $\epsilon_z \approx 60 \text{ cm}^2/\text{sec}$ , ranging between 50 and 110  $\text{cm}^2/\text{sec}$ . These values are consistent with (3.25) provided the mean velocity was about 0.10 - 0.20 m/sec. Indeed, the observed current shear was  $4.1 \times 10^{-2} \text{ sec}^{-1}$ ; for a linear velocity profile,

the velocity at 10m depth (where the dye was injected) would then be approximately 0.16 m/sec. A summary of measurements in deeper waters is presented in (36). In surface layers of up to 200m thickness, values of  $\epsilon_z$  up to  $100 \text{ cm}^2/\text{sec}$  have been reported. Much smaller values have also been reported, apparently due to significant stratification over such large layer thicknesses. Values around  $100 \text{ cm}^2/\text{sec}$  were found for  $\frac{1}{\rho} \frac{\partial \rho}{\partial z} \sim 10^{-6} \text{ m}^{-1}$ , i.e., a density difference of  $0.01^0/\text{oo}$  over 10m, negligible when compared to the density discontinuities considered in the present two-layer discretization. Further, the value  $100 \text{ cm}^2/\text{sec}$  is proposed as typical for a well-mixed upper layer of 200 ft ( $\approx 60$  meters) thickness. This is consistent with (3.25) provided the mean velocity in the layer is about 0.04 m/sec (velocity magnitudes were not given).

An alternative way of expressing the vertical eddy diffusivity is in terms of representative vertical eddy characteristics, as was done for the horizontal exchange. Thus, one may write (16):

$$\epsilon_z = \tilde{w} L_z \quad (3.26)$$

where  $\tilde{w}$  is the r.m.s. vertical velocity fluctuation and  $L_z$  is the vertical length scale. As has already been indicated in Section 3.2,  $L_z$  is of the order of 0.08 to 0.10 of the layer depth. The vertical velocity fluctuations are generally smaller than the horizontal ones; according to (91),  $\tilde{w}/\tilde{u} \approx 0.5$ . Applying for  $\tilde{u}$  the value of one tenth of the mean velocity, commonly used for shear flows, one finally obtains from (3.26):



$$\epsilon_z \approx 0.05 \bar{U} \times 0.08 H = 4.10^{-3} \bar{U} H$$

in agreement with (3.25).

In conclusion, it appears that Equation (3.25) gives a reasonable approximation to the vertical eddy diffusivity. When this expression is substituted in Equations (3.22), the dispersion coefficients are only related to the mean velocities and the layer thickness, which are the simplest flow characteristics in a layered system. Of course, in (3.25) the magnitude of the velocity vector should be used for  $\bar{U}$ . In this formula the effect of wind is only implicitly taken into account, i.e., through its contribution to the layer velocity. A discussion of vertical exchange caused primarily by the wind can be found in (85). Finally, waves may significantly affect the vertical diffusion near the sea surface. Measurements for low to moderate sea states have resulted in the empirical formula (36)  $\epsilon_{z,s} = 0.02 H_w^2 / T_w$  for the value of  $\epsilon_z$  at the surface, where  $H_w$  is the wave height and  $T_w$  the wave period. Thus, a 3 foot wave would imply  $\epsilon_{z,s} = 50-90 \text{ cm}^2/\text{sec}$ . This is of the same order of magnitude as the average values of  $\epsilon_z$  for the top layer discussed earlier. Therefore, moderate waves may be considered as a factor justifying a uniform distribution of the diffusion coefficient over the top layer thickness.

## CHAPTER 4

### INTERFACIAL TRANSPORT

#### 4.1 Description of the Phenomenon

The transport of material through the interface separating two layers constitutes in the model the only link between them. If such transport is absent, any quantity introduced into a layer will be simply dispersed within the layer, under the appropriate circulation pattern. When the interface is identified with a strong density gradient (eg. the thermocline in oceans or lakes, or an atmospheric inversion in the atmosphere), it has been common practice in the past to neglect any transport through it, on the grounds that it is very small. An additional reason has probably been the difficulty of quantifying this transport. Even though a density gradient does, indeed, have an adverse effect on the quantity of the material being transferred between adjacent layers, this quantity may not always be negligibly small, and its contribution may be significant over the large length scales characteristic of coastal areas. In the case where the constituent has some vertical mobility, e.g. settling velocity, neglecting the interfacial transport is clearly unacceptable.

Focusing on the two-layer system, which has been formulated in detail in Chapter 2, we may recall that the rate of transport of a constituent through the interface is expressed as:

$$Q_{21} = (w_e - w_s) \frac{c_1 + c_2}{2} + \alpha(c_2 - c_1) \quad (4.1)$$

where  $Q_{21}$  is considered positive when the overall transfer is from layer 2 (bottom) to layer 1 (top). The "settling velocity"  $w_s$  is a characteristic of the constituent under consideration and will be supposedly known. For example, for fine non-flocculating suspended sediments it may be determined from Stoke's law. In this chapter the physical meaning of  $w_e$  and  $\alpha$  is discussed and a quantification of them is attempted.

Neglecting settling, the interfacial transport of a neutrally buoyant constituent is written as:

$$Q_{21} = w_e \frac{c_1 + c_2}{2} + \alpha(c_2 - c_1) \quad (4.2)$$

As already indicated in Section 2.1, the first term of Equation (4.2) expresses the transport associated with the relative vertical motion of the interface and the neighboring water particles, while the second term represents diffusive flux through the interface, associated with the concentration difference between the layers. Thus, the former involves a net water flow across the interface, while the latter does not.

It is well known that a turbulent layer flowing in relatively quiescent ambient water causes "erosion" or "entrainment" of the adjacent fluid, that is, a net mass flux from it. The term entrainment is most familiar in jet theory, where the "entrainment velocity", quantifying the intensity of this mass flux, is considered proportional to some characteristic jet velocity (33). In a lake or in the ocean

a strong wind stress producing a high flow velocity in the top layer causes entrainment of the lower layer and erosion (deepening) of the thermocline (67). In the case of a jet the entrainment process need not be associated with a density difference, since a jet is easily identified because of its high momentum relative to the ambient water. In large water bodies, however, the density "discontinuity" may actually define the layer, as is the case in the present work.

The mechanism of erosion of a density interface has been examined mostly experimentally (15,52,79) and mechanistically explained by Pedersen (66). The turbulence in one of the layers causes a system of irregular interfacial cusps. Turbulent eddies appear to scour the interface by detaching wisps or streamers from the crests of the disturbances and rapidly removing them from the vicinity of the interface and diffusing them within the turbulent layer. Thus, some of the non-turbulent fluid is being swept away from a cusp and becomes entrained into the turbulent layer. This mixing process occurs in bursts and, according to (15), a point at the interface may be subject to one such "event" about every 100 seconds. Evidently, this type of mixing is a one-way transport of water from the non-turbulent to the turbulent fluid. However, when both layers are turbulent, a two-way transport has to take place, the interface being eroded by eddies coming from both sides. According to Turner (79), the events causing removal of fluid from the interfacial cusps are rare enough, so that they can be considered statistically independent, as experimental

evidence also indicates.

Let us consider two turbulent layers, moving at arbitrary velocities (Figure 4.1). Denote by  $m_{21}$  and  $m_{12}$  the volume rates (per unit projected area) of transport of water through the interface from layer 2 to 1 and from 1 to 2, respectively. The net volume rate moving through the interface can then be expressed as their difference. This net rate has been identified as the "entrainment" velocity in Section 2.1, i.e.

$$w_e = m_{21} - m_{12} \quad (4.3)$$

Consider now a constituent having concentrations  $c_1$  and  $c_2$  in layers 1 and 2, respectively. Arguing that the wisps being removed from each layer and being incorporated into the other contain these concentrations, we may write for the net transport from layer 2 to layer 1 the following expression:

$$Q_{21} = m_{21}c_2 - m_{12}c_1 \quad (4.4)$$

This can be easily rewritten as:

$$Q_{21} = (m_{21} - m_{12}) \frac{c_1 + c_2}{2} + \frac{m_{21} + m_{12}}{2} (c_2 - c_1) \quad (4.5)$$

By comparing Equations (4.5) and (4.2) and using Equation (4.3) it is seen that

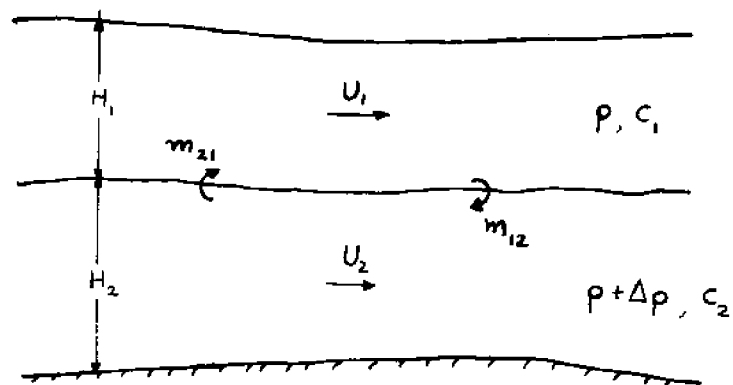


Figure 4.1 Schematization of Interfacial Transport

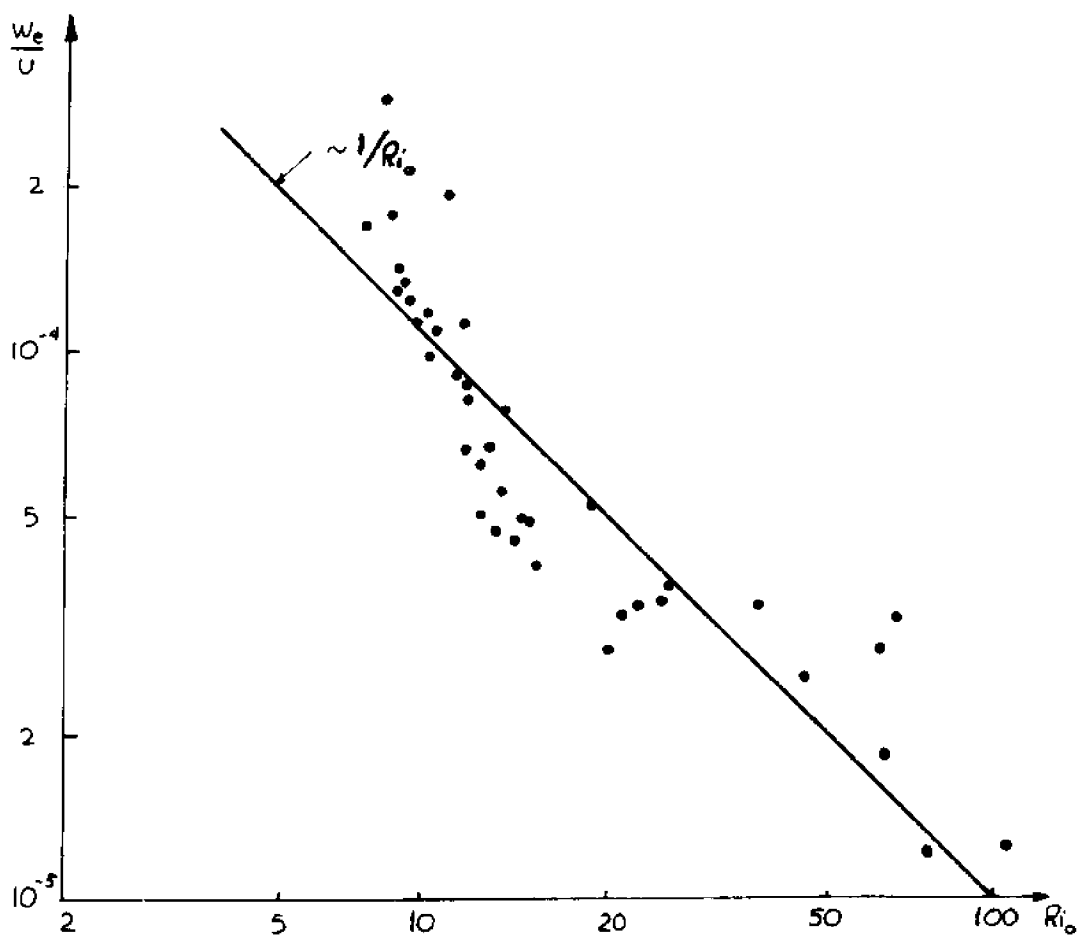


Figure 4.2 Experimental Results of Lofquist, Replotted in (7)

$$\alpha = \frac{m_{12} + m_{21}}{2} \quad (4.6)$$

Thus, the interfacial transport rate is simply expressed as the net entrainment rate times the average concentration of the layers plus an average entrainment rate times the difference in layer concentrations. When one of the layers (say, layer 2) is non-turbulent, Equation (4.5) or its equivalent Equation (4.4) reduces to

$$Q_{21} = m_{21}c_2 \quad (4.7a)$$

which is consistent with the visualization of the mixing process as a one-way transport in this case. When both layers have identical characteristics, it is  $m_{21} = m_{12} = \bar{m}$ , and the transport rate is expressed as:

$$Q_{21} = \frac{m_{21} + m_{12}}{2} (c_2 - c_1) = \bar{m}(c_2 - c_1) \quad (4.7b)$$

In this case there is no net water movement through the interface, which is a common assumption for hydrodynamic models at steady state; however, transfer of matter through the interface does occur, and it may be significant if the concentration difference between the layers is large.

The problem of relating the entrainment rates to the structure of the turbulence, let alone the mean flow characteristics, remains unsolved (67). In the next section a review of relevant studies is

made in an attempt to arrive at reasonably general quantitative expressions for the interfacial transport processes.

#### 4.2 Review of Related Work

Several experimental and semi-empirical studies have been conducted in the past concerning mass transport in stratified systems. Most of the information available at present comes from simple laboratory experiments made under horizontally one-dimensional flow conditions. However, the various investigators have often been using different length and velocity scales, so that it is quite difficult to compare quantitatively their results. In addition, the applicability of some of the results in a real water body is doubtful, due to the particular experimental conditions.

Experiments on a two-layer system were made by Turner (78), who induced turbulence in one of the layers by means of an oscillating grid and measured the rate of thickening of the layer due to entrainment. He used as length ( $\ell$ ) and velocity ( $U$ ) scales those associated with the grid turbulence and hence dependent on the mesh size and stirring frequency. His results showed a different functional relation of the entrainment velocity to the overall Richardson number, depending on whether the density stratification was caused by temperature or salinity. Thus,



$$w_e/U \propto Ri_o^{-3/2} \quad (\text{Salt}) \quad (4.8a)$$

$$w_e/U \propto Ri_o^{-1} \quad (\text{Heat}) \quad (4.8b)$$

for

$$Ri_o = \frac{g \frac{\Delta \rho}{\rho} \ell}{U^2} > 1$$

It may be argued on dimensional grounds (78), that three non-dimensional parameters may, in general, affect the interfacial transport process. In addition to the Richardson number, these are the Reynolds number

$$Re = \frac{U \ell}{\nu} \quad , \quad \nu = \text{kinematic viscosity}$$

and the Peclet number

$$Pe = \frac{U \ell}{\kappa} \quad , \quad \kappa = \text{molecular diffusivity of substance}$$

As discussed in (78) and (15), the effect of molecular diffusion for low Peclet numbers ( $Pe < 200$ ) may account, at least qualitatively, for the observed difference between (4.8a) and (4.8b). Long (49), however, has attributed this difference to erroneous interpretation of earlier experimental results and accepts (4.8b) as fundamental.

Apart from the fact that grid turbulence experiments do not seem

directly extendable to natural coastal waters (where most of the turbulent energy is associated with shear), the latter are normally characterized by high Reynolds numbers. In fully established turbulent flows the effect of the Reynolds number is traditionally considered unimportant. A high Reynolds number implies a high Peclet number, too, since in most cases  $\nu \gg \kappa$ . Therefore, the only parameter to be considered in practical cases is the Richardson number.

Turner's experiments have made clear that, in the absence of mean flow, the entrainment rate is essentially proportional to the turbulent intensity of the corresponding layer near the interface. When both layers were stirred at the same frequency, the interface remained fixed in the centre. When stirring was unsymmetrical, the interface tended to move away from the region of more vigorous stirring.

When a mean flow is present in a layer, the turbulent intensity is often considered proportional to the mean velocity. Experiments with mean flow have been mostly carried out with one layer quiescent. By measuring the rate of thickening of the turbulent layer, the following relation was found:

$$w_e / \bar{U} = c / Ri_o \quad (4.9)$$

where

$$Ri_o = \frac{g \frac{\Delta \rho}{\rho} H}{\bar{U}^2}$$

H being the layer depth and  $\bar{U}$  its mean velocity.

Early experimental investigations by Ellison and Turner (19) on a surface jet flowing over heavier fluid and on a salt water layer flowing under fresh water, both on a sloping channel, established the validity of Equation (4.9) with  $c \approx 5 \times 10^{-3}$ . However, their overall Richardson number was less than unity, which is not common in natural stably stratified waters. Lofquist (46) experimented on a salty layer flowing under quiet fresh water and found a dependence on the densimetric Froude number, but not on the Reynolds number. His results were replotted in (7) vs. the Richardson number,  $Ri = 1/Fr^2$ , and presented as Figure 4.2. This indicates a value of  $c \sim 10^{-3}$ . The hydraulic radius was used instead of the layer depth, to account for the limited width of the channel.

Later, Kato and Phillips (35) determined experimentally the rate of motion of the interface associated with a shear stress applied on the surface of an initially linearly stratified fluid. Using the shear velocity at the surface,  $U_s$ , as their velocity scale, they found a value of  $c \approx 2.5$  (Figure 4.3). The layer-average velocity was observed to be about half the velocity of the screen, with which the surface stress was achieved. From the given measurements of this stress, it follows (49) that  $\bar{U} \approx 10 U_s$ . Thus, the constant  $c$  of Equation (4.9) is found to be  $2.5 \times 10^{-3}$ , in reasonable agreement with Lofquist's value.

However, the above experiment is not really representative of a two-layer system, because of the initial linear stratification (which continues to be maintained below the interface). Wu (90) studied the

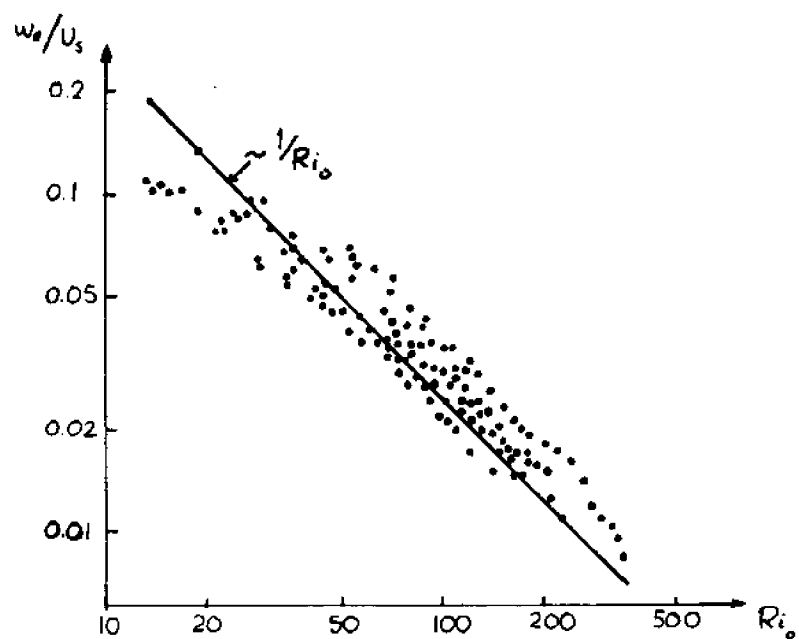


Figure 4.3 Experimental Results of Kato and Phillips (35)

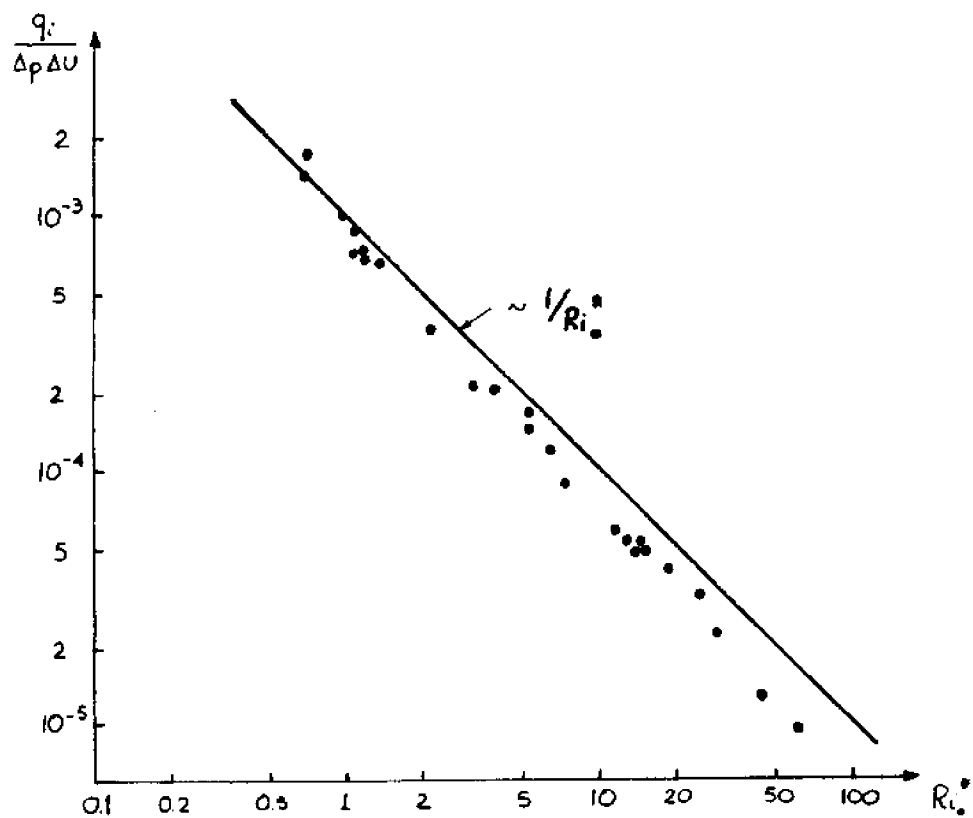


Figure 4.4 Experimental Results of Moore and Long (52)

entrainment due to wind acting on the free surface of a two-layer system. Using the same velocity scale as Kato and Phillips, he concluded that  $c \approx 0.234$ , i.e., an order of magnitude smaller than before. He suggested that the discrepancy may be due to different velocity profiles in the two cases. In his experiments, there was a significant countercurrent over the lower 3/5 of the top layer and there was no net overall velocity. This countercurrent was observed to be about three times the surface friction velocity. The velocity scale  $U_s$  used by Wu was found by applying a reduction factor of 0.685 to this friction velocity. If we use in Equation (4.9) the velocity of the countercurrent,  $U = 3 U_s / 0.685 = 4.38 U_s$ , which is adjacent to the interface, the coefficient  $c$  becomes equal to  $2.7 \times 10^{-3}$ , in close agreement with the previous results. Wu's results were later confirmed in Delft (7).

Recently, Hansen (25) carried out a theoretical investigation on the rate of deepening of the surface layer of a small lake due to wind stress. For moderate to large times, the balance between surface stress and pressure forces yielded Equation (4.9) with  $c = 2.36$ , which is essentially the same as Kato and Phillips' result. It also agrees well with Lofquist's data slightly modified by Hansen.

Finally, Long (50), in modeling a two-layer estuary with a deep quiescent lower layer and using the r.m.s. turbulent velocity  $\tilde{U}$  as velocity scale, concludes that  $c \approx 0.1$ , based on some of his own theoretical considerations (49). He subsequently argues that  $\tilde{U}$  is of the same order of magnitude as the mean layer velocity in this

case, although certainly smaller. It may be seen that a ratio of  $\bar{U}/\tilde{U} \approx 4$  reduces the coefficient  $c$  to the order of the values found by the previous investigators.

In conclusion, there seems to be agreement on the validity of Equation (4.9) for expressing the one-way interfacial transport, where the value of  $c$  is of the order of  $10^{-3}$ . It is worth noticing that the quantity  $\bar{U}^3/H$  is proportional to the rate of change of turbulent kinetic energy in the layer ( $e$ ). By rewriting Equation (4.9) as

$$w_e = \frac{c\bar{U}^3}{g \frac{\Delta\rho}{\rho} H} \propto \frac{e}{g \frac{\Delta\rho}{\rho}} \quad (4.10)$$

one may view entrainment as the result of consumption of part of the turbulent kinetic energy for shifting the level of the density discontinuity, thereby altering the potential energy of the system. The relation of entrainment to the energy characteristics of the two-layer system has long been recognized and examined in most studies on the subject. Long (49), in particular, proceeds in using energy arguments in an effort to offer a unified view of experiments with and without shear.

So far, the quantification of one-way transport, from a quiescent to a flowing turbulent layer, has been examined. At the other extreme, in the case of a counterflow, the interface must remain fixed, because of symmetry. However, interfacial transfer of properties does occur. This problem was experimentally investigated by Moore

and Long (52), who measured the turbulent buoyancy flux  $q_1 = \overline{w'\rho'}$  in one-dimensional counterflow and proposed the empirical relation (Figure 4.4)

$$\frac{q_1}{\Delta U \Delta \rho} = \frac{8 \cdot 10^{-4}}{Ri_o^*} \quad (4.11)$$

where

$$Ri_o^* = \frac{g \frac{\Delta \rho}{\rho} h}{(\Delta U)^2}$$

where  $\Delta U$  is the velocity difference, double each layer's velocity  $\bar{U}$  and  $h$  is the total depth, double each layer's depth  $H$ .

Equation (4.11) may be rewritten:

$$q_1 = \frac{8 \cdot 10^{-4} \cdot 2\bar{U}}{g \frac{\Delta \rho}{\rho} 2H / (\Delta U)^2} \Delta \rho$$

Since  $\Delta \rho$  is here the "concentration" difference, comparison with Equation (2.7) yields

$$\alpha = \frac{1}{2} \cdot \frac{8 \cdot 10^{-4} \cdot 2\bar{U}}{g \frac{\Delta \rho}{\rho} H / (\Delta U)^2} = \frac{1}{2} \cdot \frac{8 \cdot 10^{-4} \cdot 2\bar{U}}{g \frac{\Delta \rho}{\rho} H / (\Delta U)^2} \quad (4.12)$$

where  $Ri_o$  is based on each layer's depth. By comparing Equation (4.12) to Equation (4.6), and since  $m_{12} = m_{21}$  due to symmetry, we obtain

$$m_{12} = m_{21} = \frac{8.10^{-4}U}{Ri_0}$$

This is similar to the result found earlier for the entrainment rate when only one-way transport occurs. It is seen that the agreement in the coefficient  $c$  is very good and its value around  $10^{-3}$  appears well established.

An alternative way of expressing the diffusive flux of a substance is by using the concept of eddy diffusion coefficient, assuming Fickian behavior. This coefficient is widely used in homogeneous flows and was discussed in Chapter 3. In continuously stratified flows the decrease of vertical turbulent fluxes has been described by a reduction of the vertical diffusion coefficient and its dependence on the density gradient has been the subject of several investigations (7).

In nature there is always a zone of certain thickness over which the density change takes place, under even the strongest stratification. Despite our two-layer idealization, the diffusion coefficient concept could still be used, provided there was some knowledge of the width of the transition zone. In two-layer counterflow experiments this has been found to be approximately 0.08 times the total depth (48), or 0.16 times one layer's depth, for a wide range of the overall Richardson number (2 to 120).

In stirring grid experiments (15) it was also concluded that the thickness of the interface zone is independent of  $Ri_0$  in the range



4 to 1500 and equals 1.5 times the turbulence length scale (for high Peclet numbers). Since this length scale is of the order of 1/10 of the layer depth (see Chapter 3), the width of the zone comes to be about 0.15 times the layer depth, in close agreement with the previous value. This would imply that a thermocline at 10m from the surface will have a minimum thickness of about 1.5 meters. This is of the order of observed values, although natural conditions are certainly not as ideal as in laboratory experiments.

To quantify the vertical eddy diffusivity in the region of the interface, resort can be made again to the theory of locally isotropic turbulence (see Chapter 3). Arguing that eddies larger than a certain critical size cannot take part in the vertical mass transfer, Osmidov (62) obtains as a maximum value for the vertical diffusivity, effective through a density gradient

$$\epsilon_{z,i} = \frac{c_1 \rho}{g \frac{\partial \rho}{\partial z}} \quad (4.13)$$

where  $c_1 \sim 0(0.1)$

and  $e$  the rate of energy input into the system.

Using a typical value of  $e \approx 10^{-2} \text{ cm}^2/\text{sec}^{-3}$  one obtains

$$\epsilon_{z,i} = \frac{10^{-8}}{\frac{1}{\rho} \frac{\partial \rho}{\partial z}} (\text{m}^2/\text{sec}) = \frac{10^{-4}}{\frac{1}{\rho} \frac{\partial \rho}{\partial z}} (\text{cm}^2/\text{sec}) \quad (4.14)$$

where  $\frac{1}{\rho} \frac{\partial \rho}{\partial z}$  has to be given in  $\text{m}^{-1}$ .

Expression (4.14) has been, in fact, proposed (36) as the statistically best fit to available data in stratified regions. For  $\frac{\Delta\rho}{\rho} \approx 3^0/00$ , taking place over a 1.5 meters distance, eg. (4.14) yields:

$$\epsilon_{z,i} \approx \frac{10^{-4}}{2 \cdot 10^{-3}} = 0.05 \text{ cm}^2/\text{sec}$$

Observed values of the effective vertical diffusivity in the region of the thermocline in the oceans range below  $1 \text{ cm}^2/\text{sec}$  to  $0.01 \text{ cm}^2/\text{sec}$  (56). Using (4.14), the interfacial diffusive flux may be written

$$q_i = (\epsilon_z \frac{\partial c}{\partial z})_{-h_1} = \frac{10^{-8}}{\frac{1}{\rho} \frac{\partial \rho}{\partial z}} \frac{\partial c}{\partial z}$$

or, considering the concentration and density gradients taking place over the same thickness:

$$q_i = \frac{10^{-8}}{\frac{\Delta\rho}{\rho}} \Delta c \quad (4.15)$$

By comparison with Equation (2.7) and (4.12), it is seen that

$$\frac{10^{-8}}{\frac{\Delta\rho}{\rho}} = \alpha = \frac{10^{-3} \bar{U}}{Ri_o}$$

For  $\bar{U} \sim 0(0.10 \text{ m/sec})$

and  $\frac{\Delta\rho}{\rho} \sim 0 (10^{-3})$

one obtains  $Ri_0 \sim 0(10)$

and  $\alpha \sim 0(10^{-5} \text{ m/sec})$ .

This seemingly small value of  $\alpha$  is, nevertheless, of the order of settling velocities of fine suspended particles, and its contribution becomes significant over relatively large length and time scales, especially when multiplied by a large concentration difference.

It is worth mentioning here that, despite its small value, the effective diffusivity of  $0.05 \text{ cm}^2/\text{sec}$  found earlier is still several orders of magnitude larger than molecular diffusion coefficients of most substances. For example, the molecular coefficient for salt is barely  $10^{-5} \text{ cm}^2/\text{sec}$ . Certainly, in an actual two-layer system, with a near-discontinuity in the profile of density and any other constituent, the transport caused by molecular diffusion would be significant. But, since in nature there is always a transition zone of finite thickness, molecular effects tend to be unimportant and can be safely neglected within the scope of the present work.

#### 4.3 Generalizations and Conclusions

The experimental evidence discussed in the previous section points out to the following expression for the one-way transport rate from layer  $j$  to  $i$ :

$$m_{ji} \approx \frac{10^{-3} \bar{U}_i}{Ri_0} \quad (4.16)$$

where  $\bar{U}_i$  the mean velocity of layer i

and  $Ri_o$  the overall Richardson number of the two-layer system

When both layers are flowing at different velocities, the Richardson number has to be expressed in terms of their relative velocity, which controls the stability of the interface. In the general case of a horizontally two-dimensional flow field the Richardson number is defined in terms of the vector difference of the layer velocities. Thus

$$Ri_o = \frac{g \frac{\Delta \rho}{\rho} H}{(\vec{U}_i - \vec{U}_j)^2} \quad (4.17)$$

The proper H to be used in this formula is not quite clear. Experiments with both layers flowing do not exist except for the symmetrical counterflow case where the layer thicknesses are the same. The coefficient  $10^{-3}$  in (4.16) was seen to be consistent when one layer's depth is used in the definition of  $Ri_o$ . When the two layers have different thicknesses, their average can be used as a reasonable value for H. This is consistent with considering the velocity gradient taking place over the distance between the center levels of the two layers.

Using Equations (4.3) and (4.16) we can now write for the net entrainment rate between layers 1 and 2:

$$w_e = m_{21} - m_{12} \approx \frac{10^{-3} (|U_1| - |U_2|)}{Ri_o} \quad (4.18)$$

Similarly, from Equations (4.6) and (4.16) one obtains

$$\alpha = \frac{m_{12} + m_{21}}{2} \approx \frac{1}{2} \frac{10^{-3} (|U_1| + |U_2|)}{Ri_o} \quad (4.19)$$

where in both expressions  $Ri_o$  is given by (4.17). The use of absolute values of the layer velocities in (4.18) and (4.19) is justified from the fact that the interfacial transport is a scalar quantity and consequently should not be affected by changes in the velocity directions (apart from their effect on the stability of the system, as expressed through the Richardson number). This is especially important to realize in a two-dimensional flow field, where  $\bar{U}_1$  and  $\bar{U}_2$  will, in general, have different directions. In particular, when  $|\bar{U}_1| = |\bar{U}_2|$ , irrespective of direction, there should be no net entrainment, since it is difficult to accept a preferential motion either upwards or downwards.

The above treatment essentially links the interfacial transport process to the mean flows in the adjacent layers. This is not a bad assumption for tide dominated flows which characterize coastal waters although, in general, interfacial transport may well exist when mean flow is absent, as indicated by the stirring grid experiments.

The problem of properly describing the mechanisms of interfacial transport is by no means solved. The quantitative expressions given

above are believed to be as good as can be obtained at present from the limited experience available from one-dimensional investigations. Future research is undoubtedly needed in this area, and this will certainly be no easy task. In the meanwhile, the sensitivity of the two-layer dispersion solutions to the values of  $w_e$  and  $\alpha$  may be examined, in order to assess how critical the correct specification of interfacial mixing is in various classes of problems. A first step in this direction will follow in Chapter 6.

## CHAPTER 5

### ANALYTICAL SOLUTIONS

The essential features of the phenomenon of dispersion in a two-layer system can be best illustrated through analytical solutions. However, such solutions can only be obtained under very simple flow conditions. The simplest case which may be examined is the counter-flow in an infinite domain, shown schematically in Figure 5.1. When  $U_1 = U_2 = U$ , the net entrainment at the interface vanishes, i.e.  $w_e = 0$ , according to Equation (4.18). Assuming the interface essentially horizontal and consequently the layer depths constant, the one-dimensional governing equations in this ideal case reduce to:

$$\frac{\partial C_1}{\partial t} + U_1 \frac{\partial C_1}{\partial x} = E \frac{\partial^2 C_1}{\partial x^2} - kC_1 + \alpha'(C_2 - C_1) + R_1 \quad (5.1a)$$

$$\frac{\partial C_2}{\partial t} - U_2 \frac{\partial C_2}{\partial x} = E \frac{\partial^2 C_2}{\partial x^2} - kC_2 - \alpha'(C_2 - C_1) + R_2 \quad (5.1b)$$

where  $C_{1,2}$  are the layer integrated concentrations  
 $R_{1,2}$  are the source terms  
 $E$  is the common dispersion coefficient, assumed constant  
 $k$  is the decay rate, and  
 $\alpha' = \frac{\alpha}{H}$ , where  $\alpha$  the proportionality constant for the  
interfacial transport and  $H$  the layer thickness.

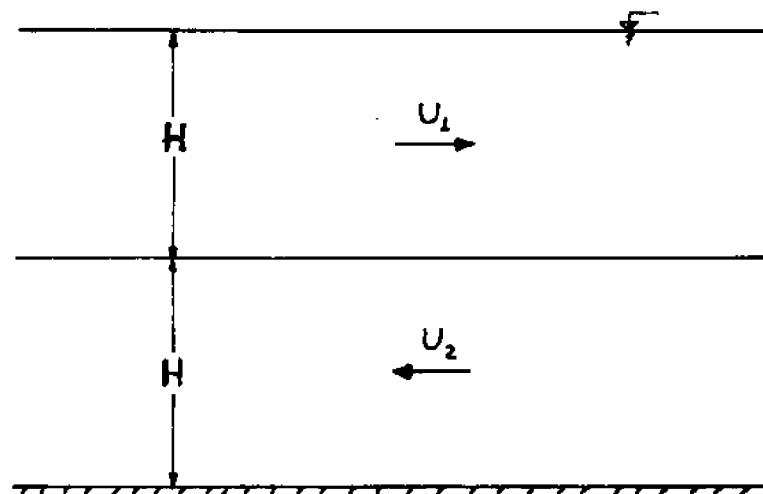


Figure 5.1 Flow Field Assumed for Analytical Solutions

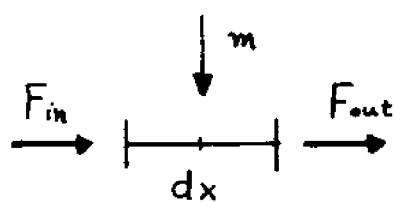


Figure 5.2 Mass Balance at the Location of the Source



Although the two equations are coupled in a very simple way, obtaining closed form solutions in the general transient case with arbitrary sources proves to be extremely difficult. In the following sections, two practically important problems, that of an instantaneous and that of a continuous injection in one of the layers, are examined.

### 5.1 1-D Instantaneous Injection

Of fundamental importance in all dispersion problems is the "unit impulse response", i.e., the solution for a unit load introduced instantaneously at a point, from which, by superposition, further solutions, for more complicated loads, may be constructed. In the particular counterflow situation one may consider a quantity  $M$  being introduced instantaneously in one of the layers, say the top, at  $x = 0$ . For the sake of generality, the solution will be developed for  $U_1 \neq U_2$ , arguing that the net entrainment  $w_e$  can still be neglected, provided the velocity magnitudes are not much different.

Since in stably stratified systems the interfacial transport is generally small and since the material is introduced only in layer 1, it will be  $C_2 \ll C_1$  for sufficiently small times. Equations (5.1a,b) may then be simplified as follows:

$$\frac{\partial C_1}{\partial t} + U_1 \frac{\partial C_1}{\partial x} = E \frac{\partial^2 C_1}{\partial x^2} - (\alpha' + k)C_1 + M \delta(t) \delta(x) \quad (5.2a)$$

$$\frac{\partial C_2}{\partial t} - U_2 \frac{\partial C_2}{\partial x} = E \frac{\partial^2 C_2}{\partial x^2} - (\alpha' + k)C_2 + \alpha' C_1 \quad (5.2b)$$

Equation (5.2a) contains now only  $C_1$  and its solution is well known (26):

$$C_1 = \frac{M}{\sqrt{4\pi Et}} \exp\left[-\frac{(x-U_1 t)^2}{4Et} - (\alpha' + k)t\right] \quad (5.3)$$

valid for small times.

Introducing this expression to (5.2b):

$$\begin{aligned} \frac{\partial C_2}{\partial t} - U_2 \frac{\partial C_2}{\partial x} = E \frac{\partial^2 C_2}{\partial x^2} - (\alpha' + k)C_2 \\ + \frac{\alpha' M}{\sqrt{4\pi Et}} \exp\left\{-\frac{x^2}{4Et} + \frac{xU_1}{2E} - \frac{U_1^2}{4E} t - (\alpha' + k)t\right\} \end{aligned} \quad (5.4)$$

This may be solved by use of the Laplace transform ( $t \rightarrow s$ ;  $C_2 \rightarrow y$ ).

The transformed equation is ( ):

$$\begin{aligned} sy - U_2 \frac{dy}{dx} = E \frac{d^2 y}{dx^2} - (\alpha' + k)y + \frac{\alpha' M}{2\sqrt{E}} \exp\left\{\frac{xU_1}{2E}\right\} \frac{\exp\left[-\frac{|x|}{\sqrt{E}} \sqrt{s + \alpha' + k + \frac{U_1^2}{4E}}\right]}{\sqrt{s + \alpha' + k + \frac{U_1^2}{4E}}} \\ \text{or} \\ Ey'' + Uy' - (\alpha' + k + s)y = - \frac{\alpha' M}{2\sqrt{E}} \frac{\exp\left\{\frac{xU_1}{2E} - \frac{|x|}{\sqrt{E}} \sqrt{s + \alpha' + k + \frac{U_1^2}{4E}}\right\}}{\sqrt{s + \alpha' + k + \frac{U_1^2}{4E}}} \end{aligned} \quad (5.5)$$

This is an ordinary linear differential equation of second order.

The corresponding homogeneous equation is

$$E_y'' + U_2 y' - (\alpha' + k + s)y = 0$$

with characteristic:

$$E\omega^2 + U_2\omega - (\alpha' + k + s) = 0$$

This has two real roots

$$r_{1,2} = \frac{-U_2 \pm \sqrt{U_2^2 + 4E(\alpha' + k + s)}}{2E} = -\frac{U_2}{2E} \pm \frac{1}{\sqrt{E}} \sqrt{s + \alpha' + k + \frac{U_2^2}{4E}}$$

Therefore, the homogeneous solution is:

$$y_h = A_1 \exp \left[ -\frac{xU_2}{2E} + \frac{x}{\sqrt{E}} \sqrt{s + \alpha' + k + \frac{U_2^2}{4E}} \right] + A_2 \exp \left[ -\frac{xU_2}{2E} - \frac{x}{\sqrt{E}} \sqrt{s + \alpha' + k + \frac{U_2^2}{4E}} \right] \quad (5.6)$$

Requiring that the solution be finite (indeed, tend to zero) as  $x \rightarrow \pm \infty$ , it is seen that

$$A_1 = 0 \quad \text{for } x \geq 0$$

and

$$A_2 = 0 \quad \text{for } x \leq 0$$

To find now a particular solution of Equation (5.5) for  $x \geq 0$ , set:

$$y_p = \lambda_1 \exp \left[ \frac{xU_1}{2E} - \frac{x}{\sqrt{E}} \sqrt{s + \alpha' + k + \frac{U_1^2}{4E}} \right] \quad (5.7)$$

The value of  $\lambda_1$  is obtained by substituting this expression in (5.5):

$$\lambda_1 = \frac{\alpha' M}{2(U_1 + U_2) \sqrt{s + \alpha' + k + \frac{U_1^2}{4E}} \left( \sqrt{s + \alpha' + k + \frac{U_1^2}{4E}} - \frac{U_1}{2\sqrt{E}} \right)} \quad (5.7a)$$

Finally, to find a particular solution for  $x \leq 0$ , set

$$y_p = \lambda_2 \exp \left( \frac{xU_1}{2E} + \frac{x}{\sqrt{E}} \sqrt{s + \alpha' + k + \frac{U_1^2}{4E}} \right) \quad (5.8)$$

which, by substitution in (5.5) yields:

$$\lambda_2 = - \frac{\alpha' M}{2(U_1 + U_2) \sqrt{s + \alpha' + k + \frac{U_1^2}{4E}} \left( \sqrt{s + \alpha' + k + \frac{U_1^2}{4E}} + \frac{U_1}{2\sqrt{E}} \right)} \quad (5.8a)$$

By combining (5.6), (5.7) and (5.8), the general solution is obtained, as follows,

$$y = A_2 \exp \left( - \frac{xU_2}{2E} \right) \exp \left( - \frac{x}{\sqrt{E}} \sqrt{s + \alpha' + k + \frac{U_2^2}{4E}} \right) + \frac{\alpha' M}{2(U_1 + U_2)} \frac{\exp \left( \frac{xU_1}{2E} \right) \exp \left( - \frac{x}{\sqrt{E}} \sqrt{s + \alpha' + k + \frac{U_1^2}{4E}} \right)}{\sqrt{s + \alpha' + k + \frac{U_1^2}{4E}} \left( \sqrt{s + \alpha' + k + \frac{U_1^2}{4E}} - \frac{U_1}{2\sqrt{E}} \right)} \quad \text{for } x \geq 0 \quad (5.9a)$$

$$y = A_1 \exp \left( - \frac{xU_2}{2E} \right) \exp \left( \frac{x}{\sqrt{E}} \sqrt{s + \alpha' + k + \frac{U_2^2}{4E}} \right) - \frac{\alpha' M}{2(U_1 + U_2)} \frac{\exp \left( \frac{xU_1}{2E} \right) \exp \left( - \frac{x}{\sqrt{E}} \sqrt{s + \alpha' + k + \frac{U_1^2}{4E}} \right)}{\sqrt{s + \alpha' + k + \frac{U_1^2}{4E}} \left( \sqrt{s + \alpha' + k + \frac{U_1^2}{4E}} + \frac{U_1}{2\sqrt{E}} \right)} \quad \text{for } x \leq 0 \quad (5.9b)$$

To determine the values of the constants  $A_1$  and  $A_2$ , the two branches of the solution have to be matched at  $x = 0$ . The concentration is continuous

at  $x = 0$  and, since there is no source at this point, the first derivative also has to be continuous. These properties also hold for the transformed variable  $y$ .

The first condition,  $y|_{0-} = y|_{0+}$ , implies

$$A_1 - A_2 = \frac{\alpha' M}{2(U_1 + U_2) \sqrt{s + \alpha' + k + \frac{U_1^2}{4E}}} \left[ \frac{1}{\sqrt{s + \alpha' + k + \frac{U_1^2}{4E}} - \frac{U_1}{2\sqrt{E}}} + \frac{1}{\sqrt{s + \alpha' + k + \frac{U_1^2}{4E}} + \frac{U_1}{2\sqrt{E}}} \right]$$

or,

$$A_1 - A_2 = \frac{\alpha' M}{(U_1 + U_2)(s + \alpha' + k)} \quad (5.10)$$

The second condition,  $\frac{dy}{dx}|_{0-} = \frac{dy}{dx}|_{0+}$ , implies

$$\begin{aligned} A_1 \left( -\frac{U_2}{2E} + \frac{1}{\sqrt{E}} \sqrt{s + \alpha' + k + \frac{U_2^2}{4E}} \right) \\ - \frac{\alpha' M}{2(U_1 + U_2)} \frac{\left( \frac{U_1}{2E} + \frac{1}{\sqrt{E}} \sqrt{s + \alpha' + k + \frac{U_1^2}{4E}} \right)}{\sqrt{s + \alpha' + k + \frac{U_1^2}{4E}} \left( \sqrt{s + \alpha' + k + \frac{U_1^2}{4E}} + \frac{U_1}{2\sqrt{E}} \right)} = \\ = -A_2 \left( \frac{U_2}{2E} + \frac{1}{\sqrt{E}} \sqrt{s + \alpha' + k + \frac{U_2^2}{4E}} \right) + \frac{\alpha' M}{2(U_1 + U_2)} \frac{\left( \frac{U_1}{2E} - \frac{1}{\sqrt{E}} \sqrt{s + \alpha' + k + \frac{U_1^2}{4E}} \right)}{\sqrt{s + \alpha' + k + \frac{U_1^2}{4E}} \left( \sqrt{s + \alpha' + k + \frac{U_1^2}{4E}} - \frac{U_1}{2\sqrt{E}} \right)} \end{aligned}$$

or,

$$(A_1 + A_2) \frac{1}{\sqrt{E}} \sqrt{s + \alpha' + k + \frac{U_2^2}{4E}} = (A_1 - A_2) \frac{U_2}{2E} + 0$$

and, by using Eq. (5.10):

$$A_1 + A_2 = \frac{\alpha' M U_2}{2(U_1 + U_2) \sqrt{E} (s + \alpha' + k) \sqrt{s + \alpha' + k + \frac{U_2^2}{4E}}} \quad (5.11)$$

Solving the system of equations (5.10) and (5.11), the values of  $A_1$  and  $A_2$  are obtained:

$$A_1 = \frac{\alpha' M \left( \sqrt{s + \alpha' + k + \frac{U_2^2}{4E}} + \frac{U_2}{2\sqrt{E}} \right)}{2(U_1 + U_2) (s + \alpha' + k) \sqrt{s + \alpha' + k + \frac{U_2^2}{4E}}} \quad (5.12a)$$

$$A_2 = - \frac{\alpha' M \left( \sqrt{s + \alpha' + k + \frac{U_2^2}{4E}} - \frac{U_2}{2\sqrt{E}} \right)}{2(U_1 + U_2) (s + \alpha' + k) \sqrt{s + \alpha' + k + \frac{U_2^2}{4E}}} \quad (5.12b)$$

After introducing the above into the expressions (5.9a,b) and rewriting the factor  $(s + \alpha' + k)$  in the denominator as

$$s + \alpha' + k = \left( \sqrt{s + \alpha' + k + \frac{U_2^2}{4E}} - \frac{U_2}{2\sqrt{E}} \right) \left( \sqrt{s + \alpha' + k + \frac{U_2^2}{4E}} + \frac{U_2}{2\sqrt{E}} \right)$$

the final form of the solution in the transformed variables is:

$$\begin{aligned}
y = \frac{\alpha' M}{2(U_1 + U_2)} \left\{ - \frac{\exp(-\frac{xU_2}{2E}) \exp(-\frac{x}{\sqrt{E}} \sqrt{s + \alpha' + k + \frac{U_2^2}{4E}})}{\sqrt{s + \alpha' + k + \frac{U_2^2}{4E}} (\sqrt{s + \alpha' + k + \frac{U_2^2}{4E}} + \frac{U_2}{2\sqrt{E}})} \right. \\
\left. + \frac{\exp(-\frac{xU_1}{2E}) \exp(-\frac{x}{\sqrt{E}} \sqrt{s + \alpha' + k + \frac{U_1^2}{4E}})}{\sqrt{s + \alpha' + k + \frac{U_1^2}{4E}} (\sqrt{s + \alpha' + k + \frac{U_1^2}{4E}} - \frac{U_1}{2\sqrt{E}})} \right\} \quad \text{for } x \geq 0 \quad (5.13a)
\end{aligned}$$

$$\begin{aligned}
y = \frac{\alpha' M}{2(U_1 + U_2)} \left\{ \frac{\exp(-\frac{xU_2}{2E}) \exp(\frac{x}{\sqrt{E}} \sqrt{s + \alpha' + k + \frac{U_2^2}{4E}})}{\sqrt{s + \alpha' + k + \frac{U_2^2}{4E}} (\sqrt{s + \alpha' + k + \frac{U_2^2}{4E}} - \frac{U_2}{2\sqrt{E}})} \right. \\
\left. - \frac{\exp(-\frac{xU_1}{2E}) \exp(\frac{x}{\sqrt{E}} \sqrt{s + \alpha' + k + \frac{U_1^2}{4E}})}{\sqrt{s + \alpha' + k + \frac{U_1^2}{4E}} (\sqrt{s + \alpha' + k + \frac{U_1^2}{4E}} + \frac{U_1}{2\sqrt{E}})} \right\} \quad \text{for } x \leq 0 \quad (5.13b)
\end{aligned}$$

From Tables ( 73 ) , the inverse transform is found to be:

$$\begin{aligned}
C_2 &= \frac{\alpha' M}{2(U_1 + U_2)} \exp\{-(\alpha' + k)t\} \left[ -\operatorname{erfc} \frac{x + U_2 t}{\sqrt{4Et}} + \operatorname{erfc} \frac{x - U_1 t}{\sqrt{4Et}} \right] \\
&= \frac{\alpha' M}{2(U_1 + U_2)} \exp\{-(\alpha' + k)t\} \left[ \operatorname{erf} \frac{x + U_2 t}{\sqrt{4Et}} - \operatorname{erf} \frac{x - U_1 t}{\sqrt{4Et}} \right] \quad ; \quad x \geq 0
\end{aligned}$$

$$\begin{aligned}
C_2 &= \frac{\alpha' M}{2(U_1 + U_2)} \exp\{-(\alpha' + k)t\} \left[ \operatorname{erfc}\left(-\frac{x + U_2 t}{\sqrt{4Et}}\right) - \operatorname{erfc}\left(\frac{-x + U_1 t}{\sqrt{4Et}}\right) \right] \\
&= \frac{\alpha' M}{2(U_1 + U_2)} \exp\{-(\alpha' + k)t\} \left[ \operatorname{erf}\left(\frac{x + U_2 t}{\sqrt{4Et}}\right) - \operatorname{erf}\left(\frac{x - U_1 t}{\sqrt{4Et}}\right) \right] ; \quad x \leq 0
\end{aligned}$$

that is, for all  $x$

$$C_2 = \frac{\alpha' M}{2(U_1 + U_2)} \exp\{-(\alpha' + k)t\} \left[ \operatorname{erf}\left(\frac{x + U_2 t}{\sqrt{4Et}}\right) - \operatorname{erf}\left(\frac{x - U_1 t}{\sqrt{4Et}}\right) \right] \quad (5.14)$$

The location  $x_0$  of the peak of the distribution can be found by differentiation:

$$\frac{2}{\sqrt{4\pi Et}} \exp\left[-\frac{(x_0 + U_2 t)^2}{4Et}\right] - \frac{2}{\sqrt{4\pi Et}} \exp\left[-\frac{(x_0 - U_1 t)^2}{4Et}\right] = 0$$

This yields

$$(x_0 + U_2 t)^2 = (x_0 - U_1 t)^2$$

i.e.,

$$x_0 = \frac{U_1 - U_2}{2} t \quad (5.15)$$



and the value of the peak concentration is:

$$C_{20} = \frac{\alpha' M}{(U_1 + U_2)} \exp\{-(\alpha' + k)t\} \operatorname{erf}\left(\frac{U_1 + U_2}{2} t\right) \quad (5.16)$$

Therefore, the peak concentration at the bottom layer moves at a velocity  $\frac{U_1 - U_2}{2}$ , the direction being controlled by the relative magnitude of  $U_1$  and  $U_2$ . By comparing to the velocity  $U_1$  of the peak at the top layer (see Eq. 5.3), it is seen that the bottom peak is moving much slower, since  $U_1$  and  $U_2$  are assumed about equal. The functional form of  $C_2$  also indicates that the distribution is symmetrical about the peak and very "diffuse" in character, due to the presence of the slowly varying error functions. This is, of course, explained physically by the distributed nature of the transfer of material to the bottom layer through the interface.

In the particular case that  $U_1 = U_2 = U$ , it is

$$C_{20} = \frac{\alpha' M}{2U} \exp\{-(\alpha' + k)t\} \operatorname{erf}\left(\frac{Ut}{\sqrt{4Et}}\right) \quad (5.17)$$

and  $x_0 = 0$ , that is, the highest concentration in the bottom layer remains stationary at the position of the original source.

The above conclusions were based on the small time approximation  $C_2 \ll C_1$ . It is appropriate, at this point, to examine the time scale of the validity of this assumption, which allows the simplification of the original equations. An order of magnitude of the desired time scale can be

obtained from a restriction on the ratio  $C_{20}/C_{10}$ , although the two peak concentrations do not occur at the same point. For small arguments (10)

$$\operatorname{erf} X = \frac{2}{\sqrt{\pi}} \sum_{n=0}^{\infty} \frac{(-1)^n X^{2n+1}}{(2n+1)n!}$$

Keeping only the leading term ( $n=0$ ), Eq. (5.17) becomes approximately

$$C_{20} = \frac{\alpha' M}{2U} \exp\{-(\alpha+k)t\} \frac{2}{\sqrt{\pi}} \frac{Ut}{\sqrt{4Et}}$$

and therefore,

$$\frac{C_{20}}{C_{10}} = \frac{\alpha' Mt / \sqrt{4\pi Et}}{M / \sqrt{4\pi Et}} = \alpha' t$$

Requiring that  $C_{20}/C_{10} < 5\%$  implies

$$t < 0.05/\alpha' \quad (5.18)$$

Eq. (5.18) indicates that the time scale of the validity of the approximate solution increases in inverse proportion to  $\alpha'$ . This could be intuitively expected, since the smaller the diffusion through the interface, the lower the concentrations in the bottom layer.

## 5.2 1-D Continuous Injection

The steady-state solution under continuous release of a constituent at a point is of great practical interest, since it reveals the kind of impact of such sources as sewage outfalls or power plants, which operate, more or less, on a continuous basis. The problem, in the case of counter-flow, is described by the following set of equations:

$$U \frac{dC_1}{dx} = E \frac{d^2C_1}{dx^2} - kC_1 + \alpha'(C_2 - C_1) + R_1 \quad (5.19a)$$

$$-U \frac{dC_2}{dx} = E \frac{d^2C_2}{dx^2} - kC_2 - \alpha'(C_2 - C_1) \quad (5.19b)$$

where  $R_1 = m \cdot \delta(x)$ , and the other symbols have been defined in Eqs. (5.1a,b). The layer velocities are assumed here exactly equal; this is done for two reasons. First, neglecting the net entrainment associated with even a small difference between  $U_1$  and  $U_2$  is not justified because of the large time scale required for the system to reach steady state. Second, by setting  $U_1 = U_2 = U$  the mathematical treatment is significantly simplified, because odd order derivatives vanish, as will be seen shortly.

Solving Eq. (5.19a) for  $C_2$ , and neglecting for the moment the source term which will be treated later through boundary conditions, one obtains:

$$C_2 = \frac{1}{\alpha'} [ (\alpha' + k)C_1 + U \frac{dC_1}{dx} - E \frac{d^2C_1}{dx^2} ] \quad (5.20)$$

Substituting in (5.19b), an equation for  $C_1$  only is obtained:

$$E^2 \frac{d^4 C_1}{dx^4} - [2(\alpha' + k)E + U^2] \frac{d^2 C_1}{dx^2} + k(2\alpha' + k)C_1 = 0 \quad (5.21)$$

The corresponding characteristic is:

$$E^2 \omega^4 - [2(\alpha' + k)E + U^2] \omega^2 + k(2\alpha' + k) = 0 \quad (5.22)$$

with roots:

$$r_{1,3}^2 = \frac{2(\alpha' + k)E + U^2 \pm \sqrt{4\alpha'^2 E^2 + U^4 + 4(\alpha' + k)EU^2}}{2E^2}$$

These are both positive and, therefore, Eq. (5.22) has four real roots,  $\pm r_1, \pm r_3$ , where

$$r_{1,3} = \frac{1}{E} \sqrt{\frac{2(\alpha' + k)E + U^2 \pm \sqrt{4\alpha'^2 E^2 + U^4 + 4(\alpha' + k)EU^2}}{2}} \quad (5.23)$$

The general solution of Eq. (5.21) is:

$$C_1 = A_1 e^{r_1 x} + A_2 e^{-r_1 x} + A_3 e^{r_3 x} + A_4 e^{-r_3 x}$$

where  $A_1, A_2, A_3, A_4$  are constants to be specified through the boundary conditions, which the layer concentrations and their derivatives have to comply with.

As in Section 5.1, distinction must be made between the regions  $x > 0$  and  $x < 0$  because of the exponential terms that grow without bound as

$|x| \rightarrow \infty$ . Consequently, the solution for  $C_1$  is:

$$C_1 = A_2 e^{-r_1 x} + A_4 e^{-r_3 x} \quad ; \quad x \geq 0 \quad (5.24)$$

$$C_1 = A_1 e^{r_1 x} + A_3 e^{r_3 x} \quad ; \quad x \leq 0$$

Using these expressions in Eq. (5.20), one obtains for  $C_2$ :

$$C_2 = \frac{1}{\alpha'} \{ (\alpha' + k - Ur_1 - Er_1^2) A_2 e^{-r_1 x} + (\alpha' + k - Ur_3 - Er_3^2) A_4 e^{-r_3 x} \};$$

$$x \geq 0 \quad (5.25)$$

$$C_2 = \frac{1}{\alpha'} \{ (\alpha' + k + Ur_1 - Er_1^2) A_1 e^{r_1 x} + (\alpha' + k + Ur_3 - Er_3^2) A_3 e^{r_3 x} \};$$

$$x \leq 0$$

For matching the solutions at  $x = 0$ , the following conditions must be satisfied:

(i) Continuity of  $C_1$  at  $x = 0$ , i.e.

$$(C_1)_{0-} = (C_1)_{0+} \quad (5.26)$$

From (5.24)

$$A_1 + A_3 = A_2 + A_4 \quad (5.27)$$

(ii) Due to the presence of the source in layer 1 at  $x = 0$ , the first derivative of  $C_1$  is discontinuous at that point. Mass balance per unit time over an infinitesimal length  $dx$  (Figure 5.2) implies:

$$F_{out} - F_{in} = m$$

$$\text{i.e. } (UC_1 - E \frac{dC_1}{dx})_{o+} - (UC_1 - E \frac{dC_1}{dx})_{o-} = m$$

and, taking into account (5.26), this yields:

$$(\frac{dC_1}{dx})_{o-} - (\frac{dC_1}{dx})_{o+} = \frac{m}{E} \quad (5.28)$$

Using (5.24)

$$r_1 A_1 + r_3 A_3 - (-r_1 A_2 - r_3 A_4) = \frac{m}{E}$$

or

$$r_1 (A_1 + A_2) + r_3 (A_3 + A_4) = \frac{m}{E} \quad (5.29)$$

(iii) Continuity of  $C_2$  at  $x = 0$ , i.e.

$$(C_2)_{o-} = (C_2)_{o+} \quad (5.30)$$

from (5.25)

$$(\alpha' + k - Er_1^2)(A_1 - A_2) + Ur_1(A_1 + A_2) + (\alpha' + k - Er_3^2)(A_3 - A_4) + Ur_3(A_3 + A_4) = 0 \quad (5.31)$$

(iv) Continuity of the first derivative of  $C_2$  at  $x = 0$ , since there is no source in the bottom layer:

$$\left(\frac{dC_2}{dx}\right)_{0-} = \left(\frac{dC_2}{dx}\right)_{0+} \quad (5.32)$$

Differentiating (5.25), we obtain

$$\begin{aligned} &(\alpha' + k - Er_1^2)r_1(A_1 + A_2) + Ur_1^2(A_1 - A_2) \\ &+ (\alpha' + k - Er_3^2)r_3(A_3 + A_4) + Ur_3^2(A_3 - A_4) = 0 \end{aligned} \quad (5.33)$$

Solving the system of equations (5.27), (5.29), (5.31) and (5.33), the values of  $A_1, A_2, A_3, A_4$  are found to be

$$A_1 = \frac{Um}{2E^2(r_1^2 - r_3^2)} + \frac{m}{2E(r_1^2 - r_3^2)r_1} \left( \frac{\alpha' + k}{E} + \frac{U^2}{E^2} - r_3^2 \right) \quad (5.34a)$$

$$A_2 = -\frac{Um}{2E^2(r_1^2 - r_3^2)} + \frac{m}{2E(r_1^2 - r_3^2)r_1} \left( \frac{\alpha' + k}{E} + \frac{U^2}{E^2} - r_3^2 \right) \quad (5.34b)$$

$$A_3 = -\frac{Um}{2E^2(r_1^2 - r_3^2)} - \frac{m}{2E(r_1^2 - r_3^2)r_3} \left( \frac{\alpha' + k}{E} + \frac{U^2}{E^2} - r_1^2 \right) \quad (5.34c)$$

$$A_4 = \frac{Um}{2E^2(r_1^2 - r_3^2)} - \frac{m}{2E(r_1^2 - r_3^2)r_3} \left( \frac{\alpha' + k}{E} + \frac{U^2}{E^2} - r_1^2 \right) \quad (5.34d)$$

Substitution in Eqs. (5.24) yields:

$$\begin{aligned}
C_1 = & \frac{Um}{2E^2(r_1^2 - r_3^2)} (e^{-r_3 x} - e^{-r_1 x}) \\
& + \frac{m}{2E(r_1^2 - r_3^2)r_1 r_3} \left( \frac{\alpha' + k}{E} + \frac{U^2}{E^2} \right) (r_3 e^{-r_1 x} - r_1 e^{-r_3 x}) \\
& + \frac{m}{2E(r_1^2 - r_3^2)r_1 r_3} (r_1^3 e^{-r_3 x} - r_3^3 e^{-r_1 x}) \quad \text{for } x \geq 0
\end{aligned}$$

$$\begin{aligned}
C_1 = & \frac{Um}{2E^2(r_1^2 - r_3^2)} (e^{r_1 x} - e^{r_3 x}) \\
& + \frac{m}{2E(r_1^2 - r_3^2)r_1 r_3} \left( \frac{\alpha' + k}{E} + \frac{U^2}{E^2} \right) (r_3 e^{r_1 x} - r_1 e^{r_3 x}) \\
& + \frac{m}{2E(r_1^2 - r_3^2)r_1 r_3} (r_1^3 e^{r_3 x} - r_3^3 e^{r_1 x}) \quad \text{for } x \leq 0
\end{aligned}$$

These can be written in a compact form as:

$$\begin{aligned}
C_1 = & \frac{m}{2E(r_1^2 - r_3^2)r_1 r_3} \left\{ \left( \frac{\alpha' + k}{E} + \frac{U^2}{E^2} \right) (r_3 e^{-r_1 |x|} - r_1 e^{-r_3 |x|}) \right. \\
& + r_1^3 e^{-r_3 |x|} - r_3^3 e^{-r_1 |x|} \} \\
& + (\text{sing } x) \frac{Um}{2E^2(r_1^2 - r_3^2)} (e^{-r_3 |x|} - e^{-r_1 |x|})
\end{aligned}$$

and further simplified by multiplying the first term by  $\frac{r_1 r_3}{r_1 + r_3}$  and using the fact that

$$r_1^2 r_3^2 = \frac{k(2\alpha' + k)}{E^2}$$

The expression for  $C_1$  finally becomes



$$C_1 = \frac{m}{2(r_1^2 - r_3^2)} \left[ \frac{(\alpha' + k)r_1 r_3}{k(2\alpha' + k)} + \frac{1}{E} \right] (r_1 e^{-r_3|x|} - r_3 e^{-r_1|x|}) - \frac{m[r_1 + r_3 - (\text{sign } x) \frac{U}{E}]}{2E(r_1^2 - r_3^2)} (e^{-r_3|x|} - e^{-r_1|x|}) \quad (5.35)$$

where  $r_1, r_3$  are given by Eq. (5.23).

Substituting this expression for  $C_1$  in Eq. (5.20) and after several algebraic manipulations, the solution for  $C_2$  is obtained as follows:

$$C_2 = \frac{\alpha' m r_1 r_3}{2k(2\alpha' + k)(r_1^2 - r_3^2)} (r_1 e^{-r_3|x|} - r_3 e^{-r_1|x|}) \quad (5.36)$$

Eq. (5.36) shows that the distribution of  $C_2$  is symmetrical about  $x = 0$ , where its highest value is achieved. This would be also the case for  $C_1$  in the absence of advection; indeed, Eq. (5.35) indicates that the only distinction between  $x > 0$  and  $x < 0$  is associated with the appearance of the velocity  $U$ . However, symmetry characterizes the bottom layer at any advection rate and it is certainly due to the exactly equal and opposite layer velocities.

The total mass present in each layer at steady state is of particular interest. This can be obtained by integrating each concentration distribution over  $x$ . Thus,

$$M_1 = \int_{-\infty}^0 C_1 dx + \int_0^{+\infty} C_1 dx = 2 \left\{ \frac{m}{2(r_1^2 - r_3^2)} \left[ \frac{r_1 r_3 (\alpha' + k)}{k(2\alpha' + k)} + \frac{1}{E} \right] \left( \frac{r_1}{r_3} - \frac{r_3}{r_1} \right) - \frac{m(r_1 + r_3)}{2E(r_1^2 - r_3^2)} \left( \frac{1}{r_3} - \frac{1}{r_1} \right) \right\}$$

which reduces to

$$M_1 = \frac{(\alpha' + k)m}{k(2\alpha' + k)} \quad (5.37)$$

Similarly

$$\begin{aligned} M_2 &= \int_{-\infty}^0 C_2 dx + \int_0^{+\infty} C_2 dx = \\ &= 2 \frac{\alpha' m}{2k(2\alpha' + k)} \frac{r_1 r_3}{r_1^2 - r_3^2} \left( \frac{r_1}{r_3} - \frac{r_3}{r_1} \right) \end{aligned}$$

i.e.

$$M_2 = \frac{\alpha' m}{k(2\alpha' + k)} \quad (5.38)$$

The total mass in the system is, of course

$$M = M_1 + M_2 = \frac{(\alpha' + k)m}{k(2\alpha' + k)} + \frac{\alpha' m}{k(2\alpha' + k)} = \frac{m}{k} \quad (5.39)$$

as expected, since at steady state the rate of input  $m$  must be equal to the total decay rate  $kM$ . Moreover, the ratio of the two masses is:

$$\frac{M_2}{M_1} = \frac{\alpha'}{\alpha' + k} = \frac{1}{1 + k/\alpha'} \quad (5.40)$$

that is, always less than unity and decreasing as the ratio of decay to the interfacial diffusion coefficient increases.

### 5.3 2-D Continuous Injection

Having examined the main features of the problem in the one-dimensional case, it is desirable to obtain an analytical solution in a two-dimensional flow field. This is easier attainable under steady state conditions, since the time variable is eliminated. The appropriate equations for uniform counterflow  $U$  and isotropic dispersion  $E$  in both layers are:

$$U \frac{\partial C_1}{\partial x} = E \frac{\partial^2 C_1}{\partial x^2} + E \frac{\partial^2 C_1}{\partial y^2} - kC_1 + \alpha'(C_2 - C_1) \quad (5.41a)$$

$$-U \frac{\partial C_2}{\partial x} = E \frac{\partial^2 C_2}{\partial x^2} + E \frac{\partial^2 C_2}{\partial y^2} - kC_2 - \alpha'(C_2 - C_1) \quad (5.41b)$$

The unavailability of boundary conditions along the  $x$ - or  $y$ -axes, which in fact are part of the solution, still poses a serious difficulty in a formal mathematical treatment. In this section a heuristic approach is undertaken for obtaining an approximate solution of Eqs. (5.41a,b) under a continuous input  $m$  per unit time at  $(x=0, y=0)$  in the top layer. The contribution of the longitudinal dispersion term is considered negligible compared to the advection term in similar one-layer problems (26) and therefore only transverse dispersion will be taken into account. Provided the entrainment is small, the steady state solution for the top layer should be very close to that of a single layer, i.e.

$$C_1 \approx \frac{m}{\sqrt{4\pi EUx}} \exp\left[-\frac{y^2 U}{4Ex} - \frac{(\alpha' + k)}{U} x\right] ; x > 0 \quad (5.42)$$

$$C_1 \approx 0 \quad ; x < 0 \quad (5.42a)$$

The above solution may be thought of as derived from the transient solution of (5.41a) for a load  $mdt$ :

$$C_1 \approx \frac{mdt}{\sqrt{4\pi Et}} \exp\left[-\frac{y^2}{4Et} - (\alpha' + k)t\right]$$

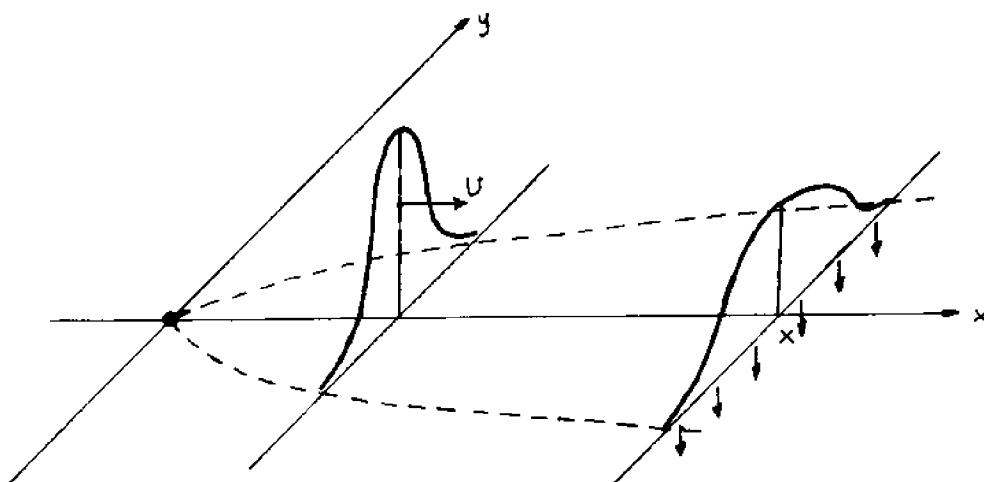
by replacing the time  $t$  by  $x/U$ , i.e. the distance travelled from the source at  $x=0$  to  $x=x$  divided by the velocity of travel.

Consider now a stripe of unit width in the bottom layer, parallel to the  $y$ -axis (Figure 5.3). This is moving at a velocity  $U$  at the direction of the negative  $x$ -axis. At each  $x$ -position it collects from the stripe directly above it (in the top layer) an input of  $\alpha' C_1$  per unit time--or  $\frac{\alpha' C_1}{U}$  per unit width, that is, for the whole stripe. Whatever comes down from a particular top layer stripe has then a certain distribution, as given by Eq. (5.42), multiplied by  $\frac{\alpha'}{U}$ . This distribution will continue to expand at the same rate  $E$  while the stripe in the bottom layer moves from  $x$  back to a certain position  $\bar{x}$ . A particle released from the source at  $x=0$  has travelled a distance  $x$  in the top layer and then  $(x-\bar{x})$  in the bottom layer. By analogy to Eq. (5.42), the contribution coming from  $x$  of the top layer to the steady-state concentration at  $\bar{x}$  of the bottom layer must be:

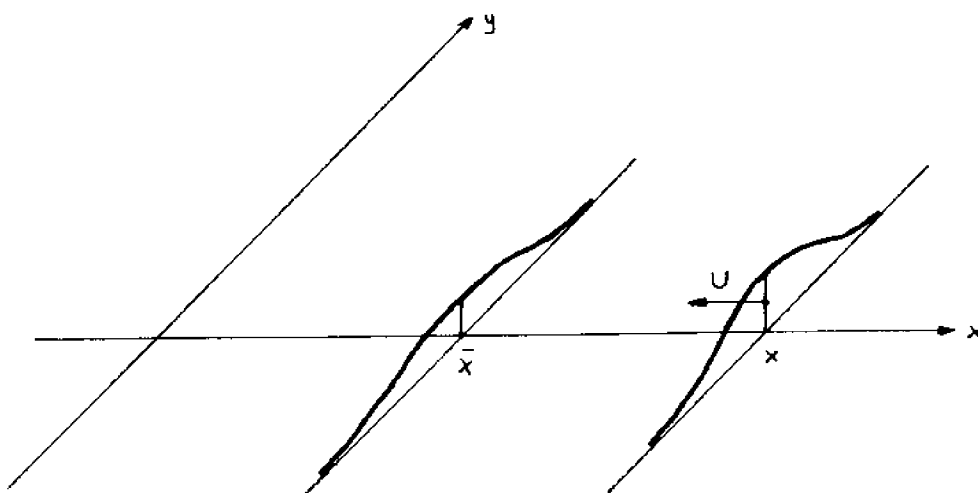
$$\frac{\alpha'}{U} \frac{m}{\sqrt{4\pi EU(2x-\bar{x})}} \exp\left[-\frac{y^2 U}{4E(2x-\bar{x})} - \frac{\alpha' + k}{U} (2x-\bar{x})\right]$$

Therefore, taking into account contributions from all  $x$ :

$$C_{z, \bar{x}} = \int_{\min(0, \bar{x})}^{+\infty} \frac{\alpha' m}{U \sqrt{4\pi EU(2x-\bar{x})}} \exp\left[-\frac{y^2 U}{4E(2x-\bar{x})} - \frac{\alpha' + k}{U} (2x-\bar{x})\right] dx \quad (5.43)$$



(a) Top Layer



(b) Bottom Layer

Figure 5.3 Concentration Distributions in 2-D Counterflow Case

The lower limit of integration is based on the following considerations:  
 if  $\bar{x} \geq 0$ , all  $x > \bar{x}$  have a positive concentration  $C_1$  and give a contribution. However, if  $\bar{x} < 0$ , contributions come only from  $x \geq 0$ , since  $C_1 = 0$  for  $x < 0$ , according to Eq. (5.42a). Further, by substituting  $z = 2x - \bar{x}$ , the limits of integration become:

$$\text{for } \bar{x} < 0: \quad x = 0 \rightarrow z = -\bar{x}$$

$$\text{for } \bar{x} > 0: \quad x = \bar{x} \rightarrow z = \bar{x}$$

$$\text{i.e., always } z = |\bar{x}|$$

The above integral may then be written:

$$C_{2,\bar{x}} = \int_{|\bar{x}|}^{\infty} \frac{\alpha'_m}{2U\sqrt{4\pi EUz}} \exp\left[-\frac{y^2 U}{4Ez} - \frac{\alpha'+k}{U} z\right] dz \quad (5.44)$$

It is evident from this equation that the bottom layer concentration distribution is symmetrical about  $\bar{x} = 0$ , as was the case in the one-dimensional problem.

For the particular case that  $y = 0$ , that is, for the  $x$ -axis, the integration (5.44) can be easily carried out. Dropping the overbar from  $\bar{x}$  and considering  $x \geq 0$ :

$$C_2 = \int_x^{\infty} \frac{\alpha'_m}{2U\sqrt{4\pi EUz}} \exp\left(-\frac{\alpha'+k}{U} z\right) dz$$

By setting  $\sqrt{\frac{\alpha'+k}{U}} z = \omega$ , one obtains:

$$C_2 = \frac{1}{U} \sqrt{\frac{U}{\alpha'+k}} \frac{\alpha'_m}{\sqrt{4\pi EU}} \int_{\sqrt{\frac{\alpha'+k}{U}} x}^{\infty} \exp(-\omega^2) d\omega$$

i.e.

$$C_2 = \frac{\alpha'_m}{4U\sqrt{E(\alpha'+k)}} \operatorname{erfc} \left( \sqrt{\frac{\alpha'+k}{U}} x \right)$$

Since the distribution is symmetrical about  $x = 0$ , we may write in general

$$C_2 = \frac{\alpha'_m}{4U\sqrt{E(\alpha'+k)}} \operatorname{erfc} \left( \sqrt{\frac{\alpha'+k}{U}} |x| \right); \quad \text{for } y = 0 \quad (5.45)$$

The presence of the complementary error function in the solution indicates that the distribution in the bottom layer falls off rather rapidly with distance from the source.

When  $y \neq 0$ , the integral of (5.44) is much more difficult to evaluate. In general, a numerical integration scheme can be employed to obtain  $C_2$  at certain points for given values of the parameters. The main purpose here being to provide an idea of the behavior of the solution, an approximation to the integral in terms of simple functions is desired. This can be obtained by expanding the exponential term and keeping only the three leading terms:

$$\exp\left(-\frac{y^2 U}{4Ez}\right) \approx 1 - \frac{y^2 U}{4Ez} + \frac{1}{2} \left(\frac{y^2 U}{4Ez}\right)^2 \quad (5.46)$$

This approximation will slightly overestimate the result, since the first term neglected is negative, therefore it is conservative. Of course, its validity is restricted to the case that

$$\frac{y^2 U}{4Ez} < 1$$

Since  $z$  varies between  $|x|$  and  $+\infty$ , the above inequality is covered by

$$\frac{y^2 U}{4E|x|} < 1 \quad (5.47)$$

Introducing (5.46) in Eq. (5.44) yields:

$$\begin{aligned} C_{2,x} &= \int_{|x|}^{\infty} \frac{\alpha' m}{2U\sqrt{4\pi EUz}} \exp\left(-\frac{\alpha'+k}{U} z\right) \left[1 - \frac{y^2 U}{4Ez} + \frac{1}{2} \frac{y^4 U^2}{16E^2 z^2}\right] dz \\ &= \frac{\alpha' m}{4U\sqrt{\pi EU}} \left\{ I_0 - \frac{y^2 U}{4E} I_1 + \frac{y^4 U^2}{32E^2} I_2 \right\} \end{aligned}$$

where

$$I_0 = \int_{|x|}^{\infty} \frac{1}{\sqrt{z}} \exp\left(-\frac{\alpha'+k}{U} z\right) dz = \sqrt{\frac{U}{\alpha'+k}} \sqrt{\frac{\pi}{2}} \operatorname{erfc} \sqrt{\frac{\alpha'+k}{U} |x|}$$

as found earlier, and

$$I_1 = \int_{|x|}^{\infty} \frac{1}{z^{3/2}} \exp\left(-\frac{\alpha'+k}{U} z\right) dz = \frac{2}{|x|} \exp\left(-\frac{\alpha'+k}{U} |x|\right) - 2 \frac{\alpha'+k}{U} I_0$$

$$\begin{aligned} I_2 &= \int_{|x|}^{\infty} \frac{1}{z^{5/2}} \exp\left(-\frac{\alpha'+k}{U} z\right) dz = \frac{2}{3|x|^{3/2}} \exp\left(-\frac{\alpha'+k}{U} |x|\right) - \frac{2}{3} \frac{\alpha'+k}{U} I_1 \\ &= \frac{2}{3|x|^{3/2}} \left(1 - 2 \frac{\alpha'+k}{U} |x|\right) \exp\left(-\frac{\alpha'+k}{U} |x|\right) + \frac{4}{3} \left(\frac{\alpha'+k}{U}\right)^2 I_0 \end{aligned}$$

Substituting these expressions, the solution for  $C_2$  finally becomes:

$$\begin{aligned} C_2 &\approx \frac{\alpha' m}{4U\sqrt{E(\alpha'+k)}} \operatorname{erfc}\left(\sqrt{\frac{\alpha'+k}{U} |x|}\right) \left[1 - \frac{y^2(\alpha'+k)}{2E} + \frac{1}{6} \left(\frac{y^2(\alpha'+k)}{2E}\right)^2\right] - \\ &- \frac{\alpha' m y^2}{8E\sqrt{\pi EU|x|}} \exp\left(-\frac{\alpha'+k}{U} |x|\right) \left[1 + \frac{1}{6} \left(\frac{y^2(\alpha'+k)}{2E} - \frac{y^2 U}{4E|x|}\right)\right] \quad (5.48) \end{aligned}$$



Comparisons of all three analytical solutions derived in this Chapter were made to results of the numerical model for verification purposes and are presented in Chapter 9.

## CHAPTER 6

### SENSITIVITY ANALYSIS

Irrespective of errors introduced in the numerical computations, an issue which is often not given the proper attention is that of parameter or input uncertainty. No matter how accurate the solution of the equations representing the mathematical abstraction to the natural process is, it can be no better in reality than the inputs used to generate it.

In the dispersion problem the basic parameters of interest are the velocity field, the dispersion coefficients, the decay and entrainment coefficients. The values assigned to the parameters may be obtained through theoretical considerations, field experiments, past experience, etc. There is always some uncertainty about the proper values to be used in any particular problem. The question that arises is: Is it worthwhile to resort to a highly accurate and expensive numerical scheme when some of the relevant parameters are known, say, only within an order of magnitude? The answer depends on the sensitivity of the solution to the value of the uncertain parameters.

The great practical importance of sensitivity analysis is that it reveals how the solution changes relative to changes in the parameters. By identifying the most critical parameters, the engineer can focus his efforts on determining them as accurately as possible, while not worrying too much about the remaining parameters.

Systematic sensitivity analysis can be easily carried out when an analytical solution exists. This happens under simple flow conditions only. However, the conclusions on the relative importance of the various parameters should be essentially the same in more complicated situations. Numerical experimentation can, of course, be used, but this is far more costly and less revealing than the simple analytical expressions.

In the following sections, the parameter sensitivity of the solution to some basic one and two-layer dispersion problems is studied. In particular, the sensitivity of the two most significant features of the solution i.e., the peak concentration and the extent (length, width) of the plume, is examined. With respect to the latter, since theoretically the concentration goes to zero only at an infinite distance, two definitions can be used: The "relative" extent of the plume is defined such that the concentration at the edge is a certain percentage (say 1% or 5%) of the peak concentration. The "absolute" extent is defined such that the concentration at the edge is a certain prescribed value; for example that imposed by existing environmental standards.

## 6.1 One-Dimensional One-Layer Flow

### 6.1.1 Instantaneous Source

The solution to the convection-diffusion equation for an instantaneous source of strength  $M$  is

$$C = \frac{M}{\sqrt{4\pi Et}} \exp \left[ -\frac{(x-ut)^2}{4Et} - kt \right] \quad (6.1)$$

The peak concentration at time  $t$  is

$$C_o = \frac{M}{\sqrt{4\pi Et}} \exp(-kt) \quad (6.2)$$

It is seen that the magnitude of  $C_o$  is independent of the velocity, which, however, determines the location of the peak (at  $x=Ut$ ).

Differentiating with respect to the dispersion coefficient yields

$$\frac{\partial C_o}{\partial E} = - \frac{M \exp(-kt)}{2E^{3/2} \sqrt{4\pi t}} = - \frac{C_o}{2E}$$

or,

$$\frac{\delta C_o}{C_o} = - \frac{1}{2} \frac{\delta E}{E} \quad (6.3)$$

where  $\delta$  denotes a differential change in magnitude. Equation (6.3) implies that a 10% increase in  $E$  would cause a 5% decrease in the peak concentration and indicates a moderate sensitivity of  $C_o$  to  $E$ .

The distribution (6.1) is symmetrical about  $x=Ut$ . As shown in Figure 6.1, the half-length of the plume at that time can be defined as

either i)  $L_r$ , where  $C = \beta C_o$  ( $\beta \ll 1$ , constant) or

ii)  $L_a$ , where  $C = \bar{C}$  (prescribed)

In the former case  $L_r$  can be found from

$$\exp \left( - \frac{L_r^2}{4Et} \right) = \beta$$

This leads to

Table 6.1

## Parameter Sensitivity for 1-D Instantaneous Injection

Quantity $Y$	$Y =$	$\frac{\delta Y}{Y} / \frac{\delta E}{E}$	$\frac{\delta Y}{Y} / \frac{\delta k}{k}$
$C_o$	$\frac{M}{\sqrt{4\pi Et}} \exp(-kt)$	$-\frac{1}{2}$	$-kt$
$L_r$	$\sqrt{4Et \ln \frac{1}{\beta}}$	$\frac{1}{2}$	$0$
$\max L_a$	$\sqrt{4Et^*(\frac{1}{2} + kt^*)}$	$\frac{kt^*}{1 + 2kt^*}$	$-\frac{kt^*}{1 + 2kt^*}$

Note:  $t^*$  is given by Equation (6.7)

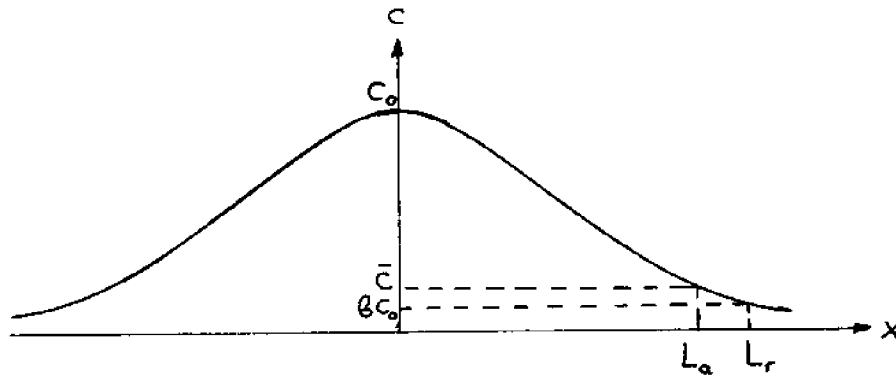


Figure 6.1 Typical Distribution after an Instantaneous Injection in 1-D Flow

$$L_r = \sqrt{4Et \ln \frac{1}{\beta}} \quad (6.4)$$

It is seen that  $L_r$  depends only on  $E$  and the choice of  $b$ . Furthermore,

$$\frac{\partial L_r}{\partial E} = \frac{1}{2\sqrt{E}} \sqrt{4t \ln \frac{1}{\beta}} = \frac{L_r}{2E} \quad (6.5)$$

$$\text{or,} \quad \frac{\delta L_r}{L_r} = \frac{1}{2} \frac{\delta E}{E}$$

indicating that the relative plume length would increase at half the rate of an increase of  $E$ .

In a similar way, one finds that

$$L_a = \sqrt{4Et \ln \frac{C_o}{\bar{C}}} = \sqrt{4Et \left( \ln \frac{M}{\bar{C}\sqrt{4\pi Et}} - kt \right)} \quad (6.6)$$

which, of course, has meaning only when  $C_o > \bar{C}$ . Of interest is the maximum value that  $L_a$  will ever reach. This can be found by differentiating  $L_a$  (or  $L_a^2$ ) with respect to time and setting the derivative equal to zero. Thus, one obtains:

$$\ln \frac{M}{\bar{C}\sqrt{4\pi Et}} = \frac{1}{2} + 2kt \quad (6.7)$$

which, unfortunately, has to be solved for the time to  $\max L_a$  by a trial and error procedure. Substituting (6.7) in Equation (6.6) yields:

$$\max L_a = \sqrt{4Et\left(\frac{1}{2} + kt\right)} \quad (6.8)$$

In the particular case of no decay, Equation (6.7) can be directly solved for  $t$ , giving

$$\sqrt{t}\Big|_{\max} = \frac{M}{e\bar{C}\sqrt{4\pi E}}$$

and consequently, from Equation (6.8)

$$\max L_a = \sqrt{\frac{M}{\pi e\bar{C}}} \quad (6.8a)$$

which is independent of both  $E$  and  $U$  and is only related to the value of  $\bar{C}$ .

In the more general case, when  $k > 0$ , the sensitivity of the maximum length of the cloud to the values of dispersion and decay coefficients can be found by employing partial differentiation on Equation (6.6) and using Equation (6.7). The resulting expressions, along with the previous sensitivity results, are summarized in Table 6.1.

#### 6.1.2 Continuous Source

The steady-state solution for a continuous input  $m$  (units/sec) at  $x = 0$  is (26):

$$C = \frac{m}{\sqrt{U^2 + 4kE}} \exp\left[\frac{x}{2E}(U \mp \sqrt{U^2 + 4kE})\right] \quad (6.9)$$

where

- for downstream ( $x > 0$ )

+ for upstream ( $x < 0$ )

The peak value occurs at  $x = 0$ ;

$$C_o = \frac{m}{\sqrt{U^2 + 4kE}} \quad (6.10)$$

Employing partial differentiation;

$$\frac{\delta C_o}{C_o} = - \frac{1}{2} \frac{1}{1 + \frac{U^2}{4kE}} \frac{\delta E}{E} \quad (6.11)$$

$$\frac{\delta C_o}{C_o} = - \frac{\frac{U^2}{4kE}}{1 + \frac{U^2}{4kE}} \frac{\delta U}{U} \quad (6.12)$$

$$\frac{\delta C_o}{C_o} = - \frac{1}{2} \frac{1}{1 + \frac{U^2}{4kE}} \frac{\delta k}{k} \quad (6.13)$$

Comparing (6.11) to (6.3) shows that the peak concentration is less sensitive to changes in  $E$  for a continuous source than for an instantaneous injection. As the non-dimensional parameter  $U^2/4kE$  increases, the peak tends to become increasingly sensitive to the velocity magnitude and less sensitive to the dispersion coefficient.



This should be expected, since a large value of  $U^2/4kE$  indicates that the process is advection-dominated.

For typical values in estuaries and coastal waters:

$$U \approx 0.10 \text{ m/sec}, \quad E \approx 10 \text{ m}^2/\text{sec}, \quad k \approx 10^{-5} \text{ sec}^{-1} \quad (\sim 1 \text{ day}^{-1})$$

$$U^2/4kE \approx 25$$

Then

$$\frac{\delta C_o}{C_o} = - \frac{25}{26} \frac{\delta U}{U}$$

$$\frac{\delta C_o}{C_o} = - \frac{1}{26} \frac{\delta E}{E}$$

which indicates that advection is the critical parameter and a misjudgement in the value of the dispersion coefficient has a negligible effect. This insensitivity to even an order of magnitude change in the dispersion coefficient in cases of continuous releases has been observed in the past (30).

The distribution (6.9) is illustrated in Figure 6.2. The downstream length of the plume  $L_{dr}$ , where  $C = \beta C_o$ , can be determined from

$$\exp\left[\frac{L_{dr}}{2E} (U - \sqrt{U^2 + 4kE})\right] = \beta$$

which yields

$$L_{dr} = \frac{2E \ln \beta}{U - \sqrt{U^2 + 4kE}} \quad (6.14)$$

Table 6.2

## Parameter Sensitivity for 1-D Continuous Source

Quantity Y	Y =	$\frac{\delta Y}{Y} / \frac{\delta E}{E}$	$\frac{\delta Y}{Y} / \frac{\delta U}{U}$	$\frac{\delta Y}{Y} / \frac{\delta k}{k}$
$C_o$	$\frac{m}{\sqrt{U^2 + 4kE}}$	$-\frac{1}{2} \frac{1}{1+\sigma}$	$-\frac{\sigma}{1+\sigma}$	$-\frac{1}{2} \frac{1}{1+\sigma}$
$L_{dr}$	$\frac{2E \ln \beta}{U - \sqrt{U^2 + 4kE}}$	$1 + \frac{1}{2} \frac{1}{\sqrt{\sigma(1+\sigma)} - (1+\sigma)}$	$\frac{1}{1+\sigma}$	$\frac{1}{2} \frac{1}{\sqrt{\sigma(1+\sigma)} - (1+\sigma)}$
$L_{da}$	Eq. (6.18)	Eq. (6.19)	Eq. (6.20)	

\* Note:  $\sigma = U^2/4kE$

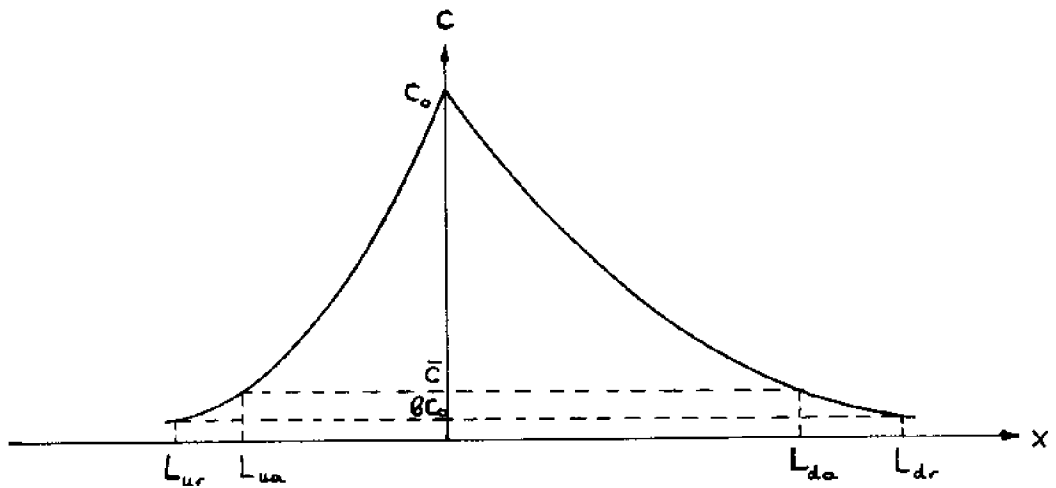


Figure 6.2 Typical Steady State Distribution for a Continuous Source in 1-D Flow

Differentiating with respect to E:

$$\frac{\delta L_{dr}}{L_{dr}} = \left[ 1 + \frac{1}{2} \frac{1}{\sqrt{\frac{U^2}{4kE} \left( 1 + \frac{U^2}{4kE} \right) - \left( 1 + \frac{U^2}{4kE} \right)}} \right] \frac{\delta E}{E} \quad (6.15)$$

Moreover, differentiating with respect to U:

$$\frac{\delta L_{dr}}{L_{dr}} = \frac{1}{\sqrt{1 + \frac{U^2}{4kE}}} \frac{\delta U}{U} \quad (6.16)$$

and with respect to k:

$$\frac{\delta L_{dr}}{L_{dr}} = \frac{1}{2} \frac{1}{\sqrt{\frac{U^2}{4kE} \left( 1 + \frac{U^2}{4kE} \right) - \left( 1 + \frac{U^2}{4kE} \right)}} \frac{\delta k}{k} \quad (6.17)$$

Evidently, the sensitivity of the plume length depends again on the value of  $U^2/4kE$ . For large values of this non-dimensional parameter, the coefficients of  $\delta E/E$  and  $\delta U/U$  tend to zero and unity, respectively. For  $U^2/4kE \rightarrow 0$ , these coefficients tend to 1/2 and zero, respectively. A similar analysis can be carried out for the upstream length of the plume,  $L_{ur}$ , which is, nevertheless, always smaller than  $L_{dr}$ , becoming equal when  $U = 0$ .

The absolute downstream length, defined by a prescribed concentration  $\bar{C}$ , is determined from

$$\bar{C} = \frac{m}{\sqrt{U^2 + 4kE}} \exp\left[-\frac{L_{da}}{2E} (U - \sqrt{U^2 + 4kE})\right]$$

i.e.,

$$L_{da} = \frac{2E}{U - \sqrt{U^2 + 4kE}} \ln \frac{\bar{C} \sqrt{U^2 + 4kE}}{m} \quad (6.18)$$

Partial differentiation yields

$$\frac{\delta L_{da}}{L_{da}} = \left[ 1 + \frac{1}{2} \frac{1}{\sqrt{\frac{U^2}{4kE} \left(1 + \frac{U^2}{4kE}\right) - \left(1 + \frac{U^2}{4kE}\right)}} + \frac{1}{2} \frac{1}{\left(1 + \frac{U^2}{4kE}\right) \ln \left(\frac{\bar{C}U}{m} \sqrt{1 + \frac{4kE}{U^2}}\right)} \right] \frac{\delta E}{E} \quad (6.19)$$

$$\frac{\delta L_{da}}{L_{da}} = \left[ -\frac{1}{\sqrt{1 + \frac{4kE}{U^2}}} + \frac{1}{\left(1 + \frac{4kE}{U^2}\right) \ln \left(\frac{\bar{C}U}{m} \sqrt{1 + \frac{4kE}{U^2}}\right)} \right] \frac{\delta U}{U} \quad (6.20)$$

As the value of the logarithm is always negative and usually large in magnitude (because  $\bar{C} \ll \frac{m}{\sqrt{4kE+U^2}} = C_o$  for the analysis to have some meaning), Equations (6.19) and (6.20) indicate that  $L_{da}$  is less sensitive to  $E$  and  $U$  than  $L_{dr}$ . Another non-dimensional parameter enters here, namely  $\bar{C}U/m$ . A very small value of  $\bar{C}U/m$ , associated with a low prescribed level  $\bar{C}$ , makes (6.19) and (6.20) approach (6.15) and (6.16), respectively.

The sensitivity results obtained in this section for the case of a continuous injection are summarized in Table 6.2 and presented graphically in Figure 6.3.

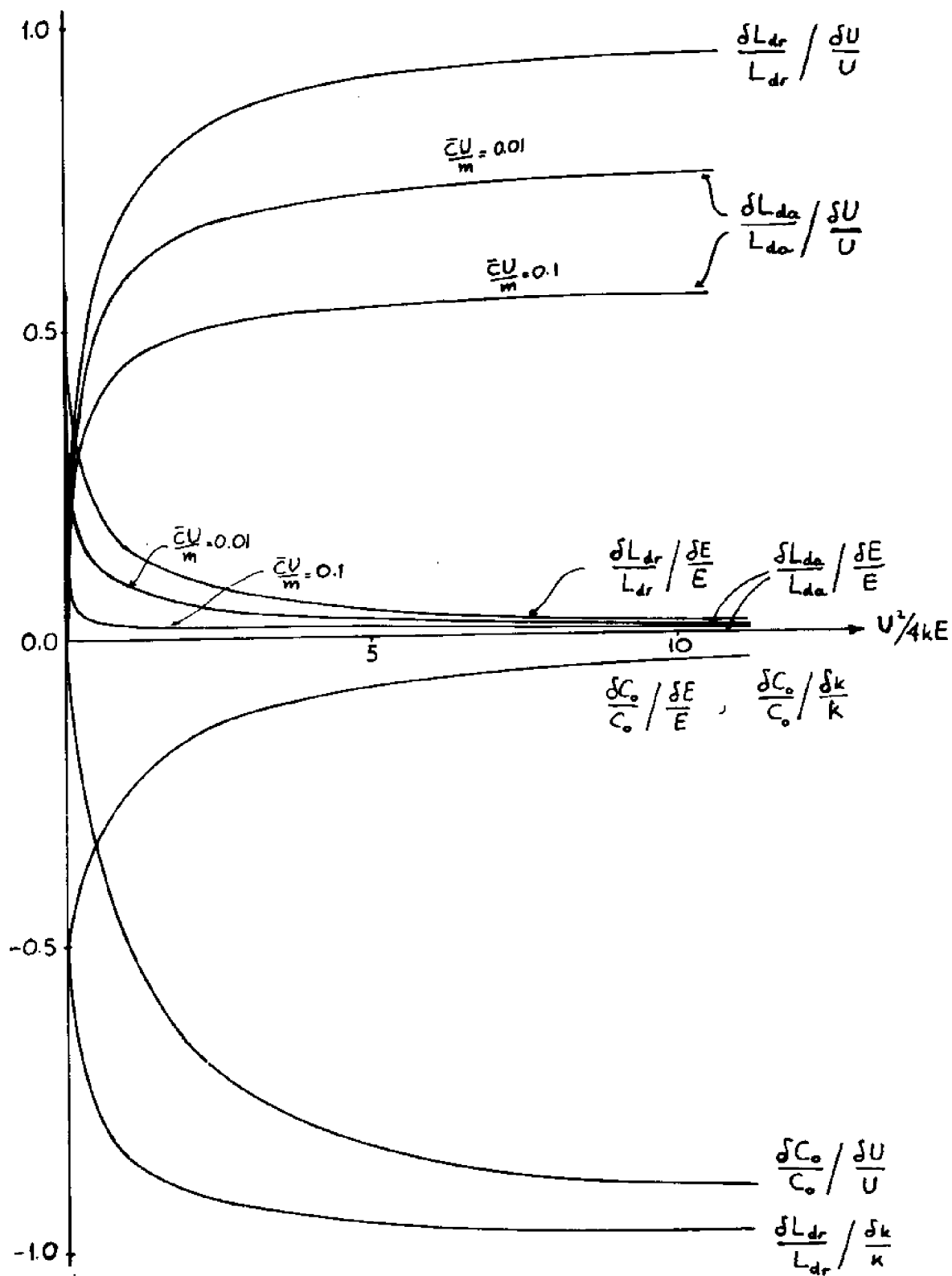


Figure 6.3 Sensitivity Curves for 1-D Continuous Source

## 6.2 Two-Dimensional One-Layer Flow

### 6.2.1 Instantaneous Source

The concentration distribution for an instantaneous source of strength  $M$  in a two-dimensional flow field is given by:

$$C = \frac{M}{\sqrt{4\pi E_x t} \sqrt{4\pi E_y t}} \exp\left[-\frac{(x-Ut)^2}{4E_x t} - \frac{(y-Vt)^2}{4E_y t} - kt\right] \quad (6.21)$$

The peak concentration at time  $t$  is located at  $(x=Ut, y=Vt)$  and has a magnitude, under isotropic conditions ( $E_x = E_y = E$ ) of:

$$C_o = \frac{M}{4\pi E t} \exp(-kt) \quad (6.22)$$

It is seen that  $C_o$  is independent of the velocity, which, nevertheless, defines its location, as in the one-dimensional case. The distribution is symmetrical around the peak (Figure 6.4) and can be expressed as:

$$C = C_o \exp\left(-\frac{r^2}{4Et}\right) \quad (6.23)$$

where  $r=0$  refers to  $(x = Ut, y = Vt)$ . The radius at which the concentration drops to a certain fraction  $\beta$  of the peak is then determined by

$$R_r = \sqrt{4Et \ln \frac{1}{\beta}} \quad (6.24)$$

which is similar to (6.4). Partial differentiation of (6.22) and (6.24) with respect to  $E$  and  $k$  reveals the sensitivity of the peak and the cloud radius to these parameters, as tabulated in Table 6.3.

Table 6.3

Parameter Sensitivity for 2-D Instantaneous Injection

Quantity Y	Y =	$\frac{\delta Y}{Y} / \frac{\delta E}{E}$	$\frac{\delta Y}{Y} / \frac{\delta k}{k}$
$C_o$	$\frac{M}{4\pi Et} \exp(-kt)$	-1	-kt
$R_r$	$\sqrt{4Et \ln \frac{1}{\beta}}$	$\frac{1}{2}$	0
$\max R_a$	$\sqrt{4Et^*(1 + kt^*)}$	$\frac{1}{2} \frac{kt^*}{1 + kt^*}$	$-\frac{1}{2} \frac{kt^*}{1 + kt^*}$

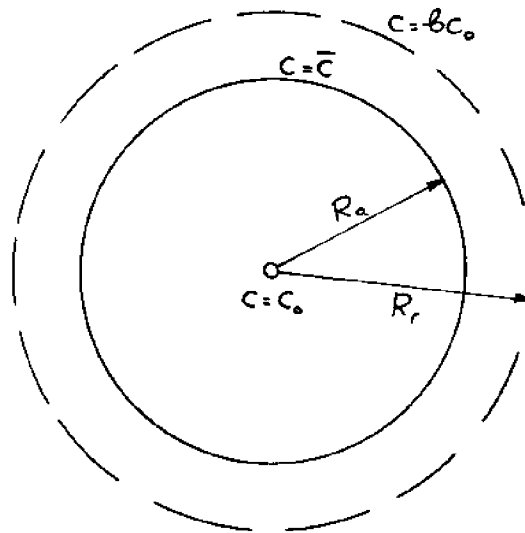
Note:  $t^*$  is given by Equation (6.26)

Figure 6.4 Typical Distribution after an Instantaneous Injection in a 2-D Domain

The radius at which the concentration drops to a prescribed value  $\bar{C}$  ( $< C_0$ ) can be found from:

$$\bar{C} = \frac{M}{4\pi Et} \exp\left(-\frac{R_a^2}{4Et} - kt\right)$$

i.e.

$$R_a = \sqrt{4Et\left(\ln \frac{M}{4\pi Et\bar{C}} - kt\right)} \quad (6.25)$$

To find the maximum area which will be subjected to concentrations higher than  $\bar{C}$ , partial differentiation with respect to time is used, as in Sec. 6.1.1. The corresponding time has to satisfy the following equation:

$$\ln \frac{M}{4\pi Et\bar{C}} = 1 + 2kt \quad (6.26)$$

which has to be solved, in general, by a trial and error procedure.

In the case of no decay, Equation (6.26) is simplified to:

$$t\big|_{\max} = \frac{M}{4\pi eE\bar{C}} \quad (6.26a)$$

Substitution in (6.25) yields

$$\max R_a = \sqrt{\frac{M}{\pi e\bar{C}}}$$

and consequently the maximum area is

$$\max A = \pi \cdot \max R_a^2 = \frac{M}{e\bar{C}} \quad (6.27)$$



This is independent of any of the flow characteristics and depends only on the source strength and the choice of  $\bar{C}$ . Of course, the dispersion coefficient controls the time to max A, according to (6.26a), while the location of the cloud at that time is determined by the flow velocity. In a time-varying flow field the average velocity during the time given by (6.26a) can be used. Incidentally, solving (6.27) for  $\bar{C}$  and substituting in (6.25) allows determination of the dispersion coefficient; this method has been used in conjunction with observations of the visible radius of smoke puffs in the atmosphere (64).

To determine the sensitivity of  $R_a$  at any time, one obtains from Eq. (6.25):

$$\frac{\delta R_a}{R_a} = \frac{1}{2} \left( 1 - \frac{1}{\ln \frac{M}{4\pi Et \bar{C}} - kt} \right) \frac{\delta E}{E} \quad (6.28)$$

and

$$\frac{\delta R_a}{R_a} = - \frac{1}{2} \frac{kt}{(\ln \frac{M}{4\pi Et \bar{C}}) - kt} \frac{\delta k}{k} \quad (6.29)$$

At the time of max  $R_a$ , Equation (6.26) holds. Then, the above expressions are simplified as follows:

$$\frac{\delta R_{a,\max}}{R_{a,\max}} = \frac{1}{2} \frac{kt}{1+kt} \frac{\delta E}{E} \quad (10.28a)$$

$$\frac{\delta R_{a,\max}}{R_{a,\max}} = - \frac{1}{2} \frac{kt}{1+kt} \frac{\delta k}{k} \quad (10.29a)$$

The results of this section are summarized in Table 6.3.

### 6.2.2 Continuous Source

The solution for a continuous source of strength  $m$ , assuming the flow is along the  $x$ -axis and neglecting the contribution of longitudinal dispersion, is (26):

$$C = \frac{m}{\sqrt{4\pi EUx}} \exp\left(-\frac{y^2 U}{4Ex} - \frac{kx}{U}\right) \quad (6.30)$$

valid for  $x > 0$ .

At the origin, the value of  $C$  is infinite, and hence there will be no attempt to examine the peak concentration in this case. Moreover, no "relative" dimensions of the plume can be defined here.

Obviously, the shape of the plume will be elongated along the  $x$ -axis, even under isotropic dispersion (Figure 6.5). The "absolute" length of the plume  $L$ , where  $C = \bar{C}$ , can be found after taking into consideration that the furthest point longitudinally will lie on the  $x$ -axis, having  $y = 0$ . Equation (6.30) then yields:

$$\bar{C} = \frac{m}{\sqrt{4\pi EU L}} \exp\left(-\frac{kL}{U}\right)$$

i.e.

$$\frac{kL}{U} = \ln \frac{m}{\bar{C} \sqrt{4\pi EU L}} \quad (6.31)$$

In the special case of no decay, this can be solved for  $L$  directly, giving

Table 6.4

Parameter Sensitivity for 2-D Continuous Source

Quantity $Y$	$Y =$	$\frac{\delta Y}{Y} / \frac{\delta E}{E}$	$\frac{\delta Y}{Y} / \frac{\delta U}{U}$	$\frac{\delta Y}{Y} / \frac{\delta k}{k}$
$L$	Eq. (6.31)	$-\frac{1}{1+2\sigma}$	$\frac{2\sigma-1}{2\sigma+1}$	$-\frac{2\sigma}{1+2\sigma}$
$W$	Eq. (6.37)	$\frac{\lambda\sigma}{1+2\lambda\sigma}$	$-\frac{1}{1+2\lambda\sigma}$	$-\frac{\lambda\sigma}{1+2\lambda\sigma}$

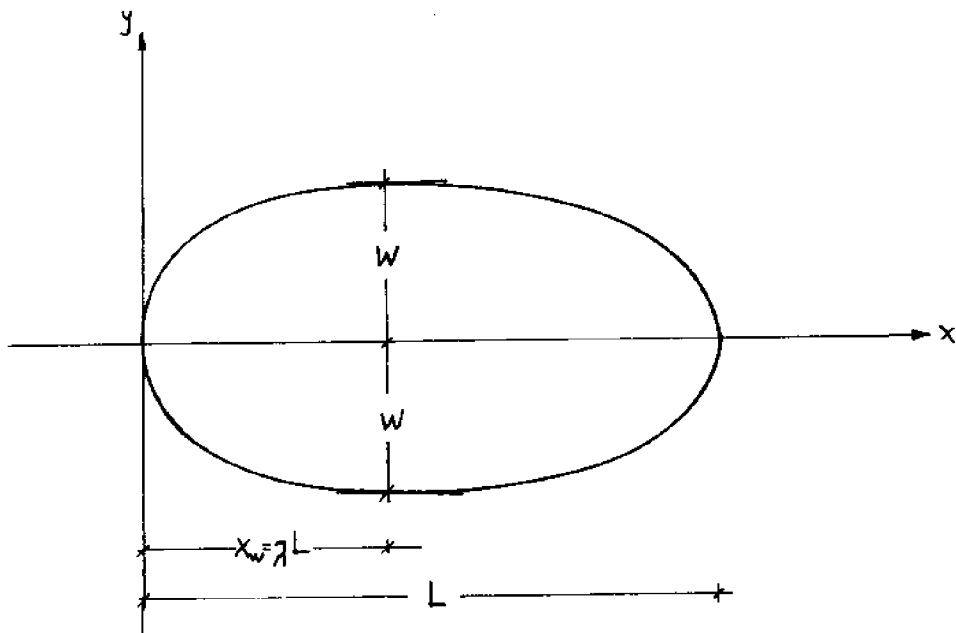
Note:  $\sigma = kL/U$  ;  $\lambda$  is given by (6.36)

Figure 6.5 Typical Steady State Distribution for a Continuous Source in a 2-D Domain

$$L = \frac{\bar{m}^2}{4\pi EU\bar{C}^2} \quad (6.31a)$$

but, in general, Equation (6.31) requires a trial and error solution. Even when  $L$  is not available explicitly, its sensitivity to the various parameters can be determined by differentiating (6.31), rewritten in the more convenient form:

$$\ln \frac{\bar{C}\sqrt{4\pi EU}}{\bar{m}} + \ln\sqrt{L} + \frac{kL}{U} = 0$$

After some algebraic manipulations, one obtains:

$$\frac{\delta L}{L} = \frac{\frac{2kL}{U} - 1}{\frac{2kL}{U} + 1} \frac{\delta U}{U} \quad (6.32)$$

$$\frac{\delta L}{L} = - \frac{1}{1 + \frac{2kL}{U}} \frac{\delta E}{E} \quad (6.33)$$

$$\frac{\delta L}{L} = - \frac{\frac{2kL}{U}}{1 + \frac{2kL}{U}} \frac{\delta k}{k} \quad (6.34)$$

It is seen that the only parameter controlling the sensitivity of the plume length is  $kL/U$ . For any particular problem, this is known, after  $L$  has been determined from (6.31). A small value of  $kL/U$  indicates high sensitivity of  $L$  to the dispersion coefficient

and low sensitivity to decay, while the opposite is implied by a large  $kL/U$ . It is worth noticing that, unlike the 1-D case, an increase in dispersion results, according to (6.33), in a decrease in the plume length, due to higher lateral spreading. An unusual behavior is indicated by (6.32): the coefficient of  $\frac{\delta U}{U}$  becomes zero at  $2kL/U = 1$  and negative when  $2kL/U$  drops below unity. Thus, if  $0 < 2kL/U < 1$ , the plume length tends to decrease with increasing velocity. The behavior of (6.32) to (6.34) over the range of values of  $kL/U$  is shown in Fig. 6.6.

In addition to the max length of the plume, its maximum width is also of interest. Denoting that by  $W$  (Figure 6.5), it will be

$$\bar{C} = \frac{m}{\sqrt{4\pi EUx_w}} \exp\left[-\frac{W^2 U}{4Ex_w} - \frac{kx_w}{U}\right]$$

However,  $x_w$  is yet unknown. Setting  $x_w = \lambda L$  and solving the equation for  $W$ :

$$W^2 = \frac{4E\lambda L}{U} \left( \ln \frac{m}{\bar{C}\sqrt{4\pi EU\lambda L}} - \frac{k\lambda L}{U} \right)$$

Using Equation (6.31), we obtain further:

$$W^2 = \frac{4EL\lambda}{U} \left[ (1-\lambda) \frac{kL}{U} - \ln\sqrt{\lambda} \right] \quad (6.35)$$

The value of  $\lambda$  can be determined from the condition that  $\frac{\partial W}{\partial \lambda} = 0$ .

This implies

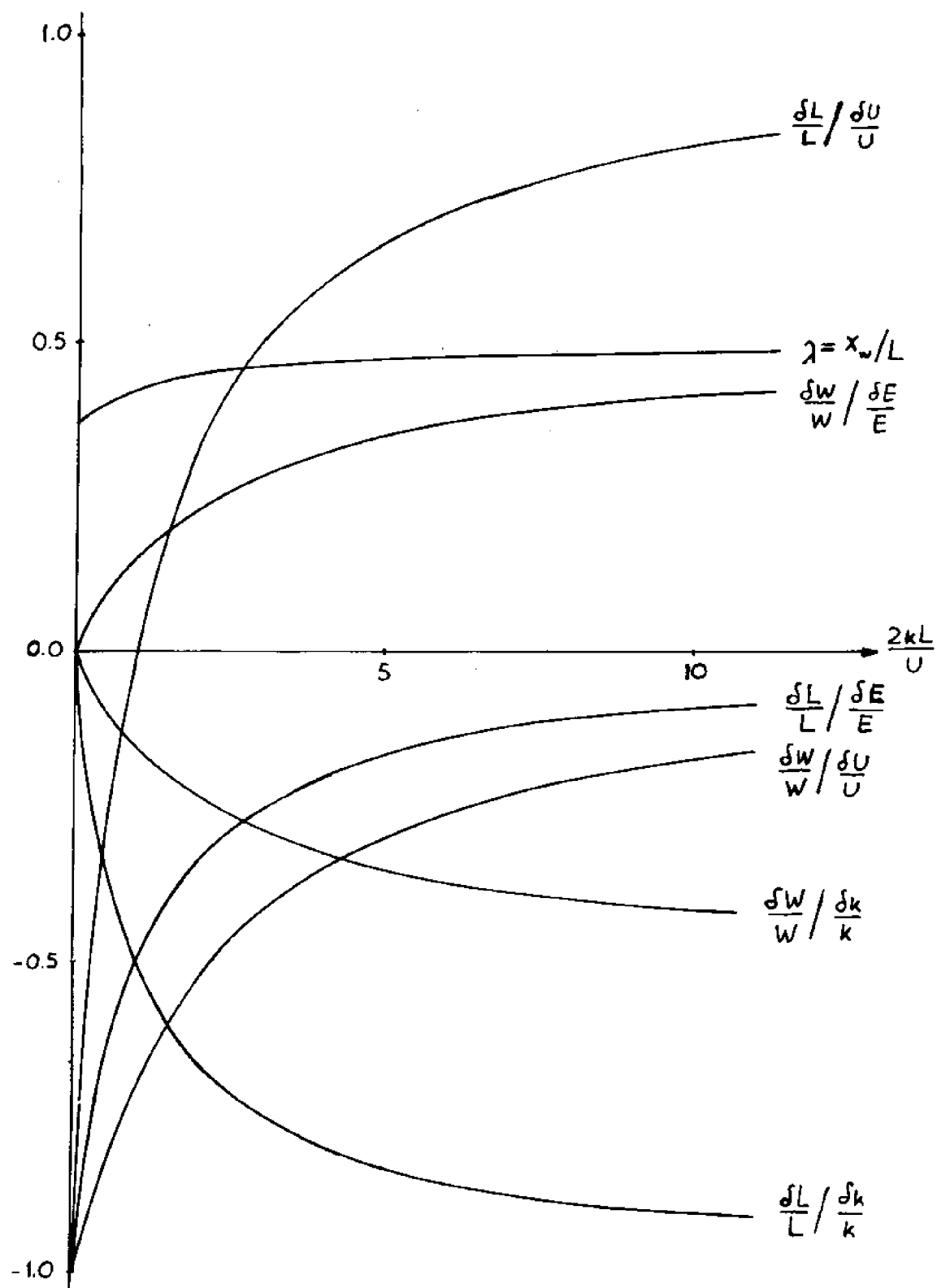


Figure 6.6 Sensitivity Curves for 2-D Continuous Source

$$\ln\sqrt{\lambda} = \frac{kL}{U}(1-2\lambda) - \frac{1}{2} ; \quad 0 < \lambda < 1 \quad (6.36)$$

This can be solved by trial and error and will obviously give  $\lambda$  as a function of  $kL/U$  only, i.e.,  $\lambda = \lambda(kL/U)$ . Rewriting (6.36) as

$$1 - 2\lambda = \frac{\ln\sqrt{\lambda} + \frac{1}{2}}{\frac{kL}{U}}$$

it is clear that, as  $kL/U$  becomes large,  $\lambda$  tends to  $1/2$ . On the other extreme, Equation (10.36) shows that, for  $kL/U = 0$ ,  $\lambda = 1/e = 0.368$ . The variation of  $\lambda$ , as shown in Figure (6.6) is found to be very small over the range of values of  $kL/U$ . Eliminating  $\ln\sqrt{\lambda}$  between (6.35) and (6.36):

$$W^2 = \frac{2EL\lambda}{U} \left( 2\lambda \frac{kL}{U} + 1 \right) \quad (6.37)$$

To examine the sensitivity of the width  $W$  to the parameters of the problem, it will be assumed for simplification that  $\lambda \approx \text{constant}$  and only the variability of  $L$  will be taken into account.

In view of the very small variability of  $\lambda$  discussed above, this is a good approximation, especially for  $kL/U > 1$ , when  $\lambda$  is essentially equal to  $1/2$ .

By partially differentiating (6.37) with respect to  $E$ ,  $U$ ,  $k$  and using Equations (6.32), (6.33) and (6.34) for the derivatives of  $L$ , we obtain

$$\frac{\delta W}{W} = - \frac{1}{1 + \lambda \frac{2kL}{U}} \frac{\delta U}{U} \quad (6.38)$$

$$\frac{\delta W}{W} = \frac{\lambda \frac{kL}{U}}{1 + \lambda \frac{2kL}{U}} \frac{\delta E}{E} \quad (6.39)$$

$$\frac{\delta W}{W} = - \frac{\lambda \frac{kL}{U}}{1 + \lambda \frac{2kL}{U}} \frac{\delta k}{k} \quad (6.40)$$

These expressions show that, again, the non-dimensional ratio  $kL/U$  controls the sensitivity of  $W$ , in addition to that of  $L$ . In the above formulas either the exact value of  $\lambda$  for a particular  $kL/U$ , obtained from (6.36), or simply the value  $\lambda = 1/2$  can be used. The sensitivity behavior of the width  $W$  for various  $kL/U$  is also shown in Figure 6.6. At large values of  $kL/U$  the width becomes insensitive to the velocity magnitude, while it is moderately sensitive to both the dispersion and the decay coefficient. On the contrary, at small values of  $kL/U$  the width is highly sensitive to the velocity but not to the other parameters.

The results of this section are summarized in Table 6.4.



### 6.3 Two-Layer Flow

Having examined the sensitivity of the solution in the one-layer case, this section will focus primarily on determining the sensitivity of the results in two-layer systems to variations in the magnitude of interfacial transport as well as identifying possible differences from the behavior of one-layer systems. Since analytical solutions are available only under very simple flow conditions (see Chapter 5), the analysis will be necessarily restricted to those cases, with the expectation that the basic conclusions will hold in more general situations. In the following sections the main parameter of interest will be the interfacial diffusion coefficient  $\alpha'$ . All two-layer results are summarized in Table 6.5.

#### 6.3.1 1-D Instantaneous Source

When the top layer is loaded with an amount  $M$  and the interfacial transport is small, the approximate transient solution, developed in Section 5.1, is:

$$C_1 \approx \frac{M}{\sqrt{4\pi Et}} \exp\left[-\frac{(x-U_1 t)^2}{4Et} - (\alpha' + k)t\right] \quad (6.41)$$

$$C_2 \approx \frac{\alpha' M}{2(U_1 + U_2)} \exp[-(\alpha' + k)t] \left[ \operatorname{erf} \frac{x+U_2 t}{\sqrt{4Et}} - \operatorname{erf} \frac{x-U_1 t}{\sqrt{4Et}} \right] \quad (6.42)$$

valid for

$$t < 0.05/\alpha' \quad (6.43)$$

The top layer concentration,  $C_1$ , behaves as in a single layer, with

some additional loss through the interface. The peak concentration in the bottom layer occurs at  $x=(U_1-U_2)t/2$  and is equal to

$$C_{20} = \frac{\alpha' M}{U_1 + U_2} \exp[-(\alpha' + k)t] \operatorname{erf} \frac{(U_1 + U_2)t}{2\sqrt{4Et}} \quad (6.44)$$

Partial differentiation with respect to  $\alpha'$  yields:

$$\frac{\delta C_{20}}{C_{20}} = (1 - \alpha't) \frac{\delta \alpha'}{\alpha'} \quad (6.45)$$

Equation (6.45) indicates that the sensitivity of  $C_{20}$  to  $\alpha'$  is highest at  $t=0$  and decreases with time. Due to the restriction (6.43), the coefficient of  $\delta \alpha'/\alpha'$  in (6.45) stays above 0.95 for the time range of validity of the approximate solution. On the contrary, the respective change in the peak top layer concentration

$$C_{10} = \frac{M}{\sqrt{4\pi Et}} \exp[-(\alpha' + k)t]$$

with respect to  $\alpha'$  is given by

$$\frac{\delta C_{10}}{C_{10}} = -\alpha't \frac{\delta \alpha'}{\alpha'} \quad (6.46)$$

This is quite small, since  $\alpha't < 0.05$ . Indeed, the small-time approximation of Section 5.1 is based on the assumption that interfacial mixing affects  $C_1$  very little.

For the small times for which (6.44) is valid, a further approximation may be made by setting  $\operatorname{erf} y = 2y/\sqrt{\pi}$ . Then

$$C_{20} \approx \alpha' M \sqrt{\frac{t}{\pi E}} \exp[-(\alpha' + k)t]$$

and consequently,

$$\frac{\delta C_{20}}{C_{20}} = - \frac{1}{2} \frac{\delta E}{E} \quad (6.47)$$

It follows that the bottom layer peak is moderately sensitive to the dispersion coefficient but independent of the velocity magnitudes.

To find the length of the plume in the bottom layer, having  $C_2 \geq \bar{C}$ , the equation

$$\frac{\alpha M}{U} \exp[-(\alpha+k)t] \left[ \operatorname{erf}\left(\frac{L+Ut}{\sqrt{4Et}}\right) - \operatorname{erf}\left(\frac{L-Ut}{\sqrt{4Et}}\right) \right] = \bar{C}$$

has to be solved by trial and error. However, at least for small times,  $C_2 \ll C_1$  and therefore there is no point in pursuing further the examination of the extent of contamination in the bottom layer in this case.

### 6.3.2 1-D Continuous Source

The steady state solution for a continuous source of strength  $m$  at  $x=0$  in the top layer has been given in Section 5.2. The resulting expressions for  $C_1$  and  $C_2$  are rather complicated and an analytical sensitivity analysis will not be attempted here. Nevertheless, the final distribution of mass between the layers can be easily examined. According to Section 5.2, the mass in the top layer is

$$M_1 = \frac{(\alpha' + k)m}{k(2\alpha' + k)} \quad (6.48)$$

while in the bottom layer

$$M_2 = \frac{\alpha' m}{k(2\alpha' + k)} \quad (6.49)$$

To determine the sensitivity of this mass breakdown to the value of  $\alpha'$ , one has to employ partial differentiation to the above expressions. The results are:

$$\frac{\delta M_1}{M_1} = - \frac{\frac{\alpha'}{k}}{(1 + \frac{\alpha'}{k})(1 + 2\frac{\alpha'}{k})} \frac{\delta \alpha'}{\alpha'} \quad (6.50)$$

$$\frac{\delta M_2}{M_2} = \frac{1}{1 + 2\frac{\alpha'}{k}} \frac{\delta \alpha'}{\alpha'} \quad (6.51)$$

It is seen that the ratio of interfacial diffusion to decay is the controlling non-dimensional parameter. As that ratio increases,  $M_2$  tends to become insensitive to changes in  $\alpha'$ . However,  $M_1$  is insensitive to the interfacial transport rate at either very small or very large values of  $\alpha'/k$ . The highest sensitivity of  $M_1$  is attained at  $\alpha'/k = 1/\sqrt{2}$ , corresponding to

$$\frac{\delta M_1}{M_1} = -0.172 \frac{\delta \alpha'}{\alpha'}$$

which is still rather low.

Looking now at the ratio  $M_2/M_1$ , given by

$$\frac{M_2}{M_1} = \frac{\alpha'}{\alpha' + k} \quad (6.52)$$

one obtains

$$\frac{\delta(M_2/M_1)}{M_2/M_1} = \frac{1}{1 + \frac{\alpha'}{k}} \frac{\delta\alpha'}{\alpha'} \quad (6.53)$$

This further confirms that the distribution of the constituent between the two layers is not sensitive to the interfacial transport rate, provided this is at least moderately higher than the decay rate. In the case of a very low value of  $\alpha'/k$ , however, the overall mass distribution becomes highly sensitive to the value of the interfacial diffusion rate; this is due to the sensitivity of  $M_2$ , i.e., the mass of the bottom layer, which is all gained through the interface. The behavior of Equations (6.50), (6.51) and (6.53) is shown in Figure 6.7.

### 6.3.3 2-D Continuous Source

The approximate steady-state solution for a continuous source in the top layer of a counterflow is given in Section 5.3. For the top layer the solution is essentially the same as for a single layer and the conclusions of Section 6.2.2 apply. The bottom layer concentration along the x-axis is given by:

$$C_2 = \frac{\alpha' m}{4U\sqrt{E(\alpha' + k)}} \operatorname{erfc}\left(\sqrt{\frac{\alpha' + k}{U}} |x|\right); y=0 \quad (6.54)$$

The peak concentration, at  $(x=0, y=0)$  is

$$C_{20} = \frac{\alpha' m}{4U\sqrt{E(\alpha' + k)}} \quad (6.55)$$

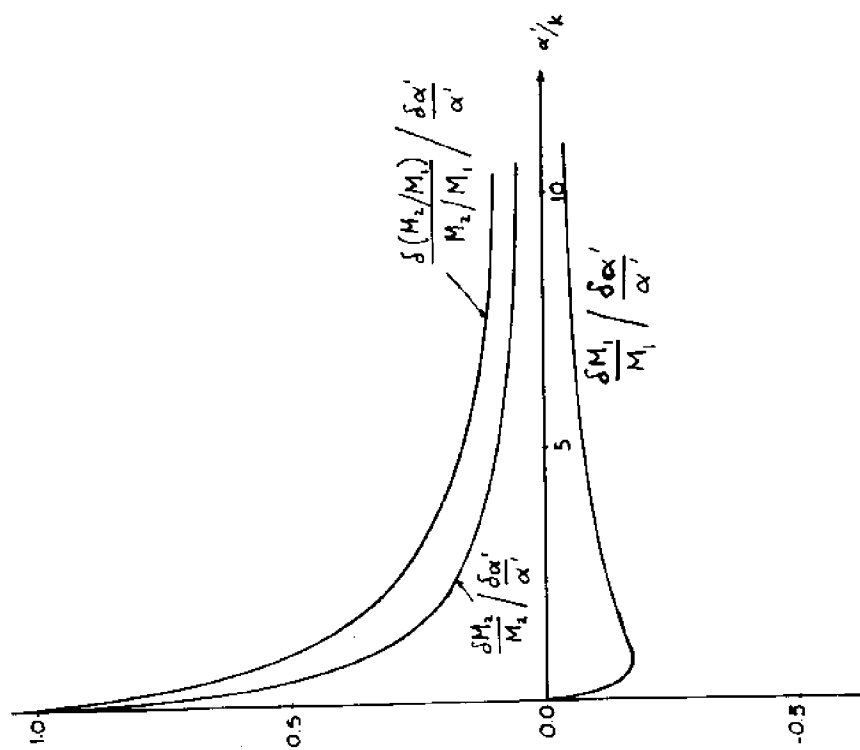


Figure 6.7 Sensitivity Curves for a Continuous Source in a 2-Layer 1-D Counterflow

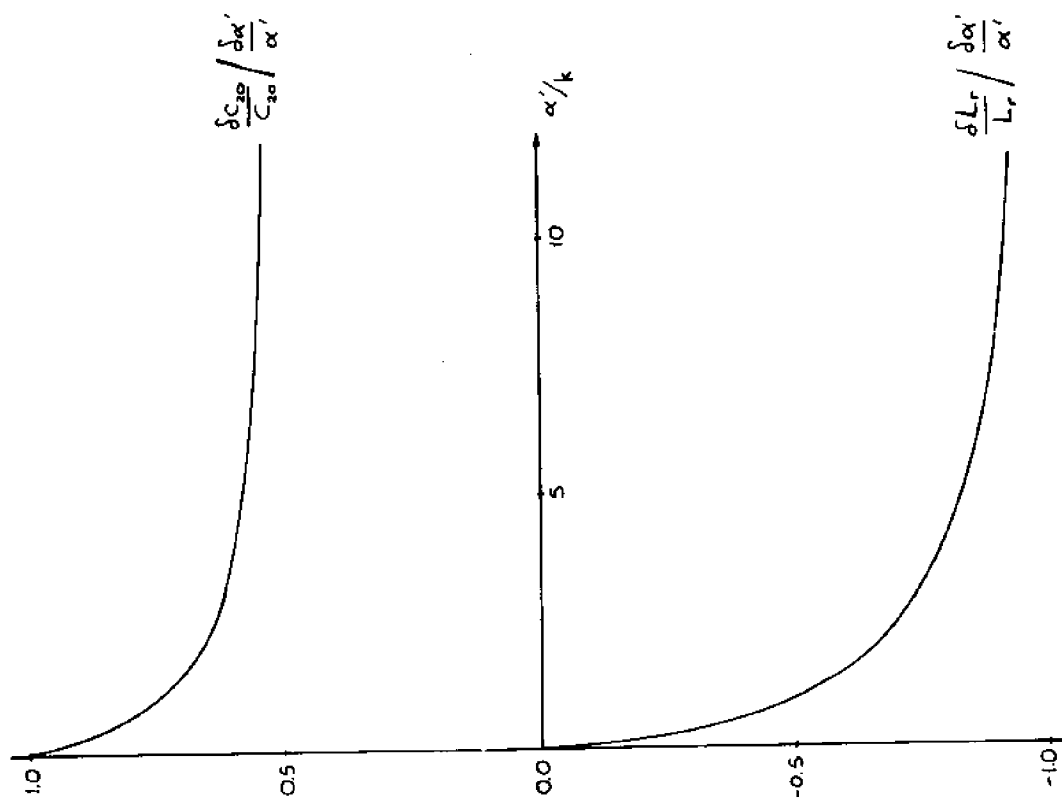


Figure 6.8 Sensitivity Curves for a Continuous Source in a 2-Layer 2-D Counterflow

From (6.55)

$$\frac{\delta C_{20}}{C_{20}} = \frac{1}{2} \frac{2 + \frac{\alpha'}{k}}{1 + \frac{\alpha'}{k}} \frac{\delta \alpha'}{\alpha'} \quad (6.56)$$

This indicates a considerable sensitivity of the lower layer peak to interfacial diffusion for both small or large values of  $\alpha'/k$ , the coefficient of  $\delta \alpha'/\alpha'$  tending to 1 and 1/2, respectively. The detailed behavior of (6.56) is presented in Figure 6.8.

The "relative" half-length of the (symmetrical about  $x=0$ ) plume can be found from

$$\beta C_{20} = C_{20} \operatorname{erfc}\left(\sqrt{\frac{\alpha' + k}{U}} L_r\right)$$

i.e.,

$$\operatorname{erfc}\left(\sqrt{\frac{\alpha' + k}{U}} L_r\right) = \beta \quad (6.57)$$

with the help of tables of the error function, once the parameters of the problem and  $\beta$  are known. For a fixed  $\beta$ , the argument of the error function is also fixed, say  $\beta^*$ . Therefore,

$$L_r = \frac{U}{\alpha' + k} \beta^{*2} \quad (6.58)$$

Differentiating with respect to  $\alpha'$ ,

$$\frac{\delta L_r}{L_r} = - \frac{\frac{\alpha'}{k}}{1 + \frac{\alpha'}{k}} \frac{\delta \alpha'}{\alpha'} \quad (6.59)$$

As shown in Figure 6.8, the length of the plume is quite sensitive

to  $\alpha'$  for large values of  $\alpha'/k$ , but not for  $\alpha'/k \ll 1$ .

The above results as well as the sensitivity of  $C_{20}$  and  $L_r$  to the velocity and dispersion coefficient are summarized in Table 6.5. Elaboration in determining the plume width from the general expression of  $C_2$  given in Section 5.3 is not justified in view of the very approximate nature of that expression and the restriction of its validity to a narrow range of  $y$  only.

In concluding this chapter, some important points should be emphasized. Firstly, as the previous analysis has indicated, the significance of the various parameters in determining the peak concentration and the dimensions of the area affected by a pollutant source depends on the problem (i.e., continuous or instantaneous, 1-D or 2-D, etc.). Within each class of problems there is a non-dimensional combination of the parameters which governs the behavior of the above mentioned plume measures. In particular, in two-layer steady state problems the ratio of interfacial diffusion to decay rate is of basic importance, with respect to concentrations in the layer with no source.

In most cases, the dispersion coefficient seems to be less critical to the results than the velocity magnitude. In a complex circulation field the velocity direction must also be of importance, controlling the direction of motion of the plume, on the average. In this context, the advantage of the two-layer formulation is the more detailed description of the velocity field. A relevant question is, of course, that of the uncertainty of the velocity



Table 6.5

## Parameter Sensitivity in Two-Layer Systems

Case	Quantity $Y$	$Y =$	$\frac{\delta Y}{Y} / \frac{\delta \alpha'}{\alpha'}$	$\frac{\delta Y}{Y} / \frac{\delta E}{E}$	$\frac{\delta Y}{Y} / \frac{\delta U}{U}$
1-D Instantaneous	$C_{20}$	Eq. (6.44)	$1 - \alpha' t$	$\approx -\frac{1}{2}$	0
1-D Continuous	$M_1$	$\frac{(\alpha' + k)m}{k(2\alpha' + k)}$	$-\frac{\sigma}{(1+\sigma)(1+2\sigma)}$	0	0
	$M_2$	$\frac{\alpha' m}{k(2\alpha' + k)}$	$\frac{1}{1+2\sigma}$	0	0
	$M_2/M_1$	$\frac{\alpha'}{\alpha' + k}$	$\frac{1}{1+\sigma}$	0	0
2-D Continuous	$C_{20}$	$\frac{\alpha' m}{4U\sqrt{E(\alpha' + k)}}$	$\frac{1}{2} \frac{2+\sigma}{1+\sigma}$	$-\frac{1}{2}$	-1
	$L_r$	$\frac{U}{\alpha' + k} (\text{erfc}^{-1} \beta)^2$	$-\frac{\sigma}{1+\sigma}$	0	1

Note:  $\sigma = \alpha'/k$

field used. This has to be tracked to the circulation model or measurements used to provide the velocity inputs and is beyond the scope of the present work.

It should be clear that the conclusions reached on sensitivity strictly apply for marginal changes in the parameters only. A large change in any parameter may significantly change the value of the non-dimensional ratio controlling the sensitivity; nevertheless in regions where the sensitivity curves are leveled off, even the effect of large parameter changes can be readily predicted.

## CHAPTER 7

### THE FINITE ELEMENT FORMULATION

#### 7.1 The Weak Form

The governing equations (2.11, 2.14) for each layer have the following form:

$$\frac{\partial C}{\partial t} + \frac{\partial}{\partial x} (\bar{u}C) + \frac{\partial}{\partial y} (\bar{v}C) = - \frac{\partial}{\partial x} Q_x - \frac{\partial}{\partial y} Q_y + P \quad (7.1)$$

where

$$Q_x = -E_{xx} H \frac{\partial \bar{C}}{\partial x} - E_{xy} H \frac{\partial \bar{C}}{\partial y} \quad (7.1a)$$

$$Q_y = -E_{xy} H \frac{\partial \bar{C}}{\partial x} - E_{yy} H \frac{\partial \bar{C}}{\partial y} \quad (7.1b)$$

and P includes sources, decay and exchange between the layers. The boundary conditions are (Figure 7.1):

- i) Essential, i.e. the concentration is specified on the boundary segment  $S_c$ :

$$C = C^* \quad \text{on } S_c \quad (7.2a)$$

- ii) Natural, i.e. the normal concentration gradient or, equivalently, the normal dispersive flux is specified on the boundary segment  $S_q$ :

$$Q_n = Q_n^* \quad \text{on } S_q \quad (7.2b)$$

In seeking an approximate solution  $\hat{C}$ , the partial differential equation (7.1) along with the boundary condition (7.2b) are transformed to an

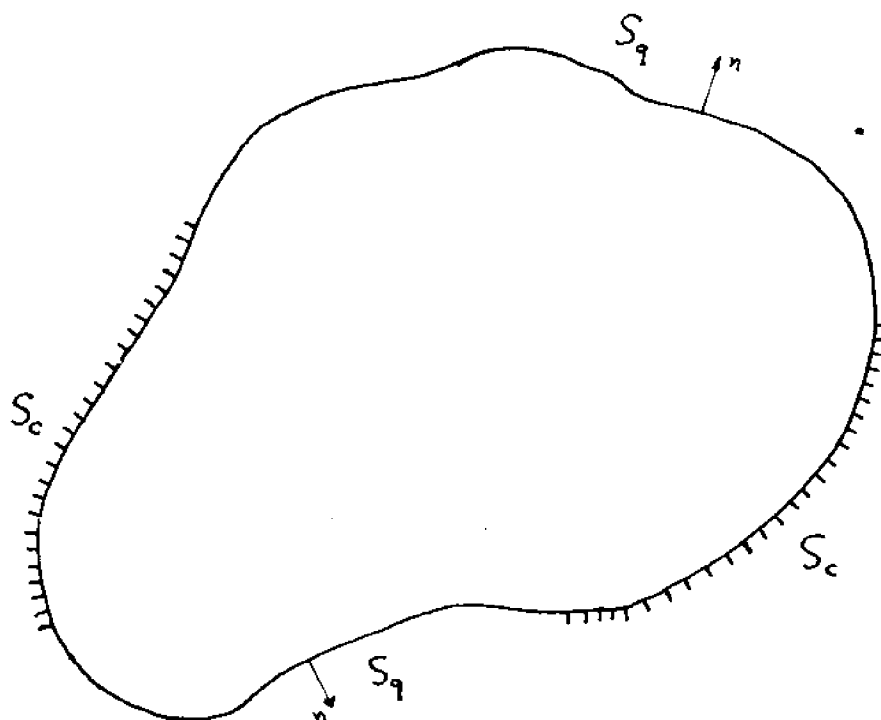


Figure 7.1 Solution Field and Boundary Conditions

integro-differential equation by multiplying with a weighting or test function  $W$ , integrating over the total domain, and requiring the resulting expression to vanish:

$$R = \iint_A \left\{ \frac{\partial \hat{C}}{\partial t} + \frac{\partial (\bar{u}\hat{C})}{\partial x} + \frac{\partial (\bar{v}\hat{C})}{\partial y} + \frac{\partial}{\partial x} Q_x + \frac{\partial}{\partial y} Q_y - P \right\} W dA + \int_{S_q} (Q_n^* - Q_n) W dS = 0 \quad (7.3)$$

The trial function  $\hat{C}$ , is required to satisfy the essential boundary condition (7.2a), and the weighting function to satisfy the homogeneous form, i.e.,  $W = 0$  on  $S_c$ .

Employing partial integration, i.e., writing

$$\left( \frac{\partial}{\partial x} Q_x \right) W = \frac{\partial}{\partial x} (Q_x W) - Q_x \frac{\partial W}{\partial x}$$

$$\left( \frac{\partial}{\partial y} Q_y \right) W = \frac{\partial}{\partial y} (Q_y W) - Q_y \frac{\partial W}{\partial y}$$

and applying Gauss' theorem,

$$\iint_A \left\{ \frac{\partial}{\partial x} (Q_x W) + \frac{\partial}{\partial y} (Q_y W) \right\} dA = \int_S Q_n W dS$$

Eq. (7.3) is transformed to

$$R = \iint_A \left[ \left\{ \frac{\partial \hat{C}}{\partial t} + \frac{\partial (\bar{u}\hat{C})}{\partial x} + \frac{\partial (\bar{v}\hat{C})}{\partial y} - P \right\} W - Q_x \frac{\partial W}{\partial x} - Q_y \frac{\partial W}{\partial y} \right] dA + \int_{S_q} Q_n^* W dS = 0 \quad (7.4)$$

Since Eq. (7.4) involves only first derivatives of  $C$ , the trial functions can be simple piecewise continuous functions, which require only continuity of the function itself within the domain. Also, since the equation involves only first derivatives of  $W$ , the test functions have the same requirement as the trial functions. Eq. (7.4) is called the "symmetrical weak form". Transforming (7.3) to (7.4) makes it easier to find a solution because simpler trial functions can be used. However, uniqueness of the solution is harder to prove. According to Wang and Connor (86), the symmetrical weak form is the optimum form, constituting a balance between existence and uniqueness of the solution, and allowing  $\hat{C}$  and  $W$  to be chosen from the same solution space. The application of the finite element method is thus facilitated.

In the finite element method, the domain is subdivided into smaller areas, called elements, and the total residual  $R$ , evaluated as the sum of the element residuals, is required to vanish:

$$R = \sum_e R^e = 0 \quad (7.5)$$

The solution variable, here the concentration  $C$ , is approximated in each element by a trial function, which interpolates between the concentrations at certain points in the element. Thus, the continuous problem is transformed into a discrete problem with the concentrations at these points as the unknowns. Depending on the form of the integral equation, the trial functions have to satisfy certain continuity conditions (13). The simplest element for a two-dimensional domain is the triangle. The admissibility of simple piecewise continuous trial (and test) functions allows

the use of linear interpolating functions within the triangles, resulting eventually in transformation of (7.3) to a set of ordinary differential equations with the values of concentration at the corners of the triangles as unknowns.

The finite element formulation for this simple case is outlined in the next section (see also Leimkuhler (43) ). Various other element shapes as well as interpolation functions can be used. A great advantage of the finite element method is that the basic formulation remains the same, irrespective of the specific type of approximation employed. Another basic advantage of the finite element method, a consequence of the division of the domain into individual elements, is the capability for easily handling spatial variability of properties or parameters. Finally, the finite element discretization is well suited for the description of irregular boundaries, common in coastal water bodies, and has great flexibility in providing variable spatial resolution, as may be desired.

## 7.2 The Finite Element Approximation

Using a local coordinate system for a triangle (Figure 7.2), the concentration expansion corresponding to a linear interpolation is written as

$$C = \xi_1 C_1 + \xi_2 C_2 + \xi_3 C_3$$

where

$$\xi_3 = 1 - \xi_1 - \xi_2$$

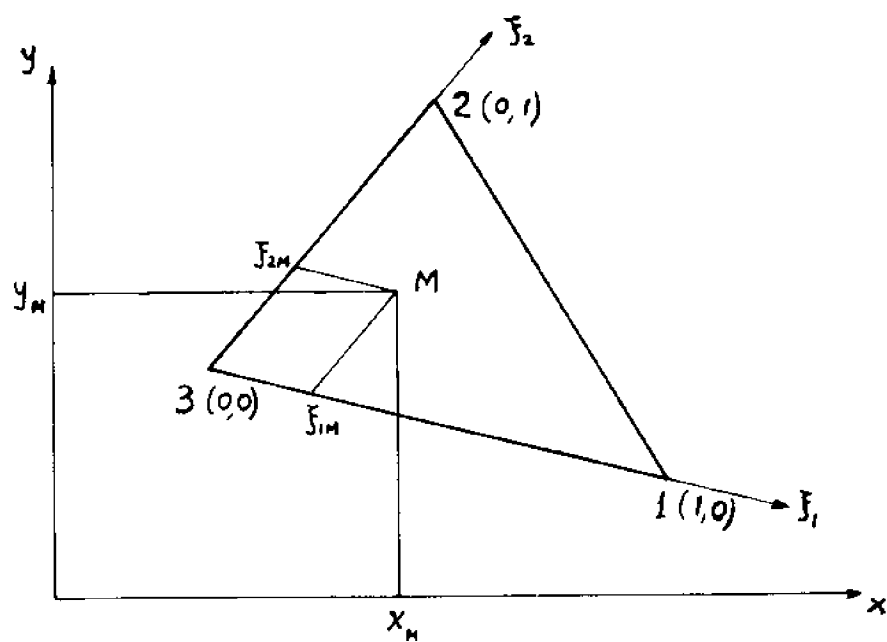


Figure 7.2 Local Element Coordinate System

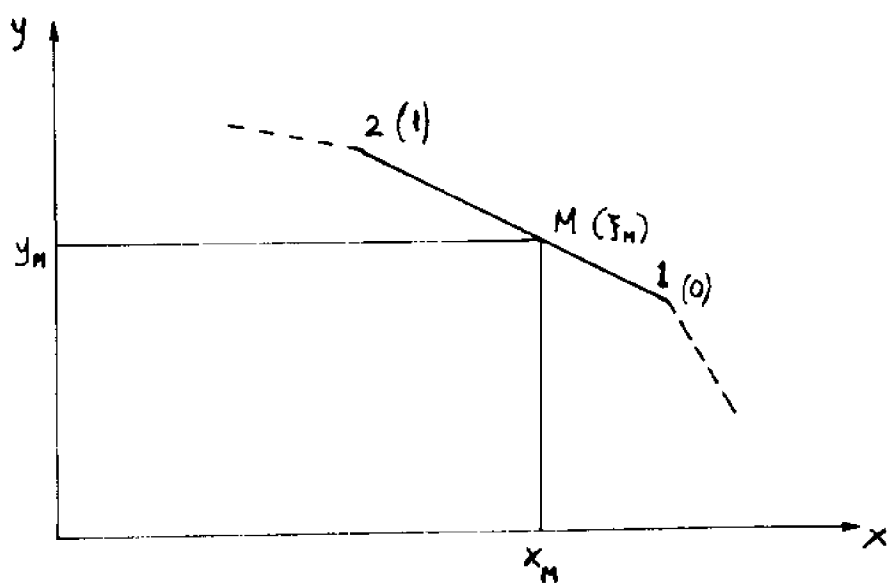


Figure 7.3 Local Boundary Segment Coordinate System



The matrix form is

$$C = \underset{\sim}{N} \underset{\sim}{C}^e \quad (7.6)$$

where

$$\underset{\sim}{N} = [ \xi_1 \quad \xi_2 \quad \xi_3 ]$$

and

$$\underset{\sim}{C}^e = \begin{bmatrix} c_1 \\ c_2 \\ c_3 \end{bmatrix}$$

the superscript (e) denoting element property throughout this chapter. The following relations hold between the local and global coordinates, provided the nodes are numbered counterclockwise (13,93):

$$\begin{aligned} \xi_1 &= \frac{1}{2A} (k_1 + b_1 x + a_1 y) \\ \xi_2 &= \frac{1}{2A} (k_2 + b_2 x + a_2 y) \\ \xi_3 &= 1 - \xi_1 - \xi_2 \end{aligned} \quad (7.7)$$

where

$$\begin{aligned} a_1 &= x_3 - x_2 & b_1 &= y_2 - y_3 \\ a_2 &= x_1 - x_3 & b_2 &= y_3 - y_1 \\ a_3 &= x_2 - x_1 & b_3 &= y_1 - y_2 \end{aligned} \quad (7.8)$$

and

$$A = \frac{1}{2} (b_1 a_2 - b_2 a_1) = \text{the area of the triangle} \quad (7.9)$$

while  $k_1, k_2$  are constants of no particular significance.

The boundary segments are handled similarly (Figure 7.3):

$$C_b = \xi_1 C_1 + \xi_2 C_2$$

or

$$C_b = \tilde{N}^b \tilde{C}^b$$

where

$$\tilde{N}^b = [\xi_1 \quad \xi_2]$$

$$\tilde{C}^b = \begin{bmatrix} C_1 \\ C_2 \end{bmatrix}$$

and

$$\xi_2 = 1 - \xi_1$$

For a fixed grid,  $\tilde{N}$  is invariant with time, while  $\tilde{C}^e$  is independent of space for a given element. Therefore, the derivatives of  $C$  can be expressed as

$$\begin{aligned} \frac{\partial C}{\partial t} &= \tilde{N} \frac{d\tilde{C}^e}{dt} \\ \frac{\partial C}{\partial x} &= \frac{\partial \tilde{N}}{\partial x} \tilde{C}^e \\ \frac{\partial C}{\partial y} &= \frac{\partial \tilde{N}}{\partial y} \tilde{C}^e \end{aligned} \tag{7.11}$$

The derivatives of  $\tilde{N}$  are found from (7.6),

$$\frac{\partial \tilde{N}}{\partial x} = \frac{1}{2A^e} [b_1 \ b_2 \ b_3] = \frac{1}{2A^e} b \quad (7.12)$$

$$\frac{\partial \tilde{N}}{\partial y} = \frac{1}{2A^e} [a_1 \ a_2 \ a_3] = \frac{1}{2A^e} a$$

These are special applications of the general chain-differentiation rule, through which the derivatives of an arbitrary function  $f$  can be expressed as:

$$\frac{\partial f}{\partial x} = \sum_{i=1}^3 \frac{\partial f}{\partial \xi_i} \frac{\partial \xi_i}{\partial x} = \frac{1}{2A^e} \sum_{i=1}^3 b_i \frac{\partial f}{\partial \xi_i} \quad (7.13)$$

$$\frac{\partial f}{\partial y} = \sum_{i=1}^3 \frac{\partial f}{\partial \xi_i} \frac{\partial \xi_i}{\partial y} = \frac{1}{2A^e} \sum_{i=1}^3 a_i \frac{\partial f}{\partial \xi_i}$$

The following integration formula (93) is useful

$$\int_{A^e} \xi_1^\lambda \xi_2^\mu \xi_3^\nu dA = \frac{\lambda! \mu! \nu!}{(\lambda + \mu + \nu + 2)!} 2A^e \quad (7.14)$$

For  $\lambda = \mu = 1, \nu = 0$ , this simplifies to:

$$\iint_{A^e} \xi_1 \xi_j dA = \frac{A^e}{12} (1 + \delta_{1j})$$

where  $\delta_{ij}$  the Kronecker delta  $\left\{ \begin{array}{ll} \delta_{ij} = 1 & \text{for } i = j \\ \delta_{ij} = 0 & \text{for } i \neq j \end{array} \right.$

The test function is taken to have the same form as the trial function.

In particular,

$$W = \Delta C = \tilde{N} \Delta C^e \quad (7.15)$$

Differentiation formulas similar to (7.11) apply for  $\Delta C$  as well.

Now substituting back in Eq. (7.4), the weighted residual for one element becomes

$$\begin{aligned} R^e = & \iint_{A^e} \left[ \tilde{N} \frac{dC^e}{dt} + \frac{\partial}{\partial x} (\bar{u}C) + \frac{\partial}{\partial y} (\bar{v}C) - P \right] \tilde{N} \Delta C^e - \\ & - \left( Q_x \frac{\partial \tilde{N}}{\partial x} + Q_y \frac{\partial \tilde{N}}{\partial y} \right) \Delta C^e \bigg] dA + \int_{S_q^e} Q_n^* \tilde{N} \Delta C^e dS \end{aligned}$$

or, by rearranging:

$$R^e = (\Delta C^e)^T (\tilde{M}^e \frac{dC^e}{dt} - \tilde{P}^e) + (\Delta C^e)^T \tilde{F}^{be} \quad (7.16)$$

where

$$\tilde{M}^e = \iint_{A^e} \tilde{N}^T \tilde{N} dA \quad (7.17a)$$

$$\tilde{P}^e = \iint_{A^e} \left[ \tilde{N}^T (P - \frac{\partial}{\partial x} (\bar{u}C) - \frac{\partial}{\partial y} (\bar{v}C) + \frac{\partial \tilde{N}^T}{\partial x} Q_x + \frac{\partial \tilde{N}^T}{\partial y} Q_y) \right] dA \quad (7.17b)$$

$$\tilde{F}^{be} = \int_{S_q^e} \tilde{N}^{bT} Q_n^* dS \quad (7.17c)$$

Of course, the boundary term enters only for elements that have a side on  $S_q$ .

The matrix  $\tilde{M}^e$  is time invariant and depends only on the geometry of the element. Using (7.14):

$$\begin{aligned}\tilde{M}^e &= \iint_{A^e} \tilde{N}^T \tilde{N} dA = \iint_{A^e} \begin{bmatrix} \xi_1 \\ \xi_2 \\ \xi_3 \end{bmatrix} [\xi_1 \ \xi_2 \ \xi_3] dA = \\ &= \frac{A^e}{12} \begin{bmatrix} 2 & 1 & 1 \\ 1 & 2 & 1 \\ 1 & 1 & 2 \end{bmatrix}\end{aligned}\quad (7.18)$$

The  $\tilde{P}^e$  vector includes the contributions of the advective, dispersion and source/sink terms. Using the approximations

$$\bar{u} = \tilde{N} \tilde{u}^e$$

$$C = \tilde{N} \tilde{C}^e$$

we obtain

$$\begin{aligned}\frac{\partial}{\partial x} (\bar{u}C) &= \frac{\partial \tilde{N}}{\partial x} \tilde{u}^e \tilde{N} \tilde{C}^e + \tilde{N} \tilde{u}^e \frac{\partial \tilde{N}}{\partial x} \tilde{C}^e \\ &= \tilde{N} \tilde{C}^e \frac{\partial \tilde{N}}{\partial x} \tilde{u}^e + \tilde{N} \tilde{u}^e \frac{\partial \tilde{N}}{\partial x} \tilde{C}^e\end{aligned}\quad (7.19)$$

Because  $\tilde{C}^e$ ,  $\tilde{u}^e$ ,  $\frac{\partial \tilde{N}}{\partial x}$  are independent of space,

$$\iint_{A^e} \tilde{N}^T \frac{\partial}{\partial x} (\bar{u}C) dA = \left( \iint_{A^e} \tilde{N}^T \tilde{N} dA \right) \tilde{C}^e \frac{\partial \tilde{N}}{\partial x} \tilde{u}^e + \left( \iint_{A^e} \tilde{N}^T \tilde{N} dA \right) \tilde{u}^e \frac{\partial \tilde{N}}{\partial x} \tilde{C}^e$$

Similarly

$$\iint_{A^e} \tilde{N}^T \frac{\partial}{\partial y} (\bar{v}C) dA = \left( \iint_{A^e} \tilde{N}^T \tilde{N} dA \right) \tilde{C}^e \frac{\partial \tilde{N}}{\partial y} \tilde{v}^e + \left( \iint_{A^e} \tilde{N}^T \tilde{N} dA \right) \tilde{v}^e \frac{\partial \tilde{N}}{\partial y} \tilde{C}^e$$

Hence, the contribution of the advective terms can be expressed as:

$$\begin{aligned}
 & - \iint_{A^e} \tilde{N}^T \left( \frac{\partial}{\partial x} (\bar{u}C) + \frac{\partial}{\partial y} (\bar{v}C) \right) dA = \\
 & = - \frac{1}{24} (\bar{b}\bar{u}^e + \bar{a}\bar{v}^e) \begin{bmatrix} 2 & 1 & 1 \\ 1 & 2 & 1 \\ 1 & 1 & 2 \end{bmatrix} \tilde{C}^e - \frac{1}{24} \begin{bmatrix} 2 & 1 & 1 \\ 1 & 2 & 1 \\ 1 & 1 & 2 \end{bmatrix} (\bar{u}^e\bar{b} + \bar{v}^e\bar{a}) \tilde{C}^e \\
 & = -\tilde{A}^e \tilde{C}^e \tag{7.20}
 \end{aligned}$$

Noting that  $\bar{b}\bar{u}^e + \bar{a}\bar{v}^e$  is a scalar, it is seen that the first part of the "advection" matrix  $\tilde{A}^e$  is symmetric, but vanishes under uniform flow conditions, since  $\sum b_i = \sum a_i = 0$ .

The contribution of the dispersion terms is given by:

$$\iint_{A^e} \left( \frac{\partial \tilde{N}^T}{\partial x} Q_x + \frac{\partial \tilde{N}^T}{\partial y} Q_y \right) dA = \frac{1}{2} (\bar{b}^T Q_x + \bar{a}^T Q_y) \tag{7.21}$$

where  $Q_x, Q_y$  are obtained by expanding (7.1a,b):

$$\begin{aligned}
 Q_x &= - \frac{E_{xx}}{2A^e} (\bar{b}\bar{C}^e - \frac{C}{H} \bar{b}\bar{H}^e) - \frac{E_{xy}}{2A^e} (\bar{a}\bar{C}^e - \frac{C}{H} \bar{a}\bar{H}^e) \\
 Q_y &= - \frac{E_{xy}}{2A^e} (\bar{b}\bar{C}^e - \frac{C}{H} \bar{b}\bar{H}^e) - \frac{E_{yy}}{2A^e} (\bar{a}\bar{C}^e - \frac{C}{H} \bar{a}\bar{H}^e)
 \end{aligned}$$

The dispersion coefficients are treated as an element property and assumed constant within each element. For simplicity, instead of expanding the ratio  $C/H$ , its average value over the element may be used, i.e.

$$\frac{C}{H} \approx \left(\frac{C}{H}\right)_{av} = \frac{1}{3} \sum_{i=1}^3 \frac{C_i}{H_i}$$

Thus, the dispersion term takes the form:

$$\begin{aligned} \frac{1}{2} (\tilde{b}^T Q_x + \tilde{a}^T Q_y) &= - \frac{1}{4A^e} (E_{xx} \tilde{b}^T \tilde{b} + E_{xy} \tilde{b}^T \tilde{a} + E_{xy} \tilde{a}^T \tilde{b} + E_{yy} \tilde{a}^T \tilde{a}) \tilde{C}^e \\ &+ \left(\frac{C}{H}\right)_{av} \frac{1}{4A^e} (E_{xx} \tilde{b}^T \tilde{b} + E_{xy} \tilde{b}^T \tilde{a} + E_{xy} \tilde{a}^T \tilde{b} + E_{yy} \tilde{a}^T \tilde{a}) \tilde{H}^e \\ &= - \tilde{K}^e \tilde{C}^e + \left(\frac{C}{H}\right)_{av} \tilde{K}^e \tilde{H}^e \end{aligned} \quad (7.22)$$

In the particular case that the layer thickness is constant over the domain,

$$\begin{aligned} \tilde{b}^T \tilde{b} \tilde{H}^e &= \tilde{b}^T (\tilde{b} \tilde{H}^e) = \tilde{b}^T (b_1 H + b_2 H + b_3 H) = 0 \\ \tilde{b}^T \tilde{a} \tilde{H}^e &= \tilde{a}^T \tilde{b} \tilde{H}^e = \tilde{a}^T \tilde{a} \tilde{H}^e = 0 \end{aligned}$$

and the last term in (7.22) vanishes.

The remaining part of  $\tilde{P}^e$  contains the distributed source and sink terms, as well as interfacial transport between the layers. The contribution of a linear decay term  $-kC$  over the element is

$$\begin{aligned} - \iint_{A^e} \tilde{N}^T k C dA &= - \iint_{A^e} \tilde{N}^T k \tilde{N} \tilde{C}^e dA = - k \left( \iint_{A^e} \tilde{N}^T \tilde{N} dA \right) \tilde{C}^e = \\ &= - k \tilde{M}^e \tilde{C}^e = - \tilde{D}^e \tilde{C}^e \end{aligned} \quad (7.23)$$

Assuming a linear distributed source,

$$\iint_{A^e} \tilde{N}^T R dA = \left( \iint_{A^e} \tilde{N}^T \tilde{N} dA \right) \tilde{R}^e = \frac{A^e}{12} \begin{bmatrix} 2 & 1 & 1 \\ 1 & 2 & 1 \\ 1 & 1 & 2 \end{bmatrix} \tilde{R}^e = \tilde{S}^e \quad (7.24)$$

where  $\tilde{R}^e$  denotes the sources at the element nodes, if any.

Finally, the interfacial transport from layer 2 to layer 1 is given by

$$Q_{21} = (w_e - w_s) \frac{\bar{c}_1 + \bar{c}_2}{2} + \alpha(\bar{c}_2 - \bar{c}_1)$$

Because  $w_e$  and  $\alpha$  depend on the layer velocities, they are variable over space and time and it is convenient to work here with the overall quantity  $Q_{21}$ . Setting

$$Q_{21} = \tilde{N} \tilde{Q}_{21}^e$$

we obtain

$$\pm \iint_{A^e} \tilde{N}^T Q_{21} dA = \pm \left( \iint_{A^e} \tilde{N}^T \tilde{N} dA \right) \tilde{Q}_{21}^e = \pm \tilde{M}_{21}^e \tilde{Q}_{21}^e = \pm \tilde{E}^{*e} \quad (7.25)$$

where  $\tilde{Q}_{21}^e$  is the vector of interfacial fluxes at the nodal points and the plus and minus signs apply to the top (sub. 1) and bottom (sub. 2) layer, respectively. This treatment of the interfacial exchange term is similar to that of a distributed external source. However, unlike  $\tilde{R}^e$ ,  $\tilde{Q}_{21}^e$  depends on the layers concentrations and has to be updated as they change during the solution process.



If there is no net entrainment and if  $\alpha$  is considered constant over the element, the expression for  $Q_{21}$  simplifies to

$$Q_{21} = \alpha(\bar{c}_2 - \bar{c}_1) = \alpha\left(\frac{C_2}{H_2} - \frac{C_1}{H_1}\right)$$

Assuming  $H_1 \approx H_2 \approx H$  yields an additional simplification,

$$Q_{21} \approx \alpha'(C_2 - C_1) = \alpha'(\bar{NC}_2^e - \bar{NC}_1^e)$$

where  $\alpha' = \alpha/H$ . Finally,

$$\begin{aligned} \pm \iint_{A^e} \tilde{N}^T Q_{21} dA &= \pm \alpha' \left( \iint_{A^e} \tilde{N}^T \tilde{N} dA \right) (C_2^e - C_1^e) \\ &= \pm \alpha' \tilde{M}^e (C_2^e - C_1^e) \\ &= \pm \tilde{E}^e (C_2^e - C_1^e) \end{aligned} \quad (7.26)$$

Summarizing, the vectors are:

$$\tilde{P}_1^e = -\tilde{A}_1^e \tilde{C}_1^e - \tilde{K}_1^e \tilde{C}_1^e + \left(\frac{C}{H}\right)_{av} \tilde{K}_1^e \tilde{H}^e - \tilde{D}_1^e \tilde{C}_1^e + \tilde{E}^{*e} + \tilde{S}_1^e \quad (7.27a)$$

$$\tilde{P}_2^e = -\tilde{A}_2^e \tilde{C}_2^e - \tilde{K}_2^e \tilde{C}_2^e + \left(\frac{C}{H}\right)_{av} \tilde{K}_2^e \tilde{H}_2^e - \tilde{D}_2^e \tilde{C}_2^e - \tilde{E}^{*e} + \tilde{S}_2^e \quad (7.27b)$$

where the various matrices are defined in Eqs. (7.20) through (7.25).

When the thicknesses and  $\alpha'$  are constant, Eqs. (7.27a,b) reduce to

$$\tilde{P}_1^e = -\tilde{A}_1^e \tilde{C}_1^e - \tilde{K}_1^e \tilde{C}_1^e - \tilde{D}_1^e \tilde{C}_1^e + \tilde{E}^e (C_2^e - C_1^e) + \tilde{S}_1^e \quad (7.28a)$$

$$\tilde{P}_2^e = -\tilde{A}_2^e \tilde{C}_2^e - \tilde{K}_2^e \tilde{C}_2^e - \tilde{D}_2^e \tilde{C}_2^e - \tilde{E}^e (C_2^e - C_1^e) + \tilde{S}_2^e \quad (7.28b)$$

With respect now to the boundary terms, we set

$$Q_n^* = \tilde{N}^b Q_n^{*be}$$

and obtain

$$\tilde{F}^{be} = \left( \int_{S_q} \tilde{N}^{bT} \tilde{N}^b dS \right) Q_n^{*be} = \frac{\ell}{6} \begin{bmatrix} 2 & 1 \\ 1 & 2 \end{bmatrix} Q_n^{*be} \quad (7.29)$$

where  $\ell$  is the length of the boundary segment.

Eq. (7.5) states that, for each layer, the sum of weighted residuals of the elements is required to vanish:

$$\sum_e (\Delta C^e)^T (\tilde{M}^e \tilde{C}^e - \tilde{P}^e + \tilde{F}^b) = 0$$

Formally carrying out the summation, we obtain the system equation:

$$\Delta C^T (\tilde{M} \dot{\tilde{C}} - \tilde{P} + \tilde{F}^b) = 0$$

Since  $\Delta C$  is arbitrary, the parenthesis must vanish, i.e., for each layer:

$$\tilde{M}_{11} \dot{\tilde{C}}_1 = \tilde{P}_1 - \tilde{F}_1^b = \hat{\tilde{P}}_1 \quad (7.30a)$$

$$\tilde{M}_{22} \dot{\tilde{C}}_2 = \tilde{P}_2 - \tilde{F}_2^b = \hat{\tilde{P}}_2 \quad (7.30b)$$

If  $\tilde{P}_1, \tilde{P}_2$  are expressible by (7.28a,b), the system equations can be written as:

$$\tilde{M}_{11} \dot{\tilde{C}}_1 + \tilde{A}_{11} C_1 + \tilde{K}_{11} C_1 + \tilde{D}_{11} C_1 + \tilde{E}(C_1 - C_2) = \tilde{S}_1 - \tilde{F}_1^b \quad (7.31a)$$

$$\tilde{M}_{22} \dot{\tilde{C}}_2 + \tilde{A}_{22} C_2 + \tilde{K}_{22} C_2 + \tilde{D}_{22} C_2 + \tilde{E}(C_2 - C_1) = \tilde{S}_2 - \tilde{F}_2^b \quad (7.31b)$$

This form of the equations is convenient for subsequent analysis of the numerical approximation, since all concentration-dependent terms are directly expressed in terms of the concentration vectors and constant (that is, not depending on concentration) coefficients (see Chapter 8). Of the matrices involved in (7.31a,b), the geometrical matrices  $\tilde{M}_1$ ,  $\tilde{M}_2$  are usually equal, since the discretization is the same for both layers. Although practically important, the case in which layers do not extend over the whole domain is not considered in this work.

### 7.3 Time Integration Strategy

The general form of the equations (7.30a,b) is more suitable for discussing the time integration scheme. These equations constitute a set of ordinary linear differential equations with the nodal concentrations of the two layers as unknowns. The trapezoidal rule is used to integrate in time.

$$\tilde{M}(\tilde{C}_{1,t+\Delta t} - \tilde{C}_{1,t}) = \frac{\Delta t}{2} (\hat{P}_{1,t+\Delta t} + \hat{P}_{1,t}) \quad (7.32a)$$

$$\tilde{M}(\tilde{C}_{2,t+\Delta t} - \tilde{C}_{2,t}) = \frac{\Delta t}{2} (\hat{P}_{2,t+\Delta t} + \hat{P}_{2,t}) \quad (7.32b)$$

Since  $\hat{P}_{1,t+\Delta t}$ ,  $\hat{P}_{2,t+\Delta t}$  depend on  $\tilde{C}_{1,t+\Delta t}$ ,  $\tilde{C}_{2,t+\Delta t}$ , these equations constitute an implicit scheme and are solved here by iteration. The values of  $\tilde{C}_{1,t}$ ,  $\tilde{C}_{2,t}$  along with the loadings and velocity inputs at time  $t$  determine  $\hat{P}_{1,t}$ ,  $\hat{P}_{2,t}$ . To obtain initial values of  $\hat{P}_{1,t+\Delta t}$  and  $\hat{P}_{2,t+\Delta t}$ , the concentrations  $\tilde{C}_{1,t+\Delta t}$ ,  $\tilde{C}_{2,t+\Delta t}$  must be given initial guesses. The simplest approach is to set

$$C_{1,t+\Delta t}^{(1)} = C_{1,t}$$

$$C_{2,t+\Delta t}^{(1)} = C_{2,t}$$

where the superscript in parenthesis denotes the iteration index. Then, new values of  $C_{1,t+\Delta t}$ ,  $C_{2,t+\Delta t}$  are determined from:

$$C_{1,t+\Delta t}^{(i+1)} = C_{1,t} + \frac{\Delta t}{2} \tilde{M}^{-1} (\hat{P}_{1,t+\Delta t}^{(i)} + \hat{P}_{1,t}) \quad (7.33a)$$

$$C_{2,t+\Delta t}^{(i+1)} = C_{2,t} + \frac{\Delta t}{2} \tilde{M}^{-1} (\hat{P}_{2,t+\Delta t}^{(i)} + \hat{P}_{2,t}) \quad (7.33b)$$

The geometrical matrix  $\tilde{M}$  is time invariant and therefore has to be computed and inverted only once. This is of major importance in practical problems with significant time variability. A direct, non-iterative solution for  $C_{t+\Delta t}$  would involve the inversion of matrices of the form  $\tilde{M} + \frac{\Delta t}{2} (\tilde{K} + \tilde{A} + \tilde{D} + \tilde{E})$  in each time step, which increases the cost of the solution considerably. In the transient case, the flow field as well as the concentration varies with time. The latter determines the advective terms, the interfacial transport coefficients and, in general, the dispersion coefficients. In addition, sources and boundary conditions may vary with time. By lumping all terms in the  $\hat{P}$  vector and employing the iteration procedure, maximum flexibility in handling time variability of any or all of the relevant parameters and loadings is achieved. Moreover, the most general case of non-linear decay, dispersion of other terms can be readily handled in this way. This is particularly significant when there is interfacial exchange

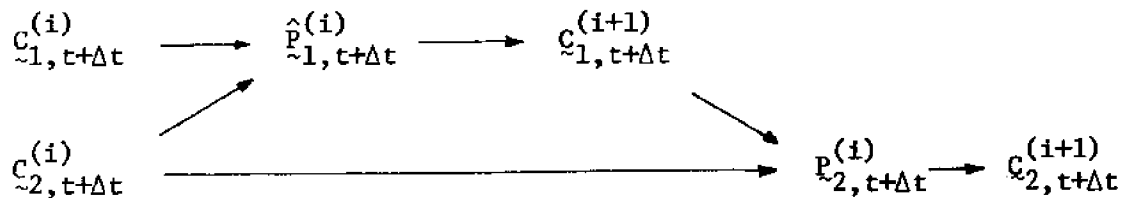
which "links" the layers and makes very difficult the exact solution of even the simplified Eqs. (7.31a,b). However, the iteration strategy requires a restriction on the time step.

In practice, the iteration continues until there is little change in concentration between the current and previous values. A tolerance limit has to be specified and compared to some measure of deviation of current nodal values from the previous ones. Thus, the iteration at  $t+\Delta t$  is considered to have converged adequately when, for each layer separately:

$$\frac{\left[ \sum_{\text{all nodes}} (C_{j,t+\Delta t}^{(i+1)} - C_{j,t+\Delta t}^{(i)})^2 \right]^{1/2}}{\left[ \sum_{\text{all nodes}} (C_{j,t+\Delta t}^{(i+1)})^2 \right]^{1/2}} < \text{Tolerance} \quad (7.34)$$

where  $j = 1,2$  refers to the layer index. An upper limit on the number of iterations at each time step may be also imposed, so that the solution proceeds to the next time step without satisfying (7.34).

In the absence of interfacial transport, Eqs. (7.33a) and (7.33b) can be solved separately. With interfacial transport, each of the vectors  $\hat{P}_1$ ,  $\hat{P}_2$  depends on both  $C_1$  and  $C_2$  as well as the velocities  $U_1$ ,  $U_2$ . To enhance the rate of convergence, the updated value  $C_{1,t+\Delta t}^{(i+1)}$  is used to calculate  $P_{2,t+\Delta t}^{(i)}$ . The scheme is illustrated below:



This procedure can be readily generalized for an arbitrary number of layers.

## CHAPTER 8

### STABILITY AND ACCURACY OF THE NUMERICAL SCHEME

In the previous chapter the finite element approximation to the problem was presented and the method of solving the resulting set of linear differential equations was discussed. As in all numerical models, two important issues relevant to the usefulness of the numerical approximation are the stability and the accuracy of the numerical solution. The former is normally associated with the selection of the time step in problems where time integration is required. Explicit schemes, i.e., determining the value at the next time directly from values at previous times, always need a restriction on the time step for stability. This is not so for implicit schemes, e.g. iterative formulations, some of which may be stable for any time step (depending also on the problem). Since the cost of the solution is directly related to the timestep, efforts are always made for devising more stable schemes. There are also other factors limiting the time-step which depend on the particular problem and the objectives of the model. For example, if it is desired to study the effect of tidal variability on the dispersion of a pollutant, the time step should at most be an order of magnitude smaller than the tidal period, so that enough resolution is provided.

The accuracy of the numerical solution, although in general may depend on the time step, is mainly associated with the space discretization. The relation of the grid size to the parameters of the problem and the particular form of the function to be approximated control how close the numerical solution can be to the true solution. Of course, the true solution cannot

be known except in simple cases, where analytical expressions are available. Starting from such simple cases, approximate general criteria can be derived which give an idea of the accuracy of the approximation in a particular problem and suggest ways for improvement. Rapidly varying boundary conditions, sources, or other forcing terms are often sources of inaccuracies and sometimes instabilities for otherwise well-behaved schemes. In particular, with respect to the convection-diffusion equation, inaccuracies originate from the fact that a fixed grid is inherently not suitable for describing a moving plume which has high concentration gradients, especially near the edges and near localized sources. Evidently, the accuracy of the approximation increases as the grid becomes finer but this is achieved at the expense of higher costs due to increased computer time. Clearly, there is a trade-off between economy and accuracy considerations. While it is not feasible to eliminate inaccuracies totally in the solution, it is possible to restrict them within acceptable limits.

In this chapter the stability and accuracy characteristics of the finite element solution strategy are discussed. Because interfacial mixing is usually small, the behavior of a single layer is of basic importance and is presented in detail. Before examining the finite element method, some background from familiar finite difference schemes is considered first.



## 8.1 Background from Finite Difference Methods

Most common finite difference schemes used for solving the convection-diffusion equation have been investigated extensively with respect to their stability and accuracy characteristics, in the search for devising better numerical approximations. Formal mathematical analyses are usually restricted to the case of constant parameters and deal mostly with the simplest one-dimensional case. An excellent review on the subject is presented by Roache ( 70 ).

Considering the one-dimensional convection-diffusion equation

$$\frac{\partial c}{\partial t} + u \frac{\partial c}{\partial x} = E \frac{\partial^2 c}{\partial x^2} \quad (8.1)$$

it can be seen that a typical Fourier component of the solution is of the form ( 82):

$$C_T = C_0 \exp[ - k^2 E t + i k (x - u t) ] \quad (8.2)$$

where  $k$  is the (real) wave number and  $C_0$  is the initial wave amplitude. Approximating (8.1) by using central differences in space and forward in time (Euler method), one obtains:

$$C_j^{n+1} - C_j^n = \frac{E \Delta t}{\Delta x^2} (C_{j+1}^n + C_{j-1}^n - 2C_j^n) - \frac{u \Delta t}{2 \Delta x} (C_{j+1}^n - C_{j-1}^n) \quad (8.3)$$

where the subscript is used as the space index and the superscript as the index. The solution of Eq. (8.3) has the form

$$C_j^n = C_0 \lambda^n \exp(i k j \Delta x) \quad (8.4)$$

Substituting in (8.3) yields

$$\lambda = 1 + 2 \frac{E\Delta t}{\Delta x^2} (\cos k\Delta x - 1) - i \frac{u\Delta t}{\Delta x} \sin k\Delta x \quad (8.5)$$

Because  $c_j^{n+1} = \lambda c_j^n$ , the coefficient  $\lambda$  is called the "amplification factor" and is, in general, complex. To ensure stability as the solution proceeds in time,  $\lambda$  must satisfy the Von-Neumann condition

$$|\lambda| = \frac{|c_j^{n+1}|}{|c_j^n|} \leq 1 \quad (8.6)$$

which implies that a perturbation introduced into the system is bounded.

From Eq. (8.5)

$$\lambda^2 = [1 + 2 \frac{E\Delta t}{\Delta x^2} (\cos k\Delta x - 1)]^2 + [\frac{u\Delta t}{\Delta x} \sin k\Delta x]^2 \quad (8.7)$$

This indicates that for any wave number  $k$ , stability is controlled by the two non-dimensional groups  $E\Delta t/\Delta x^2$  and  $u\Delta t/\Delta x$ , involving the parameters of the problem and the time and space discretization used. When (70)

$$\frac{u\Delta x}{E} \leq 2 \quad (8.8)$$

the max value of  $\lambda^2$  occurs for  $k\Delta x = \pi$  which yields the stability criterion

$$\Delta t < \frac{\Delta x^2}{2E} \quad (8.9)$$

Eqs. (8.8) and (8.9) imply

$$\Delta t < \frac{2E}{u^2} \quad (8.10)$$

and further

$$\Delta t < \frac{\Delta x}{u} \quad (8.11)$$

which is analogous to the Courant condition in circulation problems.

However, when (8.8) is not satisfied the maximum value of  $\lambda^2$  is always larger than unity and therefore (8.8) is necessary for stability of this particular scheme.

Approximation (8.2) is an explicit scheme, which is conditionally stable, provided the time step satisfies (8.9) and (8.11). A simple implicit scheme is obtained by using the trapezoidal rule for time integration of (8.1).

$$\begin{aligned} C_j^{n+1} - C_j^n = \frac{1}{2} \left\{ \frac{E\Delta t}{\Delta x^2} (C_{j+1}^{n+1} + C_{j-1}^{n+1} - 2C_j^{n+1}) - \frac{u\Delta t}{2\Delta x} (C_{j+1}^{n+1} - C_{j-1}^{n+1}) \right\} \\ + \frac{1}{2} \left\{ \frac{E\Delta t}{\Delta x^2} (C_{j+1}^n + C_{j-1}^n - 2C_j^n) - \frac{u\Delta t}{2\Delta x} (C_{j+1}^n - C_{j-1}^n) \right\} \end{aligned} \quad (8.12)$$

Substituting Eq. (8.4) in Eq. (8.12), the expression for the amplification factor is

$$\begin{aligned} \lambda \left\{ 1 - \frac{E\Delta t}{\Delta x^2} (\cos k\Delta x - 1) + i \frac{u\Delta t}{2\Delta x} \sin k\Delta x \right\} = \\ = 1 + \frac{E\Delta t}{\Delta x^2} (\cos k\Delta x - 1) - i \frac{u\Delta t}{2\Delta x} \sin k\Delta x \end{aligned}$$

Then

$$\lambda^2 = \frac{\left[ 1 - \frac{E\Delta t}{\Delta x^2} (1 - \cos k\Delta x) \right]^2 + \left( \frac{u\Delta t}{2\Delta x} \sin k\Delta x \right)^2}{\left[ 1 + \frac{E\Delta t}{\Delta x^2} (1 - \cos k\Delta x) \right]^2 + \left( \frac{u\Delta t}{2\Delta x} \sin k\Delta x \right)^2} \quad (8.13)$$

Since  $\cos k\Delta x \leq 1$ , Eq. (8.13) indicates that  $\lambda^2 \leq 1$  for arbitrary  $\Delta t$  and the scheme is said to be unconditionally stable.

Even though a particular approximation may be stable, the solution may still be far from the true solution. Viewing the latter as a set of waves propagating downstream and diffusing according to Eq. (8.2), there are two types of errors introduced by the approximation:

- a) Amplitude errors, i.e. either excessive or inadequate damping of the wave magnitudes (numerical diffusion)
- b) Phase errors, i.e. incorrect speed of propagation of the waves (numerical dispersion).

Setting  $t = n\Delta t$  and  $x = j\Delta x$ , the exact solution (8.2) becomes

$$\begin{aligned} C_T &= C_0 [\exp(-k^2 E \Delta t)]^n \exp[ik(j\Delta x - u n \Delta t)] \\ &= C_0 [\exp(-(k\Delta x)^2 \frac{E\Delta t}{\Delta x^2})]^n \exp[ik\Delta x(j - n \frac{u\Delta t}{\Delta x})] \end{aligned} \quad (8.14)$$

The approximate solution obtained by the Euler method is given by (8.4), where  $\lambda$  is defined in (8.5).

Setting

$$\lambda = \rho e^{-i\theta} \quad (8.15)$$

Eq. (8.4) takes the form

$$\begin{aligned} C_j^n &= C_0 \rho^n \exp[i(kj\Delta x - n\theta)] \\ &= C_0 \rho^n \exp[ik\Delta x(j - n \frac{\theta}{k\Delta x})] \end{aligned} \quad (8.16)$$

From Eq. (8.5), the modulus  $\rho$  of  $\lambda$  is

$$\rho = \left[ \left( 1 + 2 \frac{E\Delta t}{\Delta x^2} (\cos k\Delta x - 1) \right)^2 + \left( \frac{u\Delta t}{\Delta x} \sin k\Delta x \right)^2 \right]^{1/2} \quad (8.17)$$

and the phase  $\theta$  is

$$\theta = \arctan \frac{\frac{u\Delta t}{\Delta x} \sin k\Delta x}{1 + 2 \frac{E\Delta t}{\Delta x^2} (\cos k\Delta x - 1)} \quad (8.18)$$

By comparing Eqs. (8.14) and (8.15) it is seen that the ratio of the approximate to the true magnitude in one time step is:

$$\frac{\rho}{\exp(-k^2 E\Delta t)} = f_1(k\Delta x, \frac{E\Delta t}{\Delta x^2}, \frac{u\Delta t}{\Delta x}) \quad (8.19)$$

and after a time  $t = n\Delta t$

$$\frac{\rho^n}{\exp(-k^2 E t)} = f_1^n \quad (8.19a)$$

On the other hand, the ratio of the distance travelled by the approximate solution to the real one in one time step is expressed as:

$$\frac{\theta/k\Delta x}{u\Delta t/\Delta x} = \frac{\theta}{ku\Delta t} = f_2(k\Delta x, \frac{E\Delta t}{\Delta x^2}, \frac{u\Delta t}{\Delta x}) \quad (8.20)$$

and apparently remains the same after time  $t = n\Delta t$ .

Although the forms of  $f_1$  and  $f_2$  depend on the particular approximation employed, it is important to realize that the two non-dimensional groups  $\frac{E\Delta t}{\Delta x^2}$  and  $\frac{u\Delta t}{\Delta x}$  which are of significance in stability considerations, also control the accuracy of the numerical approximation. Of course, the ideal case of  $f_1 = 1$  and  $f_2 = 1$  for all  $k$  is never possible, since it characterizes the true solution itself. The amplitude error may, in general, be

considered more important because of its exponential growth with time. Methods with no amplitude error do exist for simple convection ( $E = 0$ ). Indeed, the simple trapezoidal scheme for  $E = 0$  yields (from Eq. (8.12))

$$\lambda^2 = \frac{1 + \left( \frac{u\Delta t}{\Delta x} \sin k\Delta x \right)^2}{1 + \left( \frac{u\Delta t}{\Delta x} \sin x \right)^2} = 1$$

for all  $k$ , indicating that a unit wave propagates without any spurious damping. This is characteristic of time-centered approximations of the advection equation ( 53 ), which are consequently called "neutrally stable".

An alternative way of expressing the artificial damping caused by the numerical approximation was introduced by Hirt ( 29 ). Expanding all terms of (8.3) in Taylor series about the point  $C_j^n$ , the following differential equation is obtained:

$$\frac{\partial c}{\partial t} + u \frac{\partial c}{\partial x} = \left( E - \frac{u^2 \Delta t}{2} \right) \frac{\partial^2 c}{\partial x^2} + \text{higher order terms} \quad (8.21)$$

This indicates that, instead of (8.1), a different equation is solved and, in particular, a spurious diffusivity has been created

$$E_a = - \frac{u^2 \Delta t}{2} \quad (8.22)$$

Stability requires  $E > E_a$ , which is equivalent to (8.10), since otherwise the solution would grow exponentially. But, even if that is satisfied, the reduction in the effective diffusion coefficient is a source of inaccuracy. The artificial diffusivity of other finite difference schemes has been examined by Roache ( 69 ). A compact expression for first order space differences and a forward time difference is ( 3 )

$$E_a = \frac{u}{2} [(1 - 2\gamma)\Delta x - u\Delta t] \quad (8.23)$$

where

$\gamma = 0$       for backward space differences

$\gamma = 0.5$     for central space differences

$\gamma = 1$       for forward space differences

It is clear that  $E_a$  is always negative in this case, thereby reducing the magnitude of the actual diffusion coefficient. It is also seen that  $E_a$  is smallest for backward differences, which may explain their popularity in steady flow problems.

The term in (8.23) associated with  $\Delta t$  is eliminated when steady state is considered ( 69 ). It also vanishes when time centered schemes are used. Then, the choice of central space differencing completely eliminates the artificial diffusion coefficient. Any amplitude error remaining should be small and is related to the higher order terms of Eq. (8.21).

As discussed earlier, it is possible to have no amplitude error in solving the equation of pure convection. However, phase errors can never be totally eliminated ( 31 ). Fromm ( 23 ), reviewing first and higher order approximations in the search for devising a method of reduced dispersion, concludes that most finite difference schemes have lagging phase errors. In view of the previous discussion, this simply means that  $f_2 < 1$  in Eq. ( 8.20), indicating that the approximate waves lag the true waves. But, in addition, most schemes exhibit a larger phase error in the larger wavenumbers (i.e. higher frequencies). This differential error between the components of the solution causes ( 23 ) an upstream

steepening of some initial distribution shape being convected downstream, which may even lead to the appearance of spatial oscillations. The addition of a diffusion term to the convection equation, apart from changing somewhat the phase errors, acts as a damping mechanism with a higher effect at the large wavenumbers. Thus, the diffusion term helps in smoothing out the distribution and moderating the effects of numerical phase dispersion by suppressing the contributions of the most erroneous wave components.

Phase errors are, of course, irrelevant when only the steady-state solution of (8.1) is desired. Accuracy in this case is associated basically with the smoothness of the solution, which is associated with the ability of the grid to handle steep concentrations gradients, such as those occurring in the vicinity of a continuous source. The parameter  $\frac{u\Delta x}{E}$ , the so-called "grid Reynolds number" is found to be of fundamental importance, when a central difference approximation is used ( 70 ). In particular, condition (8.8) has to be satisfied for the smoothness of the exact solution of the difference analog (8.2)

## 8.2 Analysis of a Regular Finite Element Grid

### 8.2.1 Stability

For a single layer, the finite element approximation leads to the following matrix equation:

$$\underset{\sim}{M}\underset{\sim}{C} + \underset{\sim}{A}\underset{\sim}{C} + \underset{\sim}{K}\underset{\sim}{C} + \underset{\sim}{D}\underset{\sim}{C} = \underset{\sim}{S} \quad (8.24)$$

Neglecting decay and source terms and employing the trapezoidal rule for time integration, Eq. (8.24) takes the form:

$$\underset{\sim}{M}(\underset{\sim}{C}_{n+1} - \underset{\sim}{C}_n) + \frac{\Delta t}{2} (\underset{\sim}{A}\underset{\sim}{C}_n + \underset{\sim}{K}\underset{\sim}{C}_n + \underset{\sim}{A}\underset{\sim}{C}_{n+1} + \underset{\sim}{K}\underset{\sim}{C}_{n+1}) = 0 \quad (8.25)$$



where  $\tilde{A}$  and  $\tilde{K}$  are considered constant for the purposes of the following analysis and the subscripts  $n, n+1$ , refer to times  $t$  and  $t+\Delta t$ , respectively.

The techniques for studying stability and accuracy of finite difference equations, discussed in the previous sections, can be employed to Eq. (8.25) only when the finite element grid is regular, such as that shown in Fig.

8.1. To examine node A, the contributions from the six adjacent elements have to be considered. Assembling the individual matrices, defined in Section 7.2, and taking into account that the area of each element is  $A^e = \Delta s^2/12$ , Eq. (8.25) becomes:

$$\begin{aligned}
& (6 C_A^{n+1} + C_B^{n+1} + C_C^{n+1} + C_D^{n+1} + C_E^{n+1} + C_F^{n+1} + C_G^{n+1}) + \\
& + 6 \frac{E_x \Delta t}{\Delta s^2} (2C_A^{n+1} - C_C^{n+1} - C_F^{n+1}) + 6 \frac{E_y \Delta t}{\Delta s^2} (2C_A^{n+1} - C_B^{n+1} - C_E^{n+1}) \\
& + \frac{u \Delta t}{\Delta s} (C_B^{n+1} + 2C_C^{n+1} + C_D^{n+1} - C_E^{n+1} - 2C_F^{n+1} - C_G^{n+1}) \\
& + \frac{v \Delta t}{\Delta s} (-2C_B^{n+1} - C_C^{n+1} + C_D^{n+1} + 2C_E^{n+1} + C_F^{n+1} - C_G^{n+1}) \\
& = (6C_A^n + C_B^n + C_C^n + C_D^n + C_E^n + C_F^n + C_G^n) - 6 \frac{E_x \Delta t}{\Delta s^2} (2C_A^n - C_C^n - C_F^n) \\
& - \frac{6E_y \Delta t}{\Delta s^2} (2C_A^n - C_B^n - C_E^n) - \frac{u \Delta t}{\Delta s} (C_B^n + 2C_C^n + C_D^n - C_E^n - 2C_F^n - C_G^n) \\
& - \frac{v \Delta t}{\Delta s} (-2C_B^n - C_C^n + C_D^n + 2C_E^n + C_F^n - C_G^n) \tag{8.26}
\end{aligned}$$

where  $u, v$  and the  $x, y$  components of mean velocity (the overbars are implied throughout this chapter) and  $E_x, E_y$  are the  $x, y$  components of the dispersion tensor ( $E_{xy}$  is neglected here for convenience).

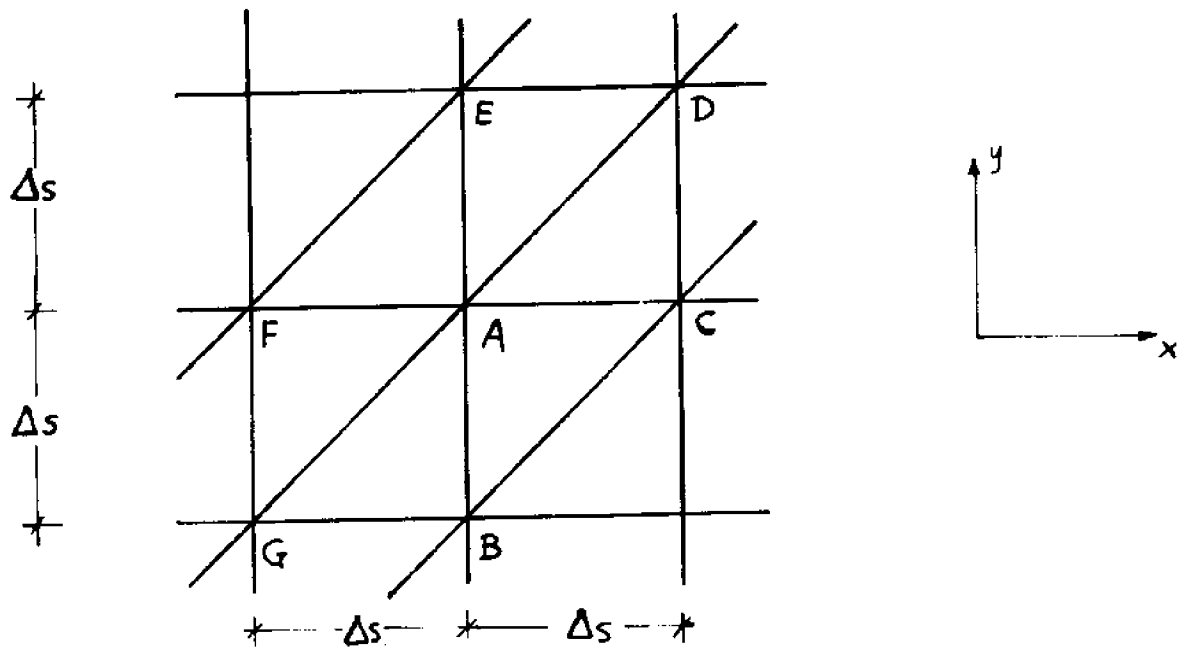


Figure 8.1 Example of a Regular Grid

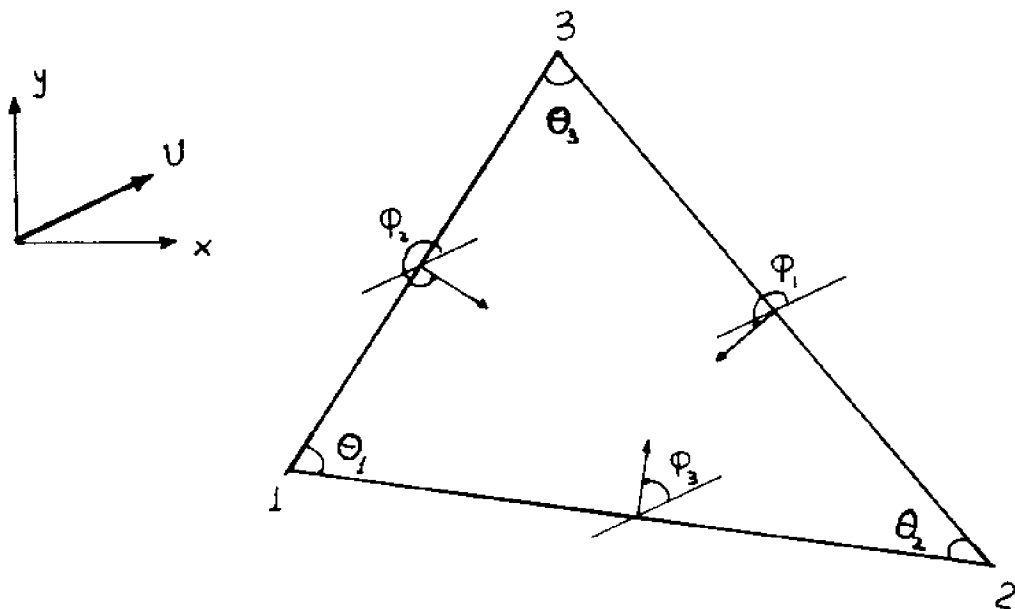


Figure 8.2 Definition of Angles for an Arbitrary Triangle

By analogy with (8.4), set

$$C_{j_x, j_y}^n = C_0 \lambda^n \exp(ik_x j_x \Delta x + ik_y j_y \Delta y) \quad (8.27)$$

Introducing this expression into (8.26) yields:

$$\begin{aligned} & \lambda \{ [6 + 2 \cos k_y \Delta s + 2 \cos k_x \Delta s + 2 \cos(k_x \Delta s + k_y \Delta s)] \\ & + 6 \frac{E_x \Delta t}{\Delta s^2} (2 - 2 \cos k_x \Delta s) + 6 \frac{E_y \Delta t}{\Delta s^2} (2 - 2 \cos k_y \Delta s) \\ & + i \frac{u \Delta t}{\Delta s} [-2 \sin k_x \Delta s + 4 \sin k_x \Delta s + 2 \sin(k_x \Delta s + k_y \Delta s)] \\ & + i \frac{v \Delta t}{6} [-2 \sin k_x \Delta s + 4 \sin k_y \Delta s + 2 \sin(k_x \Delta s + k_y \Delta s)] \} \\ & = [6 + 2 \cos k_y \Delta s + 2 \cos k_x \Delta s + 2 \cos(k_x \Delta s + k_y \Delta s)] \\ & - 6 \frac{E_x \Delta t}{\Delta s^2} (2 - 2 \cos k_x \Delta s) - 6 \frac{E_y \Delta t}{\Delta s^2} (2 - 2 \cos k_y \Delta s) \\ & - i \frac{u \Delta t}{\Delta s} [-2 \sin k_y \Delta s + 4 \sin k_x \Delta s + 2 \sin(k_x \Delta s + k_y \Delta s)] \\ & - i \frac{v \Delta t}{\Delta s} [-2 \sin k_x \Delta s + 4 \sin k_y \Delta s + 2 \sin(k_x \Delta s + k_y \Delta s)] \end{aligned}$$

Concentrating now for simplicity on the one-dimensional problem ( $v = 0$ ,

$k_y = 0, k_x = k$ ), we obtain:

$$\lambda = \frac{(4 + 2 \cos k \Delta s) - 6 \frac{E \Delta t}{\Delta s^2} (1 - \cos k \Delta s) - i 3 \frac{u \Delta t}{\Delta s} \sin k \Delta s}{(4 + 2 \cos k \Delta s) + 6 \frac{E \Delta t}{\Delta s^2} (1 - \cos k \Delta s) + i 3 \frac{u \Delta t}{\Delta s} \sin k \Delta s} \quad (8.28)$$

This is written as

$$\lambda = \frac{\beta - \gamma - i\delta}{\beta + \gamma + i\delta} \quad (8.28a)$$

where

$$\begin{aligned}\beta &= 4 + 2 \cos k\Delta s \\ \gamma &= 6 \frac{E\Delta t}{\Delta s^2} (1 - \cos k\Delta s) \\ \delta &= 3 \frac{u\Delta t}{\Delta s} \sin k\Delta s\end{aligned}\tag{8.29}$$

It follows that

$$|\lambda|^2 = \frac{(\beta - \gamma)^2 + \delta^2}{(\beta + \gamma)^2 + \delta^2}$$

since  $\cos k\Delta s < 1$ ,  $\gamma > 0$  and therefore

$$|\lambda|^2 < 1$$

which means that the scheme is unconditionally stable, for any value of  $\Delta t$ .

It is important to notice that in the absence of diffusion ( $E = 0$ ),

$$|\lambda|^2 = \frac{\beta^2 + \delta^2}{\beta^2 + \delta^2} = 1$$

indicating that a unit amplitude wave will propagate retaining the same magnitude. Thus, the scheme is neutrally stable for simple convection. The presence of diffusion enhances the stability by making the value of  $|\lambda|$  less than unity.

### 8.2.2 Amplitude Errors

The presence of amplitude errors is easily investigated by the methods discussed in Sec. 8.1. The true solution is still given by Eq. (8.14), with  $\Delta s$  in place of  $\Delta x$ , and its magnitude is at time  $t$ :

$$|C_T| = C_0 \exp(-k^2 E t) = C_0 \exp[-(k\Delta s)^2 n \frac{E\Delta t}{\Delta s^2}]$$

The magnitude of the wave propagated through the finite element grid after the same period of time is:

$$|C_N| = C_o |\lambda|^n = C_o \left[ \frac{(\beta-\gamma)^2 + \delta^2}{(\beta+\gamma)^2 + \delta^2} \right]^{n/2}$$

where  $\beta$ ,  $\gamma$ ,  $\delta$  are defined by (8.29). Using those values, the ratio

$|C_N|/|C_T|$  is expressed as:

$$\begin{aligned} \frac{|C_N|}{|C_T|} &= \left( \sqrt{\frac{[(4+2\cos k\Delta s) - 6 \frac{E\Delta t}{\Delta s^2}(1-\cos k\Delta s)]^2 + (3 \frac{u\Delta t}{\Delta s} \sin k\Delta s)^2}{[(4+2\cos k\Delta s) + 6 \frac{E\Delta t}{\Delta s^2}(1-\cos k\Delta s)]^2 + (3 \frac{u\Delta t}{\Delta s} \sin k\Delta s)^2}} \exp[(k\Delta s)^2 \frac{E\Delta t}{\Delta s^2}] \right)^n \\ &= f_1^n(k\Delta s, \frac{E\Delta t}{\Delta s^2}, \frac{u\Delta t}{\Delta s}) \end{aligned} \quad (8.30)$$

It is seen that, just as in finite difference methods, the accuracy of the approximation depends on the values of the basic parameters  $\frac{E\Delta t}{\Delta s^2}$  and  $\frac{u\Delta t}{\Delta s}$ . Table 8.1 lists the amplitude error committed after  $n = 100$  timesteps for some wave modes, for  $\frac{u\Delta t}{\Delta s} = 0.1$  and several values of  $\frac{E\Delta t}{\Delta s^2}$ , along with the true amplitude  $|C_T|$ , relative to its original value  $C_o$ .

TABLE 8.1

Amplitude Error After 100 Time Steps, for  $u\Delta t/\Delta s = 0.1$

$k\Delta s$	$E\Delta t/\Delta s^2 = 0.05$		$E\Delta t/\Delta s^2 = 0.10$		$E\Delta t/\Delta s^2 = 0.15$	
	$ C_N / C_T $	$ C_T /C_o$	$ C_N / C_T $	$ C_T /C_o$	$ C_N / C_T $	$ C_T /C_o$
$\pi/4$	0.855	0.0457	0.729	0.0021	0.620	0.0001
$\pi/5$	0.938	0.139	0.879	0.0193	0.823	0.0027
$\pi/6$	0.976	0.254	0.940	0.0644	0.914	0.0163
$\pi/10$	0.999	0.610	0.998	0.372	0.990	0.227

Errors in low frequencies are certainly more important because they are damped less strongly in the true solution. As seen from Table 8.1, lower frequencies exhibit the best behavior with respect to amplitude errors and it may be readily seen from Eq. (8.30) that  $|C_N|/|C_T|$  approaches unity as  $k\Delta s \rightarrow 0$  (i.e., for very long waves). It is also seen that, for the values of  $E\Delta t/\Delta s^2$  listed, the damping in the approximation is stronger than what it should be. A smaller diffusion coefficient that would eliminate this error can be determined for a particular frequency by solving (8.30) with  $f_1 = 1$ , by trial and error. Considering the approximation of a wave by linear expansions, it may be argued that a reasonable description requires 8 to 10 grid points per wavelength. Consequently, the highest relevant frequency that can be modeled is

$$(k\Delta s)_{\max} = \frac{\pi}{4} \quad \text{or} \quad \frac{\pi}{5}$$

For the highest frequency, as above, actual limits can be set on  $E\Delta t/\Delta s^2$  and  $u\Delta t/\Delta s$  so that the error will not exceed a specified value (say 10%) for a prescribed number of time steps ( 82 ).

It can be shown that for the regular grid of Fig. 8.1 there is no spurious diffusivity introduced through the approximation of the convective terms. The proof simply involves expanding all concentrations of Eq. (8.26) in Taylor series about node A. For the one-dimensional case and  $E = 0$ , the equation reduces to

$$\frac{\partial c}{\partial t} + u \frac{\partial c}{\partial x} = 0$$

indicating again that the finite element approximation of simple convection is free of artificial damping. This conclusion was also derived earlier

( $|\lambda| = 1$ ) and is due to the fact that the finite element approximation is essentially equivalent to central difference schemes, with spatial accuracy of order  $\Delta s^2$ .

### 8.2.3 Phase Errors

With respect to the phase error properties of the finite element method, Orszag (59) has investigated the problem of convection in a uniform 2-D rotation velocity field. His Galerkin approximation is by means of Fourier series interpolation, where 8 or 16 terms are retained. The experimental results show a behavior superior to typical second or fourth order finite difference schemes, with almost no phase error at all. This is to be expected, since the Fourier series provide an interpolation of essentially infinite order.

In the case of linear interpolation functions and for one-dimensional flow on the regular grid, the complex amplification factor  $\lambda$  is, from Eq. (8.28a):

$$\lambda = \frac{\beta - \gamma - i\delta}{\beta + \gamma + i\delta} = \frac{[(\beta - \gamma) - i\delta][(\beta + \gamma) - i\delta]}{(\beta + \gamma)^2 + \delta^2} = \frac{\beta^2 - \gamma^2 - \delta^2 - i2\beta\delta}{(\beta + \gamma)^2 + \delta^2}$$

Then, the phase  $\theta$ , defined by Eq. (8.15), is

$$\theta = \arctan \frac{-\text{Im}\lambda}{\text{Re}\lambda} = \arctan \frac{2\beta\delta}{\beta^2 - \gamma^2 - \delta^2}$$

and the ratio of the approximate to the real phase shift is

$$\begin{aligned} \frac{\theta}{ku\Delta t} &= \frac{1}{k\Delta s \frac{u\Delta t}{\Delta s}} \arctan \frac{12 \frac{u\Delta t}{\Delta s} (2 + \cos k\Delta s) \sin k\Delta s}{(4 + 2\cos k\Delta s)^2 - 36 \left(\frac{E\Delta t}{2}\right)^2 (1 - \cos k\Delta s)^2 - 9 \left(\frac{u\Delta t}{\Delta s}\right)^2 \sin^2 k\Delta s} \\ &= f_2(k\Delta s, \frac{E\Delta t}{\Delta s}, \frac{u\Delta t}{\Delta s}) \end{aligned} \quad (8.31)$$

Table 8.2 lists the ratio  $\theta/ku\Delta t$  in the case of no diffusion ( $E = 0$ ). It is seen that for pure convection the scheme is very satisfactory in terms of phase errors. The fact that the listed values are smaller than unity indicates lagging phase errors (i.e., the numerical wave lags the true wave). As can be seen from Eq. (8.31), a positive diffusion coefficient reduces the value of the denominator, thereby bringing the ratio closer to unity. The sensitivity of the ratio to  $E\Delta t/\Delta s^2$  is larger at large wavenumbers, because of the factor  $(1-\cos k\Delta s)^2$ . Thus, the most erroneous modes are the easiest to improve. A large value of  $E$  would eventually cause the ratio of Eq. (8.31) to increase beyond unity, creating leading phase errors (i.e. the numerical wave leads the true wave). By trial and error it is possible to determine the optimum value of  $E\Delta t/\Delta s^2$  such that  $f_2 = 1$  for a particular wavenumber and  $u\Delta t/\Delta s$ . The ratio  $\theta/ku\Delta t$  is listed in Table 8.3 for  $u\Delta t/\Delta s = 0.1$  and for several values of  $E\Delta t/\Delta s^2$ . The optimum value of the latter is about 0.15 for all frequencies, but in general, the phase errors are negligible.

TABLE 8.2  
Phase Error  $\theta/ku\Delta t$  for  $E = 0$

$k\Delta s$	$\frac{u\Delta t}{\Delta s} = 0.1$	$\frac{u\Delta t}{\Delta s} = 0.2$	$\frac{u\Delta t}{\Delta s} = 0.5$
$\pi/4$	0.997	0.996	0.985
$\pi/5$	0.998	0.997	0.991
$\pi/6$	0.999	0.998	0.994
$\pi/10$	$\sim 1.000$	0.999	0.998



TABLE 8.3  
Phase Error  $\theta/ku\Delta t$  for  $u\Delta t/\Delta s = 0.1$

$k\Delta s$	$\frac{E\Delta t}{\Delta s^2} = 0.05$	$\frac{E\Delta t}{\Delta s^2} = 0.10$	$\frac{E\Delta t}{\Delta s^2} = 0.15$
$\pi/4$	0.997	0.998	1.000
$\pi/5$	0.998	0.999	1.000
$\pi/6$	0.999	1.000	1.000
$\pi/10$	1.000	1.000	1.000

#### 8.2.4 Spatial Oscillations

The presence of high frequencies in the actual solution, associated with steep concentration gradients, is of major importance for the accuracy of the numerical approximation. The smoother the solution is, the better its approximation can be with a given grid and order of interpolation. The existence of high gradients in the solution of the convection-diffusion equation is associated with

- i) The type of the source, i.e. localized or distributed
- ii) The relative strength of the dispersion and advection transport mechanisms.

In general, the error norm for the approximation of a differential equation of order  $2m$  by a finite element grid of size  $\Delta s$  and degree of interpolating polynomials  $k-1$  is given by ( 75 )

$$\alpha(\omega - \omega^{\Delta s}, \omega - \omega^{\Delta s}) \leq C^2 \Delta s^{2(k-m)} |\omega|_k^2 \quad (8.32)$$

where  $C$  is a constant

$\omega$  denotes the true solution

$\omega^{\Delta s}$  is the exact solution of the discretized equations (not including time integration errors)

$|\omega|_k$  is the magnitude of the  $k^{\text{th}}$  derivative of the true solution, which is related to the  $(k-2m)^{\text{th}}$  derivative of the data  $f$ .

In our particular problem,  $m = 1$  and  $k = 2$ . Therefore, the error is

$$\alpha(\omega - \omega^{\Delta s}, \omega - \omega^{\Delta s}) \leq C^2 \Delta s^2 |\omega|_2^2 \sim C^2 \Delta s^2 |f|^2 \quad (8.33)$$

Eq. (8.33) indicates that the spatial discretization error is of order  $\Delta s^2$  and, as  $\Delta s \rightarrow 0$ , the approximate solution will converge to the true solution. But this conclusion holds only when  $f$  is smooth; when it contains a  $\delta$ -function, as is the case for point sources placed on a node, the error becomes indeterminate ( 86 ). There are certain techniques for tackling the problem in the presence of singularities, such as refining the grid in their vicinity at a rate depending on the order of the singularity, or including singular functions in the trial functions ( 75 ). While refining the grid around sources is always helpful, the best way in practice to avoid the problems associated with singularities is to avoid the singularities themselves. This is done by spreading out the localized source over several neighboring nodes or elements. Of course, if this is done, one should be prepared not to expect very good results in the immediate vicinity of the source. Depending on whether that area is of great importance, the refinement of the grid and the spatial distribution of the source should be decided.

In addition to avoiding singularities, the next important consideration refers to the ability of the grid to describe the concentration distribution and, in particular, the steep gradients that occur at the edges of the plume

under transient conditions or the vicinity of the source for steady state conditions. While in the latter case the grid can be refined locally to better handle the strong concentration gradients, this is not practical in the former case, for the edges of the plume may occur anywhere in the domain as long as the common Eulerian approach with a fixed grid is followed. Clearly, a higher order polynomial interpolation is superior to a linear approximation for describing the gaussian or exponential solutions of the convection-diffusion equation. The usual result of the inadequacy of the grid to accommodate steep gradients is the appearance of spatial oscillations and negative concentrations ( 84 ). Considering first a steady-state one-dimensional problem on the regular grid of Fig. 8.1, suppose that

- i) due to the presence of a source, the concentrations at C and D are relatively high,  $C_C \approx C_D \approx M$ ,
- ii) nodes F and G are essentially out of the plume,  $C_F \approx C_G \approx 0$ , and
- iii) nodes A, B and E have approximately the same concentration,

$$C_B \approx C_E \approx C_A < M.$$

The downstream advective transport at node A, per unit time, is then expressed as (see Eq. (8.26)):

$$\frac{u\Delta s}{6} (C_B + 2C_C + C_D - C_E - 2C_F - C_G) \approx \frac{u\Delta s M}{2}$$

while the dispersive transport is

$$E(2C_A - C_C - C_F) \approx E(2C_A - M)$$

At steady state,

$$\frac{u\Delta s M}{2} + E(2C_A - M) = 0 \quad (8.34)$$

and therefore

$$C_A \approx \frac{M}{2} \left(1 - \frac{u\Delta s}{2E}\right) \quad (8.35)$$

Eq. (8.35) shows that the sign of  $C_A$  depends on the value of  $u\Delta s/E$ . To avoid negative concentrations upstream of a continuous source, at steady-state, the following condition has to be satisfied:

$$\frac{E}{u\Delta s} > \frac{1}{2} \quad (8.36)$$

This is analogous to the restriction on the grid-Reynolds number required in finite difference schemes, as discussed in Sec. 8.1. Its applicability to finite element discretizations has been established through early numerical experiments on the one-dimensional grid shown in Fig. 8.4 ( 44 ).

Under transient conditions, the unsteady term has to be considered. Assuming the time rate of change of  $C_F$ ,  $C_G$ ,  $C_C$ ,  $C_D$  small compared to that of  $C_A \approx C_B \approx C_E$ , the latter being at the edge of the plume, the following equilibrium equation is obtained from (8.26):

$$\frac{8}{12} \Delta s^2 \frac{(C_A^{n+1} - C_A^n)}{\Delta t} + \frac{1}{2} u\Delta s M + E(C_A^n + C_A^{n+1} - M) = 0$$

which can be rewritten as:

$$C_A^{n+1} \left(1 + \frac{3}{2} \frac{E\Delta t}{\Delta s^2}\right) = C_A^n \left(1 - \frac{3}{2} \frac{E\Delta t}{\Delta s^2}\right) + \frac{3}{2} M \frac{u\Delta t}{\Delta s} \left(\frac{E}{u\Delta s} - \frac{1}{2}\right) \quad (8.37)$$

If  $C_A^n > 0$  and since normally  $3 E \Delta t / 2 \Delta s^2 < 1$  (see Sec. 8.4), a negative  $C_A^{n+1}$  would certainly require the violation of (8.36). Therefore, a conservative condition for avoiding negative concentrations in transient one-dimensional problems is still given by (8.36).

With respect to the downstream zone of the plume, the above results are applicable, if  $u$  is replaced with  $-u$ . It is then seen that there is no restriction on  $E/u\Delta s$ . In conclusion, for a steady flow, the upstream edge of the distribution is most liable to exhibit negative concentrations, and these in turn cause a wave-like pattern of negative and positive values in space, as in finite-difference schemes (42). A short duration loading is in this respect more favorable than a continuous release, because the solution of the latter has a steep exponential branch upstream of the source. In the case of tidal flow, both edges of the plume may conceivably present oscillations. Condition (8.36) must be satisfied by the highest tidal velocity in the neighborhood of the source in order to avoid negative concentrations.

We attempt now the same kind of analysis for a two-dimensional problem. Considering the edge of the plume upstream of the source at steady state and setting

$$C_o \approx M, C_A \approx C_E \approx C_C \quad \text{and} \quad C_B \approx C_F \approx C_G \approx 0,$$

in Eq. (8.26), we obtain:

$$E_x C_A + E_y C_A + \frac{u \Delta s}{6} (C_A + M) + \frac{v \Delta s}{6} (C_A + M) = 0$$

Then,

$$C_A = - \frac{M}{1 + \frac{6(E_x + E_y)}{(u+v) \Delta s}} \quad (8.38)$$

Eq. (8.38) indicates that negative concentrations always exist upstream of a localized continuous source in a two-dimensional domain. Although the analysis here is very crude, it should be expected that the two-dimensional problem will present more difficulties in numerical approximation than its one-dimensional counterpart. Indeed, the one-dimensional solution for a point source is finite everywhere, while in the two-dimensional case the solution is not defined at the source. It is essential that such a source be distributed over several elements, so that very high peaks are avoided, i.e.  $M$  is not too large in Eq. (8.38). If, in addition,

$$\frac{E_x + E_y}{(u+v)\Delta s} \gg \frac{1}{6} \quad (8.39)$$

the magnitude of (the negative value)  $C_A$ , obtained from (8.38), will be sufficiently small to be acceptable in practice. Condition (8.39) is quantitatively similar to (8.36).

The behavior of the downstream end of the plume can be examined again by substituting  $(-u, -v)$  for  $(u, v)$  in Eq. (8.38). One then obtains

$$C_A = - \frac{M}{1 - \frac{6(E_x + E_y)}{(u+v)\Delta s}}$$

which indicates that  $C_A > 0$  provided that

$$\frac{E_x + E_y}{(u+v)\Delta s} > \frac{1}{6} \quad (8.40)$$

This is less restrictive than (8.39).

### 8.3 Matrix Analysis for an Arbitrary Grid

#### 8.3.1 Time Integration Stability

As indicated in the previous section, the trapezoidal integration scheme of the finite element equations for a single layer of constant thickness has the form of Eq. (8.25) in the homogeneous case. Including the decay term, it expands to:

$$[\tilde{M} + \frac{\Delta t}{2} (\tilde{K} + \tilde{D} + \tilde{A})] \tilde{C}_{n+1} = [\tilde{M} - \frac{\Delta t}{2} (\tilde{K} + \tilde{D} + \tilde{A})] \tilde{C}_n \quad (8.41)$$

The matrices involved have been defined for individual elements in Sec. 7.2.

The geometrical matrix (Eq. 7.18)

$$\tilde{M}^e = \iint_{A^e} \tilde{N}^T \tilde{N} \, dA \quad (8.42)$$

is symmetrical positive definite and the same is true for the decay matrix, which is proportional to  $\tilde{M}^e$  (Eq. 7.23):

$$\tilde{D}^e = k \iint_{A^e} \tilde{N}^T \tilde{N} \, dA \quad (8.43)$$

The dispersion matrix has the form (Eq. 7.22)

$$\tilde{K}^e = \frac{1}{4A^e} (\tilde{E}_{xx} \tilde{b}^T \tilde{b} + \tilde{E}_{xy} \tilde{b}^T \tilde{a} + \tilde{E}_{xy} \tilde{a}^T \tilde{b} + \tilde{E}_{yy} \tilde{a}^T \tilde{a}) \quad (8.44)$$

and is symmetric and positive semidefinite. Since the system matrices  $\tilde{M}$ ,  $\tilde{D}$ ,  $\tilde{K}$ , are composed of symmetric positive definite submatrices, they also have this property. The individual advection matrix, defined by (Eq. 7.20)

$$\tilde{A}^e \tilde{C}^e = \iint_{A^e} \tilde{N}^T \left[ \frac{\partial}{\partial x}(u\tilde{C}) + \frac{\partial}{\partial y}(v\tilde{C}) \right] dA \quad (8.45)$$

is not symmetric, however, as discussed in Sec. 7.2. Introducing the continuity condition for steady but spatially variable flow

$$\frac{\partial u}{\partial x} + \frac{\partial v}{\partial y} = 0$$

we may rewrite Eq. (8.45)

$$\sum_e A^e \tilde{C}^e = \iint_{A^e} \tilde{N}^T (u \frac{\partial C}{\partial x} + v \frac{\partial C}{\partial y}) dA \quad (8.45a)$$

Integrating by parts and summing over all elements:

$$\sum_e A^e \tilde{C}^e = \sum_e \left\{ \oint \tilde{N}^T u_n C ds - \frac{1}{2A^e} \iint_{A^e} (\tilde{b}^T u + \tilde{a}^T v) C dA \right\} \quad (8.46)$$

where  $u_n$  denotes the outward normal velocity.

The concentration is expressed in terms of the nodal values through the expansion

$$C = N \tilde{C}^e$$

Since this expansion is required to be continuous across inter-element boundaries, as discussed in Sec. 7.1, and since compatible velocity expansions are used in developing the circulation field, it is seen that the line integral vanishes on the interior boundaries. Therefore,

$$\begin{aligned} \sum_e A^e \tilde{C}^e &= \int_S \tilde{N}^b T u_n C ds - \sum_e \frac{1}{2A^e} \iint_{A^e} (\tilde{b}^T u + \tilde{a}^T v) C dA \\ &= \int_S \tilde{N}^b T u_n \tilde{N}^b ds \tilde{C}^b - \sum_e \iint_{A^e} \left( \frac{\partial \tilde{N}^T}{\partial x} u + \frac{\partial \tilde{N}^T}{\partial y} v \right) \tilde{N} dA \tilde{C}^e \end{aligned} \quad (8.47)$$



Noting that by introducing the expansion of C in (8.45a) this takes the form

$$\tilde{A}^e \tilde{C}^e = \iint_{A^e} \tilde{N}^T \left( u \frac{\partial \tilde{N}}{\partial x} + v \frac{\partial \tilde{N}}{\partial y} \right) dA \tilde{C}^e \quad (8.48)$$

and combining (8.47) and (8.48), one obtains:

$$\sum_e \tilde{A}^e \tilde{C}^e = - \sum_e (\tilde{A}^e)^T \tilde{C}^e + \int_S \tilde{N}^{bT} u_{n\tilde{}} \tilde{N}^b ds \tilde{C}^b$$

or, for the system matrices:

$$\tilde{A}\tilde{C} = - \tilde{A}^T \tilde{C} + \int_{S_q} \tilde{N}^{bT} u_{n\tilde{}} \tilde{N}^b ds \tilde{C}^b \quad (8.49)$$

The line integral is restricted to the part of the boundary,  $S_q$ , where the dispersive flux is specified, because the weighting function vanishes on the segment  $S_c$  with specified concentration (Sec. 7.1).

Usually,  $S_q$  corresponds to the land boundary and there should be no velocity normal to it. Then the line integral of (8.49) vanishes entirely and the equation reduces to

$$\tilde{A} = -\tilde{A}^T \quad (8.50)$$

Eq. (8.50) indicates that the advection matrix in this case is purely skew-symmetric. This result is very important for a general stability analysis of the numerical scheme, as will be seen shortly. In addition, it is seen from Eq. (8.49) that the symmetric part of the advection matrix is associated with these portions of  $S_q$  where the normal velocity is not zero. These may represent river or estuary outlets or parts of the ocean

boundary where the gradient rather than the concentration itself is specified. This is commonly the case for outflows from the domain of interest (see Sec. 2.3). Since  $u_n > 0$  indicates flow outwards, such a flow implies a positive value of the line integral of (8.49). Setting, in general,

$$\underline{\underline{A}} = \underline{\underline{A}}_s + \underline{\underline{A}}_{ss} \quad (8.51)$$

where  $\underline{\underline{A}}_s$  denotes the symmetric part of  $\underline{\underline{A}}$  and  $\underline{\underline{A}}_{ss}$  denotes the skew-symmetric part of  $\underline{\underline{A}}$ , we may now proceed to the examination of the stability of the trapezoidal integration scheme of Eq. (8.41).

The concentration vectors at times  $t$  and  $t + \Delta t$  can be related by writing

$$\underline{\underline{C}}_{n+1} = \underline{\underline{a}} \underline{\underline{C}}_n \quad (8.52)$$

where  $\underline{\underline{a}}$  the (complex) amplification matrix, analogous to the amplification factor of Sec. (8.1). One may set, however

$$\underline{\underline{C}}_n = \lambda^n \underline{\underline{\phi}}, \text{ for all } n \quad (8.53)$$

where  $\underline{\underline{\phi}}$  an arbitrary vector (of the same dimension as  $\underline{\underline{C}}$ )

Substituting in (8.52):

$$\lambda \underline{\underline{\phi}} = \underline{\underline{a}} \underline{\underline{\phi}}$$

or

$$(\underline{\underline{a}} - \lambda \underline{\underline{I}}) \underline{\underline{\phi}} = 0 \quad (8.54)$$

This implies that the expression (8.53) is possible, provided  $\lambda$  is an eigenvalue of the amplification matrix  $\underline{\underline{a}}$ .

The necessary condition for stability is ( 68):

$$\| \underline{a} \| \leq 1 \quad (8.55a)$$

or, equivalently

$$|\lambda| \leq 1 \quad (8.55b)$$

Substituting the expression (8.53) for  $\underline{C}_n$  and  $\underline{C}_{n+1}$  in (8.41), and pre-multiplying both sides by  $\underline{\phi}^T$ , one obtains:

$$\underline{\phi}^T [\underline{M} + \frac{\Delta t}{2} (\underline{K} + \underline{D} + \underline{A})] \lambda \underline{\phi} = \underline{\phi}^T [\underline{M} - \frac{\Delta t}{2} (\underline{K} + \underline{D} + \underline{A})] \underline{\phi} \quad (8.56)$$

Since  $\underline{M}$ ,  $\underline{K}$  and  $\underline{D}$  are positive definite, it follows that

$$\underline{\phi}^T \underline{M} \underline{\phi} = m > 0 \quad (8.57a)$$

$$\underline{\phi}^T \underline{D} \underline{\phi} = d > 0 \quad (8.57b)$$

$$\underline{\phi}^T \underline{K} \underline{\phi} = \kappa \geq 0 \quad (8.57c)$$

For the advection matrix,  $\underline{A}$ , one can write

$$\underline{\phi}^T \underline{A} \underline{\phi} = a_s + i a_{ss} \quad (8.58)$$

where  $a_s$  is related to the symmetric part and

$a_{ss}$  to the skew-symmetric part of  $\underline{A}$ .

Then, Eq. (8.56) yields:

$$\lambda = \frac{m - \frac{\Delta t}{2}(\kappa + d + a_s) - i \frac{\Delta t}{2} a_{ss}}{m + \frac{\Delta t}{2}(\kappa + d + a_s) + i \frac{\Delta t}{2} a_{ss}}$$

or,

$$\lambda^2 = |\lambda|^2 = \frac{[m - \frac{\Delta t}{2}(\kappa+d+a_s)]^2 + (\frac{\Delta t}{2} a_{ss})^2}{[m + \frac{\Delta t}{2}(\kappa+d+a_s)]^2 + (\frac{\Delta t}{2} a_{ss})^2} \quad (8.59)$$

In the most common case that  $a_s = 0$ , Eq. (8.59) clearly shows that

$$|\lambda|^2 < 1$$

for any value of  $\Delta t$ . That is, the time integration scheme is unconditionally stable for an arbitrary grid.

The value of  $a_s$  may be different than zero only when there are parts of the boundary where the concentration gradient is prescribed, instead of the concentration, and the normal velocity does not vanish. Since, from (8.49),

$$a_s = \tilde{\phi}^T \tilde{A}_s \tilde{\phi} = \tilde{\phi}^T \int_{s_q} \tilde{N}^b{}^T u_n \tilde{N}^b ds \tilde{\phi}$$

it is seen that  $a_s$  has the sign of  $u_n$ . Thus, when the normal velocity is outwards,  $a_s > 0$  and Eq. (8.59) still implies that

$$|\lambda| < 1$$

Actually, the stability is enhanced in this case. However, when the normal velocity is inwards,  $a_s < 0$ . Then, the stability of the scheme depends on the relative magnitude of  $a_s$  compared to  $\kappa+d$ . In the unlikely event that  $a_s$  dominates, a value of  $|\lambda|$  larger than unity is implied. This analysis fits nicely with the considerations on boundary conditions (Sec. 2.3), where physical reasoning indicated that the concentration gradient should be prescribed only in outflow boundary segments, while during inflow the

specification of the concentration is more appropriate. If this is done,  $a_s \geq 0$  and the unconditional stability is maintained. Further, a small negative value of  $a_s$ , associated with a small inflow boundary segment, should also be acceptable in practice, being offset by the magnitude of  $K+d$ .

### 8.3.2 Iteration Convergence

The feature of unconditional stability makes the scheme (8.41) extremely attractive to use, provided that  $\tilde{K}$ ,  $\tilde{D}$  and  $\tilde{A}$  are actually constant. When they are variable, however, a new matrix has to be inverted in every time-step and this would become uneconomical for large problems. Therefore, as discussed in Sec. 7.3, an iterative scheme is employed in this case. That is, Eq. (8.41) is written as:

$$\tilde{M}C_{n+1}^{(i+1)} = [\tilde{M} - \frac{\Delta t}{2} (\tilde{K} + \tilde{D} + \tilde{A})_n] C_n - \frac{\Delta t}{2} (\tilde{K} + \tilde{D} + \tilde{A})_{n+1} C_{n+1}^{(1)} \quad (8.60)$$

The condition for the convergence of the iteration is (89):

$$\| \tilde{M}^{-1} \frac{\Delta t}{2} (\tilde{K} + \tilde{D} + \tilde{A})_{n+1} \| < 1 \quad (8.61)$$

Dropping the subscript, this implies:

$$\Delta t < \frac{2}{\| \tilde{M}^{-1} (\tilde{K} + \tilde{D} + \tilde{A}) \|} \quad (8.61a)$$

Since the norm of a sum is less than or equal to the sum of the norms, a more restrictive condition can be obtained, i.e.

$$\Delta t < \frac{2}{\| \tilde{M}^{-1} \tilde{A} \| + \| \tilde{M}^{-1} \tilde{K} \| + \| \tilde{M}^{-1} \tilde{D} \|} \quad (8.62)$$

This is a sufficient condition and is conveniently expressed in terms of the individual ratios of the various matrices to the geometrical matrix. It indicates that, because of the iteration, the choice of the time step cannot be arbitrary. Thus, there is a trade-off: the advantage of unconditional stability is lost in the attempt to handle time variability of parameters and inputs more economically. In problems where there is such variability, the advantage gained is considered more important than the one lost, since the time step would be limited anyway from considerations of resolution of the description of the phenomena.

A slightly sharper condition than (8.62) can be obtained by setting in Eq. (8.60)

$$\tilde{C}_{n+1}^{(i)} = \lambda^{*i} \phi, \quad \text{for all } i \quad (8.63)$$

in a way analogous to (8.53) used for studying the stability of the scheme. Now,  $\lambda^*$  are the eigenvalues of matrix  $\tilde{a}^*$ , defined by

$$\tilde{C}_{n+1}^{(i+1)} = \tilde{a}^* \tilde{C}_{n+1}^{(i)} \quad (8.64)$$

The condition for iteration convergence is expressed as

$$|\lambda^*| < 1 \quad (8.65)$$

Eq. (8.60) yields, after neglecting the constant term

$$\lambda^* = - \frac{\Delta t}{2} \frac{\kappa + d + a_s + ia_{ss}}{m} \quad (8.66)$$

where  $\kappa$ ,  $d$ ,  $m$ ,  $a_s$ ,  $a_{ss}$ , are as defined in (8.57) and (8.58).

For the usual case that  $a_s = 0$ ,

$$|\lambda^*| = \frac{\Delta t}{2} [(\frac{\kappa+d}{m})^2 + (\frac{a_{ss}}{m})^2]^{1/2}$$

and therefore, condition (8.65) is satisfied when

$$\Delta t < \frac{2}{[(\frac{\kappa+d}{m})^2 + (\frac{a_{ss}}{m})^2]^{1/2}} \quad (8.67)$$

Since the scalars in the denominator of (8.67) essentially represent the eigenvalues of the corresponding matrices, and the eigenvalues are commonly used as measure of the matrix norm, it can be argued that

$$\kappa/m \sim \| \tilde{M}^{-1} \tilde{K} \| \quad (8.68a)$$

$$d/m \sim \| \tilde{M}^{-1} \tilde{D} \| \quad (8.68b)$$

$$|a_{ss}/m| \sim \| \tilde{M}^{-1} \tilde{A} \| \quad (8.68c)$$

Thus the restriction on  $\Delta t$  imposed by (8.67) is expressed in the same terms as (8.62), i.e. the ratios of magnitudes of the matrices involved, as expressed by their eigenvalue norms. However, it can be readily seen that condition (8.67) is less conservative than (8.62).

Yet, neither condition is practical in this form. This is because the norm expression is rather abstract and the eigenvalues have to be derived through long machine computations once the matrices are formed. Thus, one does not have an explicit relation between the time step and the parameters of the problem. Such a relation is derived in the next section.

#### 8.4 An Approximate Criterion for the Time Step

Starting with the definitions of the matrices involved, we will attempt now to transform the right-hand side of (8.62), and (8.67), to an easily

tractable, though approximate, form. The system matrices appearing in the previous analysis all consist of sub-matrices associated with the individual elements of the solution space. The matrix eigenvalues, the most common type of norms (20), can be easily evaluated at the element level.

Provided there are no drastic changes in the grid or the parameters over the domain, the conclusions reached at the element level can be generalized for the whole area. In any case, if (8.62) or (8.67) is satisfied for the "worst" element, stability and convergence of the whole scheme is implied.

Expressions of the element matrices were presented in Sec. 7.2.

Dropping the superscript e for convenience, we summarize below the various terms:

i) The Geometrical matrix is

$$\tilde{M} = \frac{A}{12} \begin{bmatrix} 2 & 1 & 1 \\ 1 & 2 & 1 \\ 1 & 1 & 2 \end{bmatrix} \quad (8.69)$$

Therefore

$$\tilde{M}^{-1} = \frac{12}{A} \frac{1}{4} \begin{bmatrix} 3 & -1 & -1 \\ -1 & 3 & -1 \\ -1 & -1 & 3 \end{bmatrix} \quad (8.69a)$$

ii) The Dispersion matrix is, for isotropic conditions ( $E_{xx} = E_{yy} = E$ ):

$$\begin{aligned} \tilde{K} &= \frac{1}{4A} (E \tilde{b}^T \tilde{b} + E \tilde{a}^T \tilde{a}) \\ &= \frac{E}{4A} \begin{bmatrix} b_1^2 + a_1^2 & b_1 b_2 + a_1 a_2 & b_1 b_3 + a_1 a_3 \\ b_1 b_2 + a_1 a_2 & b_2^2 + a_2^2 & b_2 b_3 + a_2 a_3 \\ b_1 b_3 + a_1 a_3 & b_2 b_3 + a_2 a_3 & b_3^2 + a_3^2 \end{bmatrix} \end{aligned} \quad (8.70)$$



Noticing that products of the form  $b_i b_j + a_i a_j$  represent the inner product of  $\Delta s_i, \Delta s_j$  considered as vectors,  $\tilde{K}$  can be further written (see Figure 8.2)

$$\tilde{K} = \frac{E}{4A} \begin{bmatrix} \Delta s_1^2 & -\Delta s_1 \Delta s_2 \cos \theta_3 & -\Delta s_1 \Delta s_3 \cos \theta_2 \\ -\Delta s_1 \Delta s_2 \cos \theta_3 & \Delta s_2^2 & -\Delta s_2 \Delta s_3 \cos \theta_1 \\ -\Delta s_1 \Delta s_3 \cos \theta_2 & -\Delta s_2 \Delta s_3 \cos \theta_1 & \Delta s_3^2 \end{bmatrix} \quad (8.70a)$$

iii) The Advection matrix, for uniform flow (u,v), is:

$$\begin{aligned} \tilde{A} &= \frac{1}{24} \begin{bmatrix} 2 & 1 & 1 \\ 1 & 2 & 1 \\ 1 & 1 & 2 \end{bmatrix} (\tilde{u} \tilde{b} + \tilde{v} \tilde{d}) = \\ &= \frac{1}{24} \begin{bmatrix} 2 & 1 & 1 \\ 1 & 2 & 1 \\ 1 & 1 & 2 \end{bmatrix} \begin{bmatrix} 1 \\ 1 \\ 1 \end{bmatrix} (u[b_1 \ b_2 \ b_3] + v[a_1 \ a_2 \ a_3]) \quad (8.71) \end{aligned}$$

Since  $u b_i + v a_i$  can again be considered as the inner product of the velocity vector and a vector of magnitude  $\Delta s_i$  having the direction of the inwards normal to the element side, the above expression takes the form

$$\tilde{A} = \frac{U}{24} \begin{bmatrix} 2 & 1 & 1 \\ 1 & 2 & 1 \\ 1 & 1 & 2 \end{bmatrix} \begin{bmatrix} 1 \\ 1 \\ 1 \end{bmatrix} [\Delta s_1 \cos \phi_1 \ \Delta s_2 \cos \phi_2 \ \Delta s_3 \cos \phi_3] \quad (8.71a)$$

where  $U = (u^2 + v^2)^{1/2}$  is the velocity magnitude.

iv) The Decay matrix is

$$\tilde{D} = \frac{k_A}{12} \begin{bmatrix} 2 & 1 & 1 \\ 1 & 2 & 1 \\ 1 & 1 & 2 \end{bmatrix} = k \tilde{M} \quad (8.72)$$

One may now proceed in formulating the matrix products appearing in (8.62). It is first noticed that

$$\tilde{M}^{-1} = \frac{12}{A} \frac{1}{4} \begin{bmatrix} 3 & -1 & -1 \\ -1 & 3 & -1 \\ -1 & -1 & 3 \end{bmatrix} = \frac{12}{A} \left( I - \frac{1}{4} \begin{bmatrix} 1 & 1 & 1 \\ 1 & 1 & 1 \\ 1 & 1 & 1 \end{bmatrix} \right)$$

Due to the fact that each column of  $\tilde{K}$  adds up to zero, as seen from (8.70), only the first part of the above decomposition of  $\tilde{M}^{-1}$  will give a contribution to  $\tilde{M}^{-1}\tilde{K}$ ; since this is the identity matrix,

$$\tilde{M}^{-1}\tilde{K} = \frac{12}{A} \tilde{K} \quad (8.73)$$

For an equilateral triangle

$$\Delta s_1 = \Delta s_2 = \Delta s_3 = \Delta s$$

$$\theta_1 = \theta_2 = \theta_3 = 60^\circ$$

$$A = \frac{\Delta s^2 \sqrt{3}}{4}$$

Consequently,

$$\tilde{M}^{-1}\tilde{K} = \frac{12}{A} \frac{E \Delta s^2}{8A} \begin{bmatrix} 2 & -1 & -1 \\ -1 & 2 & -1 \\ -1 & -1 & 2 \end{bmatrix}$$

The eigenvalues of the matrix are 0,3,3. Therefore, a conservative bound on  $\Delta t$  will be obtained by using

$$\| \tilde{M}^{-1} \tilde{K} \|_{\max} = \frac{12E\Delta s^2}{8(\frac{3}{16} \Delta s^4)} 3 = 24 \frac{E}{\Delta s^2} \quad (8.73)$$

A less conservative estimate can be obtained by using for  $\| \tilde{M}^{-1} \tilde{K} \|$  the average of the three eigenvalues, bearing in mind that (8.62) is already more restrictive than the actual condition (8.61a). Then,

$$\| \tilde{M}^{-1} \tilde{K} \|_{av} = \frac{12E\Delta s^2}{8(\frac{3}{16} \Delta s^4)} 2 = 16 \frac{E}{\Delta s^2} \quad (8.73a)$$

Alternatively, for a right triangle

$$\Delta s_1 = \sqrt{2}\Delta s, \quad \Delta s_2 = \Delta s_3 = \Delta s$$

$$\theta_1 = 90^\circ \quad \theta_2 = \theta_3 = 45^\circ$$

$$A = \frac{1}{2} \Delta s^2$$

Consequently,

$$\tilde{K} = \frac{E\Delta s^2}{4A} \begin{bmatrix} 2 & -1 & -1 \\ -1 & 1 & 0 \\ -1 & 0 & 1 \end{bmatrix}$$

The matrix eigenvalues are 0, 1, 3. Therefore

$$\| \tilde{M}^{-1} \tilde{K} \|_{\max} = \frac{12E\Delta s^2}{4(\frac{1}{4} \Delta s^4)} 3 = 36 \frac{E}{\Delta s^2} \quad (8.74)$$

while

$$\| \tilde{M}^{-1} \tilde{K} \|_{av} = \frac{12E\Delta s^2}{4(\frac{1}{4}\Delta s^4)} \frac{4}{3} = 16 \frac{E}{\Delta s^2} \quad (8.74a)$$

The latter is exactly the same as (8.73a).

Eqs. (8.69) and (8.71a) imply that

$$\tilde{M}^{-1} \tilde{A} = \frac{12}{A} \frac{U}{24} \begin{bmatrix} 1 \\ 1 \\ 1 \end{bmatrix} [\Delta s_1 \cos \phi_1 \quad \Delta s_2 \cos \phi_2 \quad \Delta s_3 \cos \phi_3]$$

The norm of  $\tilde{M}^{-1} \tilde{A}$  can be obtained as the product of norms of the vector and row matrices in the above expression. Consistent with using eigenvalue norms for the square matrices, the Euclidean norms of the vector and row should be used, i.e.

$$\| \tilde{M}^{-1} \tilde{A} \| = \frac{U}{2A} \sqrt{3} \sqrt{\Delta s_1^2 \cos^2 \phi_1 + \Delta s_2^2 \cos^2 \phi_2 + \Delta s_3^2 \cos^2 \phi_3} \quad (8.75)$$

According to Figure 8.2:

$$\phi_2 = \phi_1 + \pi - \theta_3 \quad \longrightarrow \quad \cos \phi_2 = -\cos \phi_1 \cos \theta_3 - \sin \phi_1 \sin \theta_3$$

$$\phi_3 = \phi_1 - (\pi - \theta_2) \quad \longrightarrow \quad \cos \phi_3 = -\cos \phi_1 \cos \theta_2 + \sin \phi_1 \sin \theta_2$$

Then, for an equilateral triangle, Eq. (8.75) becomes:

$$\| \tilde{M}^{-1} \tilde{A} \| = \frac{U}{2(\frac{\sqrt{3}}{4} \Delta s^2)} \sqrt{3} \Delta s \sqrt{\cos^2 \phi_1 + 2(\frac{1}{4} \cos^2 \phi_1 + \frac{3}{4} \sin^2 \phi_1)}$$

that is,

$$\| \tilde{M}^{-1} \tilde{A} \| = 2 \sqrt{\frac{3}{2}} \frac{U}{\Delta s} \quad (8.76)$$

For a right triangle Eq. (8.75) gives

$$\| \tilde{M}^{-1} \tilde{A} \| = \frac{U}{2(\frac{1}{2} \Delta s^2)} \sqrt{3\Delta s \left( 2\cos^2\phi_1 + 2(\frac{1}{2} \cos^2\phi_1 + \frac{1}{2} \sin^2\phi_1) \right)}$$

i.e.,

$$\| \tilde{M}^{-1} \tilde{A} \| = \sqrt{3(2\cos^2\phi_1 + 1)} \frac{U}{\Delta s} \quad (8.77)$$

This expression indicates that the norm is not uniquely defined, but depends on the orientation of the triangle with respect to the flow. The worst case is obviously obtained when  $\phi_1 = 0^\circ$  or  $180^\circ$ , i.e. when the flow is normal to the hypotenuse, yielding

$$\| \tilde{M}^{-1} \tilde{A} \|_{\max} = 3 \frac{U}{\Delta s} \quad (8.77a)$$

When the flow is parallel to one of the legs of the right angle, it is  $\phi_1 = 45^\circ$  and therefore

$$\| \tilde{M}^{-1} \tilde{A} \| = \sqrt{6} \frac{U}{\Delta s} = 2\sqrt{\frac{3}{2}} \frac{U}{\Delta s} \quad (8.77b)$$

which is exactly the same as (8.76).

Finally it is evident from (8.72) that

$$\| \tilde{M}^{-1} \tilde{D} \| = k \quad (8.78)$$

According to the above, the criterion (8.62) can be rewritten in a variety of ways, depending on the element shape and orientation and the degree of conservatism desired. Thus, the absolute lower bounds are given by

$$\Delta t < \frac{1}{\sqrt{\frac{3}{2}} \frac{U}{\Delta s} + 12 \frac{E}{\Delta s^2} + \frac{k}{2}} \quad (8.79a)$$

$$\Delta t < \frac{1}{\frac{3}{2} \frac{U}{\Delta s} + 18 \frac{E}{\Delta s^2} + \frac{k}{2}} \quad (8.79b)$$

for equilateral and right triangles, respectively. Although the latter appears to be stricter, the different definition of  $\Delta s$  has to be taken into consideration. Using the average value of  $\| \tilde{M}^{-1} \tilde{K} \|$ , the condition becomes the same for both triangle shapes, provided the flow is parallel to one of the legs of the right triangle :

$$\Delta t < \frac{1}{\sqrt{\frac{3}{2}} \frac{U}{\Delta s} + 8 \frac{E}{\Delta s^2} + \frac{k}{2}} \quad (8.80)$$

Alternatively, using the same matrix measures in the sharper condition (8.67), we obtain

$$\Delta t < \frac{1}{\sqrt{\left(\sqrt{\frac{3}{2}} \frac{U}{\Delta s}\right)^2 + \left(8 \frac{E}{\Delta s^2} + \frac{k}{2}\right)^2}} \quad (8.81)$$

which is, in general, less conservative than (8.80) by at most 40%.

In modeling applications it is usual practice to design the grid with approximately equilateral triangles, avoiding angles in excess of  $90^\circ$ . Although a general criterion cannot be given for an arbitrary grid except in the "abstract" way of Sec. 8.3, it is believed that either of (8.80) or (8.81) should provide a good starting point for defining the time step in any given problem. The primary value of these criteria, irrespective of

the exact numerical coefficients, lies in the inclusion of all relevant parameters in a single expression. It is seen that the non-dimensional groups of interest are again  $E\Delta t/\Delta s^2$  and  $U\Delta t/\Delta s$ , while  $k\Delta t$  has to be also considered, if there is decay. So far, the effect of the various parameters has been examined separately, if at all, and only by numerical experimentation because of the inherent difficulty of a strict theoretical analysis to proceed to practically meaningful results. Thus, it has been suggested (44) that for satisfactory time integration using the same iterative scheme, the following conditions should both hold:

$$\Delta t < \frac{\Delta s^2}{10E} \quad \text{and} \quad \Delta t < \frac{\Delta s}{10U}$$

These bounds are significantly stricter than (8.80), especially with respect to advection.

Other criteria, given for explicit finite difference schemes, are of interest in comparison to (8.80) or (8.81). Some of them were presented in Sec. 8.1. For 1-D problems,

$$\Delta t < \frac{\Delta x^2}{2E}$$

$$\Delta t < \frac{\Delta x}{u}$$

$$\Delta t < \frac{2}{2 \frac{E}{\Delta x^2} + \frac{u}{\Delta x}}$$

while for 2-D problems,

$$\Delta t < \frac{1}{2E(\frac{1}{\Delta x^2} + \frac{1}{\Delta y^2})}$$

$$\Delta t < \frac{1}{\frac{u}{\Delta x} + \frac{v}{\Delta y}}$$

$$\Delta t < \frac{1}{2E(\frac{1}{\Delta x^2} + \frac{1}{\Delta y^2}) + \frac{u}{\Delta x} + \frac{v}{\Delta y}}$$

$$\Delta t < \min \left\{ \frac{\Delta x}{u}, \frac{\Delta y}{v}, \frac{\Delta x^2}{4E} \right\}$$

Using typical values of coastal environments:  $U \approx 10$  cm/sec,  
 $E \approx 30$  m<sup>2</sup>/sec,  $k \approx 1$  day<sup>-1</sup>,  $\Delta s \approx 1$  km, condition (8.80) becomes

$$\Delta t < 2718 \text{ sec}$$

while (8.81) gives

$$\Delta t < 3644 \text{ sec}$$

Thus, the restriction caused by the iteration still allows reasonably large time steps, in view of the desired accuracy of representation of the tidal variation of the flow field. Usually, the effect of decay is considerably less than that of advection and dispersion, which are, in general, of the same order of magnitude. It should be mentioned that, in problems with significant spatial variations, the largest values of  $E/\Delta s^2$  and  $U/\Delta s$  are those limiting the time step. Clearly, a refinement of the grid in a certain area for better resolution leads to higher values of these ratios and consequently a smaller allowable time step. It may be also seen that,



in a certain grid, stability problems are most likely to arise during periods of strong currents, since  $U/\Delta s$  and also  $E/\Delta s^2$  are then larger.

A comparison of (8.80) and (8.81) to time steps actually achieved in one- and two-dimensional problems, that establishes more confidence in the simple theoretical results, follows in the next section.

### 8.5 Experimental Results

Conditions (8.79a,b) or (8.80), limiting the time step, can be written in the following general form:

$$\mu_1 \frac{U\Delta t}{\Delta s} + \mu_2 \frac{E\Delta t}{\Delta s^2} + \mu_3 k\Delta t < 1 \quad (8.82)$$

Considering the non-dimensional parameter  $U\Delta t/\Delta s$ ,  $E\Delta t/\Delta s^2$  and  $k\Delta t$  as Cartesian coordinates, the inequality (8.82) implies that an "acceptable" point in that space must be between the plane

$$\mu_1 \frac{U\Delta t}{\Delta s} + \mu_2 \frac{E\Delta t}{\Delta s^2} + \mu_3 k\Delta t = 1$$

and the coordinate planes. In the absence of decay (which usually gives a negligible contribution anyway), the space is reduced to two dimensions. Using the values of the constants  $\mu_1$ ,  $\mu_2$  pertaining to (8.80), one obtains:

$$1.22 \frac{U\Delta t}{\Delta s} + 8 \frac{E\Delta t}{\Delta s^2} < 1 \quad (8.83)$$

Similarly, condition (8.81) may be written as follows:

$$\left(1.22 \frac{U\Delta t}{\Delta s}\right)^2 + \left(8 \frac{E\Delta t}{\Delta s^2}\right)^2 < 1 \quad (8.84)$$

While (8.83) determines a theoretically "safe" area on the plane

$(\frac{U\Delta t}{\Delta s}, \frac{E\Delta t}{\Delta s^2})$  bound by a straight line, (8.84) indicates an elliptical boundary which entirely contains the previous area. Thus, (8.84) is less conservative, extending the admissibility of combinations  $(\frac{U\Delta t}{\Delta s}, \frac{E\Delta t}{\Delta s^2})$  over a larger part of the plane. Both boundaries are drawn in Figure 8.3.

Given the parameters E, U and the numerical discretization  $\Delta t$ ,  $\Delta s$  of a problem, the two ratios can be formed and the location of the point corresponding to their coordinates can be found. If it lies within the safe region, there should be no difficulty with the convergence and stability of the solution.

A large number of runs was carried out on the one-dimensional grid shown in Figure 8.4. A point source was simulated by loading the three nodes marked with dots. Most runs involved continuous releases, but instantaneous injections were also made. For each run the corresponding point was plotted in Figure 8.3, in an effort to establish the extent to which the theoretical result of (8.83) or (8.84) is valid in practice. In the same figure, the line  $E/U\Delta s = 1/2$  is drawn. This represents the theoretically lowest ratio, below which negative upstream concentrations cannot be avoided in one-dimensional problems (Eq. (8.36)).

In Table 8.4 the various symbols used in Figure 8.3 are explained and the classification of runs is made with respect to the iteration convergence behavior and the presence or not of significant spatial oscillations in the solution.

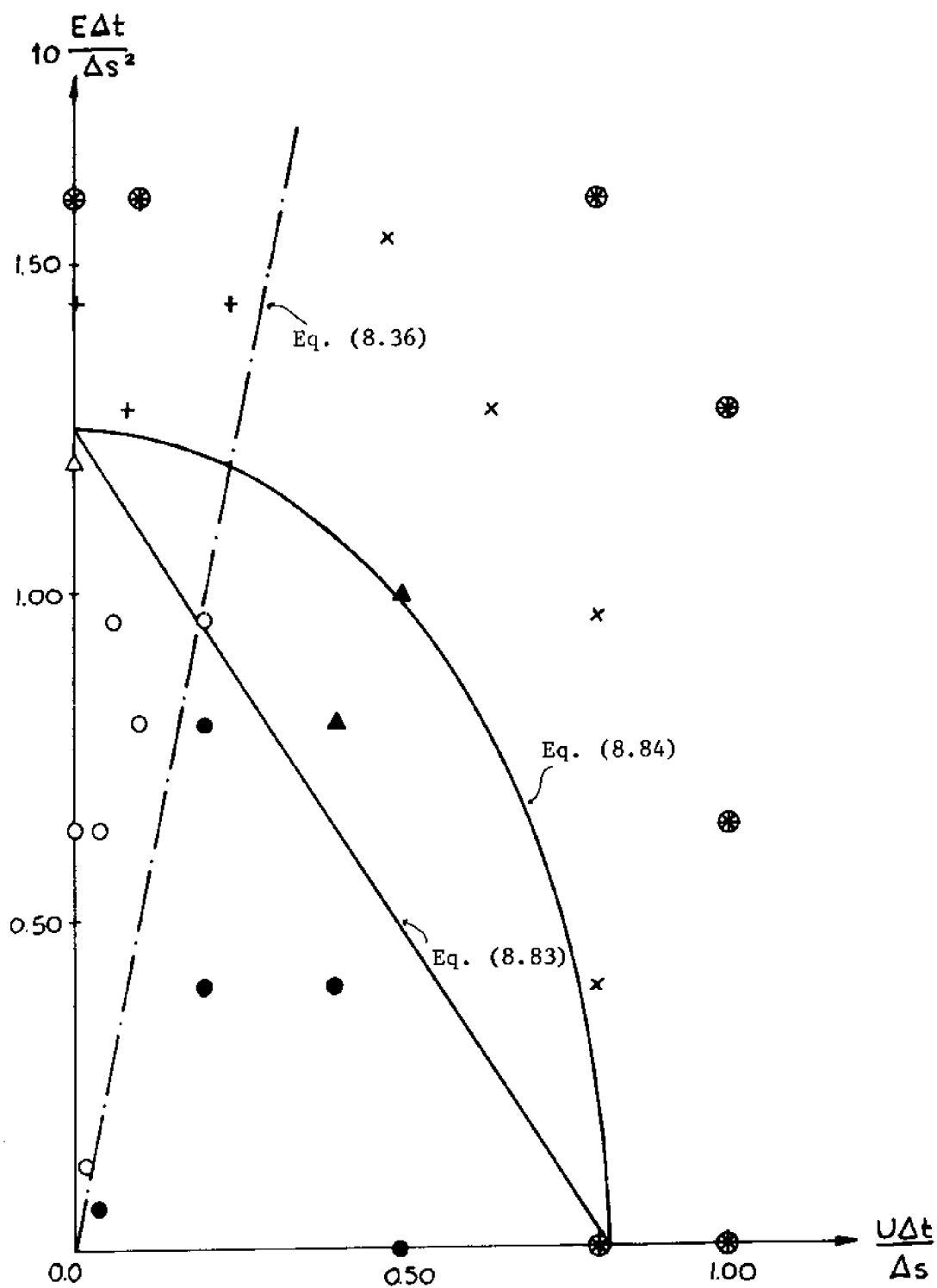


Figure 8.3 Comparison of Theoretical Bounds on the Time Step with 1-D Runs

TABLE 8.4  
Definition of Symbols Used in Figures 8.3 and 8.6

Symbol	Error After 10 Iterations	Negatives as Percent of Peak	Remarks
○	< 1%	< 10%	Good, smooth solution
●	< 1%	> 10%	Iteration converges well, but result exhibits oscillations
△	< 10%	< 10%	} Iteration error goes down rapidly as time proceeds
▲	< 10%	> 10%	
+	> 10%	< 10%	} Iteration does not always decrease rapidly (some may eventually blow up)
×	> 10%	> 10%	
⊗	-	-	Blows up

The most important conclusion from Figure 8.3 is that all runs that exhibit more or less serious problems with respect to iteration convergence lie outside the "safe" region. Actually, not too far from the elliptic boundary there are points representing runs that rapidly became unstable. Points closer to that boundary, but still outside, generally present iteration convergence errors of 20 to 75%, decreasing more or less slowly over time. Since there is a limit of 10 iterations per time step in the program, we cannot say whether these runs would eventually blow up, if allowed to continue iterating. Apparently, when the iteration is stopped with a small error, the behavior tends to improve over the next time steps.

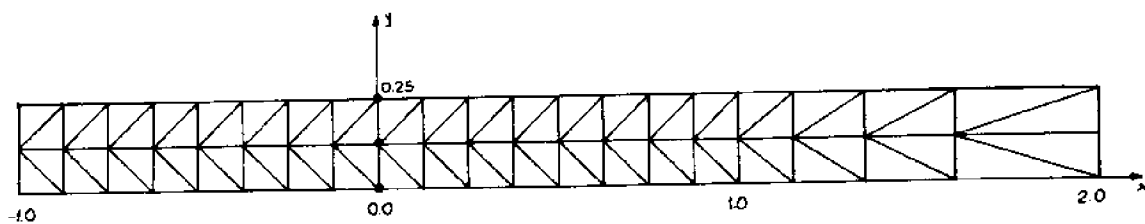


Figure 8.4 One-Dimensional Finite Element Test Grid

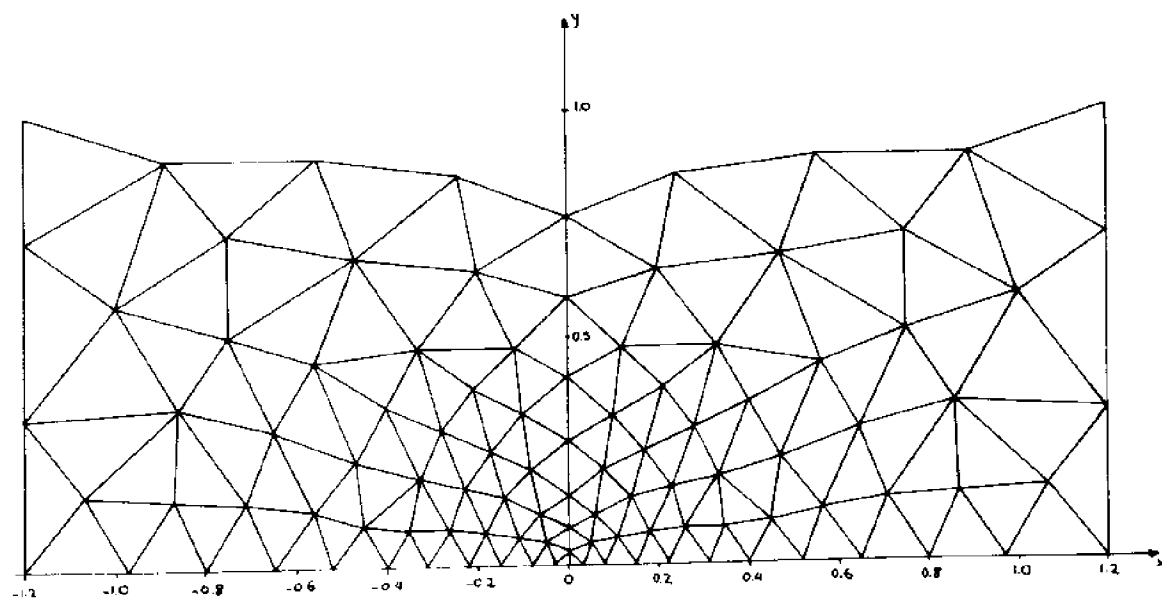


Figure 8.5 Two-Dimensional Finite Element Test Grid

Of course, these errors are accumulated in the solution. Runs between the two boundaries defined by (8.83) and (8.84) present, interestingly, "acceptable" errors of less than 10%, which actually are rapidly diminishing in subsequent time steps. Finally, runs within the inner boundary generally converge very easily, with errors less than 1%. It appears also that—since the time step increases along rays originating from the origin, for constant values of  $E$ ,  $U$ ,  $\Delta s$ —slightly better time steps can be achieved in the interior rather than close to the axes, especially the advection axis. This may just indicate a slight bias of the theoretical criteria; however, these do not seem to be too conservative in view of the relatively large errors involved in the runs outside the boundaries. On the other hand, certainly the extreme conditions (8.79a,b) are too restrictive.

The other important result of the experiments is associated with the accuracy condition (8.36). It is seen that the line  $E/U\Delta s = 1/2$  exactly separates the regions where runs do or do not show appreciable upstream negative concentrations and spatial oscillations. These oscillations become more severe near the x-axis, as the ratio  $E/U\Delta s$  diminishes and they are practically eliminated as  $E/U\Delta s$  increases slightly above  $1/2$ .

Data from various runs on two-dimensional test grids, such as that of Figure 8.5 and of (44), as well as two-dimensional grids of natural water bodies, such as the Massachusetts Bay (Fig. 9.5), Plymouth-Duxbury Bay and adjacent area (63), Great Egg Harbor, N.J. etc., have been compiled and plotted in Figure 8.6. The meaning of the various symbols is the same as in Figure 8.3. In the test grids the flow is uniform along the

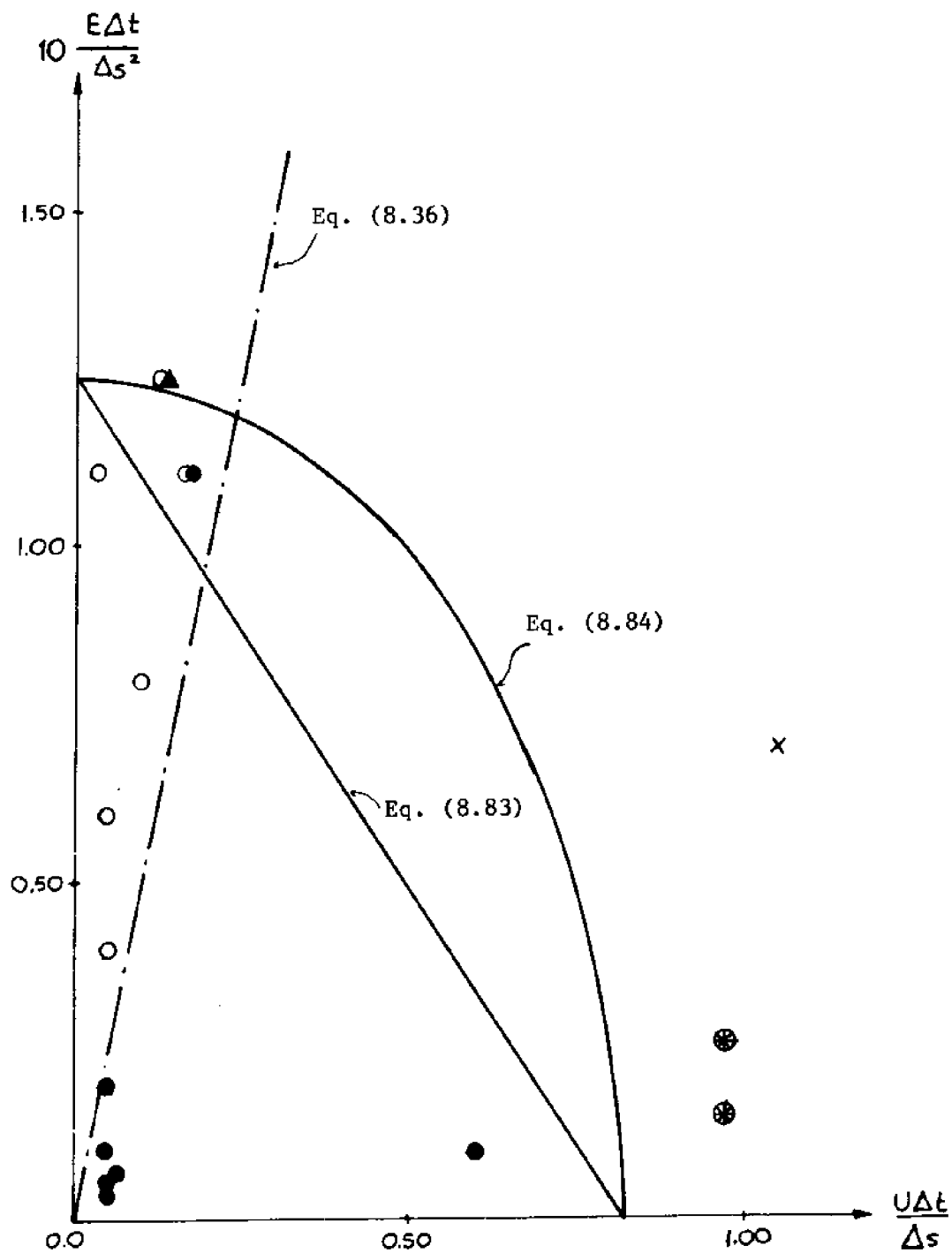


Figure 8.6 Comparison of Theoretical Bounds on the Time Step with 2-D Runs

x-axis and the dispersion only lateral, in the y-direction. In the application runs actual velocities, obtained from a compatible finite element circulation model (86), variable in space and time, are used. In view of this variability, the point having the largest sum of  $8 \frac{E\Delta t}{\Delta s^2} + 1.22 \frac{U\Delta t}{\Delta s}$  should be examined. If there is a location where this sum is much higher than over the rest of the domain, eg. caused by high velocity in a narrow zone, it might not be crucial for the stability of the whole scheme. Indeed, the point on the far right of Figure 8.6 is associated with such locally high velocities. However, points closer to the theoretical boundary, corresponding to high velocities over extended areas, indicate that the solution blows up. It is significant that all runs within the theoretically safe area do not present convergence difficulties. The boundaries can only be considered to be approximate in this case, since they are derived for one-dimensional conditions. Thus, good convergence may sometimes be achieved outside these limits. Furthermore, accuracy of the solution is more difficult in the two-dimensional case and appreciable oscillations can show up even when  $E/U\Delta s > 1/2$ . Indeed, some of the runs denoted by white circles exhibit negatives close to 10% of the peak. It is very interesting to note that there are two pairs of points having the same coordinates but different behavior. This is solely due to different source distributions. For example, both points (0.17, 1.11) represent continuous releases at the origin of the grid shown in Figure 8.5. In one case the source was distributed over two elements, while in the other over eight elements. The dramatic improvement in the numerical solution can be seen in Figure 8.7. Upstream oscillations are practically eliminated in the second case. These observations are in agreement with the theoretical arguments of Sec. 8.2.4.



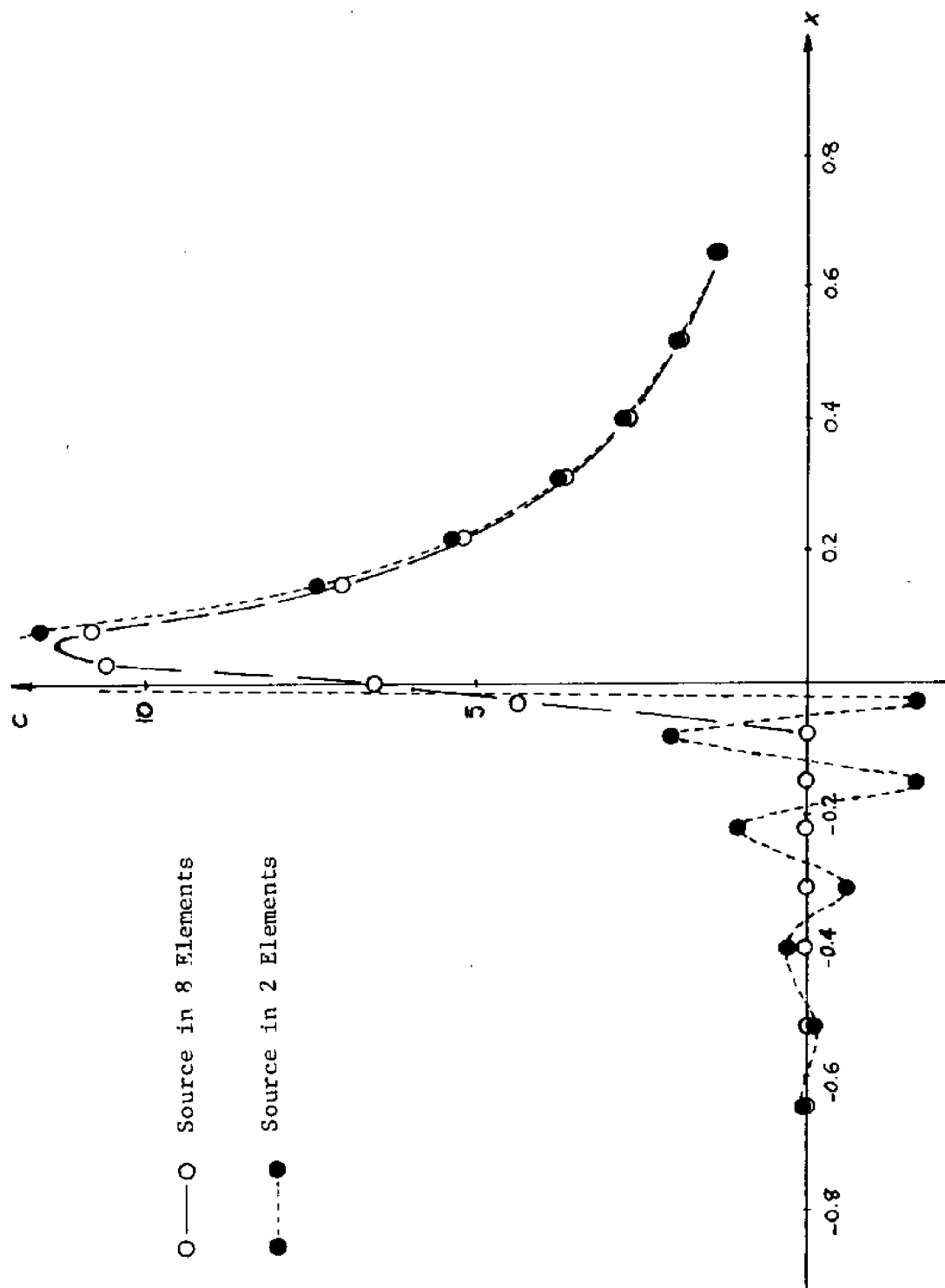


Figure 8.7 Comparison of Different Loading Strategies in a 2-D Grid

In the above, the contribution of the decay term ( $k\Delta t/2$ ) was of the order of 0.01 or less and thus neglected. If it becomes significant, it has, of course, to be taken into account by displacing inwards the limit of the safe region.

The general conclusion from the experimental results is that the theoretical bounds are very satisfactory for one-dimensional problems and still reasonably valid in a two-dimensional domain with constant or variable flow field. These bounds are appropriate not only for coastal dispersion problems but also for other dispersion problems. Condition (8.80) has been successfully applied to groundwater problems (71). Unfortunately, both theoretical and numerical results indicate that accuracy considerations significantly reduce the area of acceptability of combinations ( $U\Delta t/\Delta s$ ,  $E\Delta t/\Delta s^2$ ) to a fraction of that required for iteration convergence.

## 8.6 Stability of Two-Layer Model

It was shown in Sec. 7.2 that the discretized equations take the form (7.31a,b) under certain conditions. Considering the homogeneous case, their form is:

$$\dot{\bar{M}}_{\bar{1}} + \bar{A}_{\bar{1}}\bar{C}_{\bar{1}} + \bar{K}_{\bar{1}}\bar{C}_{\bar{1}} + \bar{D}_{\bar{1}}\bar{C}_{\bar{1}} + \bar{E}(\bar{C}_{\bar{1}} - \bar{C}_{\bar{2}}) = 0 \quad (8.85a)$$

$$\dot{\bar{M}}_{\bar{2}} + \bar{A}_{\bar{2}}\bar{C}_{\bar{2}} + \bar{K}_{\bar{2}}\bar{C}_{\bar{2}} + \bar{D}_{\bar{2}}\bar{C}_{\bar{2}} + \bar{E}(\bar{C}_{\bar{2}} - \bar{C}_{\bar{1}}) = 0 \quad (8.85b)$$

where the subscripts 1, 2 refer to the layer indices for an individual element, the interfacial diffusion matrix is expressed by (Eq. (7.26)):

$$\tilde{E}^e = \frac{\alpha'A}{12} \begin{bmatrix} 2 & 1 & 1 \\ 1 & 2 & 1 \\ 1 & 1 & 2 \end{bmatrix} = \alpha' \tilde{M} \quad (8.86)$$

The two equations (8.85a,b) are integrated successively by using the trapezoidal rule, as discussed in Sec. 7.3. That is,

$$\begin{aligned} [\tilde{M} + \frac{\Delta t}{2} (\tilde{K}_1 + \tilde{D}_1 + \tilde{A}_1 + \tilde{E})_{n+1}] \tilde{C}_{1,n+1} - \frac{\Delta t}{2} \tilde{E}_{n+1} \tilde{C}_{2,n+1} = \\ = [\tilde{M} - \frac{\Delta t}{2} (\tilde{K}_1 + \tilde{D}_1 + \tilde{A}_1 + \tilde{E})_n] \tilde{C}_{1,n} + \frac{\Delta t}{2} \tilde{E}_n \tilde{C}_{2,n} \end{aligned} \quad (8.87a)$$

$$\begin{aligned} [\tilde{M} + \frac{\Delta t}{2} (\tilde{K}_2 + \tilde{D}_2 + \tilde{A}_2 + \tilde{E})_{n+1}] \tilde{C}_{2,n+1} - \frac{\Delta t}{2} \tilde{E}_{n+1} \tilde{C}_{1,n+1} = \\ = [\tilde{M} - \frac{\Delta t}{2} (\tilde{K}_2 + \tilde{D}_2 + \tilde{A}_2 + \tilde{E})_n] \tilde{C}_{2,n} + \frac{\Delta t}{2} \tilde{E}_n \tilde{C}_{1,n} \end{aligned} \quad (8.87b)$$

Assuming for simplicity that the various coefficient matrices are constant over the time step, the above equations can be rewritten in compact form:

$$\tilde{X} \tilde{C}_{n+1} = \tilde{\Omega} \tilde{C}_n \quad (8.88)$$

where

$$\tilde{C}_{n+1} = \begin{bmatrix} \tilde{C}_{1,n+1} \\ \tilde{C}_{2,n+1} \end{bmatrix}, \quad \tilde{C}_n = \begin{bmatrix} \tilde{C}_{1,n} \\ \tilde{C}_{2,n} \end{bmatrix}$$

$$\tilde{X} = \begin{bmatrix} \tilde{M} + \frac{\Delta t}{2} (\tilde{K}_1 + \tilde{D}_1 + \tilde{A}_1 + \tilde{E}) & -\frac{\Delta t}{2} \tilde{E} \\ -\frac{\Delta t}{2} \tilde{E} & \tilde{M} + \frac{\Delta t}{2} (\tilde{K}_2 + \tilde{D}_2 + \tilde{A}_2 + \tilde{E}) \end{bmatrix}$$

$$\tilde{\Omega} = \begin{bmatrix} \tilde{M} - \frac{\Delta t}{2} (\tilde{K}_1 + \tilde{D}_1 + \tilde{A}_1 + \tilde{E}) & +\frac{\Delta t}{2} \tilde{E} \\ +\frac{\Delta t}{2} \tilde{E} & \tilde{M} - \frac{\Delta t}{2} (\tilde{K}_2 + \tilde{D}_2 + \tilde{A}_2 + \tilde{E}) \end{bmatrix}$$

Matrices  $\tilde{X}$  and  $\tilde{\Omega}$  can be decomposed as follows:

$$\tilde{X} = \tilde{B} + \frac{\Delta t}{2} (\tilde{F}_1 + \tilde{F}_2 + \tilde{G}) \quad (8.89a)$$

$$\tilde{\Omega} = \tilde{B} - \frac{\Delta t}{2} (\tilde{F}_1 + \tilde{F}_2 + \tilde{G}) \quad (8.89b)$$

where

$$\tilde{B} = \begin{bmatrix} \tilde{M} & \tilde{O} \\ \tilde{O} & \tilde{M} \end{bmatrix} \quad (8.90a)$$

$$\tilde{F}_1 = \begin{bmatrix} \tilde{K}_1 + \tilde{D}_1 & \tilde{O} \\ \tilde{O} & \tilde{K}_2 + \tilde{D}_2 \end{bmatrix} \quad (8.90b)$$

$$\tilde{F}_2 = \begin{bmatrix} \tilde{A}_1 & \tilde{O} \\ \tilde{O} & \tilde{A}_2 \end{bmatrix} \quad (8.90c)$$

$$\tilde{G} = \begin{bmatrix} \tilde{E} & -\tilde{E} \\ -\tilde{E} & \tilde{E} \end{bmatrix} \quad (8.90d)$$

Matrix  $\tilde{G}$  is singular and therefore its eigenvalues are the same as those of  $\tilde{E}$ . The latter, being composed of individual positive definite matrices  $\tilde{E}^e$ , is itself positive definite. Furthermore, matrices  $\tilde{B}$  and  $\tilde{F}_1$  are also symmetric, positive definite. Finally, if both advection matrices  $\tilde{A}_1$  and  $\tilde{A}_2$  are skew-symmetric, which is usually the case (Sec. 8.3.1),  $\tilde{F}_2$  will be skew-symmetric, too.

Writing now, as in the one layer case

$$\tilde{C}_n = \lambda^n \tilde{\phi}, \text{ for all } n,$$

substituting in (8.88), and premultiplying both sides by  $\tilde{\phi}^T$ , we obtain:

$$\lambda \tilde{\phi}^T [\tilde{B} + \frac{\Delta t}{2} (\tilde{F}_1 + \tilde{F}_2 + \tilde{G}_1 - \tilde{G}_2)] \tilde{\phi} = \tilde{\phi}^T [\tilde{B} - \frac{\Delta t}{2} (\tilde{F}_1 + \tilde{F}_2 + \tilde{G}_1 - \tilde{G}_2)] \tilde{\phi} \quad (8.91)$$

According to previous considerations

$$\tilde{\phi}^T \tilde{B} \tilde{\phi} = m > 0$$

$$\tilde{\phi}^T \tilde{G} \tilde{\phi} = \epsilon > 0$$

$$\tilde{\phi}^T \tilde{F}_1 \tilde{\phi} = \kappa + d > 0$$

$$\tilde{\phi}^T \tilde{F}_2 \tilde{\phi} = a_s + ia_{ss}$$

where the various numbers are, in general, different from those of (8.57) and (8.58), and usually  $a_s = 0$ . Eq. (8.91) implies:

$$\lambda = \frac{m - \frac{\Delta t}{2} (\kappa + d + \epsilon + a_s + ia_{ss})}{m + \frac{\Delta t}{2} (\kappa + d + \epsilon + a_s + ia_{ss})}$$

or,

$$\lambda^2 = \frac{[m - \frac{\Delta t}{2} (\kappa + d + \epsilon + a_s)]^2 + (\frac{\Delta t}{2} a_{ss})^2}{[m + \frac{\Delta t}{2} (\kappa + d + \epsilon + a_s)]^2 + (\frac{\Delta t}{2} a_{ss})^2} \quad (8.92)$$

This is analogous to the one-layer result (8.59) and indicates that the interfacial exchange, expressed by  $\epsilon$ , which is positive, is a stabilizing mechanism for the two-layer system. When  $a_s \geq 0$ , the integration scheme is unconditionally stable. Problems may arise in the unlikely case that  $a_s$  acquires large negative values, as discussed in Sec. 8.3.1. However, now a negative  $a_s$  has to be larger in magnitude than in the one layer case in order to cause instability, because of the presence of  $\epsilon$ . The stabilizing effect of the interfacial exchange (in the absence of net entrainment) should have been expected on physical grounds: when the concentration in one layer tends to increase, the diffusion of material to the other layer through the interface is enhanced. Thus, this exchange helps in "damping" high concentrations and exerts a restraint on perturbations of the numerical solution tending to grow without bound, that would eventually lead to instability. Nevertheless, in the present two-layer idealization, the rate of exchange is usually small and its effect cannot be too significant.

Despite the unconditional stability of the time integration scheme, the iterative solution actually used imposes again a restriction on the

time step. According to Sec. 7.3, the iteration proceeds successively to the next layer, using the most recent values of concentration in the previous one. That is,

$$\tilde{M}C_{1,n+1}^{(i+1)} = -\frac{\Delta t}{2} (\tilde{K}_1 + \tilde{D}_1 + \tilde{A}_1 + \tilde{E})_{n+1} C_{1,n+1}^{(i)} + \frac{\Delta t}{2} \tilde{E}_{n+1} C_{2,n+1}^{(i)} + Q_1 \quad (8.93a)$$

$$\tilde{M}C_{2,n+1}^{(i+1)} = -\frac{\Delta t}{2} (\tilde{K}_2 + \tilde{D}_2 + \tilde{A}_2 + \tilde{E})_{n+1} C_{2,n+1}^{(i)} + \frac{\Delta t}{2} \tilde{E}_{n+1} C_{1,n+1}^{(i+1)} + Q_2 \quad (8.93b)$$

where  $Q_1, Q_2$  are quantities known from the previous time step:

$$Q_1 = [\tilde{M} - \frac{\Delta t}{2} (\tilde{K}_1 + \tilde{D}_1 + \tilde{A}_1 + \tilde{E})_n] C_{1,n} + \frac{\Delta t}{2} \tilde{E}_n C_{2,n}$$

$$Q_2 = [\tilde{M} - \frac{\Delta t}{2} (\tilde{K}_2 + \tilde{D}_2 + \tilde{A}_2 + \tilde{E})_n] C_{2,n} + \frac{\Delta t}{2} \tilde{E}_n C_{1,n}$$

Eqs. (8.93a,b) can be together written as:

$$\tilde{R} \tilde{C}^{(i+1)} = \tilde{\psi} \tilde{C}^{(i)} + \tilde{Q} \quad (8.94)$$

where

$$\tilde{C}^{(i+1)} = \begin{bmatrix} C_{1,n+1}^{(i+1)} \\ C_{2,n+1}^{(i+1)} \end{bmatrix}, \quad \tilde{C}^{(i)} = \begin{bmatrix} C_{1,n+1}^{(i)} \\ C_{2,n+1}^{(i)} \end{bmatrix}$$

$$\tilde{R} = \begin{bmatrix} \tilde{M} & 0 \\ -\frac{\Delta t}{2} \tilde{E}_{n+1} & \tilde{M} \end{bmatrix}$$

$$\tilde{\psi} = \begin{bmatrix} -\frac{\Delta t}{2} (\tilde{K}_1 + \tilde{D}_1 + \tilde{A}_1 + \tilde{E})_{n+1} & \frac{\Delta t}{2} \tilde{E}_{n+1} \\ 0 & -\frac{\Delta t}{2} (\tilde{K}_2 + \tilde{D}_2 + \tilde{A}_2 + \tilde{E})_{n+1} \end{bmatrix}$$

Convergence of the iteration (8.94) requires, in general:

$$\|\tilde{R}^{-1}\tilde{\psi}\| < 1 \quad (8.95)$$

The matrix  $\tilde{R}$  can be written as a product,

$$\tilde{R} = \begin{bmatrix} \tilde{M} & 0 \\ 0 & \tilde{M} \end{bmatrix} \begin{bmatrix} \tilde{I} & 0 \\ -\frac{\Delta t}{2} \tilde{M}^{-1} \tilde{E}_{n+1} & \tilde{I} \end{bmatrix}$$

and its inverse is then:

$$\tilde{R}^{-1} = \begin{bmatrix} \tilde{I} & 0 \\ \frac{\Delta t}{2} \tilde{M}^{-1} \tilde{E}_{n+1} & \tilde{I} \end{bmatrix} \begin{bmatrix} \tilde{M}^{-1} & 0 \\ 0 & \tilde{M}^{-1} \end{bmatrix}$$

Since both  $\tilde{R}^{-1}$  and  $\tilde{\psi}$  involve triangular matrices, their eigenvalue norms are conveniently expressed in terms of their diagonal elements. Thus, the condition (8.95) is equivalent to:

$$\|\tilde{M}^{-1} \frac{\Delta t}{2} (\tilde{K}_1 + \tilde{D}_1 + \tilde{A}_1 + \tilde{E})_{n+1}\| < 1$$

implying

$$\Delta t < \frac{2}{\|\tilde{M}^{-1}(\tilde{K}_1 + \tilde{D}_1 + \tilde{A}_1 + \tilde{E})\|} \quad (8.96)$$



or, in more conservative form

$$\Delta t < \frac{2}{\| \tilde{M}^{-1} \tilde{K}_1 \| + \| \tilde{M}^{-1} \tilde{D}_1 \| + \| \tilde{M}^{-1} \tilde{A}_1 \| + \| \tilde{M}^{-1} \tilde{E} \|} \quad (8.97)$$

Conditions (8.96) and (8.97) are entirely analogous to (8.61a) and (8.62), respectively, the only difference being in the introduction of the interfacial diffusion term, due to the exchange between the layers. From (8.86) it is evident that

$$\| \tilde{M}^{-1} \tilde{E} \| = \alpha' \quad (8.98)$$

where the constant  $\alpha'$  may be spatially and temporally variable and, of course, depends on the stratification. The magnitude of the other terms appearing in (8.97) has been examined in Sec. 8.4. Using those results, the bound on the time step can be approximately written:

$$\Delta t < \frac{1}{\sqrt{\frac{3}{2}} \frac{U_i}{\Delta s} + 8 \frac{E_i}{\Delta s^2} + \frac{k}{2} + \frac{\alpha'}{2}} \quad ; i = 1, 2 \quad (8.99)$$

Usually, as discussed in Chapter 4, the value of  $\alpha'$  is expected to be of the order of  $10^{-5}$  or smaller, and its contribution in limiting the time step will therefore be usually marginal. As (8.99) shows,  $\Delta t$  is basically limited from the flow conditions in the individual layers, in particular the fastest flowing layer.

These conclusions can be easily extended to multilayer models which can be examined by a similar procedure. Condition (8.99), applied for the "worst" layer, should yield an approximate bound for the time step

applicable to the whole system. Exchange to two neighboring layers has now to be considered and the coefficient of  $\alpha'$  must be doubled. More importantly, because the layers in such formulations are often separated by only small density differences, the exchange through the interfaces will not be necessarily small and its contribution in limiting the time step may become significant.

## CHAPTER 9

### VERIFICATION AND APPLICATIONS

Model verification is necessary in order to establish its validity for describing the phenomena it has been developed for. With respect to numerical models, the first step in the verification process is to check whether the governing equations are being solved correctly. This is essentially an evaluation of the numerical approximation and involves comparison of the numerical results to analytical solutions. Clearly, the range of comparison is limited by the availability of relevant analytical expressions; these are restricted to problems involving simple geometry and flow conditions.

To establish confidence in the predictive capability of a model, further verification, consisting of comparisons to real-world cases, is necessary. This step is extremely important in providing an idea of the soundness of the conceptual idealization of the physical processes and the degree of applicability of the model under natural conditions. The agreement can never be expected to be perfect, because of the high complexity of actual hydrodynamic processes and the difficulties in obtaining reliable field measurements in the coastal environment. The quality of and the uncertainty involved in input data should always be considered when judging the model output. The compatibility of available data to the model idealization is an issue that also

deserves some thought. For example, if a model gives depth-averaged concentrations, some averaging of data taken at different points through the water column is necessary for the comparisons to be consistent.

Even if the measurements were perfect, simplifications introduced in model formulation can still prevent good agreement. With respect to the dispersion problem, the solution of the convection-diffusion equation represents the ensemble average concentration field over a small time ( $\Delta t$ ) and space ( $\Delta x$ ,  $\Delta y$ ,  $\Delta z$ ) interval (in the case of a layered structure,  $\Delta z$  will be the total layer depth). However, at any point, there is always a natural variability about this "average" value. This issue has been addressed conceptually by Csanady (16). According to his discussion, deviations from the average value by a factor of two or three can well be due to these natural fluctuations and have actually been observed in the central regions of plumes in the atmosphere. A further complication arises at the fringes of the plume, where there is a substantial probability that in a given sample there will be zero concentration. The so-called "intermittency factor" is introduced to describe this probability, but its estimation appears to be hopeless.

In view of the above comments, model comparisons to field studies have to be evaluated not as an attempt to achieve a perfect fit, but rather as an indication of the ability of the model to reproduce certain key quantitative features of the data, such as

the general direction of the plume, the peak values and the extent of its boundaries (defined by concentrations significantly higher than ambient).

In this chapter, comparisons of the two-layer model to analytical results obtained in Chapter 5 under idealized flow conditions are presented first. The generally good agreement proves the correctness of the model structure. Subsequently, the application of the model to two large scale field experiments, conducted in Massachusetts Bay under summer conditions, is discussed.

#### 9.1 1-D Verification Studies

The grid used for the one-dimensional comparisons is shown in Figure 8.4. The first test is for the transient behavior of the system after an instantaneous release simulated as of one timestep duration. A unit load is distributed between the three nodes at  $x=0$  and the results adjusted to yield values per unit width of the channel. No longitudinal spreading of the source is necessary in the 1-D examples and consequently the simulation should represent a point source quite closely. A unit depth is assumed for each layer. Zero concentration is specified at the ends of the grid, while zero flux is prescribed along the side boundaries. Table 9.1 contains a summary of the parameters considered. The value of the interfacial mixing coefficient,  $5 \times 10^{-4} \text{ sec}^{-1}$ , implies that the small time approximation of Sec. 5.1 is valid for a time period of

about 100 sec. However, to avoid the plume reaching the downstream end of the grid, the comparison is made at time  $t=10$  sec. As Figure 9.1 shows, the agreement is extremely good. The only discrepancy, at the upstream edge of the plume in the lower layer, is due to the proximity of the grid boundary. The value of the ratio  $E/U\Delta s$  ( $= 1.6$ ) was chosen larger than 0.5 to ensure a smooth numerical solution, as discussed in Section 8.2.4.

Table 9.1  
Parameters Used in Verification Studies

Parameters	1-D Instantaneous	1-D Steady State	2-D Steady State
$U_1 = -U_2$	0.05 m/sec	0.05 m/sec	0.05 m/sec
$E_{x_1} = E_{x_2}$	$0.01 \text{ m}^2/\text{sec}$	$0.01 \text{ m}^2/\text{sec}$	0
$E_{y_1} = E_{y_2}$	-	-	$0.001 \text{ m}^2/\text{sec}$
$H_1 = H_2$	1 m	1 m	1 m
$k$	0	$0.2 \text{ sec}^{-1}$	$0.2 \text{ sec}^{-1}$
$\alpha$	$5 \times 10^{-4} \text{ m/sec}$	$5 \times 10^{-2} \text{ m/sec}$	$5 \times 10^{-2} \text{ m/sec}$
$M$	1 unit	-	-
$m$	-	1 unit/sec	1 unit/sec

It is seen from Figure 9.1 that for the value of  $\alpha$  used, which is somewhat higher than values to be expected in nature, the lower layer concentrations are two orders of magnitude smaller than those of the top layer. This observation supports to some extent the treatment of the interface as a barrier. However, it may not

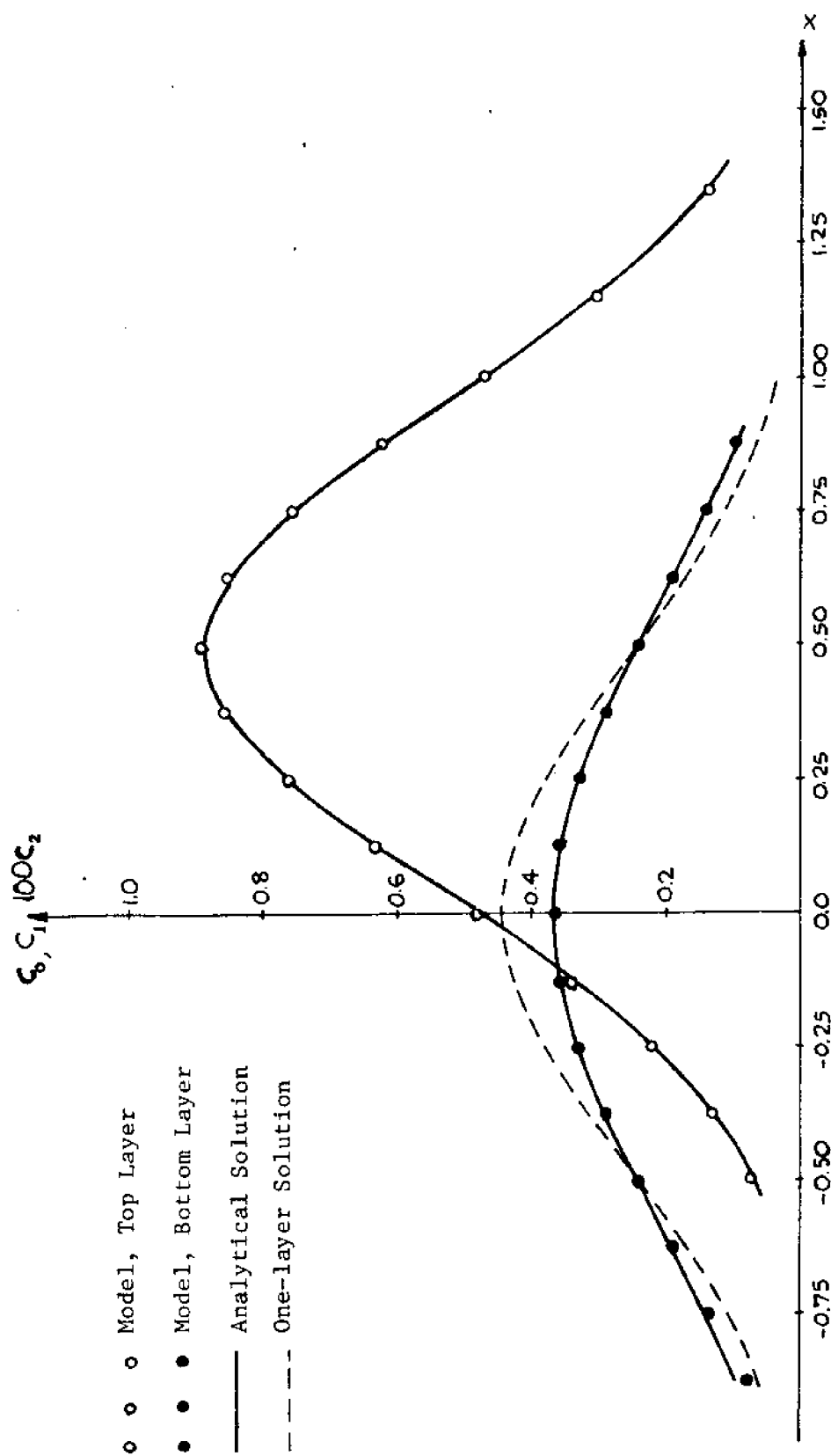


Figure 9.1 1-D Distribution at  $t=10$  sec. after an Instantaneous Injection

hold for longer time periods and is certainly not valid for substances possessing vertical mobility. Irrespective of that, it should be clear that a great advantage of the two-layer model is the more detailed description of the velocity field. In this particular counterflow case, a depth averaged treatment would imply zero overall velocity and therefore predict a stationary peak of the depth-averaged concentration distribution located at the origin and having a magnitude approximately half the actual upper layer peak. Thus, as shown in Figure 9.1, the solution for the depth-averaged velocity field is far from the actual depth-averaged concentration distribution of the two-layer system.

Next, the behavior of the model at steady state is examined. A high decay coefficient is specified to speed up the arrival to steady state and also to keep appreciable concentrations away from the boundary. The parameters used (Table 9.1) are mostly the same as in the transient test. A higher interfacial mixing coefficient was specified here so that the exchange between the layer would be more pronounced. The comparison with the analytical expressions of Section 5.2 is shown in Figure 9.2 and the agreement is, again, quite good.

Runs with no interfacial mixing were also carried out for testing purposes and the results for each layer were identical to those of the one layer model, conducted earlier by Leimkuhler (43).



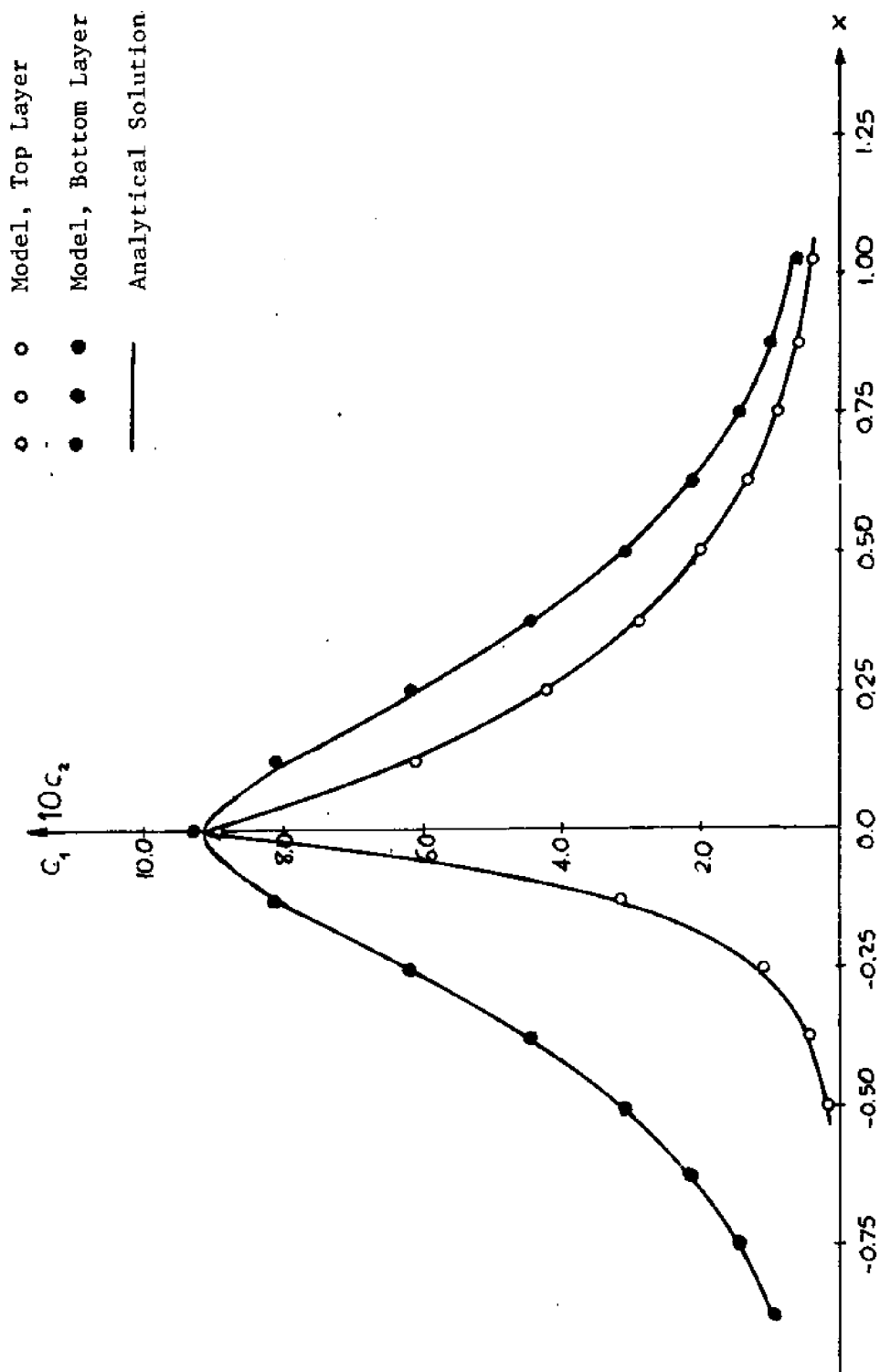


Figure 9.2 1-D Steady State Distribution

## 9.2 2-D Verification Studies

To examine the validity of the model for a two dimensional domain, a verification was attempted for a continuous source in the top layer, located at the origin of the grid shown in Figure 8.5. In the numerical simulation the load is distributed over the eight inner elements around the origin, to avoid problems associated with the singularity of the point source solution, as discussed in Section 8.2.4. Zero flux is specified along the x-axis, while a zero concentration is prescribed in all other boundaries. Again, a high decay rate is employed (Table 9.1) to contain the plume within the grid boundaries.

The steady state analytical solution for a point source, presented in Section 5.3, is compared to numerical results at  $t=20$  sec (which corresponds to steady state up to a distance of about 1 meter from the origin) in Figures 9.3 and 9.4. Figure 9.3 shows the distribution along the x-axis and a fairly good agreement is evident, except close to the origin and in particular within the area of the numerical source. This, of course, is a consequence of the spatial distribution of the source. The numerical results for the top layer along the negative x-axis are very close to zero, indicating that even for the unrealistically high interfacial diffusion assumed in this case, the approximate analytical solution is adequate. In Figure 9.4 the concentration profiles at  $x=0.22$  and at  $x=0.40$  meters are presented. The validity

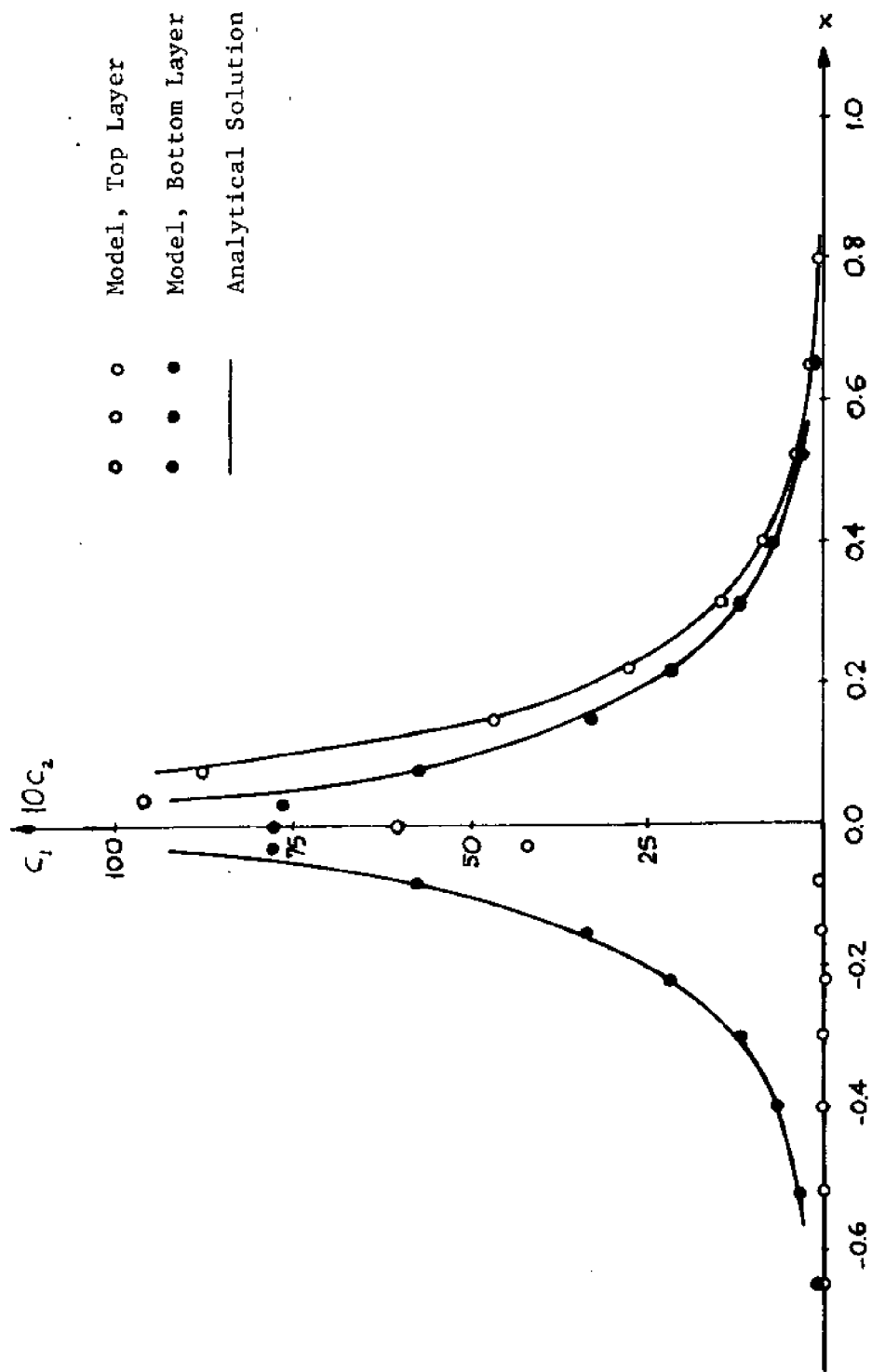


Figure 9.3 2-D Steady State Distribution along the x-axis

○ ○ ○ Model, Top Layer  
 ● ● ● Model, Bottom Layer  
 — Analytical Solution

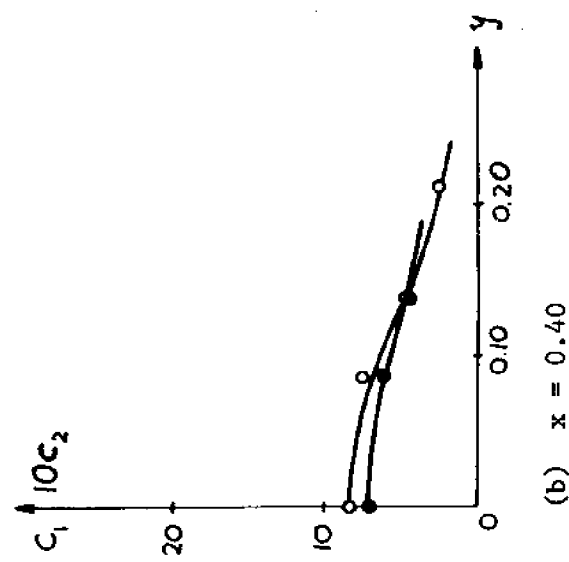
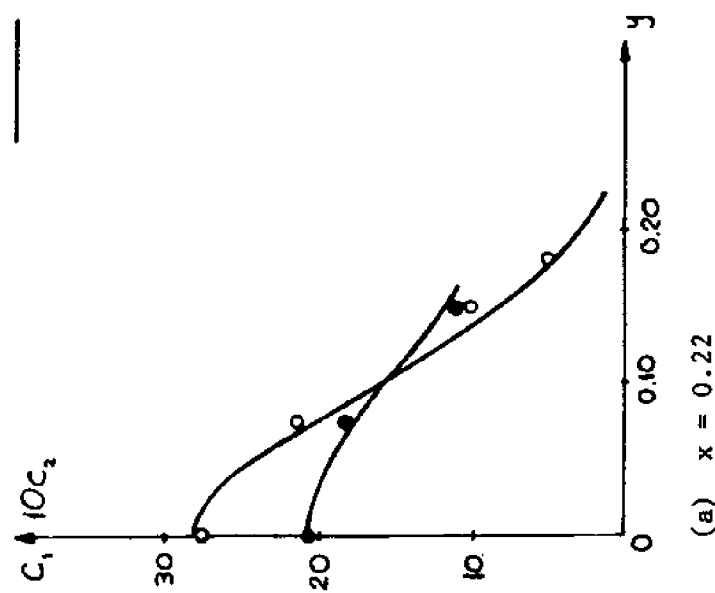


Figure 9.4 2-D Steady State Profiles Normal to x-axis

of the analytical solution (Equation 5.47) is restricted to values of  $y \leq 0.13$  and  $y \leq 0.18$  m., respectively. Within these limits the agreement with the numerical results is satisfactory.

### 9.3 Application to the NOMES Experiment

#### 9.3.1 The Experiment

In the context of the three year project NOMES (New England Offshore Mining Environmental Study) a major field experiment was carried out by NOAA in the Massachusetts Bay. The objective of the project was to study the environmental effects of offshore mining for sand and gravel in the coastal zone due mainly to fines discharged back into the water body, and an extensive experimental dredging operation was planned for the summer of 1974. A preliminary experiment, in June 1973, was aimed at gaining field experience for monitoring the actual mining operation and helping in testing and improving relevant mathematical models. On the morning of June 11, 1973, 2000 lbs of small glass beads and 1000 lbs of fluorescent sphalerite (ZnS) particles (or  $2.92 \times 10^{15}$  particles) were introduced near the water surface, about 8 miles east of Boston Harbor. The settling property of the tracers was necessary for simulating the actual dredge spoil and the use of two different kinds of particles was planned in order to assess the performance of a variety of measuring devices. The motion of the particles was tracked for more than a week, by means of samples taken throughout the water column and from the bottom. A number of current meters were installed in several stations in the vicinity

of the dump site to obtain current information, while some drogues were deployed simultaneous with the tracers to provide easy guidance with respect to sampling locations in the course of the experiment. Details on the instrumentation, the experimental procedures and data analysis can be found in (88). Difficulties with the instruments and experimental errors were inevitable in such a large scale effort. Most unfortunately, the counting of the glass bead particles was totally wrong and therefore those data are useless (54). Nevertheless, the sphalerite data are believed to be of reasonable quality. They compare well with results of the depth-integrated finite element dispersion model which preceeded the present two-layer approach (65). Indeed, the sphalerite data were used to some extent for "tuning" both the one layer circulation and dispersion models, primarily with respect to the ocean boundary condition and the dispersion coefficient.

The time of the experiment was such that, although some stratification existed, the thermocline was not as distinct as it becomes later in the summer. In fact, neither the well-mixed nor the two-layer assumption seems appropriate in this case. Nevertheless, the application of the two-layer model is of considerable interest for providing some idea about its real-world capabilities and revealing the difficulties and the sensitivity associated with numerical simulations of real problems.

The finite element grid is shown in Figure 9.5. This has been used extensively in the past in conjunction with one-layer

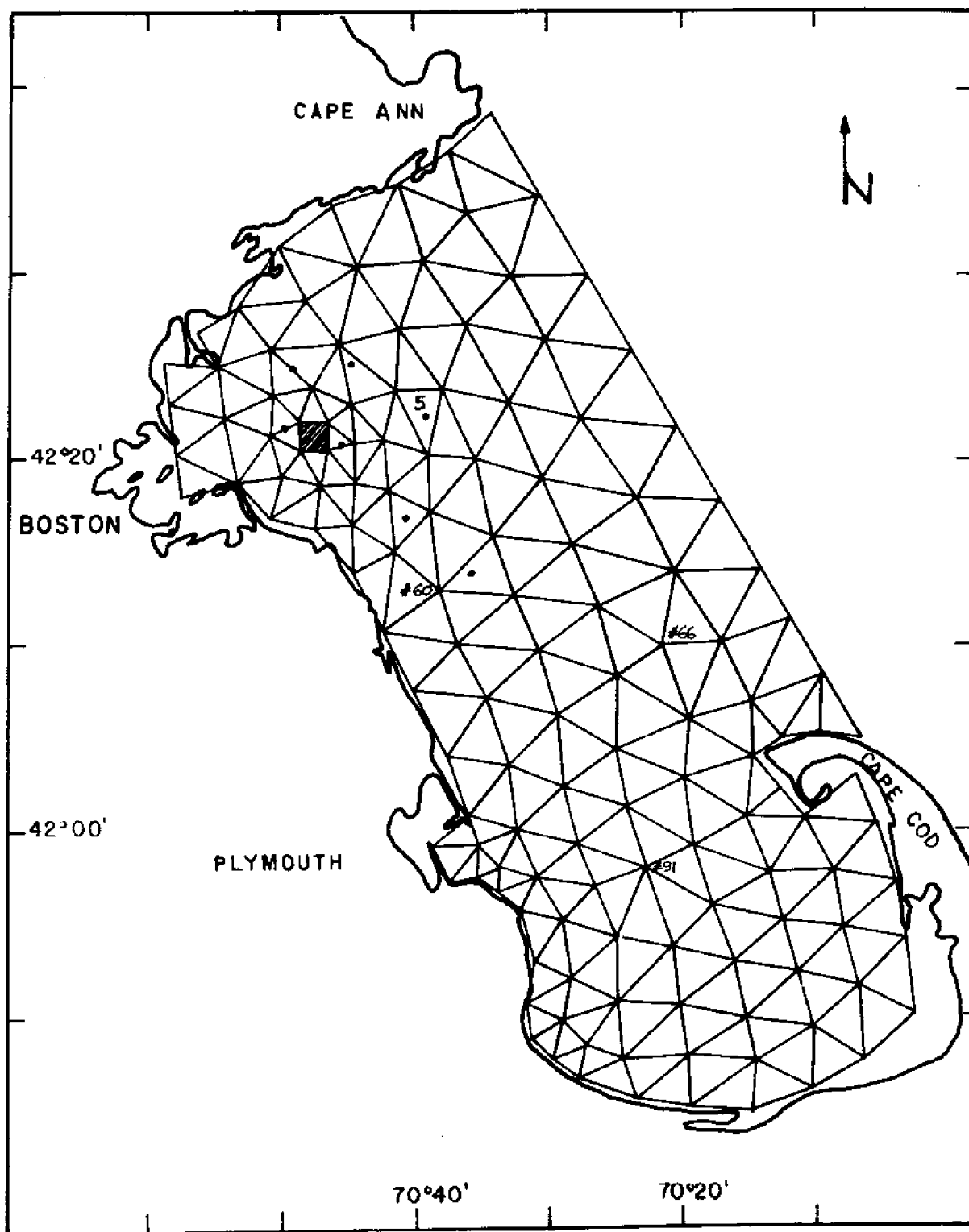


Figure 9.5 Massachusetts Bay Finite Element Grid and Location of the NOMES Experiment

models. The dumping site is denoted by the shaded area and the current meter stations are indicated by dots. Refinement of the grid in the vicinity of the source was introduced to minimize the numerical difficulties associated with large initial concentration gradients.

#### 9.3.2 The Flow Field

The hydrodynamic model developed by Wang and Connor (86) was used to generate two-layer velocity inputs for the dispersion study. Considerable preliminary effort was required since this was the first application to a real coastal water body of variable bathymetry and boundary geometry. The model requires both layers to extend over the whole domain and the depths at nodes near the land boundary had to be artificially increased to at least 15 meters in order to avoid intersection of the interface with the bottom.

A major obstacle in obtaining realistic two-layer results is associated with the proper position of the interface, in particular along the open boundary, where its spatial and temporal variation must be specified. Information relevant to the thermocline in the Bay is available in terms of a number of transects, compiled in ( 8). Vertical temperature and salinity profiles at certain locations are also available (22,9). Data of both substantial areal coverage and continuity in time, which are essential to yield a detailed enough picture of the interfacial motion, are lacking at the present time. Existing measurements show



considerable variation of the thermocline position and a significant effect of bottom topography. A major feature of the Bay bathymetry is the presence of Stellwagen Bank in the central-southern part of its entrance. Early experimental investigations on a two-layer system (47) have showed that either an internal hydraulic jump or hydraulic drop may be created on the lee of an obstacle, depending on its height relative to the layer thicknesses and the incoming flow conditions. In most circulation runs the interface was found to rise over the bank significantly higher than its specified position at the boundary and then drop further inside. A drop in the thermocline, possibly associated with phenomena of frontal nature, has been evidenced in the past west of the bank during periods of high inflow velocities (28). The behavior of the interface in the model may be considerably affected by the specification of the boundary conditions right on the bank, rather than in deep water outside. The effect of bottom anomalies is known to be critical for the position of the interface when wind provides the forcing mechanism, too (32). Specifically for Massachusetts Bay, the importance of the bottom topography, in general, and Stellwagen Bank in particular, with respect to wind driven circulation was discussed in (9).

A preliminary review of the available data for the Bay leads to the conclusion that the thermocline (or, rather, pycnocline) depth is typically about 8-10 meters during the period of strongest stratification. However, it tends to be shallower in early summer.

For the application of the model a uniform interface depth of 8 meters at low water was selected as initial condition. Along the ocean boundary in view of lack of data, the interface was assumed to vary linearly. Two extreme cases were considered: first, the interface moving at the same amplitude as the free surface and second, the interface remaining fixed throughout the tidal cycle. In the former case, the tide may be interpreted as coming through the bottom layer, while in the latter, as coming through the top layer.

A constant 10 knot west wind, typical of the period of the experiment, was imposed. A simple sinusoidal tide was specified along the ocean boundary, with amplitude linearly varying from 1.20 meters at the northern end (Cape Ann) to 1.10 meters at the southern end (Cape Cod). The amplitude was obtained from tide tables (80), as an average value over the duration of the experiment. A 10 cm "tilt" was employed initially since it was found optimum for a number of different applications of the one-layer circulation and dispersion models (65, 63), yielding results in reasonable agreement with current meters and tide gauge data taken at various locations. However, because of changes in bathymetry, the resulting southward water motion appeared too strong and it was decided to experiment with a smaller (approximately half) tidal tilt at the boundary. Primarily due to lack of data on the behavior of the interface, the results of the circulation model should be interpreted as qualitative rather than quantitative.

At present, one can only study the sensitivity of the velocity field (and ultimately that of the dispersing plumes) to variations in the imposed boundary conditions and other model parameters. Studies of this nature should be valuable in establishing the important quantities that will need to be measured in the field.

The motion of the interface within the Bay depends, in addition to the topography, on the density difference and the layer thickness (6). Sensitivity of the results to these factors was not examined further here, but the importance of the interfacial friction factor  $c_I$  was established. This was conveniently set to zero in both analytical studies and early applications of the numerical model (86), resulting in considerable oscillations of the interface and significant velocity differences between the layers, even several counterflow cases. A realistic value of the interfacial friction coefficient, of the order of  $10^{-3}$  (7), moderates those features but a higher value, of  $10^{-2}$ , yields layer velocities quite close to each other and allows little interfacial motion. Conceivably, a very high interfacial friction would essentially "tie" the two layers together, resulting in a flow pattern similar to the one-layer case. Table 9.2 summarizes the various runs carried out in conjunction with the application of the circulation model.

Table 9.2

## Summary of Circulation Runs for the NOMES Application

Name	Tidal Amplitude at Boundary	Tidal Amplitude at Boundary	Interfacial Friction Factor	Other Parameters	Relevant Figures
FTT	1.20-1.10 m	0	$10^{-3}$	Wind 10 knot west	9.7b
FTB	1.20-1.10 m	1.20-1.10 m	$10^{-3}$		9.6, 9.7a thru 9.12
FTH	1.20-1.10 m	0.60-0.55 m	$10^{-3}$	Eddy Viscosity $1000 \text{ m}^2/\text{sec}$	—
HTB	1.20-1.155 m	1.20-1.155 m	$10^{-3}$	Variable Bottom Friction	9.7c
LFT	1.20-1.10 m	0	$10^{-2}$		—
LFB	1.20-1.10 m	1.20-1.10 m	$10^{-2}$	Density Difference 1%	9.7d

The model was run until steady state was reached after 7-8 tidal cycles and the velocity field at that time is used subsequently for the dispersion calculations. Typical interfacial motions over the tidal cycle, for run FTB, at selected grid points, are shown in Figure 9.6. A comparison of simulated layer-average velocities at current meter station 5 are presented in Figure 9.7 and one of them is compared to the actual measurements in Figure 9.8. The general features seem in reasonable agreement, in view of the uncertainties involved in the application of the model, the use of constant wind and tide and the non-existence of a strong thermocline. The effect of interfacial friction in bringing the layer velocities close together can be clearly seen. Variation of the specified interface motion at the boundary relative to the surface is found to affect primarily the east-west component of the flow, i.e., that not associated with the net drift, as will be discussed shortly. The effect of the way the tide is specified to come into the bay becomes really minimal as the interfacial friction increases and is generally significant only locally near the boundary.

Typical circulation patterns for run FTB are shown in Figures 9.9 and 9.10, respectively. A quite strong outward flow is evident at the southern end of the ocean boundary, a consequence of the large tidal tilt and the wind on the one hand, and the existence of a rather narrow and deep "channel" on the other. The top layer

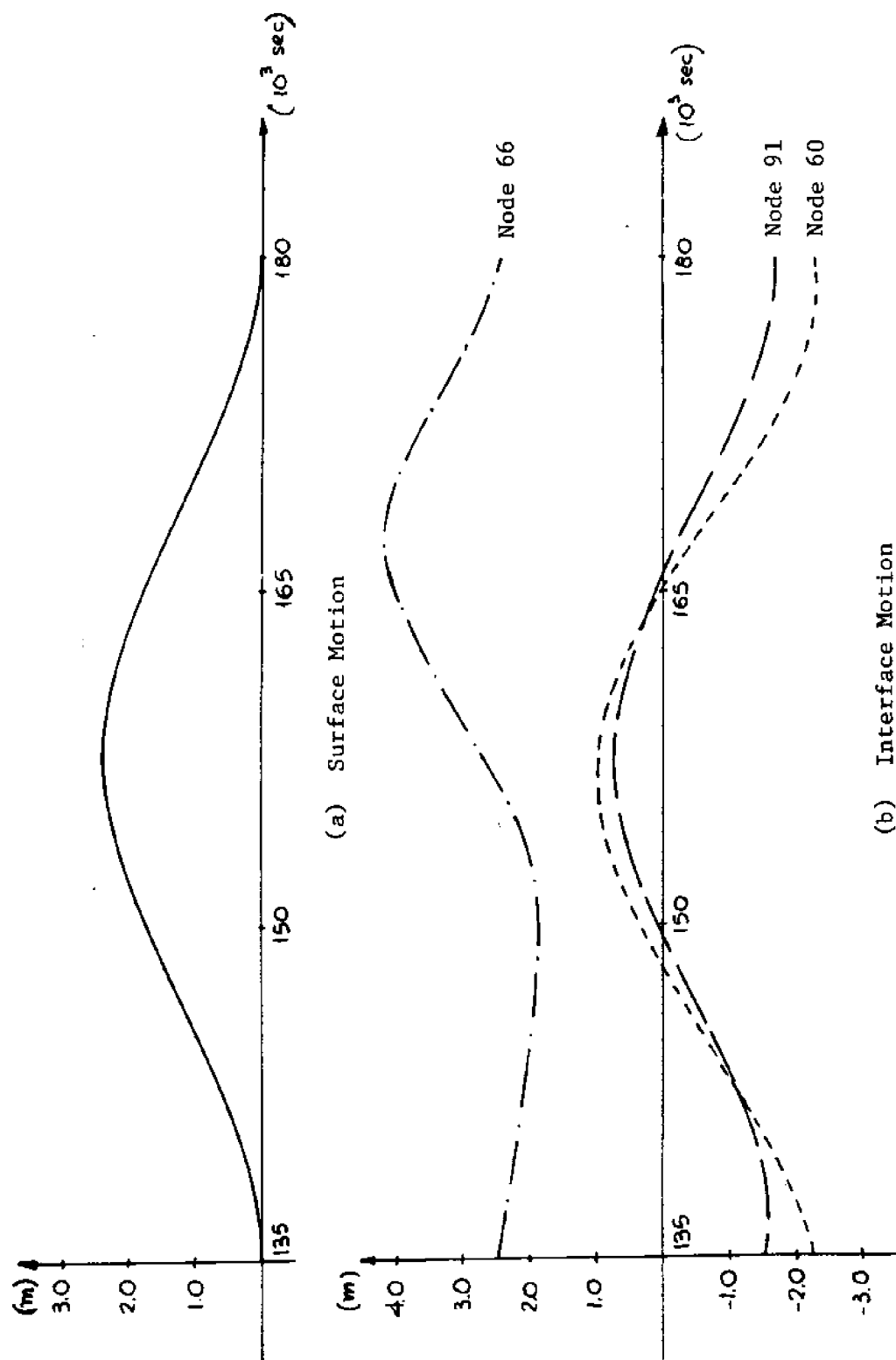


Figure 9.6 Interface Motion in FTB Run

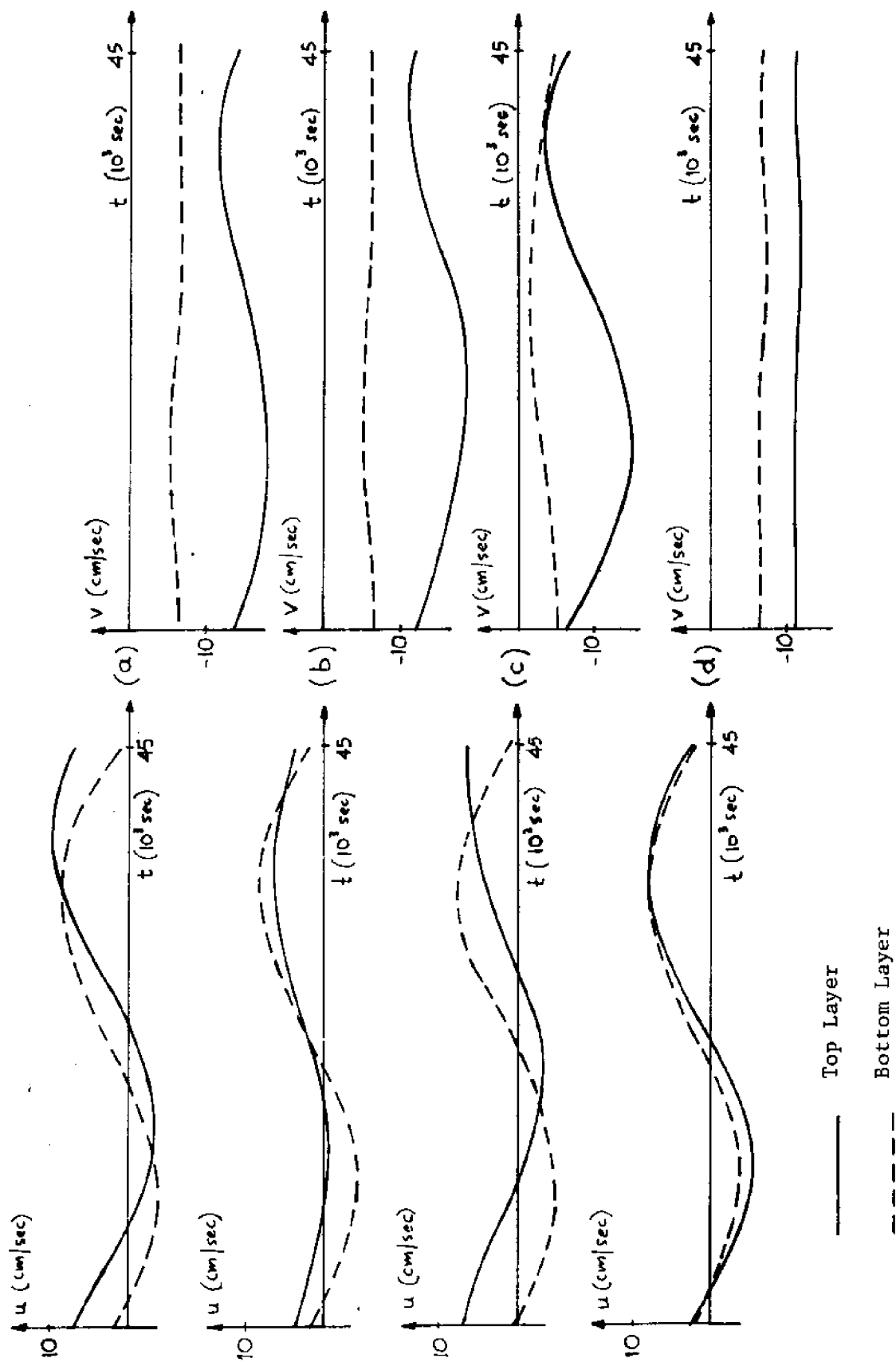


Figure 9.7 Comparison of Predicted Velocities at St. 5

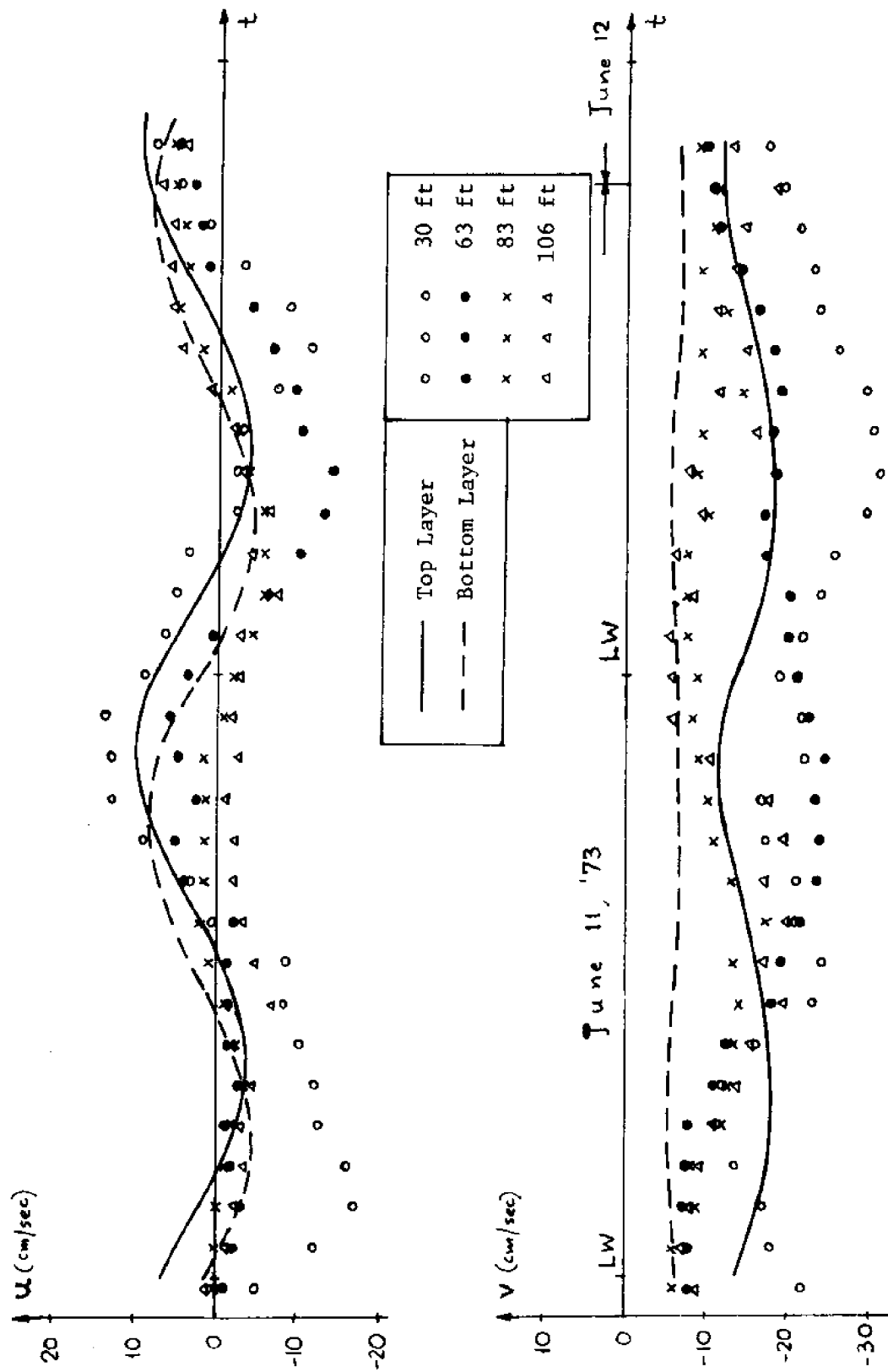


Figure 9.8 Current Data at St. 5 and FTB Model Results



velocity is, in general, larger than the bottom. However, comparison with similar one-layer circulation plots indicates that the velocities in the two-layer system are too high, primarily near the tip of Cape Cod and along the western land boundary. This is probably due to the artificial deepening of the Bay in those areas, as mentioned earlier.

An important feature of the circulation pattern as a whole is the trace of a water "particle". Particle paths can be easily computed by interpolation in space and time between the layer-average velocities given the grid points of the finite element model. Some representative paths, for a period of 7 days, originating near the dumping site, are presented in Figure 9.11. All particles in the top layer exhibit a rapid southeasterly motion in crossing the Bay. The one closest to land eventually slows down as it enters Cape Cod Bay. The other two turn to the east, as they approach the zone of high outwards velocity, and are rapidly driven out of the domain. Thus, the eventual terminal position appears to be quite sensitive to relatively small variation in the starting positions, provided they lie in the area examined. By contrast, the effect of the precise time of release within the tidal cycle is found to be of minor importance. Two "particles" were started from each location, one at low water and the other at ebb tide. As seen in the figure, the paths of each pair are essentially the same.

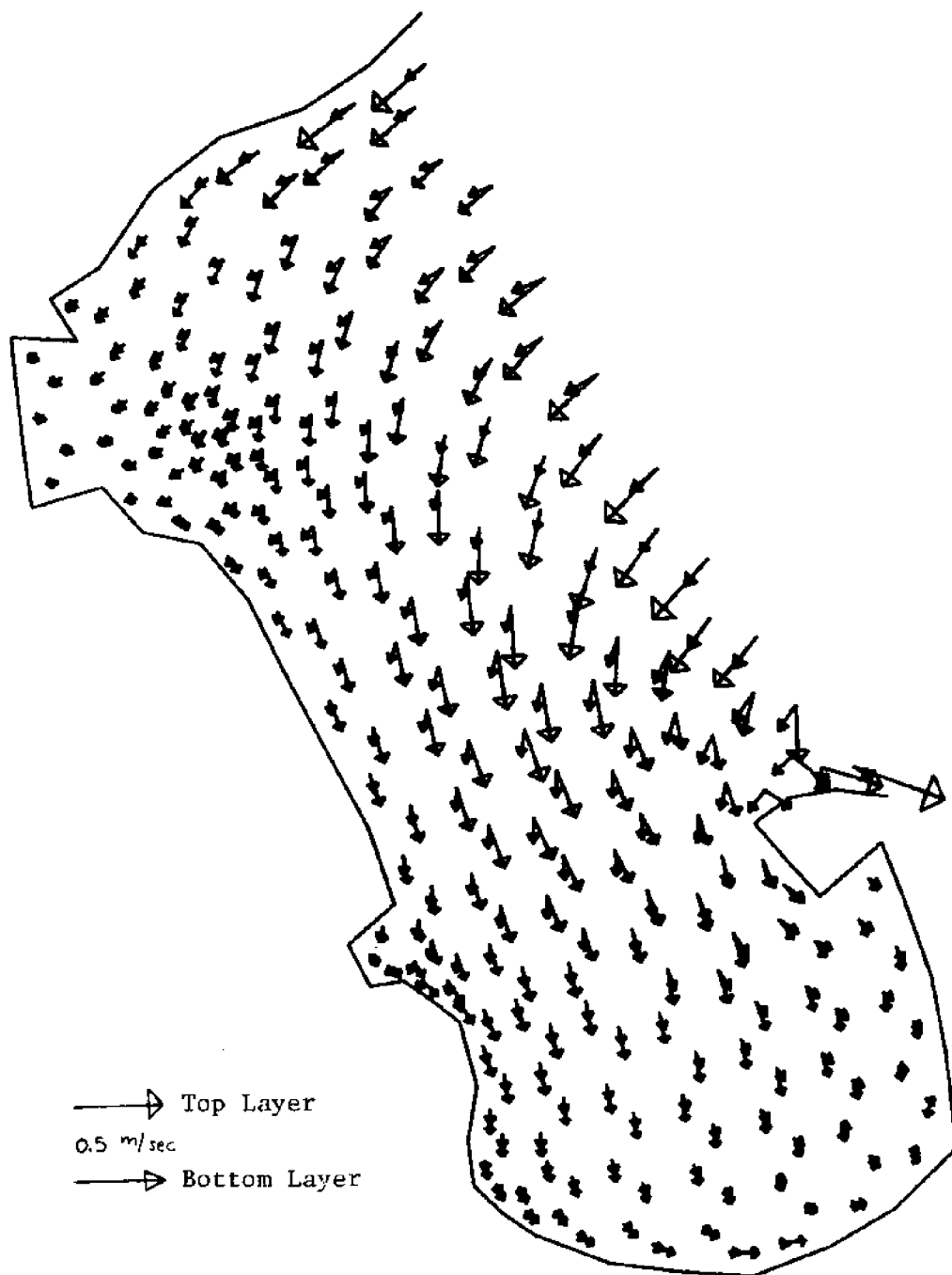


Figure 9.9 Flow Field at Flood Tide for FTB Run

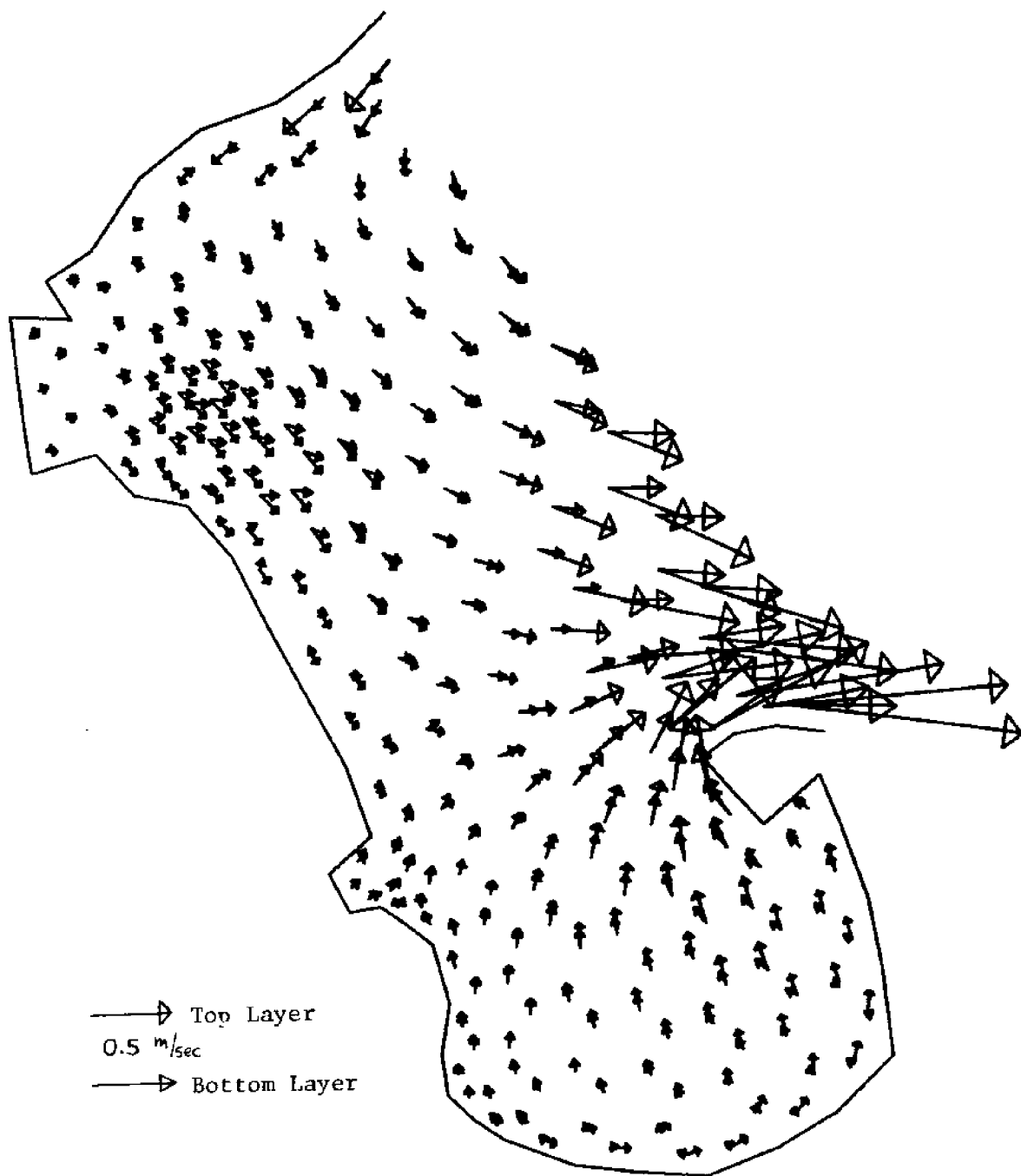
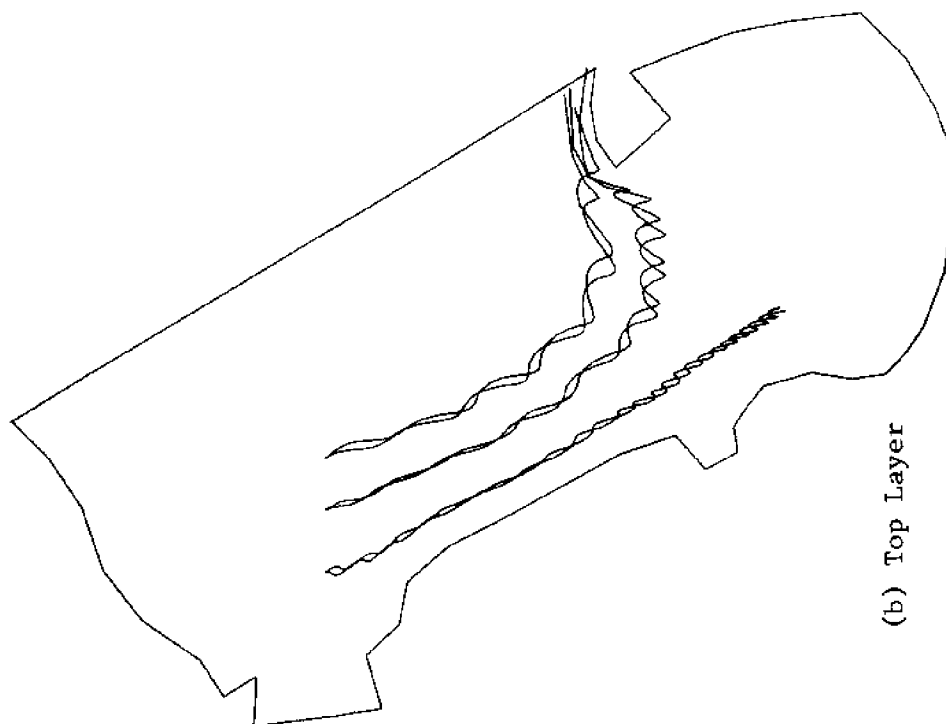
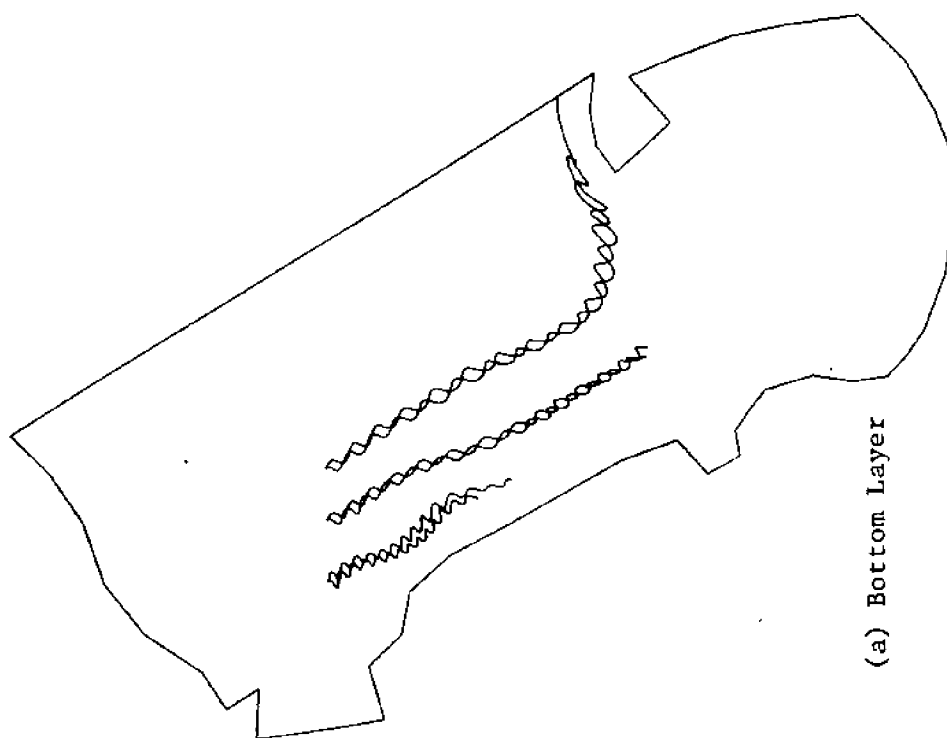


Figure 9.10 Flow Field at Ebb Tide for FTB Run



(b) Top Layer



(a) Bottom Layer

Figure 9.11 Seven-Day Particle Paths for FFB Run

To compensate for the artificial deepening of the Bay and the resulting high velocities along the western land boundary - where the highest tracer concentrations are indicated by both experimental and one-layer model results - a smaller tidal tilt was tried (Run HTB). Circulation plots for this case at flood and ebb tide, shown in Figures 9.12 and 9.13, exhibit smaller velocities both along the western bank and near the tip of Cape Cod. Particle paths, initiated at the same positions as before, are seen to move slower (Figure 9.14), although in the same direction, in general; in particular the net drift in the lower layer seems to be almost half its previous magnitude.

With respect to the comparison of the various runs to actual data in Station 5, the natural variability of the measurements is such that no conclusion can be drawn as to which one yields better agreement. Undoubtedly, an extensive undertaking is needed for a conclusive verification of the circulation model, including some carefully planned field measurements. The issue of circulation verification can no longer be pursued in the present work. Rather, two flow fields, corresponding to Runs FTB and HTB, are used as inputs to the dispersion model in an attempt to assess its sensitivity, as will be seen in the following section.

### 9.3.3 Dispersion Results

The experimental data were presented in (54) in terms of lines of equal particle counts (particles/lt) at several depths.



Figure 9.12 Flow Field at Flood Tide for HTB Run

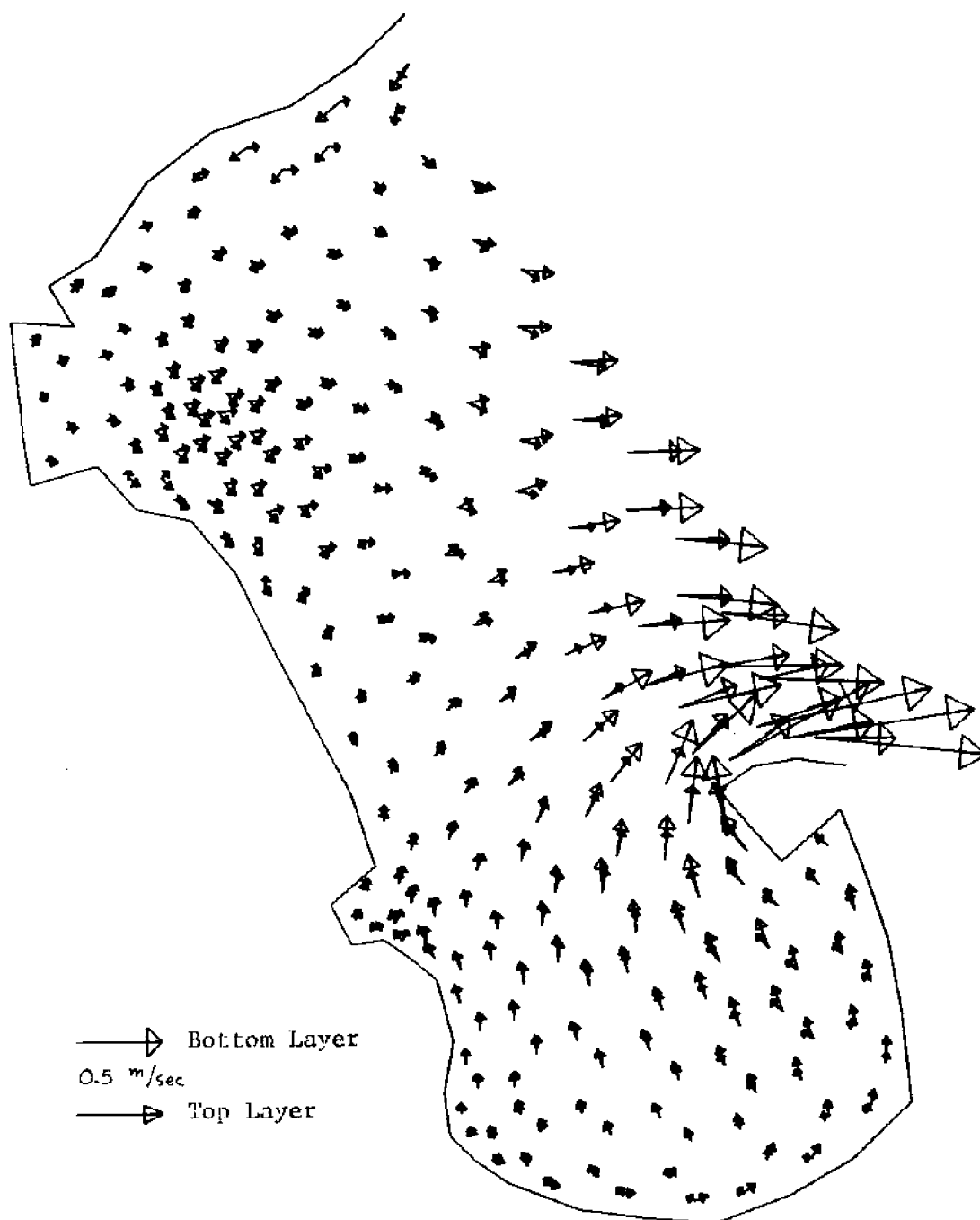
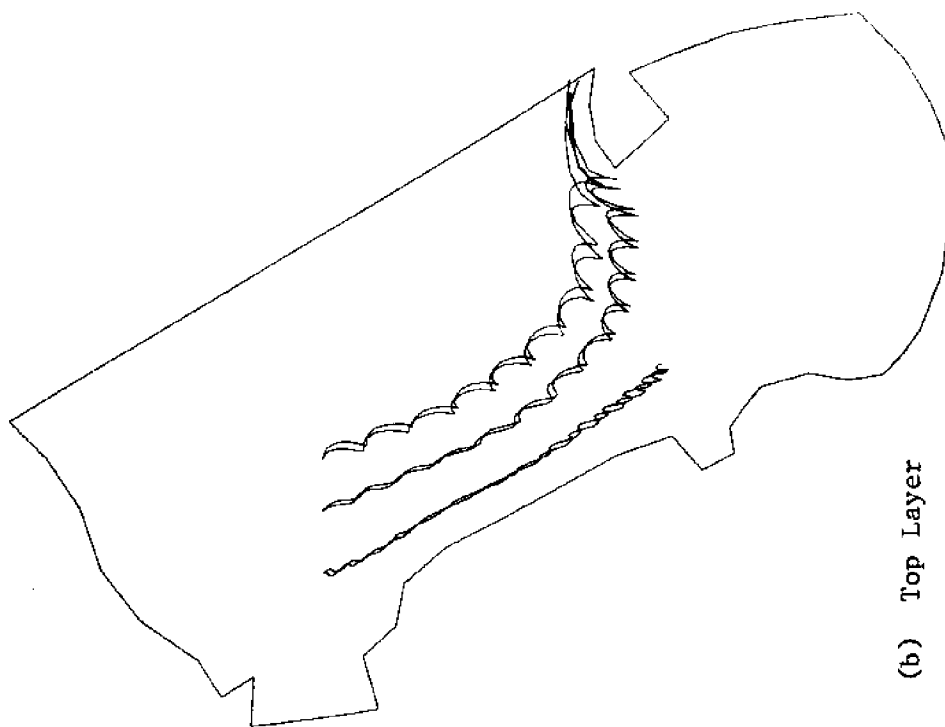
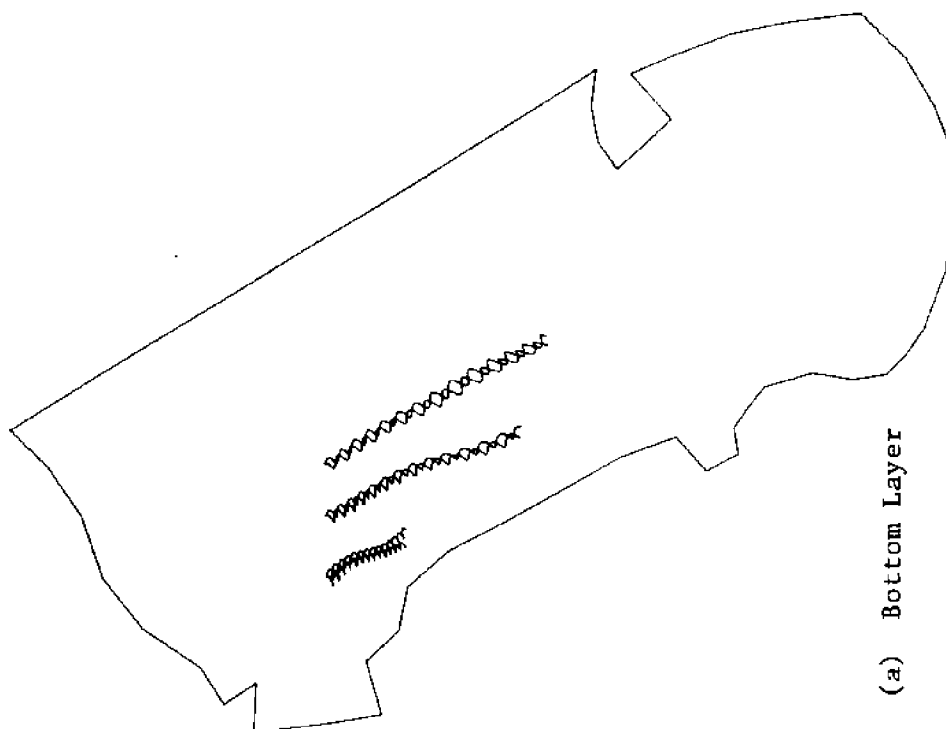


Figure 9.13 Flow Field at Ebb Tide for HTB Run



(b) Top Layer



(a) Bottom Layer

Figure 9.14 Seven-Day Particle Paths for HTB Run



These plots are shown here as Figures 9.15 through 9.17, representing the results for 2, 3, and 7 days after the introduction of the particles took place. During the early days the data were taken by boat and therefore the area that could be covered is limited. By the seventh day the particles had spread so much that boat sampling would have been meaningless. Thus, Figure 9.17 shows surface measurements, taken from a helicopter. Although monitoring of the particles continued for a few more days, their concentrations had dropped to ambient levels so that results after the seventh day are not too reliable. The data show a general southeast drift of the plume, with the peak values remaining rather close to the shoreline. In the first days, higher concentrations are found near the surface. Later, the particles move to lower levels as settling proceeds. The shape of the plume, as can be judged from the limited available measurements, is highly irregular and variable over the depth. Further, it seems to have broken into two or three different parts by the end of the experiment.

These details cannot be reproduced by deterministic modeling, which yields continuous variation of concentrations. In the numerical simulations the load was introduced at the four corners of the shaded area of Figure 9.5 over one time step. This represents an initial spreading of the source and underestimation of peaks should be anticipated for short times after the injection. All the material was considered to consist of a single representative grain

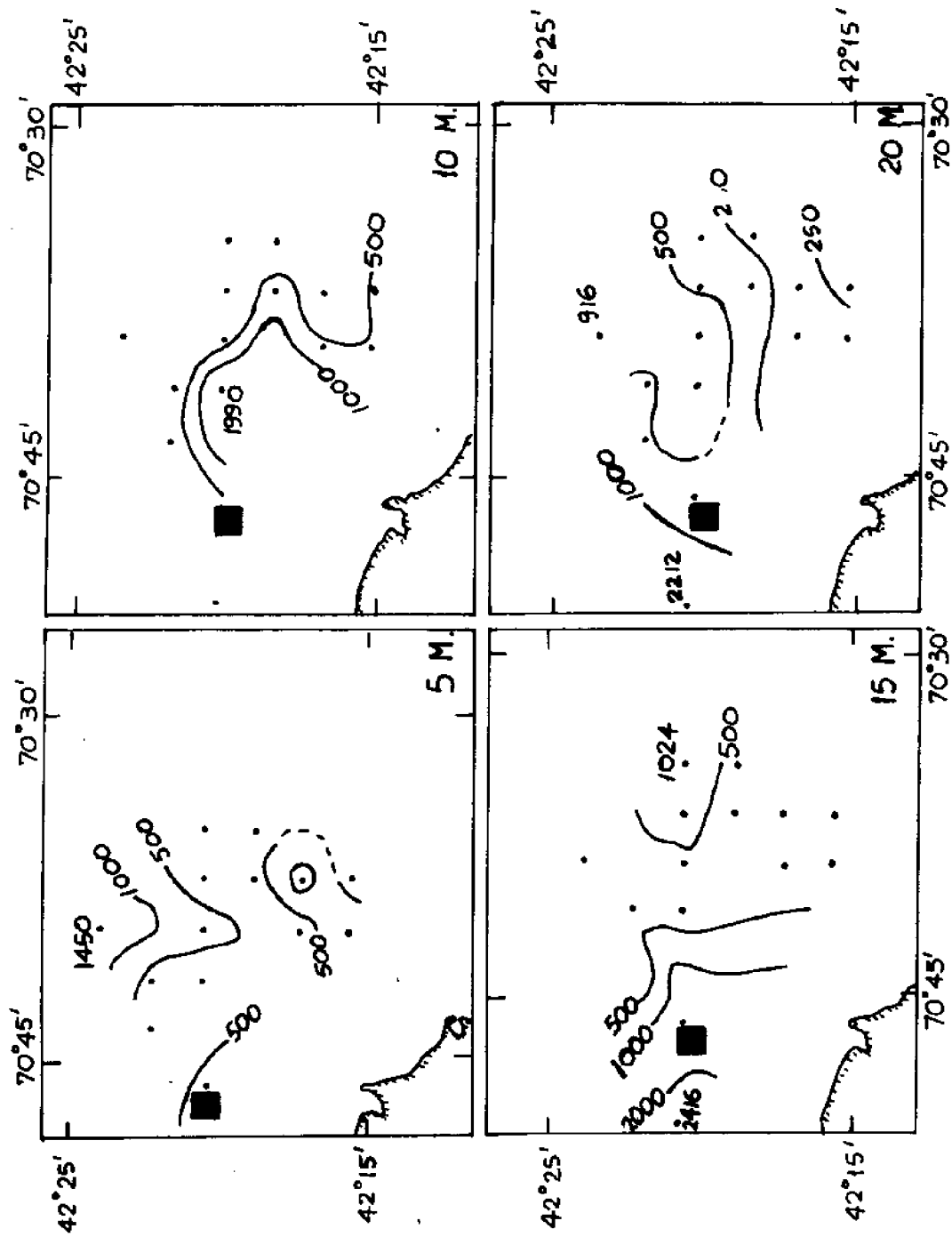


Figure 9.15 Experimental Data at Day D+2 (54)

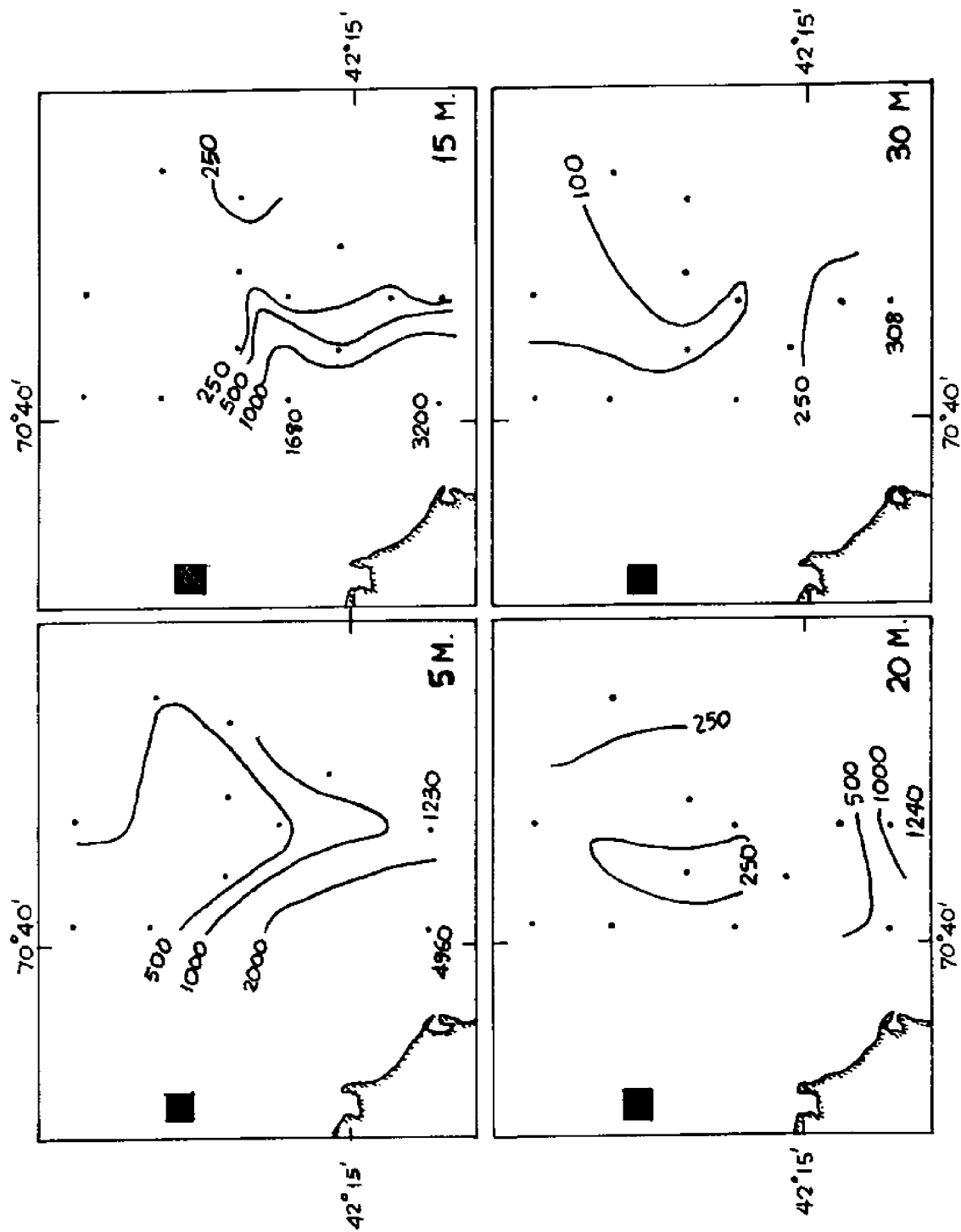


Figure 9.16 Experimental Data at Day D+3 (54)

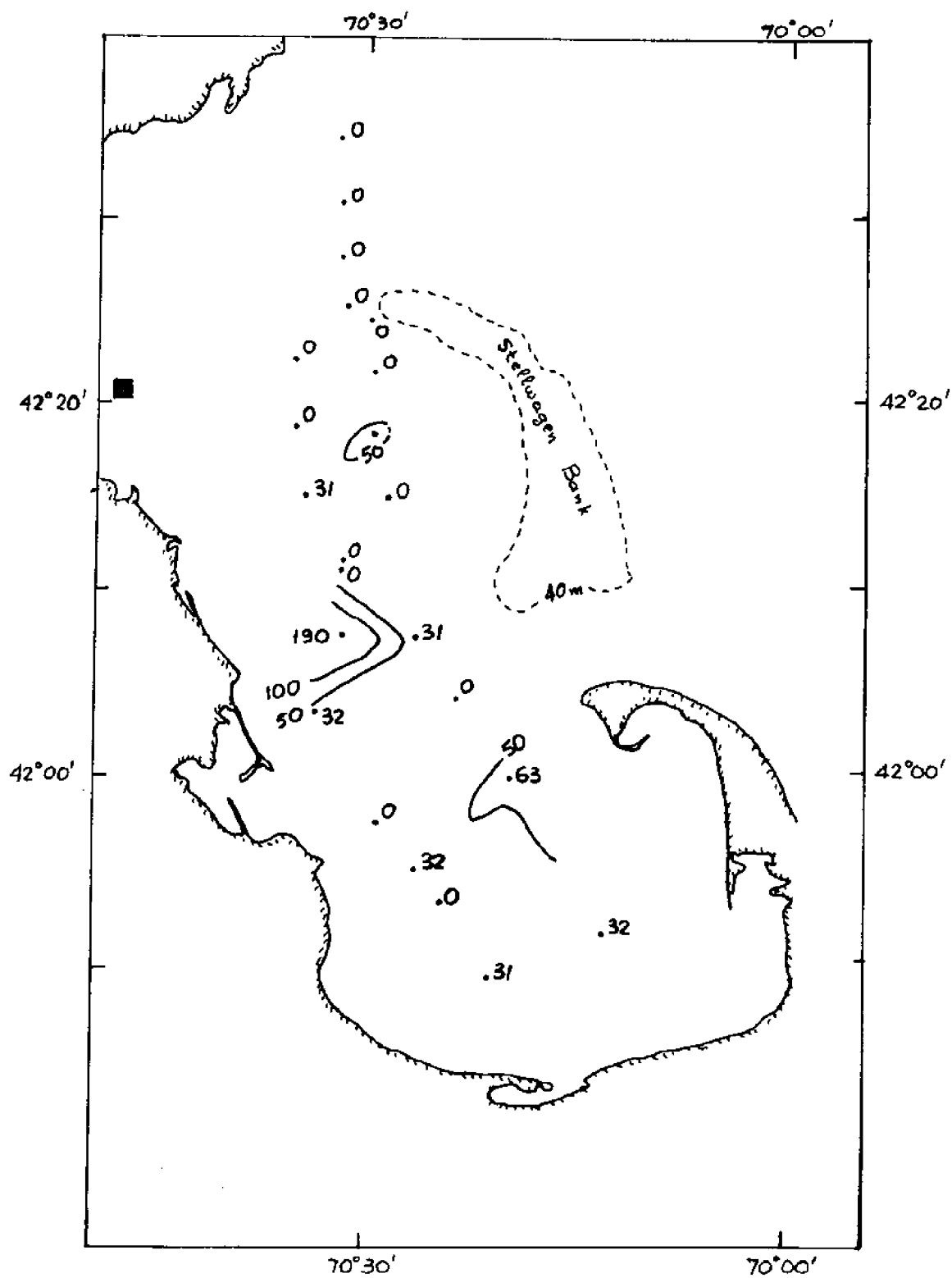


Figure 9.17 Surface Measurements at Day D+7(54)

size of 5 microns. According to Stoke's law the settling velocity of such a particle is  $3.3 \times 10^{-5}$  m/sec, assuming no interaction (eg. flocculation, etc.) between the particles. This settling rate over a layer of about 8 meters thickness is equivalent to a decay rate of about  $4 \times 10^{-6}$  sec.<sup>-1</sup>. A constant interfacial mixing coefficient of  $10^{-5}$  m/sec was used, corresponding to a (rather low) Richardson number of the order of 10. Also, a constant isotropic dispersion coefficient of  $30 \text{ m}^2/\text{sec}$ , found to yield good results in previous studies (65,63), was employed. Velocity fields from runs FTB and HTB were used as inputs to the dispersion model. The highest velocities at the area around the location of the source, where the grid is finest ( $\Delta s \approx 2.8 \text{ km}$ ), are about 10-15 cm/sec. Employing these values, as well as those of the other parameters defined above, condition (8.80) yields a bound on the time step of about 2500 to 3000 sec. The actual time step chosen was 1500 sec, for better accuracy in the representation of the velocity variability.

Using velocity input corresponding to the large tidal tilt (FTB) proved to yield results extremely sensitive to the precise tidal time of particle injection. While the actual dumping took place around ebb tide, some time has to be allowed for the cloud to reach a size comparable to that of the numerical source. Figures 9.18 through 9.20 show simulation results (in particles/lt) for a release at low water. Except for the exaggerated speed of

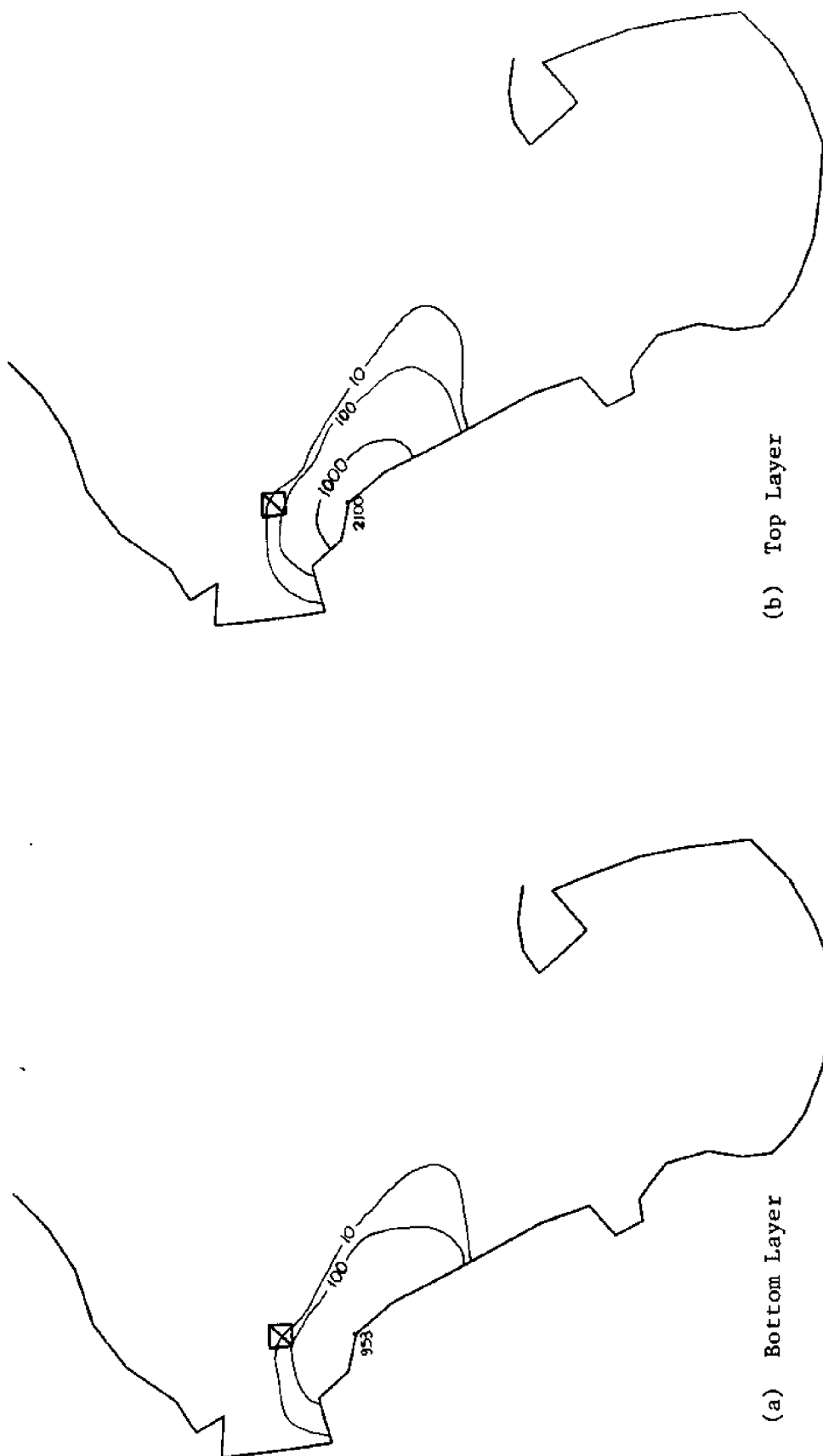
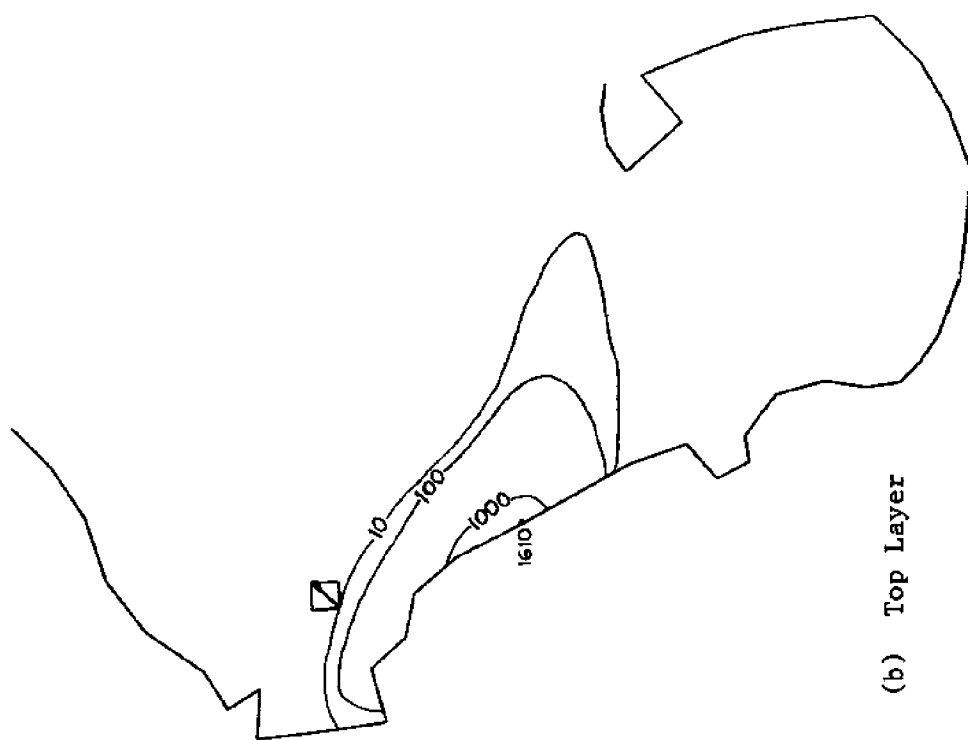
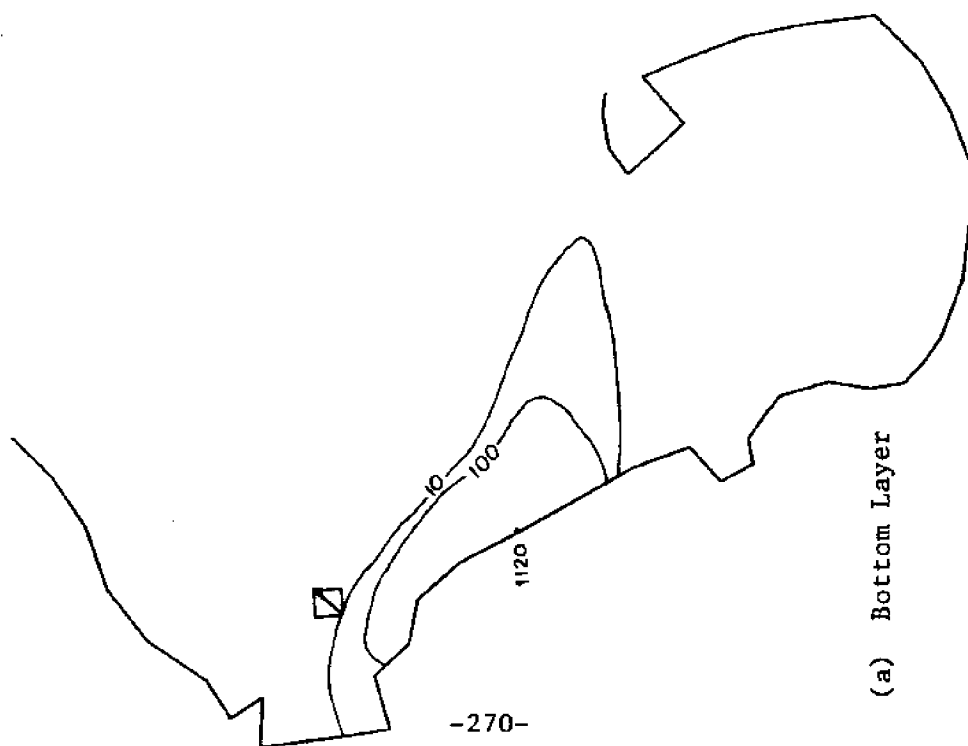


Figure 9.18 Model Results for FTB Run at Day D+2



(b) Top Layer



(a) Bottom Layer

Figure 9.19 Model Results for FTB Run at Day D+3

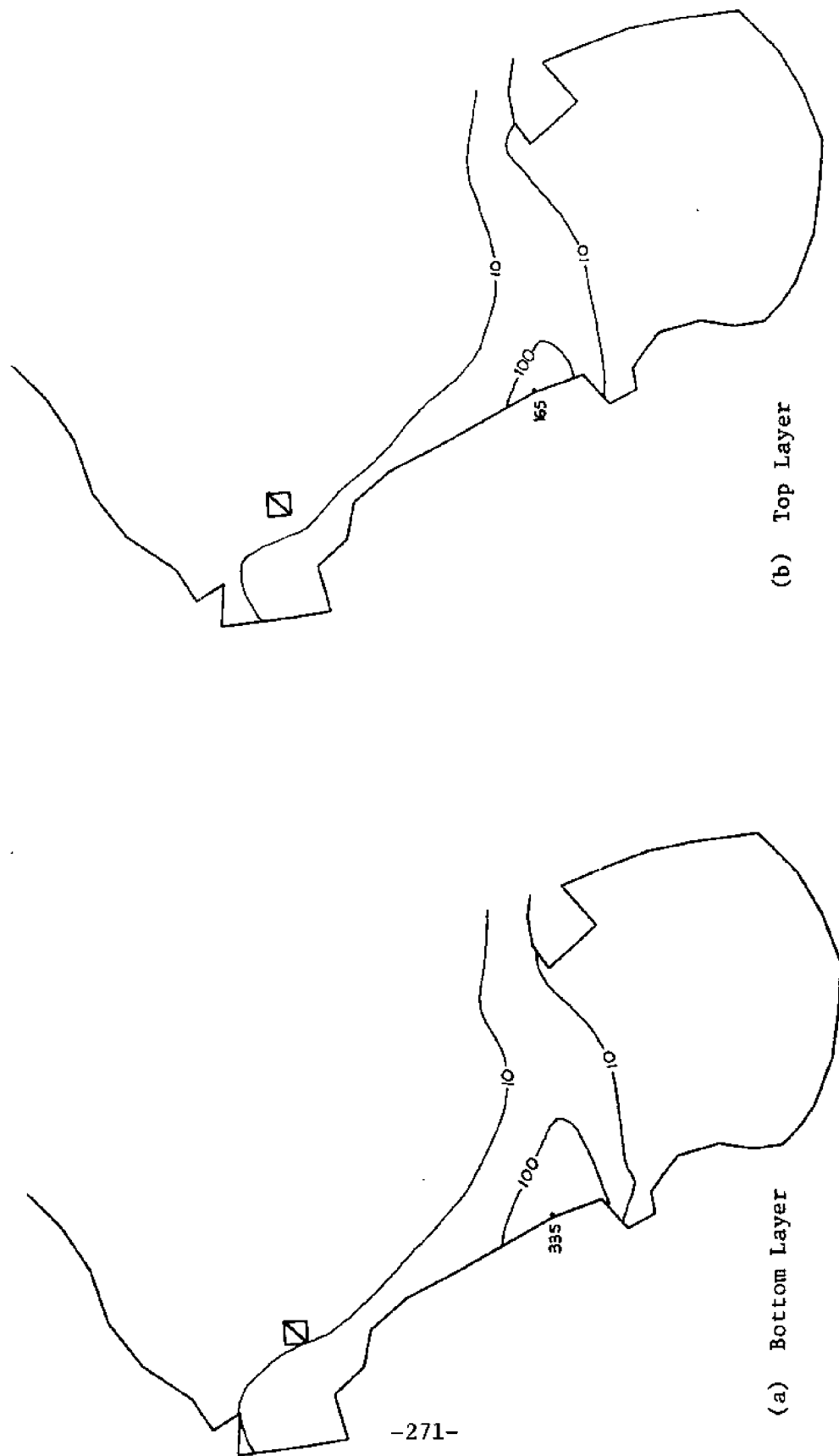


Figure 9.20 Model Results for FTB Run at Day D+7



motion southward and out of the domain, these are in reasonable agreement with the field measurements and also the one-layer results (65). However, slight variations in the time of release drastically change the picture. In particular, when the injection is made at ebb tide, the resulting cloud moves in the center of the Bay and rapidly disappears into the ocean. This unnatural sensitivity of the model can be explained based on the particle paths shown in the previous section (Figure 9.11). Apparently, if the particles are introduced close to ebb tide, the bulk of the plume gets carried enough eastward, due to the high velocities, so that it starts following the course of the paths that lead quickly out of the Bay.

Using the velocities obtained with the smaller tilt at the boundary (HTB), yields significantly different results. Figures (9.21) through (9.23) show plots corresponding to a release at low water. Comparing with analogous results associated with the previous flow field, the most striking difference is that now the plume reaches the boundary more to the north and its peak never approaches Plymouth. However, this contradicts the field data and consequently, at least in that respect, the stronger flow field is to be preferred. Figures (9.24) through (9.26) show simulation results for a release at ebb tide. Comparison with the previous set of plots again indicates considerable sensitivity of the plume motion to the time of introduction, but not as significant as found with the FTB circulation field. This is

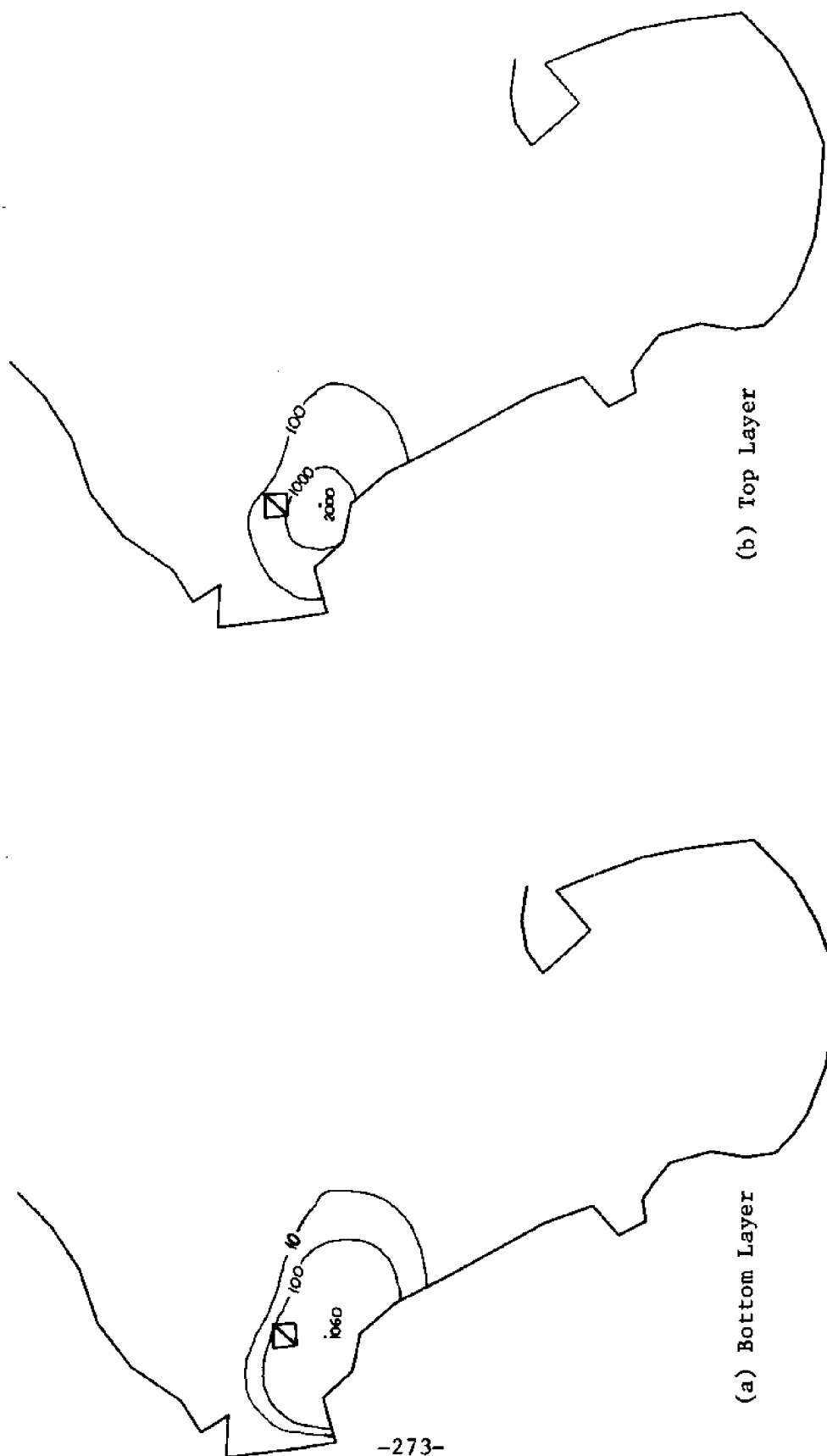


Figure 9.21 Model Results for HTB Run at Day D+2 (Release at Low Water)

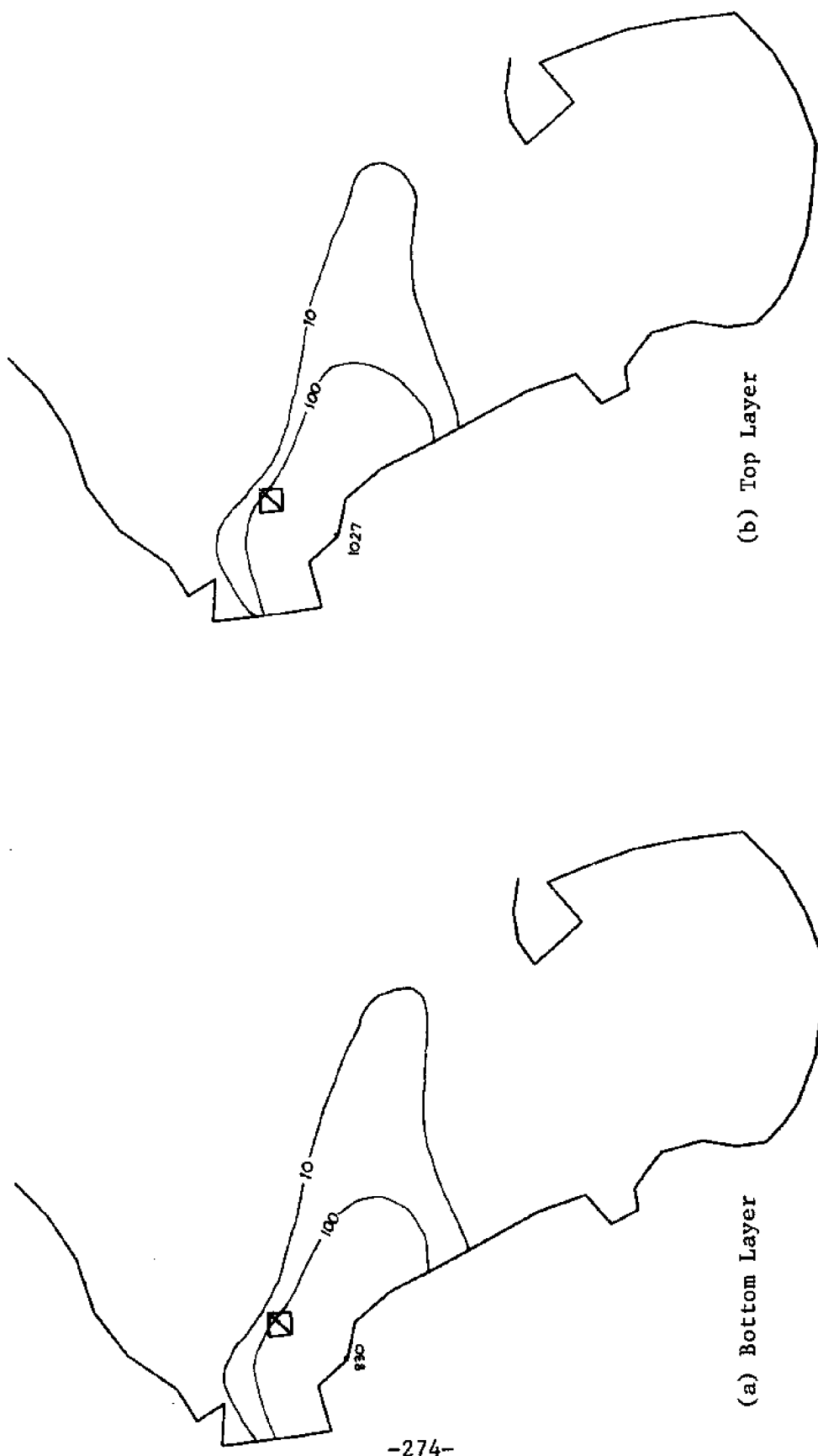


Figure 9.22 Model Results for HTB Run at Day D+3 (Release at Low Water)

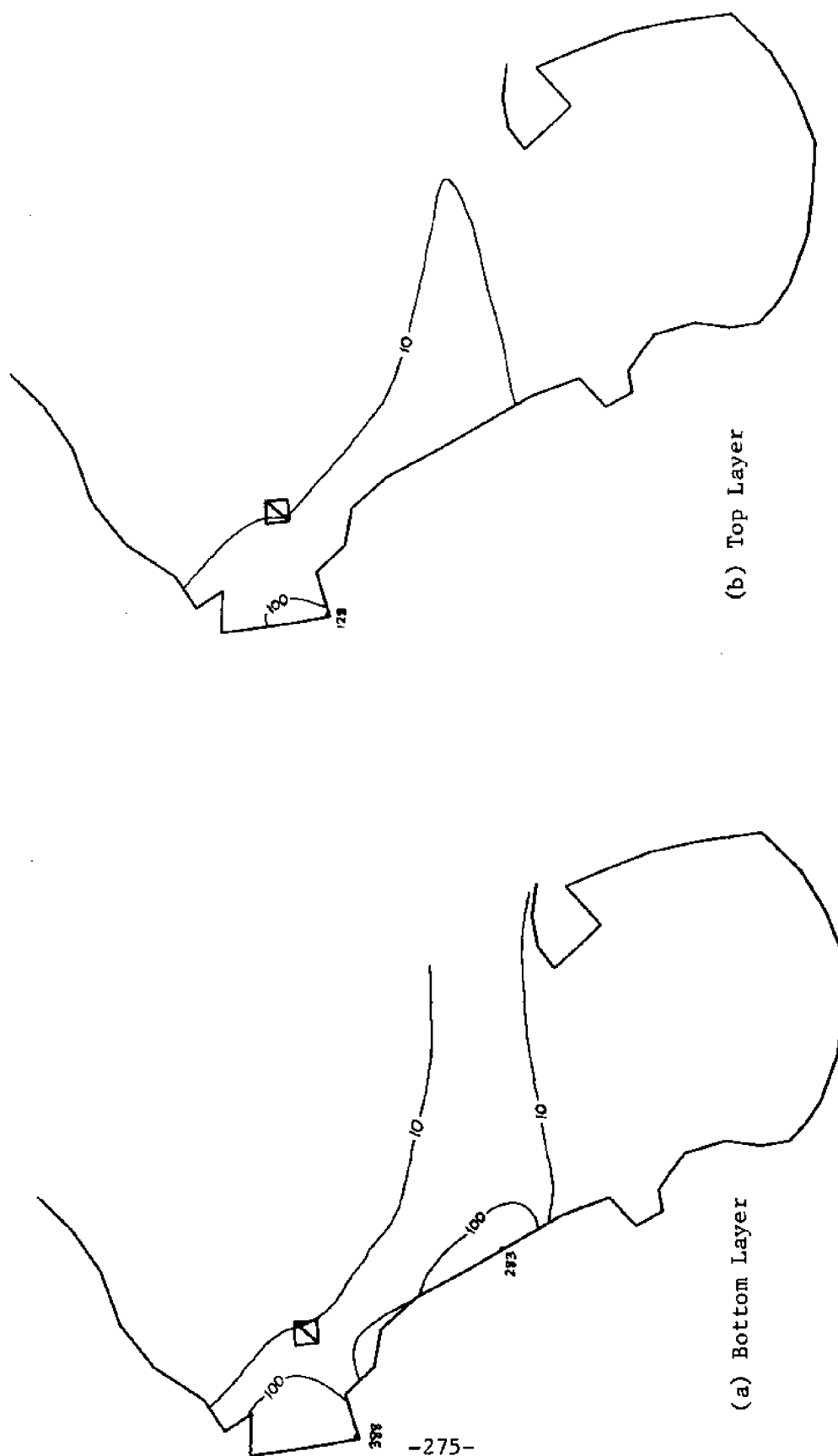


Figure 9.23 Model Results for HTB Run at Day D+7 (Release at Low Water)

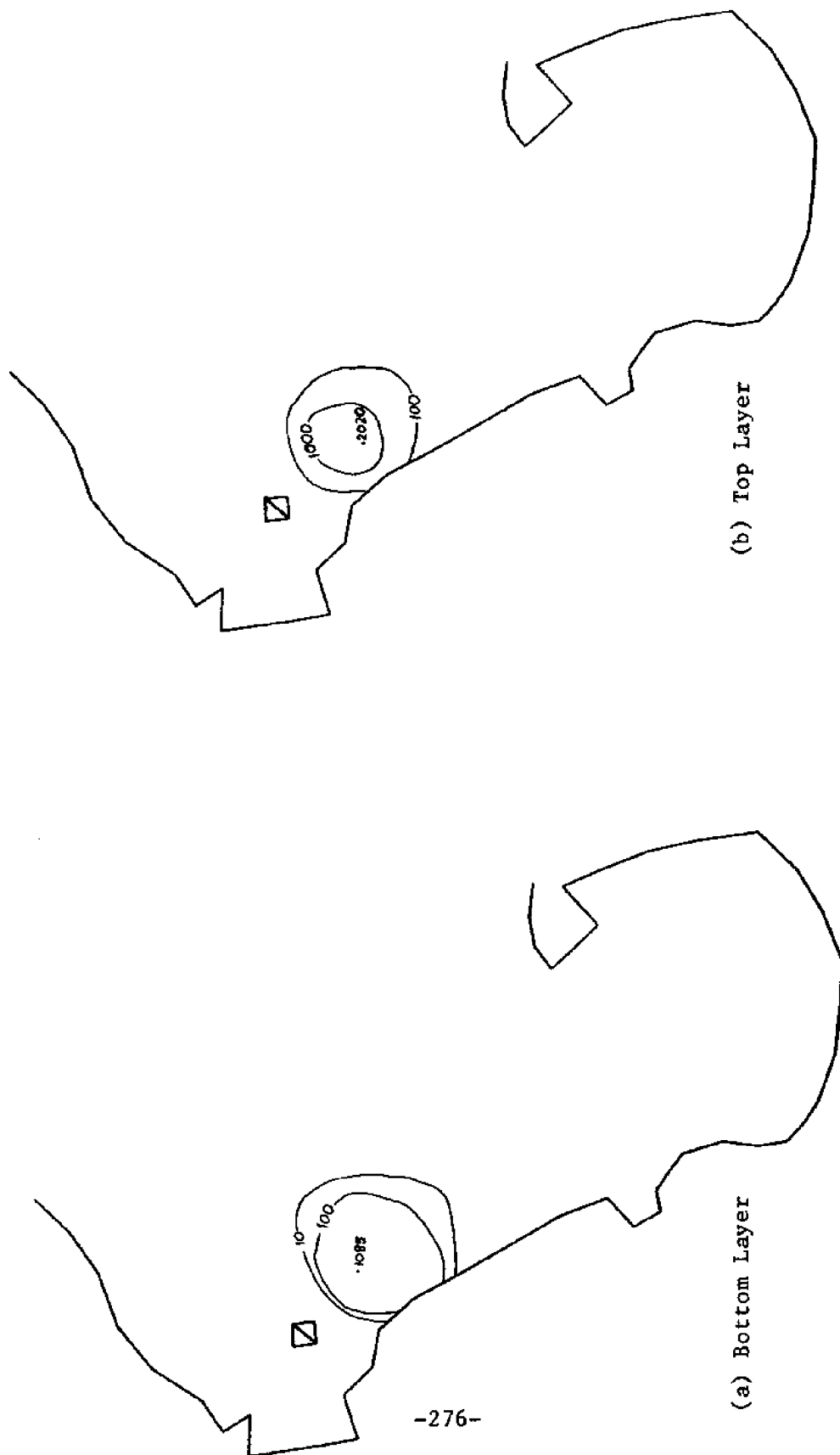


Figure 9.24 Model Results for HTB Run at Day D+2 (Release at Ebb Tide)

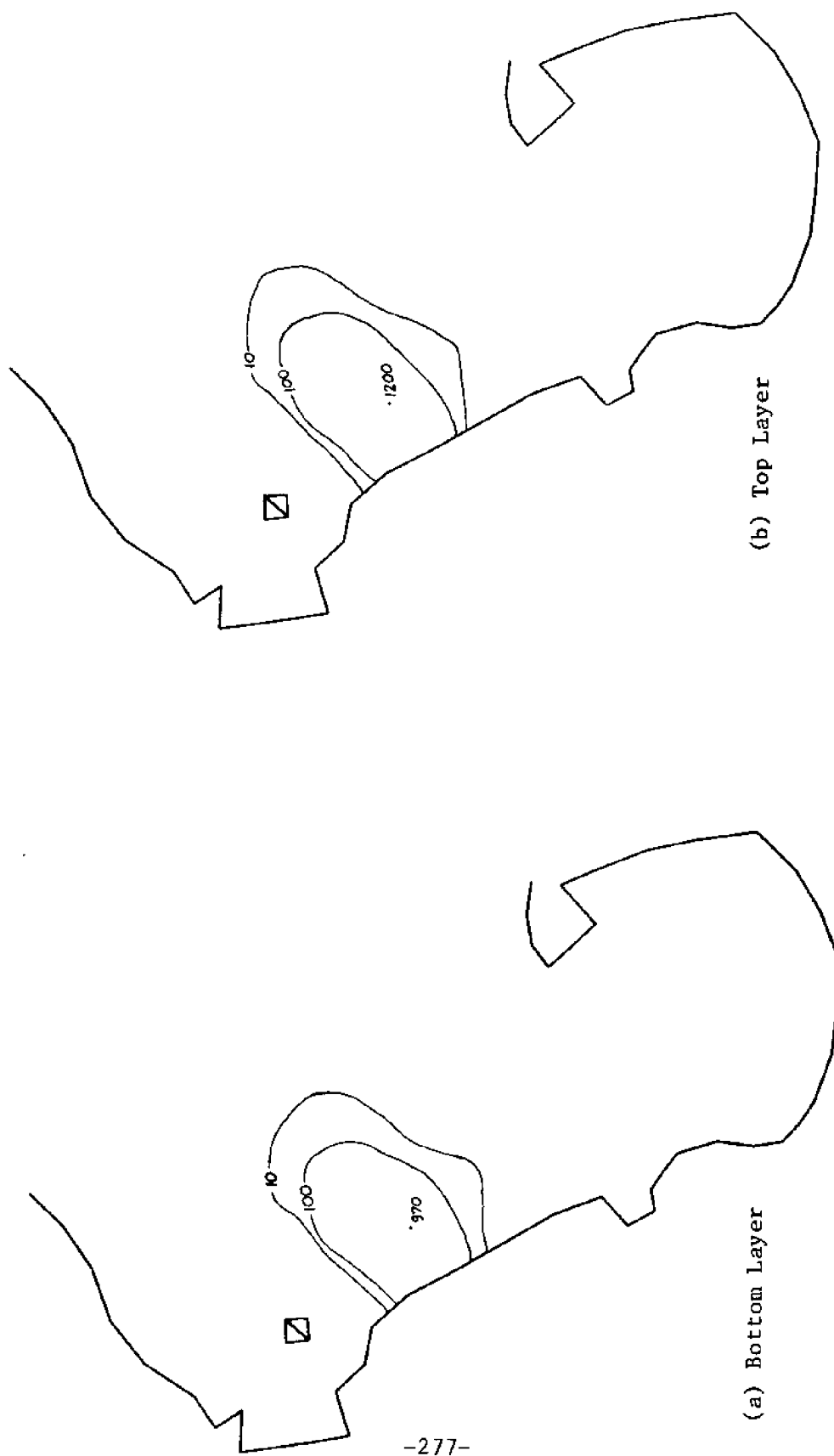


Figure 9.25 Model Results for HTB Run at Day D+3 (Release at Ebb Tide)

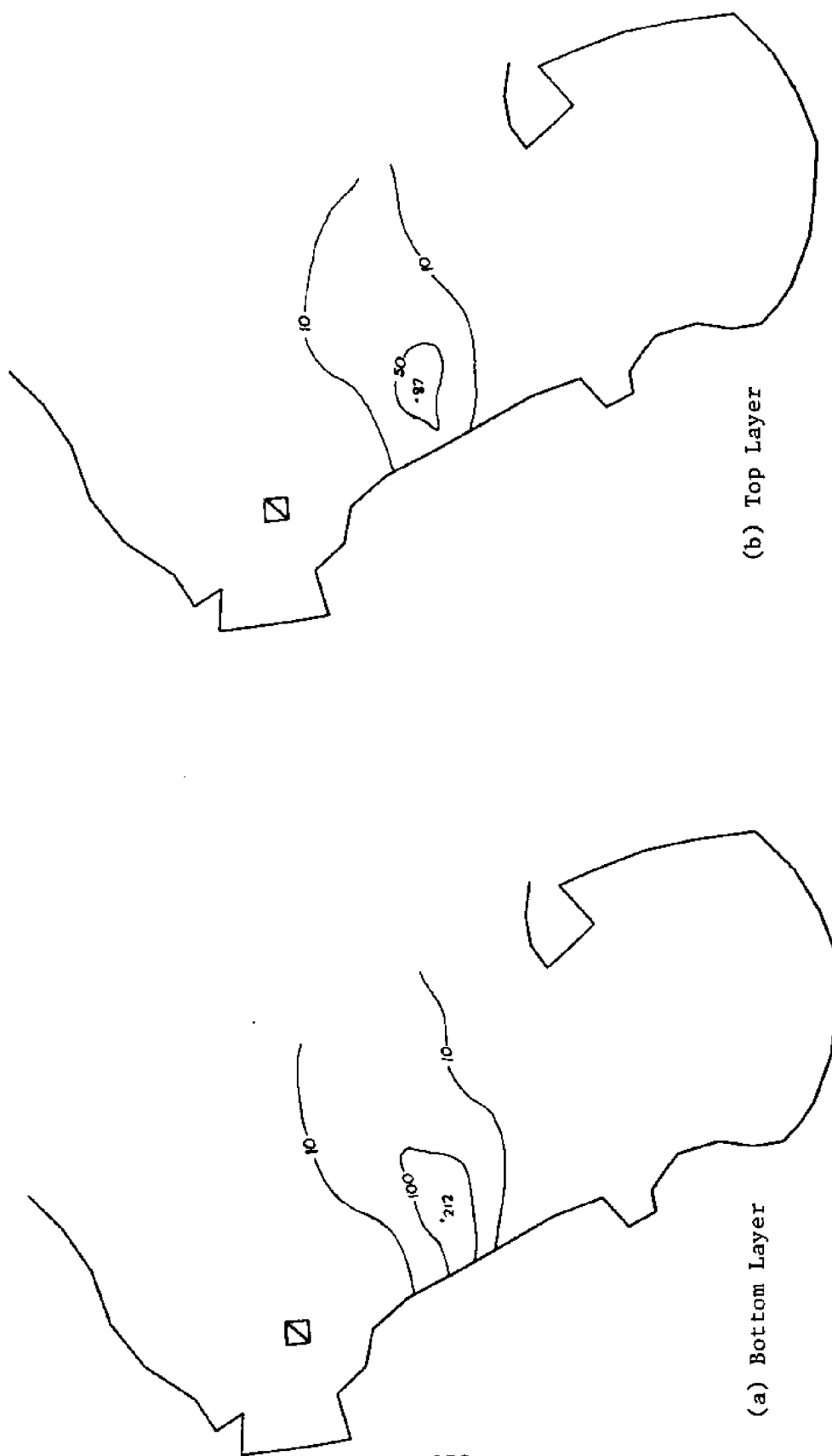


Figure 9.26 Model Results for HTB Run at Day D+7 (Release at Ebb Tide)

certainly a factor in favor of the present velocity input.

The boundary condition used in all runs of the dispersion model consisted of specifying zero concentration along the northern part of the ocean boundary and zero gradient along the southern part, where the velocity is predominantly outwards, as discussed in Section 2.3. The early arrival of appreciable concentrations at the boundary, due to the unrealistically strong flow field, may lead to inaccuracies and therefore the results near the boundary must be viewed as a crude approximation at best.

#### 9.4 Application to the MIT Experiment

##### 9.4.1 The Experiment

In conjunction with recent studies made by the R.M. Parsons Lab. of MIT (63 ) and sponsored by Boston Edison Co., of the far field effects of the Pilgrim Nuclear Power Station (PNPS), a dispersion experiment was carried out in August 1975. The power plant is located at Rocky Pt., south of Plymouth on the Massachusetts coast (Figure 9.27) and the experiment was intended to be, to some extent, site-specific in order to provide information relevant to plant discharges. However, the experimental results should be of more general value in assessing the circulation and dispersion characteristics of the adjacent water body.

The timing of the experiment, in late August, was planned so that the results could be used in connection with the two-layer numerical models. Based on previous experience with dispersion



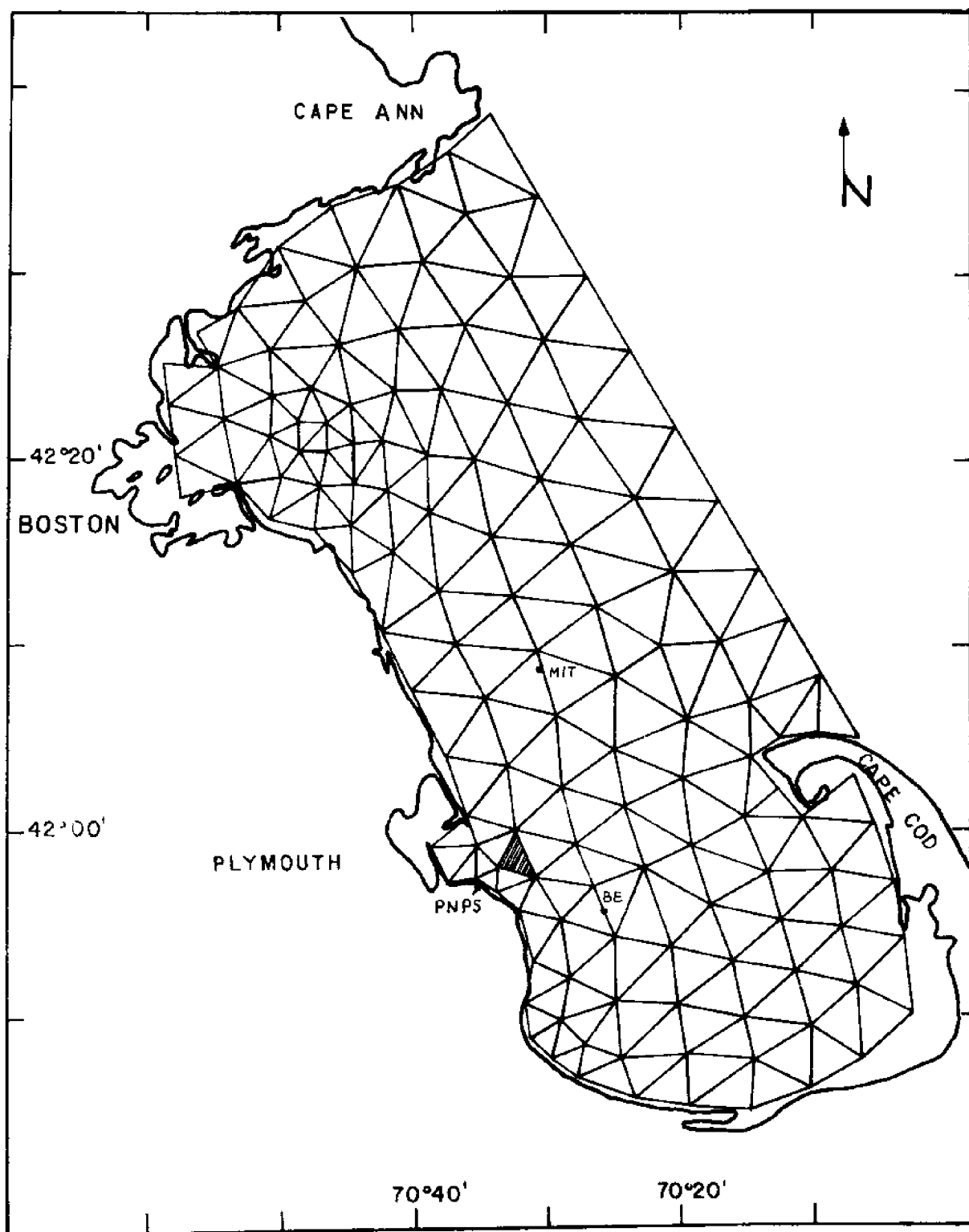


Figure 9.27 Location of the MIT Experiment

material, it was decided to use fluorescent sphalerite particles as a tracer. On the morning of August 17, 1975, 500 pounds of these particles were introduced gradually into the water over a period of about one hour, around high tide. Their motion was subsequently monitored for 5 days by boat and by helicopter. Samples were taken from the surface as well as 5, 10, 15, 20 and 25 meters depth. In addition, temperature and conductivity profiles over the depth were scheduled, but very limited data were obtained due to instrument malfunction. Two current meter stations had been installed prior to the experiment at locations shown in Figure 9.27 by dots. Details of the experimental procedures and data analysis, which has been recently completed, are given in (63).

#### 9.4.2 The Flow Field

Two sets of velocities obtained from the circulation model and corresponding to large and small tidal tilt along the boundary were used. Since the tide was slightly higher than in the NOMES experiment, the specified amplitudes were 1.22 to 1.13 meters and 1.22 to 1.175 meters, respectively. A variable wind routine was also implemented and actual time-varying wind data were used in the computations. The remaining variables, such as the interfacial friction and the depth of the interface, were assigned the same values as in the previous application. At the boundary, the interface was given the same motion as the free surface, i.e., the tide is considered to come through the bottom layer.

Comparison of the predicted currents, under the small tidal tilt, to measurements at St. BE is shown in Figure 9.28. The agreement is reasonable, especially for the lower layer, while the predicted top-layer direction differs significantly at times from the measured surface value, the latter being strongly dependent on the wind.

#### 9.4.3 Dispersion Results

The experimental results were reduced to "layer-average" concentrations. At each location, samples above and below the thermocline were averaged together to yield a single representative value for each layer. The resulting plots, in particles/lt, are shown in Figures 9.29, 9.30 and 9.31 corresponding to 1, 2 and 3 days after the dumping took place. During the fourth day no measurements were taken, while the data of the fifth day are too inconclusive - and generally low - to draw isoconcentration lines with any confidence. By that time, the plume had spread considerably to the east in comparison to earlier days, a result of a change in wind to southwest, extending probably over a large portion of Cape Cod Bay which could not be covered by the sampling means available. The plots of the first three days show the plume moving slowly to the southeast, approximately parallel to the shore. Initially the top layer has higher concentrations, as the particles were introduced a little below the surface, but later higher values occur in the bottom layer due to settling.

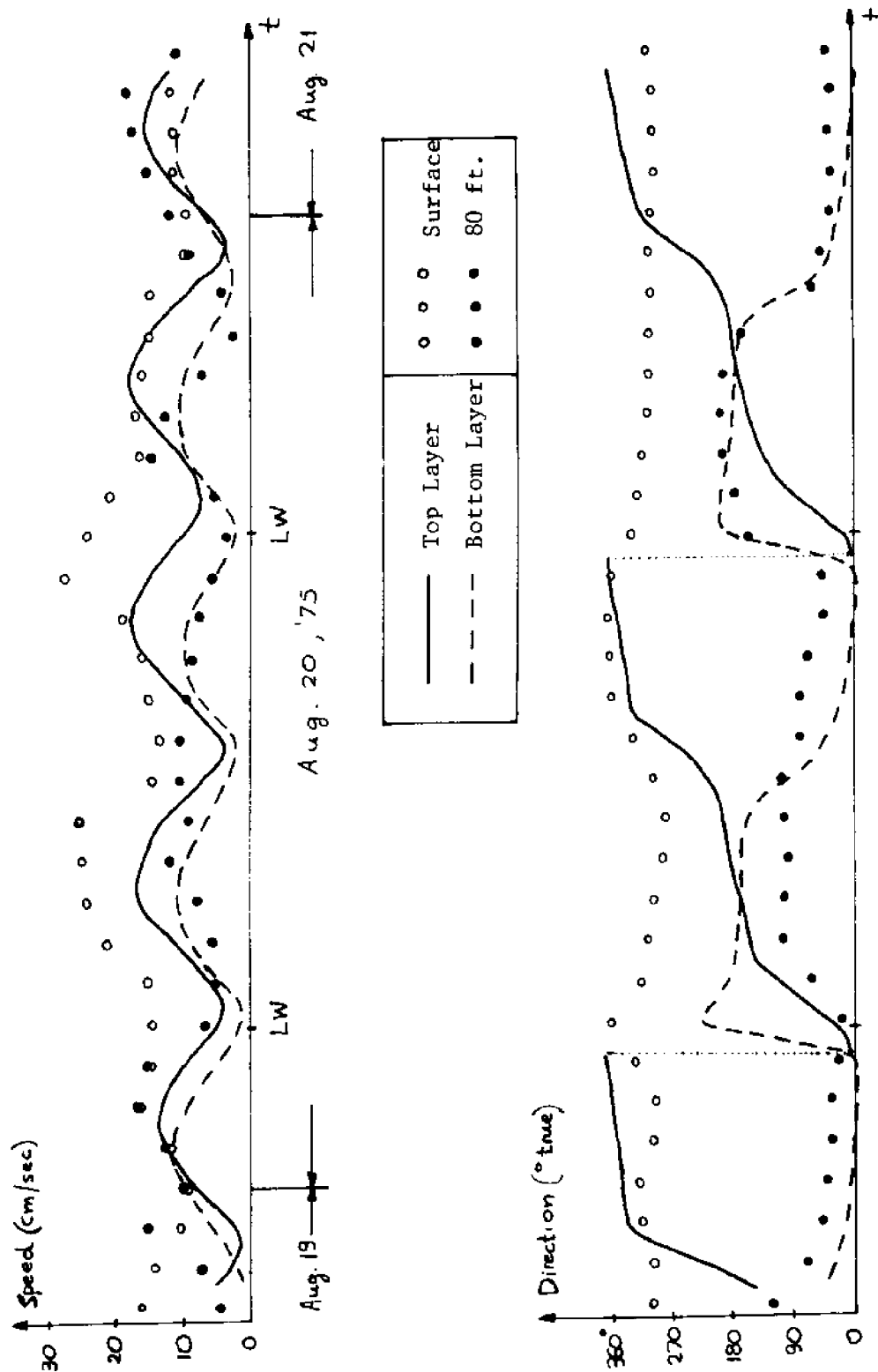
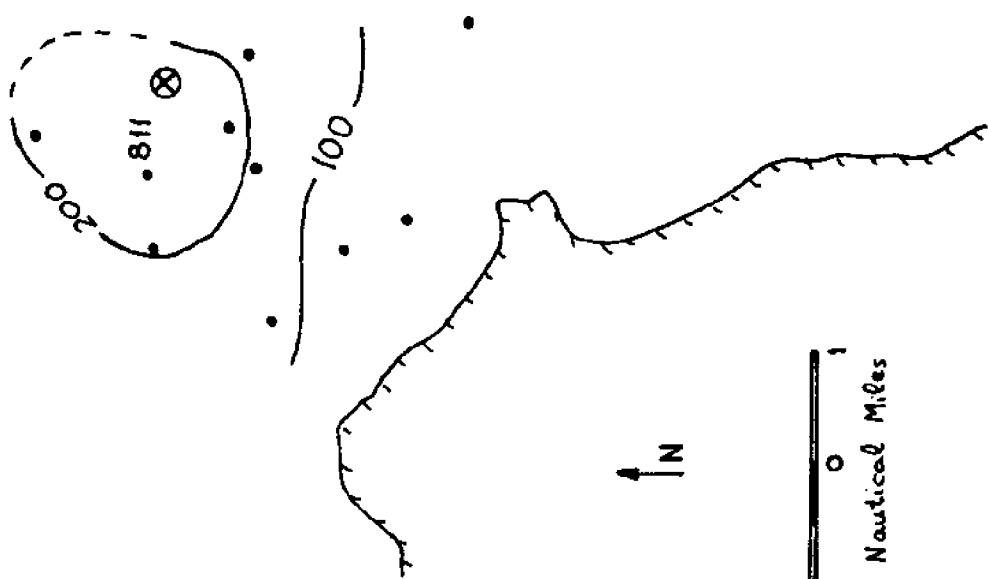
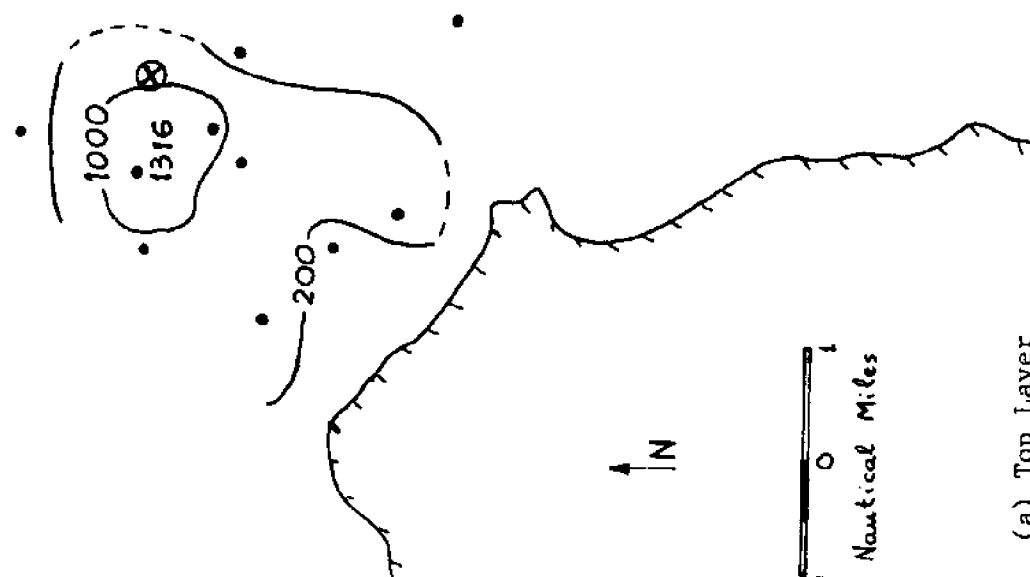


Figure 9.28 Velocity Comparison at St. BE



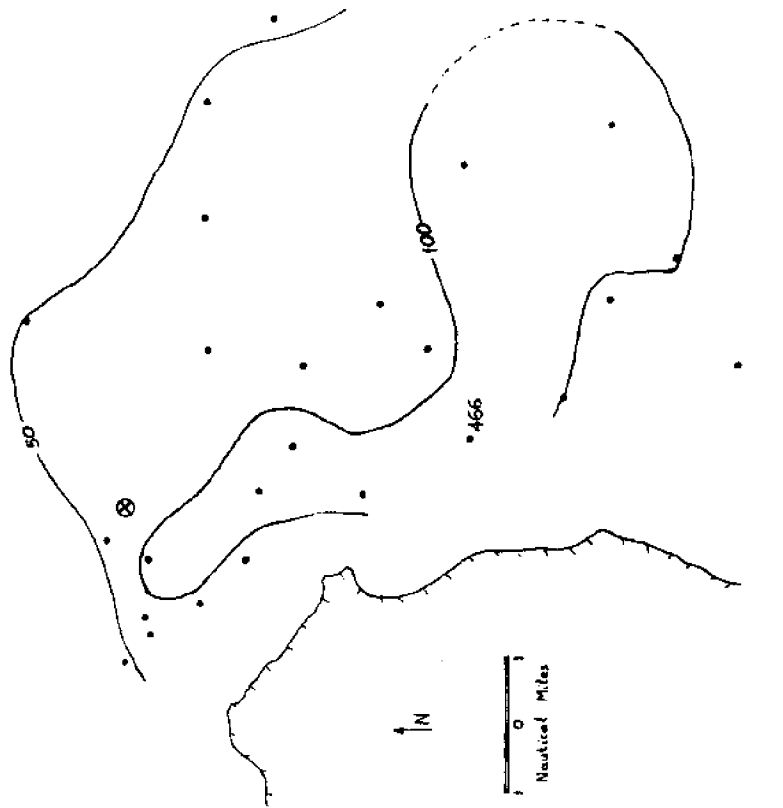
(b) Bottom Layer



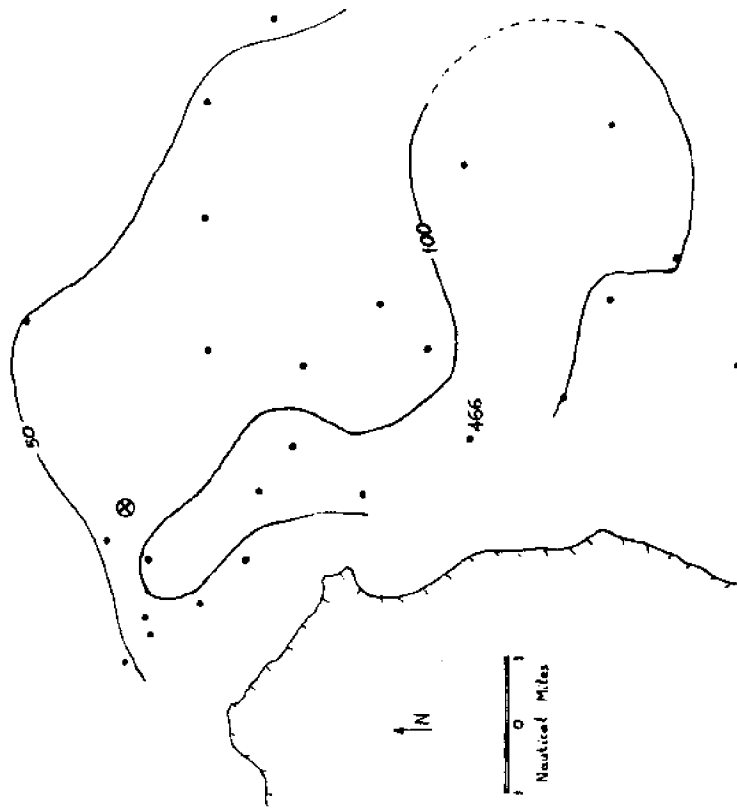
(a) Top Layer

Figure 9.29 Experimental Results at Day D+1





(a) Top Layer



(b) Bottom Layer

Figure 9.31 Experimental Results at Day D+3

In the dispersion simulations the shaded triangle was loaded over a period of three timesteps. The area of the triangle is quite large in comparison to the actual source and as a consequence, one should expect unrealistically large plume areas for short times. In fact, the finite element grid is quite coarse in the vicinity of PNPS, simply because it had not been designed to handle a source in that area. A much finer grid has been employed earlier in connection with the one-layer models to study circulation and dispersion problems in the Plymouth area, including the harbor, and may be used in the future for the two-layer models as well. At this time, the requirement that all depths be at least about 15 meters makes use of that grid meaningless.

The values of the dispersion coefficient and the interfacial mixing rate were set, as in the previous application, at  $30 \text{ m}^2/\text{sec}$  and  $10^{-5} \text{ m/sec}$ , respectively. An average particle size of 7 microns was selected as representative, following the particle distribution provided by the manufacturer. Consequently a settling velocity of  $7.3 \times 10^{-5} \text{ m/sec}$  was used in the computations. As in the previous application, various starting times of the simulation were tried. The results for the velocity field obtained under the large tidal tilt at the boundary showed again considerable sensitivity to starting times. When the release was made close to or before high water, the plume was seen to move rapidly southward close to the shore as a narrow zone; for a release after high



water the plume moved to the south more slowly and at the same time extended to the east. Taking into account our initial spreading of the source, this second starting time is more reasonable. The model results for this case are shown in Figures 9.32, 9.33 and 9.34. In addition to reasonable agreement in the location of the plume, good quantitative agreement of the peak values is observed.

Using the velocity field obtained under smaller tidal tilt at the boundary, hardly any southward movement of the plume center to the south is found. As Figures 9.36, 9.36 and 9.37 show, the plume is now more extended along the shore and appreciable concentrations occur towards Plymouth Bay. The peak values appear in satisfactory agreement with the data, although the dimensions of the plume are clearly overestimated, due to the initial spatial distribution of the source.

## 9.5 Discussion of the Results

The verification studies presented in the first part of this chapter show that the numerical model is capable of describing well the dispersion phenomenon in a two-layer system, as it is intended to. The main difficulty in its application to real world problems seems to be the lack of reliable velocity inputs. In the particular cases studied in the Massachusetts Bay, the primary obstacles are associated with the behavior of the interface at the boundary and the use of distorted topography in shallow areas.

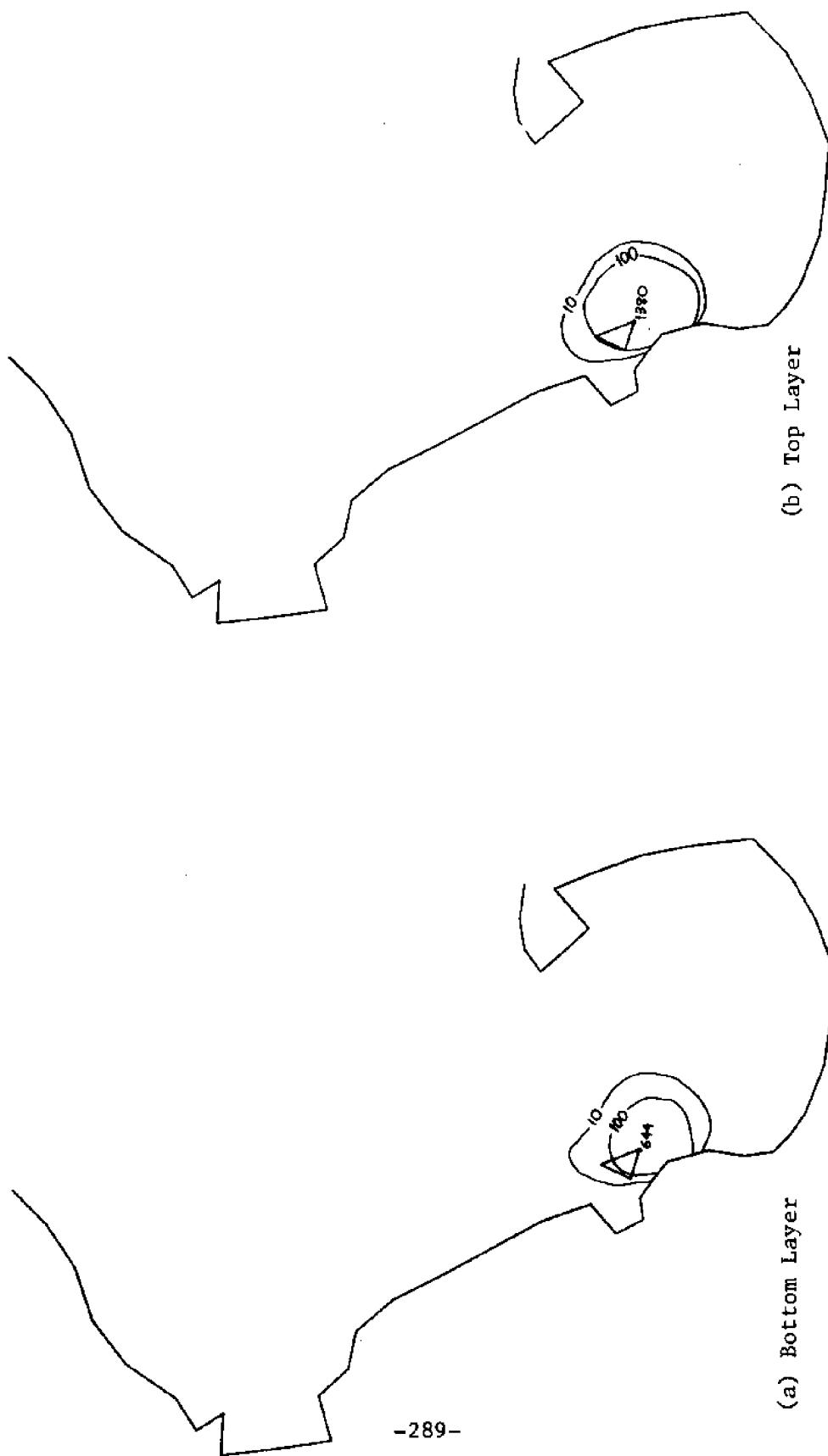


Figure 9.32 Computed Concentrations at Day D+1 (Large Tidal Tilt)

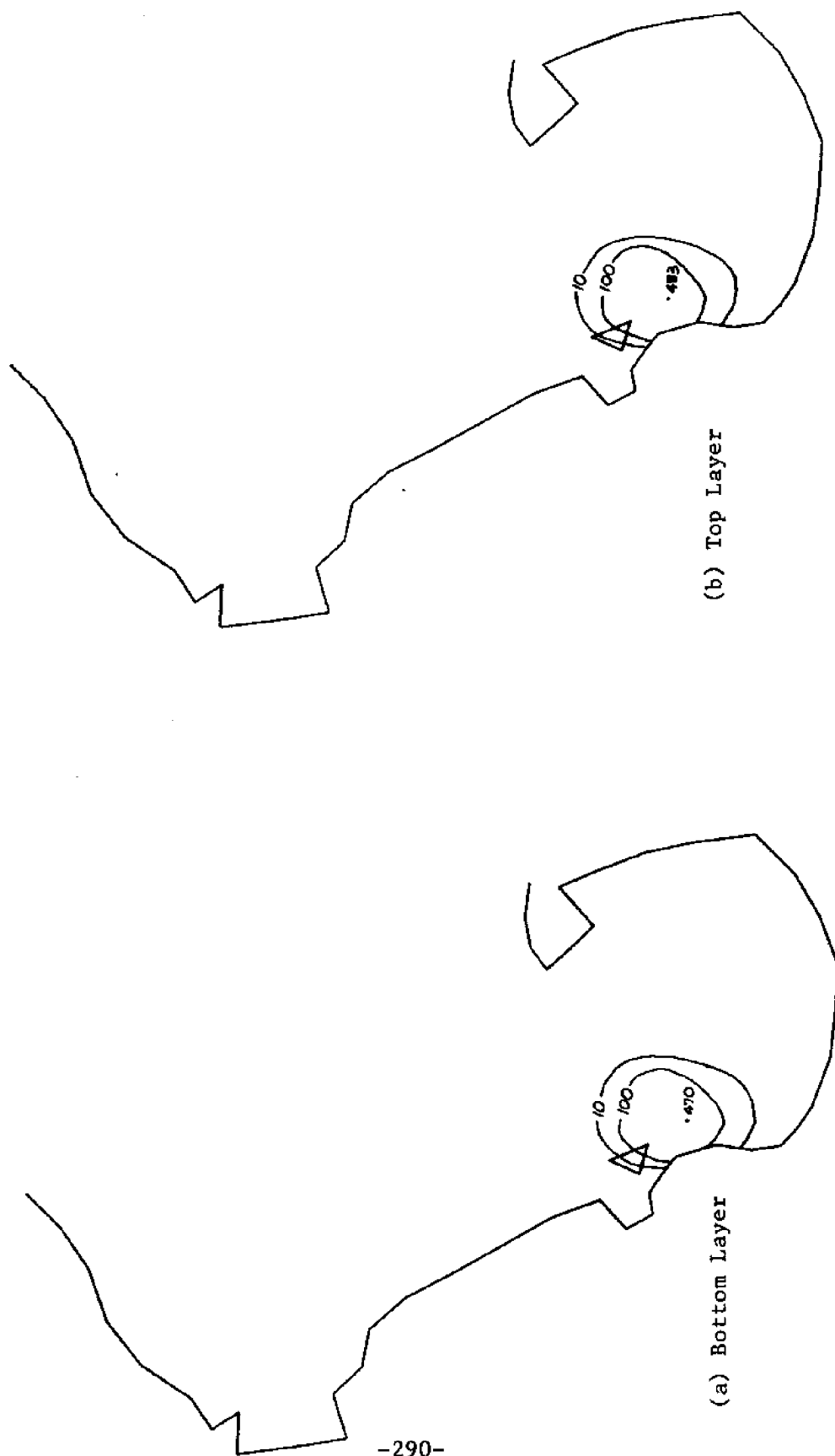


Figure 9.33 Computed Concentrations at Day D+2 (Large Tidal Tilt)

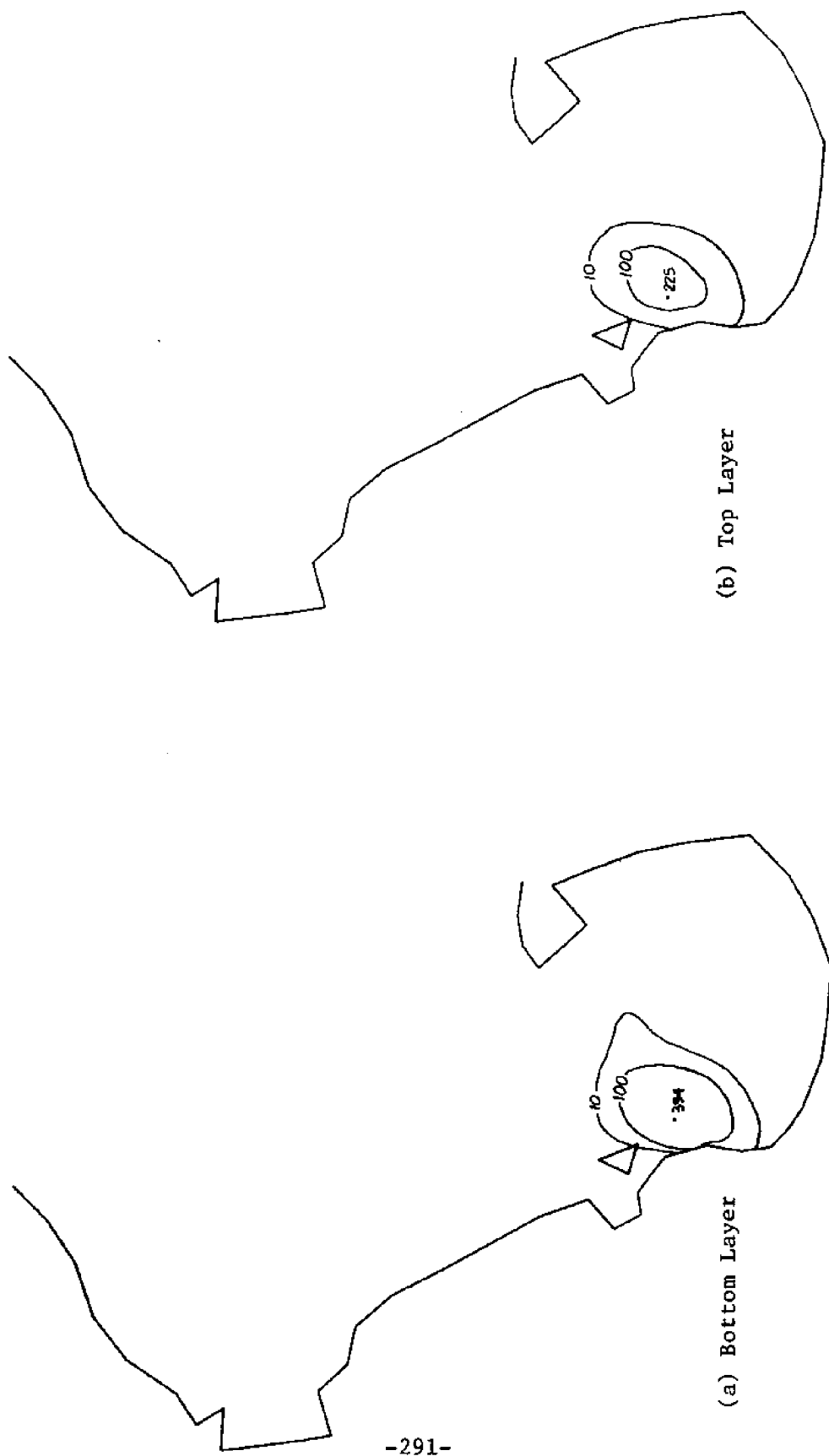


Figure 9.34 Computed Concentrations at Day D+3 (Large Tidal Tilt)

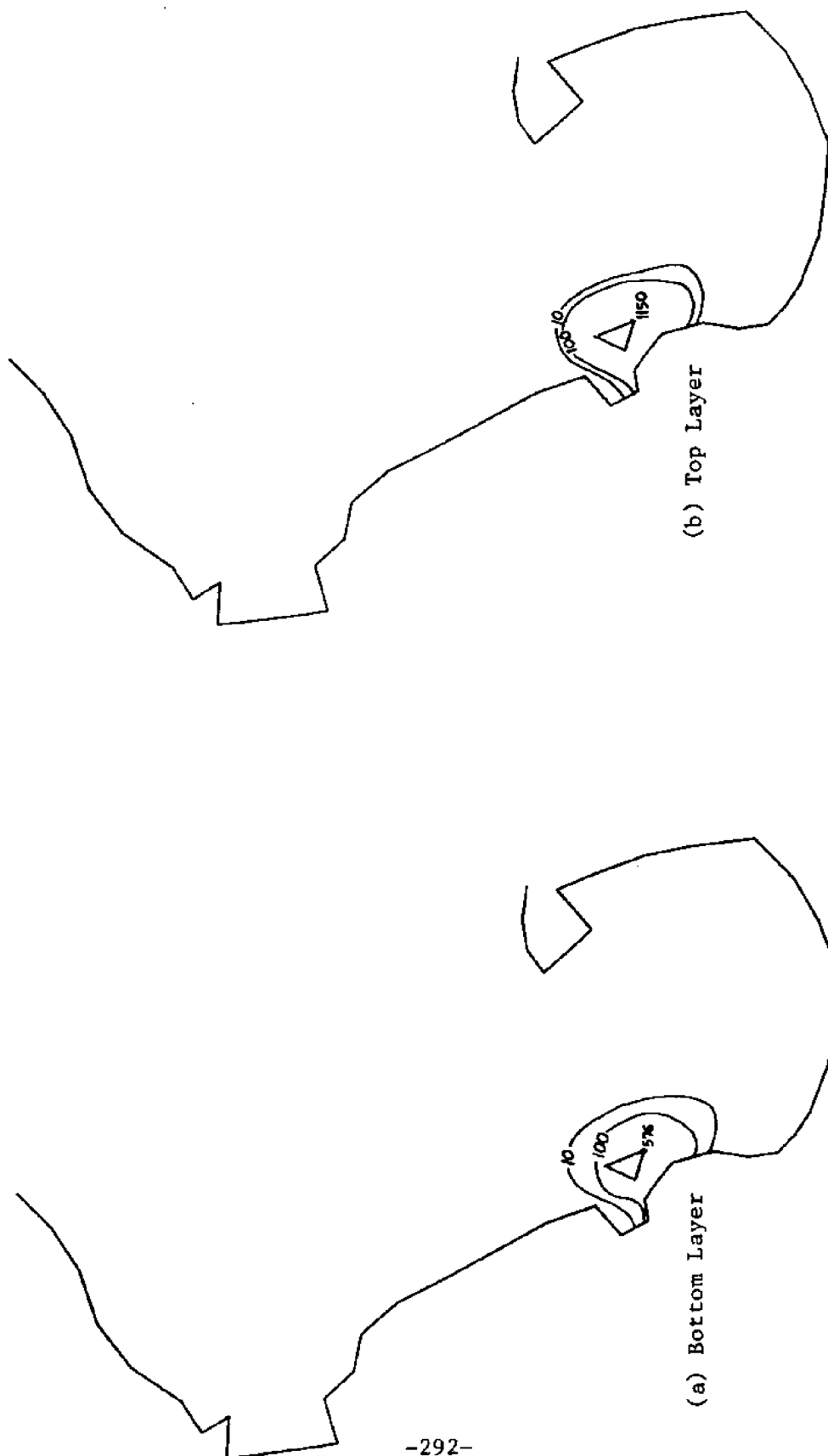


Figure 9.35 Computed Concentrations at Day D+1 (Small Tidal Tilt)

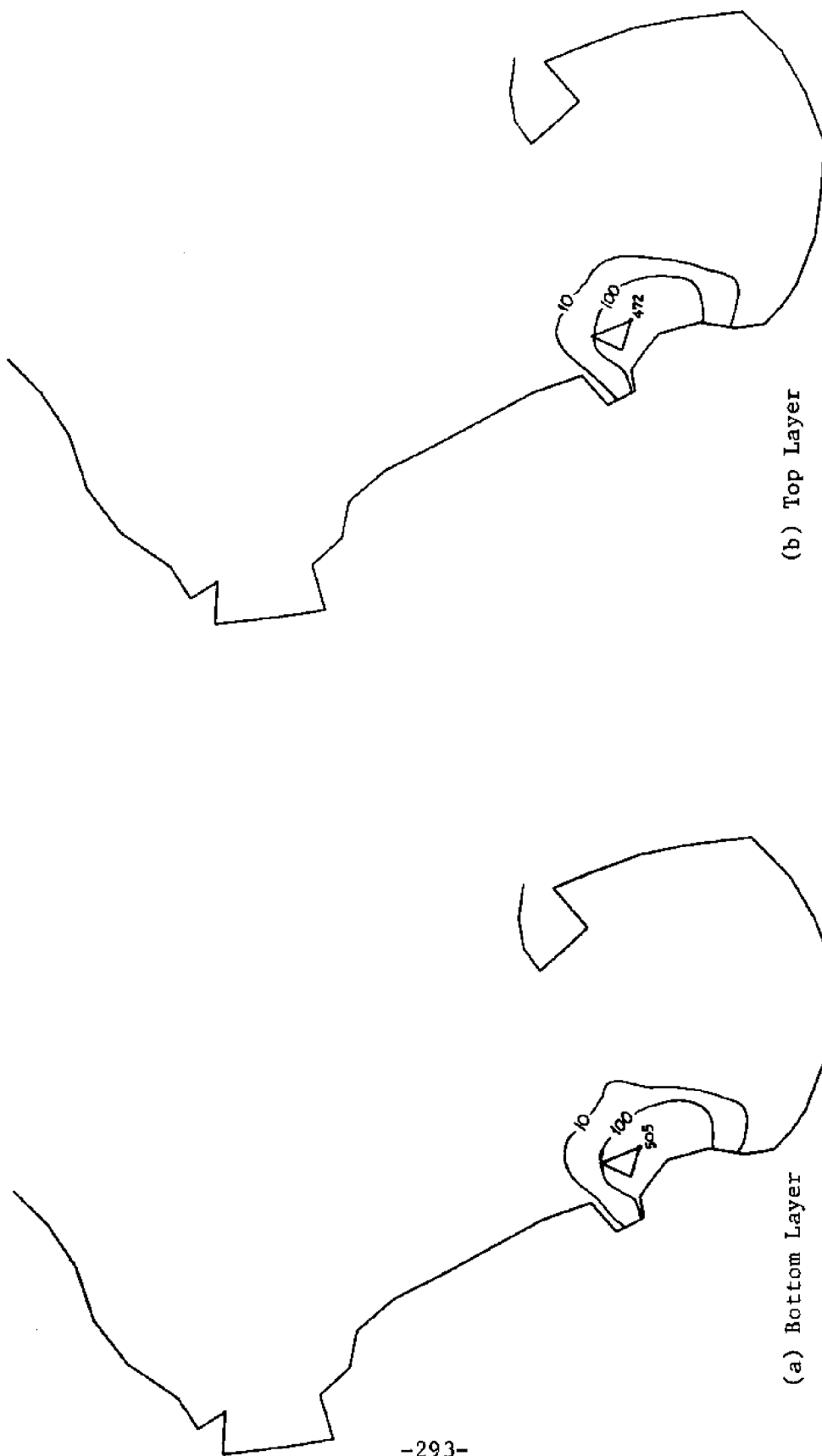


Figure 9.36 Computed Concentrations at Day D+2 (Small Tidal Tilt)

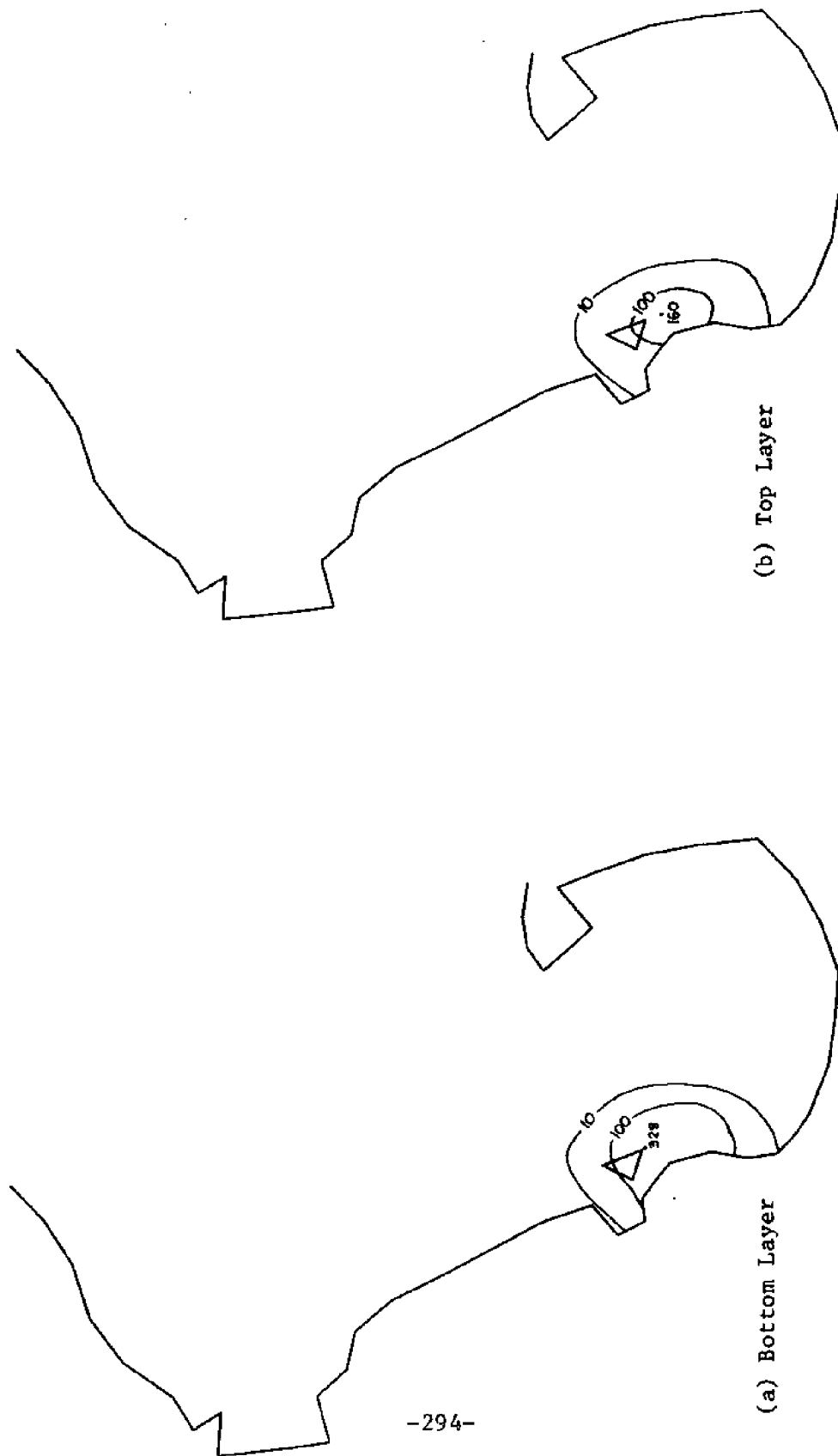


Figure 9.37 Computed Concentrations at Day D+3 (Small Tidal Tilt)

Detailed measurements should resolve the former problem, however an improved version of the circulation model, handling vanishing layers, etc., is needed to overcome the latter. The great sensitivity of the dispersion results to the velocity input, observed in the previous sections, is a factor emphasizing the need for a reliable velocity field.

In the case of Massachusetts Bay, the large tidal tilt, along with the deepening of nearshore areas, produced an exaggerated southward drift parallel to the coast, a strong counterclockwise gyre in the Cape Cod Bay and outward flow over the tip of the Cape. Although all these features do exist in weaker form, as evidenced from both measurements and one-layer model simulations, the strong velocity field causes the dispersing particles to move too fast in comparison to the actual data. It is worth noticing, however, that the location of the plumes after several days is not unreasonable and, in fact, better than that obtained under a smaller tidal tilt. In that case the southward motion is less pronounced and the plumes eventually end up more to the north than they should. The small net motion of the plume centers in the MIT experiment, both in nature and in simulations, is explained by the presence at the area of the source, of a "separation" region with very weak tidal velocities, as discussed in (63) and seen in the velocity plots of Section 9.3.3.



Another important feature of the application runs was the high sensitivity of the results to the precise tidal time of introduction of the material. This should be at least partly due to the unrealistically high velocities used, causing large tidal excursion of the particle center of mass. It is conceivable that the motion of an effluent in nature is indeed to some extent dependent on the time of injection; and this notion is being used in planning the discharges of sewage outfalls and other pollutants into the coastal waters. In view of the above and the spatial distribution of the source for purposes of the computation, it seems important that a preliminary calculation is made to evaluate the time necessary for a source of the actual size to reach its numerical size.

The value of the dispersion coefficient used in the applications gave reasonable results with respect to the quantitative features of the distributions, taking into account the initial source spreading. Nevertheless, it is low with respect to the criteria discussed in Section 8.2.4. As a consequence, appreciable negative values do appear in the fringes of the plume, and further spatial oscillations which die off rapidly. This is certainly an undesirable effect and it could be remedied by arbitrarily increasing the dispersion coefficient in cases where the solution is not sensitive to its value (see Chap. 6). In problems where this is not the case, such as the almost instantaneous sources used in the

applications, attention should be confined to the central part of the plume. This is not affected by the presence of negatives and should still contain quite good results.

Finally, some comments on the role of interfacial transport are appropriate. In the verification studies the interface was seen to represent a barrier difficult to penetrate even with unrealistically high values of the interfacial mixing rate. The picture was different in the applications because of the presence of settling on the one hand and the large time scale on the other. The velocities in the two layers were not much different and consequently the location of the plumes in the two layers was similar. However, the progressive relative increase of the lower layer concentrations with respect to those of the top was evident in all runs. Thus, in the case of settling particles, the two-layer approach is useful in providing more detail about the vertical distribution of the material as time proceeds.

## CHAPTER 10

### CONCLUSIONS

The objective of this study was to investigate the problem of dispersion in coastal or inland water bodies under conditions of strong stratification. The two-layer idealization was adopted as a useful extreme case and, at the same time, the easiest to handle mathematically. Primary emphasis was placed first on analyzing the physical mechanisms associated with the dispersion phenomenon in such a system and second on establishing the numerical requirements for its effective simulation by the finite element method.

Rational quantitative expressions for the dispersion coefficients and the interfacial transport in terms of the mean flow characteristics, which are necessary for engineering applications, were proposed. Moreover, the sensitivity of the results to variations in these and other parameters was evaluated mainly through examination of analytical solutions derived under simple flow conditions. With respect to the numerical aspects of the problem, use of the trapezoidal integration rule yielded the initial value problem unconditionally stable for an arbitrary grid. The limitation imposed by the iteration procedure, employed for economical handling of time variability, was investigated theoretically and a simple quantitative expression for selecting the time step was developed and verified by numerical experimentation.

The accuracy characteristics of the scheme, particularly in connection with the finite element spatial discretization, were also analyzed and quantified.

Verification studies showed that the numerical model adequately predicts the phenomena it is intended to. Its potential and limitations relative to real world problems was evaluated through applications to field experiments in the Massachusetts Bay. The ability of the two-layer treatment to handle transport between the layers is important, whether or not the constituent of interest has some vertical mobility, in providing a refined picture of its distribution over the depth. A further advantage of the two-layer formulation evident from both ideal and real applications, lies in the more detailed description of the velocity field. However, the sensitivity of the results to variations in the flow field points out the necessity for using realistic current input.

In order to improve the applicability of the model to natural water bodies some extensions, such as treatment of vanishing bottom layers, will have to be incorporated. But more importantly, a reliable circulation field is essential. This will require extensive field monitoring programs for obtaining information primarily on the behavior of the interface along the open boundary of the domain under consideration. Development of numerical techniques has outgrown our present ability to define realistic inputs and also our basic knowledge of turbulent mixing

processes in stratified environments. Unless the physical processes are fully understood, their proper modeling cannot be complete. Therefore, more fundamental research is needed in this area.

In view of the above, implementation of more elaborate and expensive multi-layer or three-dimensional models does not seem warranted at this time. It is believed that the present two-layer model, providing an extreme-case picture of the response of the physical system under summer conditions, can be a useful tool in coastal dispersion studies. Furthermore, the discussion of the basic physical processes and the requirements of the finite element solution should be valuable in multi-layer extensions, as well as other related problems.

## REFERENCES

1. Abbott, M.B. et.al., "Systems Modeling of Stratified Fluids", Symposium on Modeling Techniques 'Modeling 75', San Francisco, September 1975
2. Adey, R.A. and Brebbia, C.A., "Finite Element Solution for Effluent Dispersion", Proc. of Intern. Conference on Numerical Methods in Fluid Dynamics, 1973; ed. by C.A. Brebbia and J.J. Connor, Pentech Press, 1974
3. Bella, D.A. and Grenney, W.J., "Finite Difference Convection Errors", J. Sanitary Engin. Div. ASCE, Vol. 96, SA6, December 1970
4. Boericke, R.R. and Hall, D.W., "Hydraulic and Thermal Dispersion in an Irregular Estuary", J. Hydraulics Div. ASCE, Vol. 100, HY1, January 1974
5. Bowden, K.F., "Fundamentals of Dispersion", Proceedings of Symposium on 'Mathematical and Hydraulic Modeling of Estuarine Pollution', at the Water Pollution Research Labs., April 1972
6. Briggs, D.A. and Madsen, O.S., "Mathematical Models of the Massachusetts Bay, Part II: Analytical Models for One- and Two-Layer Systems in Rectangular Basins", R.M. Parsons Lab. for Water Resources and Hydrodynamics, T.R. #172, M.I.T., October 1973
7. Breusers, H.N.C. (ed.), "Momentum and Mass Transfer in Stratified Flows", Literature Study, Delft Hydraulics Lab Report R880, December 1974
8. Bumpus, D.F., "Review of the Physical Oceanography of Massachusetts Bay", Woods Hole Oceanographic Inst. Report 74-8, February 1974
9. Butman, B., "On the Dynamics of Shallow Water Currents in Massachusetts Bay and the New England Continental Shelf", Ph.D. Thesis, Dept. of Earth and Planetary Sciences, M.I.T. and Woods Hole Oceanographic Inst., April 1975
10. Carslaw, H.S. and Jaeger, J.C., "Conduction of Heat in Solids", Oxford University Press, 2nd ed., 1959
11. Christodoulou, G.C. et.al., "Mathematical Models of the Massachusetts Bay, Part III: A Mathematical Model for the Dispersion of Suspended Sediments in Coastal Waters", R.M. Parsons Laboratory for Water Resources and Hydrodynamics, T.R. #179, M.I.T., January 1974

12. Chatwin, P.C., "On the Longitudinal Dispersion of Passive Contaminants in Oscillatory Flows in Tubes", J. Fluid Mechanics, Vol. 71, Part 3, October 1975
13. Connor, J.J. and Brebbia, C.A., "Finite Element Techniques for Fluid Flow", Butterworths, 1976
14. Corrsin, S., "Theories of Turbulent Dispersion", International Symposium of the National Scientific Research Center on 'The Mechanics of Turbulence', Marseille, 1961
15. Crapper, P.F. and Linden, P.F., "The Structure of Turbulent Density Interfaces", J. Fluid Mechanics, Vol. 65, Part 1, August 1974
16. Csanady, G.T., "Turbulent Diffusion in the Environment", D. Reidel Publ. Co., 1973
17. Deardorff, J.W., "On the Magnitude of the Subgrid Scale Eddy Coefficient", J. Computational Physics, Vol. 7, Part 1, 1971
18. Elder, J.W., "The Dispersion of Marked Fluid in Turbulent Shear Flow", J. Fluid Mechanics, Vol. 5, Part 4, May 1959
19. Ellison, T.H. and Turner, J.S., "Turbulent Entrainment in Stratified Flows", J. Fluid Mechanics, Vol. 6, Part 3, October 1959
20. Fadeeva, V.N., "Computational Methods for Linear Algebra", Dover, 1959
21. Fischer, H.B., "The Mechanics of Dispersion in Natural Streams", J. Hydraulic Div. ASCE, Vol. 93, HY 6, November 1967
22. Frankel, S.L. and Pearce, B.R., "Determination of Water Quality Parameters in the Massachusetts Bay (1970-1973)", R.M. Parsons Lab for Water Resources and Hydrodynamics, T.R. #174, November 1973
23. Fromm, J.E., "Practical Investigation of Convective Difference Approximations of Reduced Dispersion", The Physics of Fluids, Vol. 12, Suppl. 2, 1969
24. Goldstein, S. (ed.), "Modern Developments in Fluid Dynamics", Vol. 1, Oxford Univ. Press, 1938

25. Hansen, N.E.O., "Effect of Wind Stress on Stratified Deep Lake", J. Hydraulics Div., ASCE, HY8, August, 1975
26. Harleman, D.R.F., "Transport Processes in Water Quality Control", R.M. Parsons Lab. for Water Resources and Hydrodynamics, M.I.T., 1973
27. Harleman, D.R.F., "One-Dimensional Models", in "Estuarine Modeling: An Assessment", published by TRACOR for EPA, February 1971
28. Halpern, D., "Observations of Short-Period Internal Waves in Massachusetts Bay", J. Marine Research, Vol. 29, 1971
29. Hirt, C.W., "Heuristic Stability Theory for Finite Difference Equations", J. Computational Physics, Vol. 2, Part 4, June 1968
30. Holley, E.R. et.al., "Dispersion in Homogeneous Estuary Flow", J. Hydraulics Div. ASCE, Vol. 96, HY8, August 1970
31. Holly, F.M. and Cunje, J.A., "Time Dependent Mass Dispersion in Natural Streams", Symposium on Modeling Techniques 'Modeling 75', San Francisco, September 1975
32. Hyden, H., "Water Exchange in Two-Layer Stratified Waters", J. Hydraulics Div. ASCE, Vol. 100, HY3, March 1974
33. Jirka, G.H. et.al., "An Assessment of Techniques for Hydrothermal Prediction", R.M. Parsons Lab for Water Resources and Hydrodynamics, T.R. #203, M.I.T., July 1975
34. Jobson, H.E. and Sayre, W.W., "Predicting Concentration Profiles in Open Channels", J. Hydraulics Div. ASCE, Vol. 96, HY10, October 1970
35. Kato, H. and Phillips, O.M., "On the Penetration of a Turbulent Layer into Stratified Fluid", J. Fluid Mechanics, Vol. 37, Part 4, July 1969
36. Koh, R.C.Y. and Fan, L.N., "Further Studies on the Prediction of the Radioactive Debris Distribution Subsequent to a Deep Underwater Nuclear Explosion", Tetra Tech Inc., Report TC 154, October 1969



37. Kullemberg, G., "Vertical Diffusion in Shallow Water", *Tellus*, Vol. 23, No. 2, 1971
38. Laevastu, T., "Multilayer Hydrodynamical-Numerical Models", Symposium on Modeling Techniques 'Modeling 75', San Francisco, September 1975
39. Launder, B.E. and Spalding, D.B., "Lectures in Mathematical Models of Turbulence", Academic Press, 1972
40. Lee, K.K., "Wind-Induced and Thermally-Induced Currents in the Great Lakes", *Water Resources Research*, Vol. 8, No. 6, December 1972
41. Leendertse, J.J. et.al., "A Three-Dimensional Model for Estuaries and Coastal Seas: Vol. I, Principles of Computation", Rand Co., December 1973
42. Leendertse, J.J. and Liu, S.K., "A Three-Dimensional Model for Estuaries and Coastal Seas: Vol. II, Aspects of Computation", Rand Co., June 1975
43. Leimkuhler, W.F., "A Two-Dimensional Finite Element Dispersion Model", Engineer's Thesis, Dept. of Civil Engineering, M.I.T., September 1974
44. Leimkuhler, W.F. et.al., "Two-Dimensional Finite Element Dispersion Model", Symposium on Modeling Techniques 'Modeling 75', San Francisco, September 1975
45. Liggett, J.A., "Stratified Lake Circulation Calculations by the Finite Element Method", Proceedings of XVI I.A.H.R. Congress, Sao Paulo, 1975
46. Lofquist, K., "Flow and Stress Near an Interface Between Stratified Liquids", *The Physics of Fluids*, Vol. 3, No. 2, March-April 1960
47. Long, R.R., "Some Aspects of the Flow of Stratified Fluids. II: Experiments with a Two-Fluid System", *Tellus*, Vol. 6, No. 2, May 1954
48. Long, R.R., "Some Properties of Turbulence in Stratified Shearing Flow", International Symposium on Stratified Flows, Novosibirsk, August 1972

49. Long, R.R., "The Influence of Shear on Mixing Across Density Interfaces", J. Fluid Mechanics, Vol. 70, Part 2, July 1975
50. Long, R.R., "Circulations and Density Distributions in a Deep, Strongly-Stratified, Two-Layer Estuary", J. Fluid Mechanics, Vol. 71, Part 3, October 1975
51. Monin, A.S. and Yaglom, A.M., "Statistical Fluid Mechanics: Mechanics of Turbulence", Vol. 1, M.I.T. Press, 1971
52. Moore, M.J. and Long, R.R., "An Experimental Investigation of Turbulent Stratified Shearing Flow", J. Fluid Mechanics, Vol. 49, Part 4, October 1971
53. Morton, K.W., "Stability and Convergence in Fluid Flow Problems", Proc. Royal Society of London, Ser. A, Vol. 323, 1971
54. Nelsen, T.A., "The New England Offshore Environmental Study (NOMES): The Character of Sphalerite Particle Dispersion in Massachusetts Bay and Adjacent Waters", Atlantic Oceanographic and Meteorological Labs, NOAA, Miami, January 1975
55. Okubo, A., "Oceanic Diffusion Diagrams", Deep Sea Research, August 1971
56. Okubo, A., "Horizontal and Vertical Mixing in the Sea", Chapter in "Impingement of Man on the Oceans", ed. by D.H. Wood, Wiley, 1971
57. Okubo, A., "The Effect of Shear in an Oscillatory Current on Horizontal Diffusion from an Instantaneous Source", J. Oceanology and Limnology, Vol. 1, No. 3, 1967
58. Okubo, A. and Osmidov, R.V., "Empirical Dependence of the Coefficient of Horizontal Turbulent Diffusion in the Ocean on the Scale of the Phenomenon in Question", Izv. Acad. of Sciences USSR, Atmospheric and Oceanic Physics, Vol. 6, No. 5, 1970
59. Orlob, G.T., "Eddy Diffusion in Homogeneous Turbulence", J. Hydraulics Div. ASCE, Vol. 85, Hy 9, September 1959
60. Orszag, S.A., "Numerical Simulation of Incompressible Flows within Simple Boundaries: Accuracy", J. Fluid Mechanics, Vol. 49, Part 1, 1971

61. Osmidov, R.V., "On the Rate of Dissipation of Turbulent Energy in Sea-Currents and on the Dimensionless Universal Constant in the  $4/3$  Power Law", Bull. Acad. of Science USSR, Geophysics Series, No. 8, 1960
62. Osmidov, R.V., "On the Turbulent Exchange in a Stably Stratified Ocean", Izv. Acad. of Science USSR, Atmospheric and Oceanic Physics, Vol. 1, No. 8, 1965
63. Pagenkopf, J.R. et.al., "Circulation and Dispersion Studies at the Pilgrim Nuclear Power Station, Rocky Point, Mass.", R.M. Parsons Lab for Water Resources and Hydrodynamics, T.R. #210, M.I.T., February 1976
64. Pasquill, F., "Atmospheric Diffusion. The Dispersion of Windborne Material from Industrial and Other Sources", Wiley, 2nd Ed., 1974
65. Pearce, B.R. and Christodoulou, G.C., "Application of a Finite Element Dispersion Model for Coastal Waters", Proceedings of XVI I.A.H.R. Congress, Sao Paulo, 1975
66. Pedersen, F.B., "Gradually Varying Two-Layer Stratified Flow", J. Hydraulics Div. ASCE, Vol. 98, HY 1, January 1972
67. Phillips, O.M., "The Dynamics of the Upper Ocean", Cambridge Univ. Press, 1966
68. Richtmeyer, R.D. and Morton, K.W., "Difference Methods for Initial Value Problems", Interscience, 1967
69. Roache, P.J., "On Artificial Viscosity", J. Computational Physics, Vol. 10, 1972
70. Roache, P.J., "Computational Fluid Dynamics", Hermosa Publ., Albuquerque, 1972
71. Sa Da Costa, A., Private Communication, M.I.T., 1976
72. Simons, T.J., "Development of Three-Dimensional Numerical Models of the Great Lakes", Scientific Series No. 12, Canada Centre for Inland Waters, Burlington, Ontario, 1973
73. Spiegel, M.R., "Laplace Transforms", SHAUM's Outline Series, McGraw-Hill, 1965

74. Sumer, M., "Mean Velocity and Longitudinal Dispersion of Heavy Particles in Turbulent Open-Channel Flow", J. Fluid Mechanics, Vol. 65, Part 1, August 1974
75. Strang, G. and Fix, G.J., "An Analysis of the Finite Element Method", Prentice Hall, 1973
76. Taylor, G.I., "The Dispersion of Matter in Turbulent Flow through a Pipe", Proc. Royal Society of London, Ser. A, Vol. 223, 1954
77. Taylor, C. and Davis, J., "Finite Element Modeling of Flow and Dispersion in Estuaries", International Symposium on River Mechanics, Bangkok, 1973
78. Turner, J.S., "The Influence of Molecular Diffusivity on Turbulent Entrainment across a Density Interface", J. Fluid Mechanics, Vol. 33, Part 4, September 1968
79. Turner, J.S., "Buoyancy Effects in Fluids", Cambridge Univ. Press, 1973
80. U.S. Dept. of Commerce, NOAA, NOS, "Tide Tables", 1973
81. U.S. Dept. of Commerce, NOAA, NOS, "Tide Tables", 1975
82. Verboom, G.K., "The Advection-Dispersion Equation for an Anisotropic Medium Solved by Fractional-Step Methods", Proc. Int. Conference on Mathematical Models for Environmental Problems, Southampton, Sept. 1975
83. Vreugdenhil, C.B. (ed.), "Computational Methods for the Vertical Distribution of Flow in Shallow Water", Literature Study, Delft Hydraulics Lab Report W 152, August 1973
84. Vreugdenhil, C.B. and Voegt, J., "Hydrodynamic Transport Phenomena in Estuaries and Coastal Waters" Scope of Mathematical Models", Symposium on Modeling Techniques 'Modeling 75', San Francisco, September 1975
85. Wada, A., "Effect of Winds on a Two-Layered Bay", Technical Lab, Central Research Inst. of Electrical Power Industry, T.R. C-66002, Tokyo, September 1966
86. Wang, J.D. and Connor, J.J., "Mathematical Modeling of Near Coastal Circulation", R.M. Parsons Lab for Water Resources and Hydrodynamics, T.R. #200, M.I.T., April 1975

87. Welander, P., "Wind Driven Circulation in One- and Two-Layer Oceans of Variable Depth", Tellus, Vol. 20, No. 1, 1968
88. Wing, R.H. (ed.), "A Test Particle Dispersion Study in Massachusetts Bay", NOAA Publication ERL-374-MESAG, September 1976 (to be published)
89. Woods, W.L., Unpublished Manuscript, the University of Reading, 11 October 1972
90. Wu, J., "Wind-Induced Turbulent Entrainment across a Stable Density Interface", J. Fluid Mechanics, Vol. 61, Part 2, November 1973
91. Yalin, M.S., "Mechanics of Sediment Transport", Pergamon Press, 1972
92. Zeidler, R.B., "Coastal Dispersion of Pollutants", J. Waterways, Harbors and Coastal Eng. Div. ASCE, Vol. 102, WW2, May 1976
93. Zienkewicz, O.C., "The Finite Element Method in Engineering Science", McGraw-Hill, 1971